The University of Nottingham

UNITED KINGDOM · CHINA · MALAYSIA

Using human induced pluripotent stem cells to study the *in vitro* phenotype of the cardiac channelopathies

Submitted by

Gary Duncan, BSc

School of Medicine

University of Nottingham

April 2017

Thesis submitted to the University of Nottingham for the degree of Doctor of Philosophy

Acknowledgements

I would like to begin by thanking my PhD supervisor Professor Chris Denning for giving me an opportunity three and a half years ago and for his continued support and advice throughout my PhD which has been invaluable.

Secondly I would like to thank our collaborators who helped shape my understanding and the direction of this project. Dr Chris George and Dr David Edwards (Cardiff University) for their help with the calcium handling aspect of this work and Dr Maria Hortigon and Dr Victor Zamora Rodriguez (University of Glasgow) for their help with the CellOPTIQ and advice regarding the voltage measurements. I would also like to thank Dr Nigel Smith (City Hospital) for his help with karyotyping, Dr Andrew Staniforth (QMC/City Hospital) for his help recruiting patients for this and other studies and Dr David Onion (QMC) for his help with flow cytometry.

My thanks to Dr Divya Mirrington, Dr Spandan Kalra and Dr Vinoj George for their initial training in cell culture and molecular biology techniques which required nearly endless patience. A special thanks go to Dr Alexander Kondrashov for all his advice and guidance with the genome engineering work of my project. Thanks also to Penny Gwynne and Kasia Lis-Slimak, without whom the labs would simply not function.

I would like thank Jamie Bhagwan, James Smith, Divya Mirrington, Luke Flatt, James Crutchley, Diogo Mosqueira, Spandan Kalra, Jamie Patient, Liz Scott, Lara Lewis, Peggy Cho Kiu Lo, Harry Hoang, Lazaros Fotopoulos and Ashley Ramsawhook for keeping me sane by listening to me rant incessantly at some point or another over the last three and a half years. I would also like to thank my friends back home in Scotland who remind me that there is more to my life than the four walls of the lab.

I would not be where I am now or have achieved what I have done without the love and support of my parents and family and for their endless support and encouragement I am very grateful.

Finally, I want to thank Aveen who has shown immeasurable patience, kindness, encouragement, love and support over the last three and half years. Without her tireless enthusiasm for rail travel between London and Nottingham almost every week I would not have had the drive to complete this project. She refused to stop believing in me even when I didn't necessarily believe in myself and without her I would never have come so far.

Declaration

I hereby declare that this thesis has been composed by myself and has not been submitted for any other degree previously. Acknowledgements of specific procedures not performed by myself are stated; otherwise, the work described is my own.

Gary Duncan:_____

Date:

Abstract

Long QT Syndrome 2 (LQTS2) and Catecholaminergic Polymorphic Ventricular Tachycardia (CPVT) are two prevalent cardiac channelopathies. LQTS2 is the second most common form of LQTS and accounts for up to 45% of cases (Schwartz et al, 2012). CPVT1 is the most common form of CPVT and relates to dysfunction of the RYR2, mutations in *RYR2* are thought to account for up to 50% of CPVT cases (Nyegaard et al, 2012). Treatment for these conditions is vital as mortality rates for untreated individuals can range from 21% to potentially as high as 50% (Leenhardt et al, 1995; Schwartz et al, 2012). Discovering novel compounds which treat these conditions is beset by suboptimal drug discovery methods which utilise animal models, which can be inaccurate due to inter-species variability in the cardiovascular system (Rajamohan et al, 2013), and heterologous overexpression systems which test the effect of a drug on specific ion channels which are limited by the inability of these systems to model the dynamic interaction between different ion channels *in vivo* (Kramer et al, 2013). Using human induced pluripotent stem cells (hiPSC) it is possible to generate cardiomyocytes which may enable the creation of humanised models of disease. Such models may enable the discovery of efficacious compounds more readily than current drug development techniques and they may also allow the study of disease pathogenesis in more detail than is currently available in human systems.

In this thesis different tissue sample types were investigated for their ability to robustly derive cell lines *in vitro* for use in reprogramming to hiPSCs. Furthermore in this thesis three different non-integrative methods of hiPSC generation, Sendai virus, episomal reprogramming using nucleofection and episomal reprogramming using GET peptide mediated transduction, were tested to assess which was able to most robustly generate hiPSCs. These hiPSCs were ultimately differentiated into cardiomyocytes (hiPSC-CMs) and used in downstream phenotyping assays. An LQTS2-hiPSC model was used as part of an *in vitro* drug assay to test the effectiveness of I_{kr}, I_{katp}, PPARδ and I_{ks} agonists in reducing the action potential duration (APD) of the LQTS2-hiPSC-CMs which would thereby indicate a role in enhancing repolarisation. The effects of these new candidate drugs were compared to the effect observed by the traditional LQTS2 therapy, β-blockers. This work was carried out using the CellOPTIQ platform and voltage was analysed by labelling the hiPSC-CMs with voltage sensitive cell dye FluoVolt. Furthermore in this thesis a CPVT-

hiPSC model was generated and genetically corrected using CRISPR/Cas9 genome engineering technology. These hiPSCs were then differentiated to cardiomyocytes and analysed for their calcium handling properties using fluorescent labelling dye Fura2-AM.

Assessment of the voltage properties of the LQTS2-hiPSC-CMs indicated that the LQTS2-hiPSC-CMs exhibit increased APD in comparison to healthy-hiPSC-CMs and an increase in triangularisation time which is indicative of repolarisation time therefore indicating a faithful recapitulation of the patient's phenotype *in vitro*. Moreover the APD of LQT2-hiPSC-CMs was found to decrease in response to treatment with I_{katp}, I_{kr}, PPARδ and I_{ks} agonists. These data indicate that the drugs tested in this thesis may provide a beneficial effect to LQTS2 patients and should be investigated further.

Assessment of the calcium handling mechanics of CPVT-hiPSC-CMs and genetically corrected CPVT-WT-hiPSC-CMs indicated that differences exist in the way in which these hiPSC-CMs handle calcium *in vitro*. The genetically corrected CPVT-WT-hiPSC-CMs were found to show enhanced functionality of RYR2 and SERCA when challenged with relevant pharmacological blockade, potentially indicating a corrected phenotype. However assessment of whether the CPVT-hiPSC-CMs exhibited a "normal" phenotype was inconclusive. There exist differences in the calcium handling properties of CPVT-WT-hiPSC-CMs and unrelated healthy-hiPSC-CMs.

To summarise, this thesis assesses the effectiveness of multiple tissue samples to elucidate a robust method to derive starting cell populations from patients. Moreover it goes on to establish a robust protocol for generating hiPSCs from these samples using a non-integrative reprogramming method. The generation of an LQTS2 disease model enabled an *in vitro* drug assay which identified 9 compounds which were able to reduce the APD in LQTS2-hiPSC-CMs, of which 7 showed utility in reducing the repolarisation time of the LQT2-hiPSC-CMs. These results indicate that these compounds may exert beneficial effects in the treatment of patients with LQTS2. In addition to this, preliminary results in the CPVT disease model created seem to indicate an increase in functionality of both RYR2 and SERCA after CRISPR/Cas9 genetic correction of the S2246L mutation. Attempts to establish if CRISPR/Cas9 genetic correction generated "normal" calcium handling properties were inconclusive. There remains a large amount of variability within genetically

distinct hiPSC-CMs with regards to their calcium handling properties, likely owing to the highly spatial and temporal nature of calcium movement in cardiomyocytes and this should be investigated further.

Table of Contents

Acknowledgements i

Declaration ii

Abstract iii

Table of Contents vi

List of Figures xii

List of Tables xiv

Abbreviations xv

Genes and Nomenclature xvii

Potassium voltage-gated channel subfamily H member 2 xvii

Mesoderm posterior bHLH transcription factor 1 xvii

1 Chapter 1 – Introduction 1

1.1 The cardiac system 1

1.1.1 The cardiac action potential and clinical electrocardiogram (ECG) 1

1.1.2 The cardiac channelopathies 7

1.2 Assessing the need for hiPSC disease models of cardiac disease 13

1.2.1 *In Vitro* systems 14

1.2.2 *In Vivo* animal models 14

1.3 Generation of hPSCs 16

1.3.1 Embryonic stem cells (ESC) 16

1.3.2 Induced pluripotent stem cells (iPSC) 17

1.3.3 Cell sources 19

1.3.4 Reprogramming factors 19

1.3.5 Integrative reprogramming methods 22

1.3.6 Non-Integrative reprogramming methods 24

1.4 Cardiac development and *In Vitro* differentiation 27

1.4.1 *In Vivo* cardiac development 27

1.4.2 Generation of cardiomyocytes from hPSCs *In Vitro* 31

1.5 The current landscape of hiPSCs in disease modelling 33

1.5.1 Cardiomyocyte phenotyping 33

1.5.2 hPSC-Cardiomyocyte structure 37

1.5.3 hPSC-Cardiomyocyte gene expression 38

1.5.4 hPSC-Cardiomyocyte electrophysiology 38
1.5.5 hPSC-Cardiomyocyte calcium handling 39
1.5.6 Long term culture of hPSC-CMs *In Vitro* 39
1.6 CRISPR/CAS9 as a genome editing tool 40
1.6.1 History of CRISPR 40
1.6.2 The CRISPR system and its use in human cells 42
1.7 Thesis rationale and objectives 44
2 Materials and Methods 46
2.1 General cell culture techniques 46
2.1.1 Derivation of starting cell populations 46
2.1.2 Culture of human fibroblasts 47
2.1.3 Culture of human induced pluripotent stem cells (hiPSC) 48
2.1.4 Tri-Lineage differentiation test 49
2.1.5 Differentiation of hiPSCs to cardiomyocytes 49
2.2 Reprogramming technologies 52
2.2.1 Sendai virus reprogramming 52
2.2.2 Episomal reprogramming 52
2.2.3 GET mediated delivery 53
2.2.4 Purification of hiPSC colonies after reprogramming 53
2.3 Human induced pluripotent stem cell characterisation 55
2.3.1 Fixing cells 55
2.3.2 Immunostaining 55
2.3.3 Flow cytometry 56
2.3.4 Karyotype analysis 56
2.3.5 Calculation of population doubling times 57
2.4 Molecular biology techniques 57
2.4.1 Genomic DNA extraction 57
2.4.2 Polymerase Chain Reaction (PCR) 58
2.4.3 Restriction digests 58
2.4.4 DNA gel electrophoresis 59
2.4.5 Gel extraction 59
2.4.6 Transformation of competent bacteria 60
2.4.7 Small scale DNA preparation 60
2.4.8 Large scale DNA preparation 61

2.4.9 PCR purification 61
2.4.10 RNA extraction 62
2.4.11 cDNA synthesis 62
2.5 CRISPR/Cas9 genome engineering 62
2.5.1 Oligonucleotide method 62
2.5.2 PiggyBac transposon method 64
2.6 CellOPTIQ assays 65
2.6.1 Voltage based assay 65
2.6.2 Calcium based assay 67
2.7 Statistical analysis 68
3 Chapter 3 – Generation and characterisation of hiPSC-and their differentiation to cardiomyocytes 70
3.1 Introduction 70
3.1.1 Identifying a starting cell population for hiPSC generation 70
3.1.2 Choosing a non-integrative reprogramming strategy for hiPSC generation 74
3.1.3 Choosing a method to differentiate hiPSCs to cardiomyocytes 78
3.1.4 Chapter aims and objectives 80
3.2 Results 82
3.2.1 Generating hiPSCs using previously established methods 82
3.2.2 Establishing the efficiency of transduction and reprogramming using non-integrative methods 85
3.2.3 Derivation of starting cell populations from different tissue samples 90
3.2.4 Pilot reprogramming of control fibroblasts like cell line using Sendai virus 93
3.2.5 Generation of hiPSCs using Sendai virus 96
3.2.6 Assessing the three germ layer differentiation potential of newly derived hiPSC line ReBl-PAT 103
3.2.7 Assessing method for hiPSC purification after reprogramming 105
3.2.8 Assessing the loss of reprogramming vectors in the newly derived hiPSCs 108
3.2.9 Using monolayer differentiation methods to generate cardiomyocytes 110
3.3 Discussion 116
4 Chapter 4 – Assessing the phenotype of LQTS2 hiPSCs and the effects of pharmacological intervention 122

4.1 Introduction 122
4.1.1 Long QT Syndrome type 2 122
4.1.2 Molecular and structural biology of I_{kr} current 123
4.1.3 The role of I_{kr} current in cardiac function 124
4.1.4 hiPSCs as a model for LQTS2 124
4.1.5 Treatment options for LQTS 125
4.1.6 Chapter aims and objectives 127
4.2 Results 129
4.2.1 Assessing cellular response to β-adrenergic stimulation 129
4.2.2 Assessing the cells behaviour as single cells and monolayers 131
4.2.3 Optimisation of the CellOPTIQ platform 133
4.2.4 Assessing LQTS2 phenotype under basal conditions 135
4.2.5 Assessing if the CellOPTIQ can detect changes in APD 137
4.2.6 Assessing LQTS2-hiPSC-CM response to E4031 140
4.2.7 Assessing effect of β-blockers on LQTS2-hiPSC-CM 142
4.2.8 Assessing effect of I_{katp} agonists on LQTS2-hiPSC-CM 145
4.2.9 Assessing effect of I_{kr} agonists on LQTS2-hiPSC-CM 149
4.2.10 Assessing effect of PPARδ agonists on LQTS2-hiPSC-CM 153
4.2.11 Assessing effect of I_{ks} agonists on LQTS2-hiPSC-CM 157
4.3 Discussion 160
5 Chapter 5 –Phenotyping a CPVT S2246L mutation in hiPSC-CMs 167
5.1 Introduction 167
5.1.1 CPVT 167
5.1.2 Molecular and structural biology of RYR2 channel 168
5.1.3 Regulation of cardiac ryanodine receptor 168
5.1.4 Calcium handling in the cardiac myocyte 170
5.1.5 CRISPR/Cas9 genome engineering to generate isogenic controls 173
5.1.6 Chapter aims and objectives 174
5.2 Results 176
5.2.1 Patient history and genetic profile 176
5.2.2 Targeting CPVT hiPSC with CRISPR/Cas9 using single stranded oligonucleotide method 178
5.2.3 Targeting CPVT hiPSC with PiggyBac transposon method 184
5.2.4 Optimisation of Amaxa 4D nucleofection 191

5.2.5 Assessment of targeting using plasmid method 193
5.2.6 Basal calcium handling data for healthy-hiPSC-CMs and CPVT-hiPSC-CMs 198
5.2.7 Assessment of LTCC blockade in healthy-hiPSC-CMs and CPVT-hiPSC-CMs 200
5.2.8 Assessment of RYR2 blockade in healthy-hiPSC-CMs and CPVT-hiPSC-CMs 204
5.2.9 Assessment of SERCA blockade in healthy-hiPSC-CMs and CPVT-hiPSC-CMs 208
5.2.10 Assessment of NCX blockade in healthy-hiPSC-CMs and CPVT-hiPSC-CMs 212
5.2.11 Assessment of IP3R blockade in healthy-hiPSC-CMs and CPVT-hiPSC-CMs 216
5.3 Discussion 220
6 General Discussion 228
6.1 Generating Disease Models 228
6.1.1 Non-integrative reprogramming technology 228
6.2 Using hiPSC-CMs to model cardiac channelopathies 229
6.2.1 LQTS2 229
6.3 Therapeutic options for LQTS2 230
6.3.1 β-blockers 230
6.3.2 I_{katp} agonists 230
6.3.3 I_{kr} agonists 231
6.3.4 PPARδ agonists 232
6.3.5 I_{ks} agonists 233
6.4 Modelling CPVT 234
6.5 The current outlook for disease modelling using hiPSC-CMs 235
6.5.1 Utility of hPSC-CMs as disease models 235
6.5.2 Limitations of hPSC-CM 237
6.6 Study limitations and future work 238
6.6.1 Use of only 1 hiPSC line per condition 238
6.6.2 Use of cell permeable fluorescent dyes 239
6.6.3 Lack of other cell types in phenotyping assays 239
6.6.4 Lack of patch clamp investigation 240
6.6.5 Variability of calcium handling data 240

6.7 Final remarks 241
7 Bibliography 242

List of Figures

Figure 1-1 - The cardiac action potential 1
Figure 1-2 - The clinical ECG 7
Figure 1-3 - Current toxicity testing models 14
Figure 1-4 - Schematic illustrating the role of pluripotency in generating disease models 16
Figure 1-5 - Schematic outlining the principles of iPSC generation 19
Figure 1-6 - The mouse as a model for cardiogenesis 30
Figure 1-7 - Schematic outlining the principles of In Vitro cardiac differentiation 33
Figure 1-8 - The four configurations of patch clamp electrophysiology 34
Figure 1-9 - Using CRISPR to edit the genome 41
Figure 1-10 - The mechanisms of immunity in the different CRISPR systems 43
Figure 2-1 - Parameters assessed in voltage traces 66
Figure 2-2 - Parameters assessed in calcium traces 67
Figure 2-3 - Box and whisker plot 68
Figure 3-1 - Schematic representation of the two main differentiation methods tested 80
Figure 3-2 Generating hiPSC lines using lentivirus as a delivery mechanism 84
Figure 3-3 Assessment of GFP transduction efficiency using Sendai virus vectors as a delivery vehicle 86
Figure 3-4 Assessment of reprogramming efficiency using different methods of vector delivery 89
Figure 3-5 Isolation of primary cells from human somatic tissue for the purposes of reprogramming 92
Figure 3-6 Sendai Virus-mediated hiPSC reprogramming 93
Figure 3-7 Assessing effectiveness of Sendai virus to produce viable hiPSC lines in our lab 95
Figure 3-8- Immunocytochemistry analysis of newly derived hiPSC lines. 99
Figure 3-9 - Flow cytometry analysis of pluripotency marker expression in newly derived hiPSCs for quantification 101
Figure 3-10 - Culture and karyotype assessment of newly derived hiPSC lines 102
Figure 3-11 - Assessing the ability of newly generated hiPSC line to generate derivatives of all three germ layers 104
Figure 3-12 - Assessing the effect of method of purification on hiPSC pluripotency and quality 107
Figure 3-13 - Detecting the presence or absence of the SeV vectors using RT-PCR 109
Figure 3-14 - Success of differentiation methods 111
Figure 3-15 - Assessing the quality of the produced cardiomyocytes 113
Figure 3-16 - Assessment of cell viability after cryopreservation 115
Figure 4-1 - The structure of hERG channel 123
Figure 4-2 - Using the Envision to assess hiPSC-CM response to isoprenaline 130
Figure 4-3 - - Analysis using confocal microscopy of calcium transients in single cells and monolayers 132
Figure 4-4 - Analysing Signal:Noise ratios of hiPSC-CMs on CellOPTIQ .. 134
Figure 4-5 - Assessment of the LQTS2-hiPSC-CMs basal APD in comparison to healthy-hiPSC-CM basal APD 136
Figure 4-6 - Assessment of NCRM5-hiPSC-CM response to E4031 139
Figure 4-7 - Assessment of ReBl-hiPSC-CM response to E4031 141
Figure 4-8 - Assessment of ReBl-hiPSC-CM response to propranolol 144
Figure 4-9 - Assessment of ReBl-hiPSC-CM response to nicorandil 147

Figure 4-10 - Assessment of ReBl-hiPSC-CM response to minoxidil..... 148
Figure 4-11 - Assessment of ReBl-hiPSC-CM response to RG3 151
Figure 4-12 - Assessment of ReBl-hiPSC-CM response to NS1643 152
Figure 4-13 - Assessment of ReBl-hiPSC-CM response to telmisartan ... 155
Figure 4-14 - Assessment of ReBl-hiPSC-CM response to GW0742 156
Figure 4-15 - Assessment of ReBl-hiPSC-CM response to ML277 159
Figure 5-1 - The cardiac calcium cycle 170
Figure 5-2 - Schematic explaining the CRISPR/Cas9 process 174
Figure 5-3 - Assessing the CP1 patient genotype 177
Figure 5-4 - Selecting the tools for the oligonucleotide method of gene targeting using CRISPR/Cas9 181
Figure 5-5 - Analysing the success of the oligonucleotide method using CRISPR/Cas9..... 183
Figure 5-6 - Schematic explaining the PiggyBac method 185
Figure 5-7 - Generating the targeting construct for use in PiggyBac system in CRISPR/Cas9 187
Figure 5-8 - Plasmid maps of CP1 targeting construct..... 188
Figure 5-9 - Generation of the gRNA plasmid..... 190
Figure 5-10 - Assessing the optimal conditions of electroporation on the Amaxa 4D system..... 192
Figure 5-11 - Analysing the success of the plasmid method of targeting using CRISPR/Cas9 194
Figure 5-12 - Assessing the left and right homology arms as well as the TTAA site after PiggyBac excision..... 197
Figure 5-13 - Basal calcium handling characteristics of CP1-, ReBl-PAT- and CP1-WT- hiPSC-CMs..... 199
Figure 5-14 - Assessment of hiPSC-CM calcium handling response to LTCC blocker nifedipine..... 202
Figure 5-15 - % change in calcium handling parameters between CP1-hiPSC-CMs and CP1-WT-hiPSC-CMs in response to different doses of nifedipine..... 203
Figure 5-16 - Assessment of hiPSC-CM calcium handling response to RYR2 blocker ryanodine 206
Figure 5-17 - % change in calcium handling parameters across hiPSC-CM panel in response to different doses of ryanodine..... 207
Figure 5-18 - Assessment of hiPSC-CM calcium handling response to SERCA blocker thapsigargin 210
Figure 5-19 - % change in calcium handling parameters across hiPSC-CM panel in response to different doses of thapsigargin 211
Figure 5-20 - Assessment of hiPSC-CM calcium handling response to NCX blocker ORM10103..... 214
Figure 5-21 - change in calcium handling parameters across hiPSC-CM panel in response to different doses of ORM10103 215
Figure 5-22 - Assessment of hiPSC-CM calcium handling response to IP3R blocker xestospongin C..... 218
Figure 5-23 - % change in calcium handling parameters across hiPSC-CM panel in response to 5μM xestospongin C..... 219
5-24 - > indicates increase, < indicates decrease while - indicates no change 222

List of Tables

Table 1-1 -LQTS subtypes and the affected genes, ... 11
Table 2-1 - Medium component table 51
Table 2-2 - Antibody table 57
Table 2-3 - Drug table 69
Table 3-1 - - List of different cell types used to generate hiPSCs 73
Table 3-2 - List of different reprogramming methods used to generate hiPSCs 75
Table 3-3 - Sendai virus vectors used to generate hiPSCs 76
Table 3-4 - List of patient samples reprogrammed during this study 85
Table 3-5 - Primer sequences to check for presence of CytoTune2.0 vectors 108
Table 4-1 - NCRM5-hiPSC-CM response to E4031 137
Table 4-2 ReBl-hiPSC-CM response to E4031 140
Table 4-3 ReBl-hiPSC-CM response to propranolol 142
Table 4-4 ReBl-hiPSC-CM response to nicorandil 145
Table 4-5 ReBl-hiPSC-CM response to minoxidil 146
Table 4-6 ReBl-hiPSC-CM response to RG3 149
Table 4-7 ReBl-hiPSC-CM response to NS1643 150
Table 4-8 ReBl-hiPSC-CM response to telmisartan 153
Table 4-9 - ReBl-hiPSC-CM response to GW0742 154
Table 4-10 - ReBl-hiPSC-CM response to ML277 157
Table 4-11 - Summary of drugs tested on LQTS2 disease model 160
Table 5-1 - Primers used to sequence CP1 179
Table 5-2 - 40bp primers used to generate targeting plasmid 186
Table 5-3 - Primer pair used to generate gRNA sequence for ligation 189
Table 5-4 - Effect of nifedipine on calcium handling mechanics 201
Table 5-5 - Effect of ryanodine on calcium handling mechanics 205
Table 5-6 - Effect of thapsigargin on calcium hanlding mechanics 209
Table 5-7 - Effect of ORM on calcium handling mechanics 213
Table 5-8 - Effect of xestospongin c on calcium handling mechanics 217
Table 5-9 - Overall effect of the drug on cell lines 222

Abbreviations

Abbreviation	Full name
ALP	Alkaline phosphatase
ATP	Adenosine triphosphate
AP	Action potential
APD	Action potential duration
APD50	Action potential duration at 50% of the repolarisation curve
APD90	Action potential duration at 90% of the repolarisation curve
AV	Atrio-ventricular
BMP	Bone morphogenic protein
cAMP	Cyclic adenosine monophosphate
cDNA	Complementary DNA
CHO	Chinese Hamster Ovary
CICR	Calcium-induced calcium release
CPVT	Catecholaminergic polymorphic ventricular tachycardia
CRISPR	Clustered regularly interspaced short palindromic repeats
DAD	Delayed after-depolarisation
DAPI	Di-amino phenyl-indole
DKK	Dickkopf-related protein 1
DMEM	Dulbecco's (Modified Eagle's) minimal essential medium
DMSO	Dimethyl sulfoxide
DNA	Deoxyribonucleic acid
dNTP	Deoxyribonucleotide triphosphate
EAD	Early after-depolarisation
EB	Embryoid body
ECC	Excitation-contraction coupling
ECG	Electrocardiogram
ECM	Extracellular matrix
EDTA	Ethylene diamine tetra-acetic acid
EHT	Engineered heart tissue
ESC	Embryonic stem cells
FBS	Foetal bovine serum
FGF	Fibroblast growth factor
FRC	Fast response cell
HEK	Human embryonic kidney
hESC	Human embryonic stem cell
hES-CM	hESC-derived cardiomyocyte
hiPSC	Human induced pluripotent stem cell
hiPSC-CM	hiPSC-derived cardiomyocyte
hPSC	Human pluripotent stem cell
hPSC-CM	hPSC-derived cardiomyocyte
HUES7	Harvard University embryonic stem cell line
ICD	Implantable cardioverter defibrillator

ICM	Inner cell mass
I_{ks}	Slowly activating K^+ current
I_{kr}	Rapidly activating K^+ current
I_{k1}	Inward rectifier current
IMS	Industrial methylated spirit
IP3	Inositol trisphosphate
iPSC	Induced pluripotent stem cell
LQTS	Long QT Syndrome
LTCC	L-Type calcium channel
MEA	Multi-electrode array
MEF	Mouse embryonic fibroblast
mRNA	Messanger RNA
NCX	Sodium-Calcium exchanger
NEAA	Non-essential amino acids
PBS	Phosphate buffered saline
PCR	Polymerase chain reaction
PFA	Paraformaldehyde
PKA	Protein kinase A
PSC	Pluripotent stem cell
PSC-CM	PSC-derived cardiomyocyte
QTc	QT interval corrected for heart rate
QT	QT interval
RNA	Ribonucleic acid
RT	Room temperature
RT-PCR	Reverse transcriptase PCR
SA	Sino-atrial
SCD	Sudden cardiac death
SD	Standard deviation of the mean
SEM	Standard error of the mean
SERCA	Sarco/endoplasmic reticulum Ca^{2+}-ATPase
SOICR	Store overload-induced calcium release
SR	Sarcoplasmic reticulum
SRC	Slow response cell
TdP	Torsades de pointes
TAE	Tris acetate buffer
TGF-β	Transforming growth factor - β
%	Percentage
^0C	Degree Celsius

Genes and Nomenclature

Gene	Full Name
BMP4	Bone morphogenic protein 4
CASQ2	Calsequestrin 2
FOXA2	Forkhead box protein A2
ISL1	Insulin gene enhancer protein
KCNE1	Potassium voltage-gated channel subfamily E member 1
KCNH2	Potassium voltage-gated channel subfamily H member 2
KCNQ1	Potassium voltage-gated channel subfamily KQT member 1
KLF4	Kruppel-like factor 4
LIN28	Protein lin-28 homolog A
MESP1	Mesoderm posterior bHLH transcription factor 1
NANOG	From Tir Na Nanog (= land of the ever young)
OCT4	Octamer 4 (aka POU5F1: POU class 5 forkhead box 1
PAX6	Paired box protein
REX1	Reduced expression 1
RYR2	Ryanodine receptor 2
SOX1	Sex-determining region Y (SRY) 1
SOX2	Sex-determining region Y (SRY) - related high mobility group (HMG) box 2
SOX17	Sex-determining region Y (SRY) 17
SSEA	Stage-specific embryonic antigen
TGF	Transforming growth factor
WNT	Wingless type

1 Chapter 1 – Introduction

1.1 The cardiac system

1.1.1 The cardiac action potential and clinical electrocardiogram (ECG)

The cardiac action potential is the cyclical depolarisation and repolarisation of cardiac myocytes driven by movement of ions across the cell membrane either spontaneously, as with pacemaker cells, or in response to external stimuli (Shih, 1994). The action potential progresses through the heart by moving across neighbouring cardiomyocytes through low resistance coupling via gap junctions (Rohr, 2004). These gap junctions are normally found at the intercalated discs near the ends of the rod shaped cardiomyocytes (Saffitz et al, 1994). The action potentials of pacemaker cells, situated within the atrioventricular (AV) and sinoatrial (SA) node, exhibit significantly different characteristics than those of the working myocardium (Grant, 2009). The action potentials of pacemaker cells can be thought of as slow response cells (SRC) whereas the myocardium and conduction system contains fast response cells (FRC) (Grant, 2009).

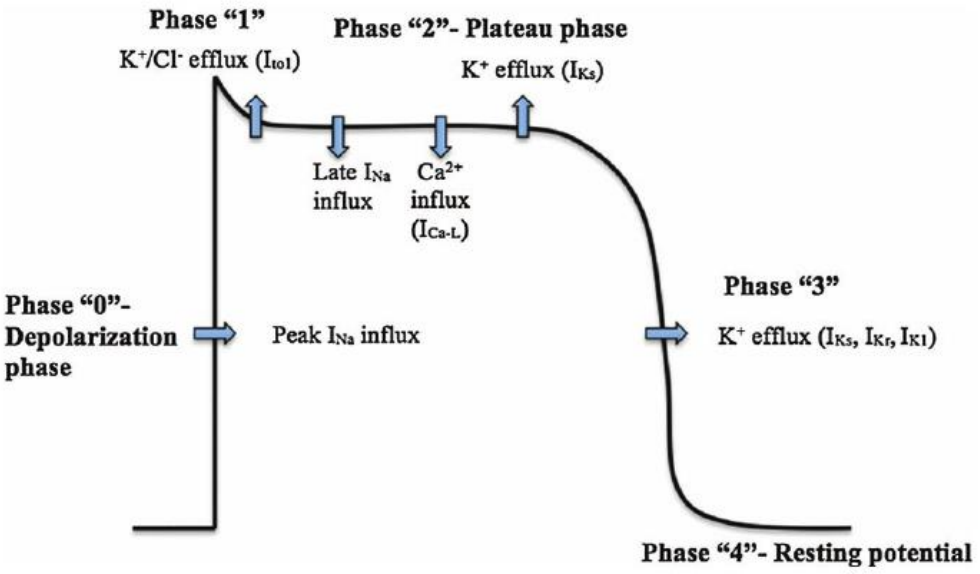


Figure 1-1 - The cardiac action potential

This schematic shows the cardiac action potential. Initially starting with phase 0, the depolarisation phase is mediated by Na^+ influx via Na_v channels. Phase 1 of the action potential is then characterised by K^+/Cl^- efflux mediated via the I_{to1} channel, identified by a characteristic notch in the action potential. Phase 2 of the action potential is the plateau phase in which there is late influx of Na^+ alongside an influx of Ca^{2+}, via L-type Ca^{2+} channel. In addition to this K^+ efflux begins through the I_{ks} current. The I_{ks} current is then joined in phase 3 by the I_{kr} current and the I_{k1} current, these three K^+ currents are responsible for

repolarisation of the cardiac myocyte. Finally the cell reaches phase 4 whereby it returns to its resting membrane potential in preparation for the next depolarisation (Saad et al 2016).

1.1.1.1 Fast Response Cells

The stable resting potential of Fast Response Cells (FRCs) in the working myocardium is maintained by the I_{k1} current, propagated through the $K_{ir}2$ channels such as $K_{ir}2.1$ (Monfredi et al, 2010). The resting membrane potential is a characteristic of phase 4 of the cardiac action potential and during this period the cardiomyocytes resting membrane potential is between -80 and -85mV (Liu et al, 2016). This phase features high K^+ conductance through I_{k1}, $K_{ir}2.1$, $K_{ir}2.2$ and $K_{ir}2.3$ inward rectifier channels which preferentially conduct K^+ when resting membrane potential is below -40mV (Liu et al, 2016). I_{k1} plays a major role in maintaining resting membrane potential of FRCs and is expressed to greater levels in the ventricles than the atria and is almost entirely absent from nodal populations (Schram et al, 2002). Phase 0 of the action potential (Figure 1.1) features a rapid upstroke via a rapid influx of Na^+ via the voltage-gated Na^+ channels, primarily $Na_v1.5$ but also $Na_v1.1$, $Na_v1.2$, $Na_v1.4$ and $Na_v1.8$ (Liu et al, 2016).

Maximum voltage of FRCs is between +20 and +40 mV and time dependant closing of the Na_v channels leads to a rapid inactivation of I_{Na} (Wang et al, 1993; Nabauer et al, 1996; Liu et al, 2016). As this inactivation of Na^+ current occurs a number of channels become active as the cells enter phase 1 of the action potential including the depolarising Ca^{2+} current which primarily acts through the L-type calcium current generated by $Ca_v1.2$ in ventricular and atrial cells and $Ca_v1.3$ in atrial cells (Liu et al, 2016). During phase 1 there are also outward transient currents generated by K_v and Ca^{2+}-activated Cl^- channels termed $I_{to1,}$ comprised of K_v components named $I_{to,f,}$ $I_{to,s,}$ and $I_{to2,}$ the molecular underpinnings of which are still poorly understood (Liu et al, 2016). Furthermore the sodium/calcium exchanger (NCX) generates an outward repolarising current by swapping 3 Na^+ ions outward in exchange for 1 Ca^{2+} ion inwardly, this mode of transport is termed reverse mode and operates synergistically with the L-type calcium channel to increase calcium influx which triggers calcium induced calcium release from the sarcoplasmic reticulum, a vital component of excitation-contraction (EC) coupling (Ramirez et al, 2011).The cardiac action potential features a characteristic notch during phase 1, a temporary hyperpolarisation of membrane potential by around -10 to -30mV (Di Diego et al, 1996; Liu et al, 2016).

Phase 2 is characterised by a plateau and very few transporters are active across the cell membrane during this time, indeed the cell exhibits a relatively high resistance. During this

phase calcium channels are closed due to Ca^{2+}-mediated inactivation after calcium induced calcium release from the sarcoplasmic reticulum (Liu et al, 2016). The membrane potential of the cardiomyocytes during phase 2 ranges from 0 to +20mV (Liu et al, 2016). As phase 2 progresses the activity of K^+ channels, I_{ks} and $I_{kr,}$ increase in what are termed the delayed rectifier currents (Liu et al, 2016). I_{kr} is known as the rapidly rectifying K^+ current and is generated by K_v11.1 channels, also known as hERG, which are encoded by the *KCNH2* gene. I_{ks} is termed the slow delayed rectifier current and is generated by K_v7.1 channels and encoded by the gene *KCNQ1*. Ultimately during phase 2 the K^+ delayed rectifier currents work with L-type calcium current (Ica_L) to repolarise the cells while depolarising currents are generated by late Na^+ entry and by the NCX operating in its forward mode where Ca^{2+} ions are extruded in favour of Na^+ ions (Liu et al, 2016).

The prevention of early after depolarisations (EAD) and arrhythmias is important at higher heart rates as action potential duration must shorten to accommodate the increased number of depolarisations required leading to a variable length of phase 2 (Liu et al, 2016). This is achieved thorough residual K^+ conductance which serves to increase the refractoriness of the myocardium (Gintant, 1996; Tseng, 2001).

Phase 3 of the cardiac action potential is initiated when the net outward movement of K^+ ions through I_{ks} and I_{kr} exceeds the inward currents generated by I_{cal} and I_{ncx} (Liu et al, 2016). As this repolarisation progresses I_{kr} takes a more prominent role due to its gating properties whereby the channels recover rapidly from inactivation when the membrane potential drops below -20mV, resulting in an increase of K^+ efflux (Liu et al, 2016). In addition to this, progressive increase in I_{k1} and I_{kr} activity during phase 3 will outweigh the Ca^{2+} entry via the L-type calcium channel returning the cell to its resting membrane potential (Liu et al, 2016).

1.1.1.2 Slow Response Cells

Nodal action potentials are propagated slower than those in the working myocardium (Grant, 2009). The synchronicity of the heart arises from the sino-atrial (SA) node (Wiese et al, 2009). Action potentials in the SA node (Figure 1.1), as well as atrio-ventricular (AV) node and HIS bundles, are distinct from the FRCs in the working myocardium due to variable resting potential (Liu et al, 2016). There is no stable resting potential in SRCs due to the absence of both I_{k1} and K_{ir}2.1 and the maximum diastolic potential (MDP) in phase 3 is typically between -70 and -55mV (Chandler et al, 2009; Liu et al, 2016). Upon reaching the MDP the SRCs

immediately begin to depolarise at a variable rate between 10-66mV/s (Verkerk et al, 2007; Hof et al, 2013). This variability in depolarisation rate is due to various overlapping currents such as funny current (I_f) (Stillitano et al, 2008), inward I_{ncx} (Maltsev et al, 2004), I_{cat} and I_{cal} (Liu et al, 2016). Whilst these currents exert a depolarising effect on the cell there remain actively repolarising currents working antagonistically, including I_{kAch} (Schram et al, 2002), I_{kr} (Ono et al, 2000) and I_{ks} (Ito and Ono. 1995). Depolarisation is accelerated when membrane potential reaches -50mV (Verkerk et al, 2007) due to the I_{cal} current which results in a clear phase 0 (Liu et al, 2016). Unlike FRCs, in SRCs it is calcium influx via I_{cal} which induces the upstroke of phase 0 (Baruscotti and Robinson, 2007), due to relatively low expression of Na_V channels in SA nodal populations (Muramatsu et al, 1996). However like FRCs, repolarisation of SA nodal populations is driven by K_v channels I_{kr} and I_{ks} (Ito and Ono 1995; Verheijck et al, 1995; Ono et al, 2000) with additional involvement of I_{to} (Arechiga-Figueroa et al, 2011) and $K_v1.5$ (Dobrzynski et al, 2000).

Uniquely, SRCs possess the I_f which is generated by hyperpolarisation-activated cyclic-nucleotide family of genes (HCN), mainly by the dominant human cardiac isoforms HCN1 and HCN4 (Chandler et al, 2009). This current is carried by Na^+ and K^+ ions (Monfredi et al, 2010). HCN channels have been suggested to play a key role in increased heart rates in response to adrenergic stimulation due to the presence of a cytoplasmic cyclic nucleotide binding domain in the HCN which is activated by cAMP produced in response to β1-adrenoceptor activation (Wainger et al, 2001). I_f is activated when the cell exhibits a negative membrane potential rather than a positive one, giving it the name pacemaker current (Liu et al, 2016). Furthermore there is also I_{kAch} current which is highly expressed in SRCs, lending to sympathetic nervous innervation, a key component during fight or flight (Mark and Herlitze, 2000). SRCs are slow responders due to the lower expression of gap junction channels compared to FRCs in addition to larger quantities of connective tissue (Monfredi et al, 2010; Csepe et al, 2015). In addition to having fewer gap junctions, those in SRCs are encoded by different genes and different connexins. SRCs are known to prominently express Cx45, Cx30 and Cx30.5 (Gros et al, 2010) in comparison to Cx40 and Cx43 which are found predominantly in the atria (Dobrzynski et al, 2007) and Cx43 (Verheijck et al, 2001) in the working ventricles.

1.1.1.3 Propagation of cardiac arrhythmias

The cardiac action potential can be thought of as a linear process whereby current flows from a depolarised cell into a neighbouring less depolarised cells through gap junctions (Kleber and

Rudy, 2004). This flow is defined by the source-sink relationship whereby a cell carrying a depolarised current is termed a source and the cells connected to it via gap junctions are its sink. As current passes through the sink cells they themselves become sources and propagate the current down to cells they are coupled to by gap junctions (Spector, 2013).

The most common cause of clinical arrhythmias is by re-entry of the action potential during propagation (Spector, 2013). Re-entry occurs when the action potential fails to extinguish itself and re-enters a region of the heart which has recovered from its refractory period (Janse and Wit, 1989). Gap junctions are vital in the propagation of action potentials and these channels are dodecameric structures consisting of two hexameric connexions, made up of six proteins called connexins (Dhein, 1998). The remodelling of gap junction architecture results in changes to action potential propagation which may result in arrhythmogenesis, this remodelling can occur from alteration in connexion transcription or degradation of the protein which occurs through a mechanism which remains poorly understood (Sicilian Gambit, 2001).

1.1.1.4 Early After Depolarisation (EAD)

An event which slows or reverses the action potential during phase 2, 3 or 4 is termed an early after depolarisations (EAD) (Priori and Corr, 1990; Weiss et al, 2010). These can occur through three major ionic mechanisms. The first being an inadequate K^+ conductance while the cells membrane potential is between -30 and 0mV, in this case I_{caL} may be able to self-amplify and reverse the depolarisation, this will lead to an upstroke as the cell attempts to depolarise (Weiss et al, 2010). The second mechanism is through the NCX, which exchanges 3 Na^+ ions for each Ca^{2+} ion it transports, during repolarisation the NCX is in forward mode and extruding Ca^{2+} from the cell, however in order to achieve this there must be an influx of Na^+ through the NCX, if this occurs synergistically with spontaneous calcium induced calcium release from the sarcoplasmic reticulum then the resulting NCX current can lead to an EAD (Weiss et al, 2010; Antzelevtich and Burashnikov, 2011). The third mechanism is through an increase in late stage I_{na} influx (Antzelevitch and Burashnikov, 2011).

1.1.1.5 Delayed After Depolarisation (DAD)

Unlike EADs, delayed after depolarisations (DADs) occur after the action potential has been completed (Cranefield, 1977). DADs are more likely to be observed under conditions which

augment intercellular calcium levels such as CPVT (Priori et al, 2001; Antzelevitch and Burashnikov, 2011; Fink et al, 2011).

Spatial repolarisation is a key process during the cardiac action potential and the ventricles of the heart are composed of three distinct cell types; epicardial, midmyocardial (M) and endocardial cells (Antzelevitch et al, 1991; Antzelevtich and Burashnikov, 2011). These subtypes of cells display different ion channel densities and as such respond differently to drugs/compounds (Burton and Cobbe, 2001). Ventricular epicardial and M cells display a prominent phase 1 due to transient outward current I_{to} which is not observed in endocardial cells (Wettwer et al, 1994; Näbauer et al, 1996). Action potential duration is longer in the endocardium than epicardium but increased numbers of M cells resulted in an increase in the QT interval (Li et al, 1998; Rivolta et al, 2015). M cells are known to express weaker I_{ks} current and a more prominent late I_{na} compared to epicardial and endocardial cells (Liu et al, 1995; Zygmunt et al, 2001). Interestingly, the heterogeneity observed in these repolarising cells of the heart is most striking in single cell analysis but is still evident in the heart, this likely points to minimisation of these differences due to electronic interaction, this is a phenomenon which can be lost in the diseased heart (Burton and Cobbe, 2001). Furthermore these heterogeneities can be exacerbated by ion channel mutations, drug interaction or sympathetic stimulation which can result in cardiac arrhythmias (Antzelevitch and Sicouri, 2012).

1.1.1.6 The clinical ECG

As electrical impulse passes through the heart, ions are transported across membranes via ion channels, this process can be measured clinically using an ECG (Dupre et al, 2009). An ECG gives a temporal readout of the propagation of an action potential across the heart (Marban, 2002). The readout from an ECG provides the waveform shown in Figure 1.2. The small P wave represent the depolarisation of the atria (Ashley and Niebauer, 2004). The QRS complex is three waves which represent the depolarisation of the ventricles with the Q wave representing the depolarisation of the interventricular septum, the R wave is the largest and represents the depolarisation of the main ventricular mass and the S wave is the final depolarisation at the base of the heart (Ashley and Niebauer, 2004). The time between atrial depolarisation and ventricular depolarisation is represented by the PR interval (Ashley and

Niebauer, 2004). The repolarisation of the atria is obscured by the large QRS complex, however the repolarisation of the ventricles is represented by the T wave (Ashley and Niebauer, 2004) therefore the QT intveral represents repolarisation of the ventricles. The time between ventricular depolarisation and repolarisation is termed the ST interval, during this time there is zero potential between depolarisation and repolarisation (Ashley and Niebauer, 2004).

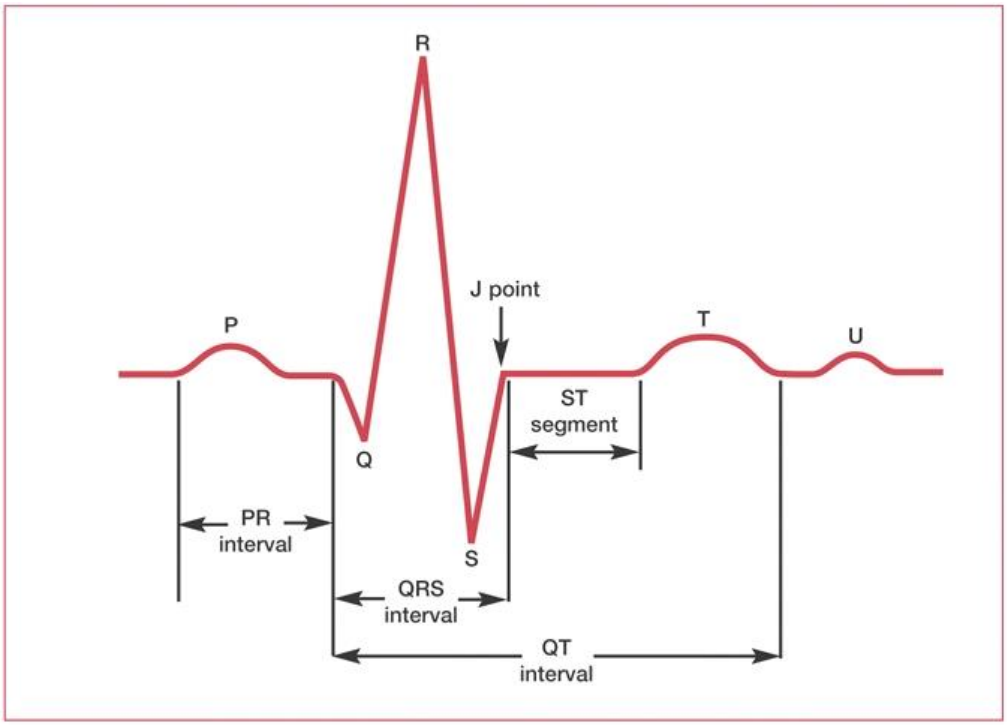


Figure 1-2 - The clinical ECG
The basic readout given from a clinical ECG where the P wave represents the atrial depolarisation followed the QRS complex which represent the depolarisation of the ventricles. The atrial repolarisation is hidden within the QRS complex and the T wave represent the repolarisation of the ventricles. The U wave is typically only seen in hypokalemic patients (Ashley and Niebauer, 2004).

1.1.2 The cardiac channelopathies

The cardiac channelopathies are a heterogenous group of diseases which manifest as a dysfunction of ion channels within cells (Kim, 2014). In the cardiac channelopathies these tend to affect the Na^+ and K^+ channels or their accessory subunits (Ackerman, 2004). Examples of cardiac channelopathies include; Long QT Syndrome (LQTS), Brugada Syndrome, Short QT Syndrome, Atrial Fibrillation and Catecholaminergic Polymorphic Ventricular Tachycardia (CPVT) (Campuzano et al, 2010). It has been estimated that in up to 50% of sudden cardiac death cases in the young death was the first manifestation of an underlying inherited cardiac

disease (Campuzano et al, 2010). The channelopathies show variable penetrance and it is possible that members of the same family carrying the same mutation will exhibit markedly different phenotypes (Bastiaenen and Behr, 2011).

1.1.2.1 Long QT Syndrome

LQTS is a genetic heart abnormality characterised by an elongation of the QT interval on an ECG alongside T-wave irregularity, ventricular tachycardia and an increased risk of sudden death (Crotti et al, 2008). The first reported cases of LQTS were termed Jervell and Lange-Nielsen syndrome and Romano-Ward syndrome (Jervell and Lange-Nielsen, 1957; Romano et al, 1963; Ward, 1964). Despite the reported 13 subtypes of LQTS (Table 1.1) the most prevalent forms of are LQTS1, 2 and 3 accounting for almost all cases (Medeiros-Domingo et al, 2007; Schwartz et al, 2012).

It has recently been estimated that the prevalence of LQTS is around 1 in 2,500 births although this fails to take into account people who silently carry a LQTS mutation (Crotti et al, 2008). Early and efficient diagnosis of LQTS is crucial as, often, the first manifestation can be life threatening (Medeiros-Domingo et al, 2007). Diagnosis can be either clinical or molecular, the disease is clinically characterised by a repeated history of syncope and an elongated QTc interval (Schwartz, 2012). The elongation of the QT interval is indicative of an extended repolarisation period for the cells of the heart. However the QT interval is variable based on the heart rate, and as such a corrected formula should be used to calculate risk, this is known as Bazett's corrected heart rate measurement (QTc) (Akhras and Rickard, 1981; Bazett, 2007).

Corrected QT (QT_C) = QT Interval / √ (R-R interval), where R-R interval is = 60/HR.

When QTc exceeds 500-550ms there is a substantial increase in risk to the patient (Priori et al, 2003). However it has been estimated that 10-35% of people may carry a mutation indicative of a form of LQTS but remain asymptomatic (Crotti et al, 2008). Therefore the only way to diagnose and treat these patients prior to syncopal or arrhythmic episodes would be through genetic screening (Napolitano et al, 2005). A patient suffering from LQTS may experience one or more syncopal episodes, brought on by Torsade-de-Pointes (TdP) which is a polymorphic ventricular tachycardia resulting in a twist of the QRS complex around the isoelectric baseline which can lead to ventricular fibrillation (Crotti et al, 2008).

1.1.2.1.1 LQTS1

LQTS1 is the most prevalent form of the syndrome and is triggered most commonly by strenuous activity (Schwartz et al, 2001). LQTS1 is caused by defective α-subunit of the K^+ channel Kv7.1 which is responsible for the generation of the I_{Ks} current (Schwartz et al, 2012). I_{Ks} is responsible for the outward flow of K^+ during the plateau phase of the cardiac action potential. In addition to this it also assists the rapidly delayed rectifier and inward rectifier currents in removing K^+ from the cells during phases 2 and 3 of the cardiac action potential. This channel is activated by sympathetic innervation and is vital for the QT interval to adapt during changes in heart rate (Schwartz et al, 2012).

1.1.2.1.2 LQTS2

The trigger for LQTS2 is emotional stress which can be brought on by auditory stimuli such as an alarm clock going off or a telephone ringing, these patients are at particular risk if such a stimulus is perceived during rest (Schwartz et al, 2001). LQTS2 is caused by a defective I_{Kr} α-subunit of the K^+ channel Kv11.1 which is responsible for the generation of the I_{Kr} current during the cardiac action potential (Schwartz et al, 2012). Like the $I_{Ks,}$ the I_{Kr} removes K^+ ions from the cell during phase 3 of the cardiac action potential (Liu et al, 2016).

1.1.2.1.3 LQTS3

In the case of LQTS3 adverse cardiac events are most likely to occur during sleep (Schwartz et al, 2001). LQTS3 is caused by mutation to the *SCN5A* gene which encodes the $Na_v1.5$ α-subunit (Medeiros-Domingo et al, 2007). The $Na_v1.5$α-subunit is responsible for generation of the inward Na^+ current which leads to initial depolarisation of the cell during an action potential. This defective Na^+ current can lead to the inward leak of Na^+ ions therefore prolonging the action potential (Schwartz et al, 2012). However there are a number of different disorders linked to variations within the Na^+ currents such as Brugada syndrome, atrial fibrillation and sick sinus node syndrome (Benson et al, 2003; Chen et al, 2007; van Hoorn et al, 2012). Furthermore a single mutation within the *SCN5A* gene can lead to either an increase or a decrease in the Na^+ current therefore the phenotype of the patient is important for an accurate diagnosis (Schwartz et al, 2012).

1.1.2.2 Treatment of LQTS

Treatment for LQTS is vital as the mortality rate for symptomatic patients who remain untreated for one year is 21% (Schwartz et al, 2012). Commonly, the patient is given antiadrenergic medication as most life threatening arrhythmias are triggered by an increase, often suddenly, in sympathetic activity which is largely due to the action of the left cardiac sympathetic nerves (Schwartz, 1984). The first line in therapy against LQTS is most often the prescription of β-blockers, in particular propranolol and nadolol (Crotti et al, 2008). β-blockers have proven to be an effective treatment for LQTS1 patients who have a mortality rate of only 0.5% when using them (Priori et al, 2004; Vincent et al, 2009). However LQTS2 patients undergoing β-blocker therapy are more likely than LQTS1 patient to experience life threatening episodes despite therapy (Priori et al, 2004) indicating the need for novel treatments. LQTS3 patients experience more life threatening events than patients who suffer from either LQTS1 or LQTS2 with episodes occurring in 10-15% of LQTS3 patients despite treatment with β-blockers (Schwartz et al, 2001; Priori et al, 2004). The failure of pharmacological therapy signals the requirement for surgical intervention.

The first surgical intervention which may be deployed is the use of an implantable cardioverter-defibrillator (ICD). It has been suggested by some that lead to a vicious cycle where the shock administered by an ICD leads to increased anxiety within the patient thus triggering more shocks (Schwartz et al, 2008). However the efficacy of ICDs has been demonstrated in a study which found patients with an ICD experienced a mortality rate of 1.3% in comparison to 16% in patients who did not have one (Zareba et al, 2003). A second surgical intervention is left cardiac sympathetic denervation (LCSD) where the first four thoracic ganglia are removed (Schwartz et al, 2004). LCSD has has been shown to significantly reduce QTc at rest and reduce the increase in heart rate during exercise but did not reduce the QTc interval during the same period; however four out of five of the patients in this study remained syncope free for 21 months after the surgery (Li et al, 2005). However further study has cast doubt on its effectiveness in patients who exhibit a severe phenotype. A retrospective study of 52 patients found that 23% who underwent LCSD experienced a cardiac event in the time since illustrating that LCSD should not be considered curative but potentially an addition to β-blocker therapy (Bos et al, 2013; Schneider et al, 2013). Overall these strategies treat the symptom, preventing an increased heart rate, rather than the disease which is an inadequate repolarisation of cardiomyocytes.

Table 1-1 -LQTS subtypes and the affected genes,

Table adapted from Schwartz et al, 2012

LQTS Subtype	Affected Gene	Locus on Affected Gene	Protein Affected	Prevalence
LQTS1	*KCNQ1*	11p15.5	I_{Ks} α-subunit	40-55%
LQTS2	*KCNH2*	7q35-36	I_{Kr} α-subunit	30-45%
LQTS3	*SCN5A*	3p21-24	$Na_v1.5$ α-subunit	5-10%
LQTS4	*ANKB*	4q25-27	Ankyrin-β	<1%
LQTS5	*KCNE1*	21q22.1p22	I_{Ks} channel β-subunit	<1%
LQTS6	*KCNE2*	21q22.1	I_{Kr} channel β-subunit	<1%
LQTS7 (Andersen-Tawil Syndrome)	*KCNJ2*	17q23	Kir2.1 α-subunit	<1%
LQTS8 (Timothy Syndrome	*CACNA1C*	12p13.3	L-type calcium channel $Ca_v1.2$	<1%
LQTS9	*CAV3*	3p25	Caveolin 3	<1%
LQTS10	*SCN4B*	11q23	I_{Na} β_4-subunit	<1%
LQTS11	*AKAP9*	7q21-q22	Yotiao	<1%
LQTS12	*SNTA1*	20q11.2	Syntrophin α1	<1%
LQTS13	*KCNJ5*	11q24	Kir3.4	<1%

1.1.2.3 Catecholaminergic Polymorphic Ventricular Tachycardia (CPVT)

Patients who suffer from CPVT often appear otherwise healthy but present with symptoms such as bidirectional polymorphic ventricular tachycardia when exposed to adrenergic stimulation (Kim et al, 2014). CPVT can be caused by mutations in *RYR2* (Priori et al, 2011), *calsequestrin 2* (*CASQ2*) (Lahat et al, 2001), *CALM1* (Hyegaard et al, 2012), *TRDN* (Roux-Buisson et al, 2012) and *TECRL* which exhibits a crossover phenotype between CPVT and LQTS (Devalla et al, 2016). The form of CPVT caused by a mutation in *RYR2* was found to be inherited in an autosomal dominant manner (Swan et al, 1999). *RYR2* is known to be important in maintaining calcium homeostasis in the heart and thus is vital in the EC coupling process which underpins the hearts electrical activity (van der Werf and Wilde, 2013). The CASQ2 protein is responsible for helping maintain a major Ca^{2+} reservoir within the sarcoplasmic reticulum and is located within the protein complex which contains the ryanodine receptor (Lahat et al, 2001). However mutations within the *RYR2* gene have only been identified as causative in around 50% of dominantly inherited CPVT cases (Nyegaard et al, 2012) underpinning the requirement for further research in order to fully ascertain the genetic causation of the condition. The spontaneous release of calcium from the sarcoplasmic reticulum during

diastole can be attributed to mutations in either *CASQ2* or *RYR2* causing sub optimally functioning ion channels (Roux-Buisson et al, 2012). In turn this increase in cystolic calcium concentration can trigger delayed after depolarisations which are a risk factor for arrhythmias, this process is particularly enhanced under adrenergic stimulation (Cerrone et al, 2007).

1.1.2.4 Prevalence of CPVT

The mean age of onset is before adolescence has been reached and it is estimated that that around 1 in 10,000 people have CPVT amongst the general population and it carries with it a 50% mortality rate in untreated seriously affected individuals under the age of 20 (Leenhardt et al, 1995; Priori et al, 2002; Postma et al, 2005). Unlike LQTS, CPVT can be difficult to diagnose as those suffering the disease will exhibit a healthy ECG (Schimpf et al, 2009). In fact the only indicator at all may be a mild sinus bradycardia (Postma et al, 2005). In the diagnosis of CPVT a graded exercise test, raising heart rate to 100-120bpm to induce reproducible arrhythmias, is the most effective method to determine a positive diagnosis (Egan et al, 2012; Faggioni et al, 2012).

1.1.2.5 Treatment for CPVT

Initial treatment for CPVT requires lifestyle changes to reduce risk of arrhythmic episodes such avoiding strenuous exercise (van der Werf and Wilde, 2014). In addition to this, the use of β-blockers is advised as studies have shown significant reduction in risk of arrhythmic episodes in up to 60% of patients (Leenhardt et al, 1995; Priori et al, 2002; Hayashi et al, 2009). This effect is thought to be mediated by reduction in heart rate and a more direct effect on calcium release from the sarcoplasmic reticulum (Napolitano et al, 2004). Importantly the dose of β-blockers should be individually assessed on a patient by patient case using the information gained by a graded increased exercise test (Heidbüchel et al, 2006). It has been shown that patients suffering CPVT who do not respond to β-blockers should be prescribed the antiarrhythmic driug flecainide in addition to their β-blockers as this has been shown to lower risk both experimentally and clinically through a mechanism involving inhibition of voltage gated sodium channels (Watanabe et al, 2009; Liu et al, 2011; Van der Werf et al, 2011). ICDs can be considered for CPVT patients but this is met with caution as ICD shocks can cause ventricular storms due to catecholamine release (Napolitano et al, 2004; Mohamed et al, 2006; Zipes et al, 2006). A final surgical intervention is the use of LCSD which has been

reported to include side effects such as palpebral ptosis, elevation of the left hemidiaphragm, and lack of sweating from the left arm and face (Napolitano et al, 2004). Furthermore there remains dubiety about the efficacy of LCSD in CPVT patients as recurrent cardiac events have been reported in patients who have underwent this therapy (Napolitano et al, 2004).

1.2 Assessing the need for hiPSC disease models of cardiac disease

The process for drug development is long and complex, beginning with high-throughput assays to search large chemical compound libraries and ending with clinical trials (Feng et al, 2005). Once a candidate drug has been identified it is then tested for primary safety data. This initial stage involves *in vitro* testing using both cell based systems, such as immortalised cell lines overexpressing ion channels, and *in vivo* animal models of disease (Figure 1.3). It has been estimated that the efficiency of current animal models in predicting heart, liver and developmental toxicity in humans is 50% (Greaves et al, 2004). Candidate drugs which exhibit low levels of toxicity and high levels of efficacy are progressed to clinical trial stage. It is estimated 85% of drugs are lost during the early phases of human clinical trials (Kola and Landis, 2004) and of those which progress to Phase III human clinical trials only half will ever make it to market (Ledford, 2011). It was recently reported that the cost of bringing a drug from initial development to the market can reach $11 Billion and take anywhere between 10-15 years (Denning et al, 2016). Clearly there is a requirement for more efficient systems which would discard toxic compounds and screen for clinically effective compounds in the earlier stages of development. Human pluripotent stem cells (hPSC) offer a highly valuable tool to model diseases *in vitro* which can strengthen and improve the current toxicity testing systems. The emergence of human induced pluripotent stem cell (hiPSC) technology enables the researcher to generate patient specific disease models which are able to accurately recapitulate the patient's phenotype *in vitro,* such advances can overcome issues such as the highly invasive and risky nature of cardiac biopsy which can make it difficult to acquire cardiac tissue to study disease states in greater detail (Rajamohan et al, 2013).

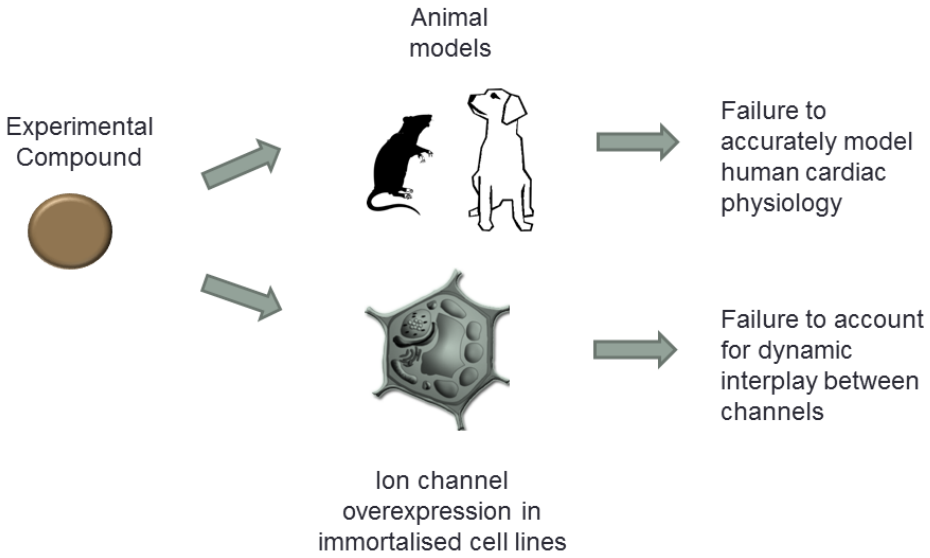


Figure 1-3 - Current toxicity testing models
Current toxicity testing models for drug compounds rely heavily on both animal models and overexpression of ion channels in immortalised cell lines. Both are limited in their ability to recapitulate the true *in vivo* system of humans.

1.2.1 *In Vitro* systems

The harvesting and prolonged culture of native human adult cardiomyocytes remains difficult and in order to assess the effect of drug compounds on cardiac ion channels many *in vitro* systems overexpress cardiac ion channels in immortalised non cardiac cell lines such as HEK and CHO cells (Giorgi et al, 2010; Haraguchi et al, 2015). Typically such cells exhibit karyotype abnormalities but more importantly are unable to accurately recapitulate the dynamic interaction ion channels exhibit *in vivo* (Wobus and Löser, 2011; Denning et al, 2016). The limitations of *in vitro* systems are perhaps best demonstrated by the case of verapamil. When verapamil was applied to CHO cells overexpressing the hERG channel it was found to block it and thus would result in a decrease in the I_{kr} current, such a decrease would result in QT prolongation (Meyer et al, 2004). However what such a system does not indicate is that verapamil also inhibits $I_{cal,}$ such an action in conjunction with I_{kr} blockade will exert a neutral effect on QT interval (Meyer et al, 2004). Therefore the suboptimal drug screening measure outlined above highlight the need for more accurate humanised models of cardiac disease.

1.2.2 *In Vivo* animal models

Much of the current knowledge relating to cardiac pharmacology and physiology is derived from mouse models as a result of the ease with which they can be maintained and bred in addition to their amenability to genetic modification (Salama and London, 2007). The murine

and human cardiovascular system exhibit major differences which can limit the conclusions which can be drawn from the murine model of cardiovascular disease. For example I_{kr} is found at very low levels in murine cardiomyocytes, however is a major determining factor in repolarisation of human cardiac cells (He et al, 2003). Mice have a life expectancy of 2-3 years and an average heart rate of about 350bpm in comparison to humans which exhibit an average heart rate of 70bpm and a life expectancy around 75-85 years (Hamlin and Altschuld, 2011). Furthermore mice have a metabolic rate somewhere in the region of 8 times greater than humans, likely as a result of increased heart rate as well as lower resting ECG duration and a shorter QT interval than humans (Wehrens et al, 2000; Hamlin and Altschuld, 2011). Moreover the murine cardiac action potential is triangular shaped without a clear plateau phase and a shorter refractory period than in the human heart (Manoach, 1984; Damiano et al, 1990; Nerbonne, 2004). This makes it harder for re-entrant arrhythmias to propagate, therefore casting doubt on their ability to model such a dysfunction (Papadimitriou et al, 2008).

One widely used alternative to murine models is rabbits. Like murine models the use of rabbits to model human cardiac diseases is limited by interspecies cardiovascular system differences as the rabbit heart is found to exhibit a heart rate in the region of 3 times greater than that of humans (Manzo et al, 2009). Moreover the rabbit heart is much smaller than the human heart and such variations in size have been known to result in differences in myocardial structure (Healy et al, 2011). A further alternative model is the use of pig hearts. There are many anatomical differences between the human and pig heart which mostly relate to the difference in bipedal and quadrupedal gait, such as the pig SA node exhibiting different innervation distribution compared to the human SA node (Lelovas et al, 2014). Such anatomical differences inhibit the use of the pig heart to study structural diseases of the human heart. With regards to the differences in electrophysiology it has been shown pig hearts exhibit greater heart rate (91-167bpm vs 60-100bpm), a shorter PR interval on an ECG (50-120ms vs 120-160ms) and a more variable QT interval (150-340ms vs 260-350ms) (Lelovas et al, 2014).

As a consequence of the shortcomings of conventional *in vitro* model systems regulatory agencies which test the safety and efficacy of new drug compounds have set guidelines which require the use of at least two different animal models, one of which must be a large non-rodent, despite the interspecies variability between humans and animals (Rajamohan et al, 2013). In 2011 over 3 million animals were used in experiments across the UK, mainly mice

(Badyal and Desai, 2014). Such extensive use of animals in experimentation is not in line with the 3Rs (Refinement, Reduction and Replacement) research policy in many countries (Naderi et al, 2012). In this respect the replacement of conventional *in vivo* animal modelling and *in vitro* overexpression systems with humanised models of cardiac disease may help improve drug safety and efficacy screening (Rajamohan et al, 2013).

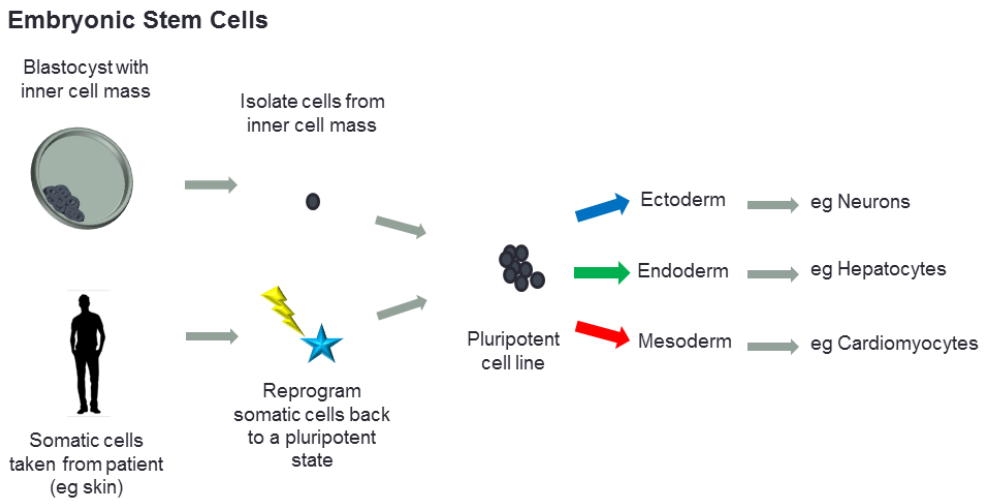


Figure 1-4 - Schematic illustrating the role of pluripotency in generating disease models

This schematic shows the two main routes which enable the generation of disease models. The first is the derivation of embryonic stem cells (ESCs) which are isolated from the inner cell mass of a developing blastocyst. The second is by reprogramming somatic cells using viral or plasmid vectors to switch on their pluripotency machinery. Both of these techniques provide pluripotent cells which can then be differentiated to a cell type of interest within any of the three germ layers

1.3 Generation of hPSCs

Recent advances in the use of hPSCs in the generation of cardiomyocytes which are able to recapitulate many of the functions of native adult cardiomyocytes has led to increased interest regarding the potential to use these hPSC-CMs in large scale drug screening and toxicity testing (Figure 1.4) (Rajamohan et al, 2013).

1.3.1 Embryonic stem cells (ESC)

Murine Embryonic Stem Cells (mESC) were first successfully cultured *in vitro* in 1981 from the inner cell mass of a murine embryo (Evans and Kaufman, 1981). These cells were derived and able to retain their pluripotency before being differentiated both *in vitro* and after transplantation *in vivo* (Evans and Kaufman, 1981). Human embryonic stem cells (hESC) were

isolated using frozen *in vitro* fertilisation (IVF) which were then propagated *in vitro* for 4-5 months while maintaining their pluripotency (Thomson et al, 1998). These ESCs, both mouse and human, display the ability to differentiate into many different cells types such as; endothelial cells (Levenburg et al, 2002), neural precursors (Zhang et al, 2001), hepatocytes (Rambhatla et al, 2003) and cardiomyocytes (He et al, 2003). This ability for pluripotent cells to be directed to differentiate to various cell types is of vital importance in the creation of disease models which can allow the study of diseases which are difficult to reproduce in culture using somatic cells. An example of this is in the cardiovascular system where heart tissue is difficult to obtain access in large quantities (From et al, 2011). Furthermore gene manipulation studies displayed promise that cells could be mutated to display a disease phenotype of interest (Zwaka and Thomson, 2003). This was further improved upon the discovery of the CRISPR/Cas9 system in recent years (Doudna and Charpentier, 2014; Ran et al, 2014).

1.3.2 Induced pluripotent stem cells (iPSC)

Traditionally it was thought that cells could differentiate towards a specific lineage but once they had started this journey they could not return, the so called Waddington's Landscape (Waddington, 1957). Cloning experiments using nuclear transfer in frogs (Briggs and King, 1952) and the generation of cloned tadpoles from intestinal cells of a frog (Gurdon, 1962) demonstrated that cells did not lose genes as they differentiated but switched them off. This indicated that the restrictions placed on cells during the developmental process may therefore be reversible.

The use of so called "discarded" IVF embryos is seen by some as a prudent use of cells which would otherwise be destroyed. However there are some who see the use of human embryos in such a manner as a destruction of human life. This has meant their use has been banned or strongly restricted in some countries such as in Germany, Poland and Italy where stem cell research is only permissible on previously established lines (Dhar and Hsi-En Ho, 2009).

In 2006 the lab of Shinya Yamanaka first reported the development of induced pluripotent stem cells (iPSC) from mouse fibroblasts (Takahashi and Yamanaka, 2006), followed a year later with confirmation that the procedure could also be applied to human cells giving rise to the term human induced pluripotent stem cells (hiPSC)(Takahashi et al, 2007). By using a retrovirus to introduce the so called Yamanaka factors; OCT4, SOX2, KLF4 and c-Myc (Figure

1.5), to the genome of fibroblast cells Yamanaka's team were able to reprogram these cells to a pluripotent state (Takahashi et al, 2007). In addition to the work carried out by Yamanaka's team in Japan, James Thomson's lab in Wisconsin also demonstrated the successful reprogramming of somatic cells to a pluripotent state relatively soon after, however as opposed to the Yamanaka factors Thomson's lab used a lentivirus to deliver; OCT4, SOX2, NANOG and LIN28 (Yu et al, 2007). The limitation of both procedures was the use of integrating methods to deliver the exogenous genes to the cell which leads to random insertions and potential mutagenesis (Kang et al, 2015).

The silencing of exogenous transgenes is crucial as it has been shown that a two fold increase in OCT4 expression within a cell will lead to differentiation into primitive endoderm or mesoderm while a down regulation of this factor leads to trophectoderm formation (Niwa et al, 2000). Furthermore data from gene therapy studies have shown that insertional mutagenesis can be a major concern in the translational use of cells reprogrammed using integrating methods (Hochedlinger and Plath, 2009; Wu and Dunbar, 2011). The use of a lentiviral vector in gene therapy studies to correct X-linked severe combined immunodeficiency (SCID-X1) demonstrated the efficacy of using lentivirus to correct genetic disease. However as a result of insertional mutagenesis 25% of patients in these studies developed leukaemia (Hacein-Bey-Abina et al, 2008; Howe et al, 2008) illustrating the need for safer methodology. Random insertions are not only a concern for the future *in vivo* use of any cells, the mutation of a gene within the cell could have effects which display a particular *in vitro* phenotype which is not an accurate recapitulation of the patients phenotype (Zheng et al, 2013).

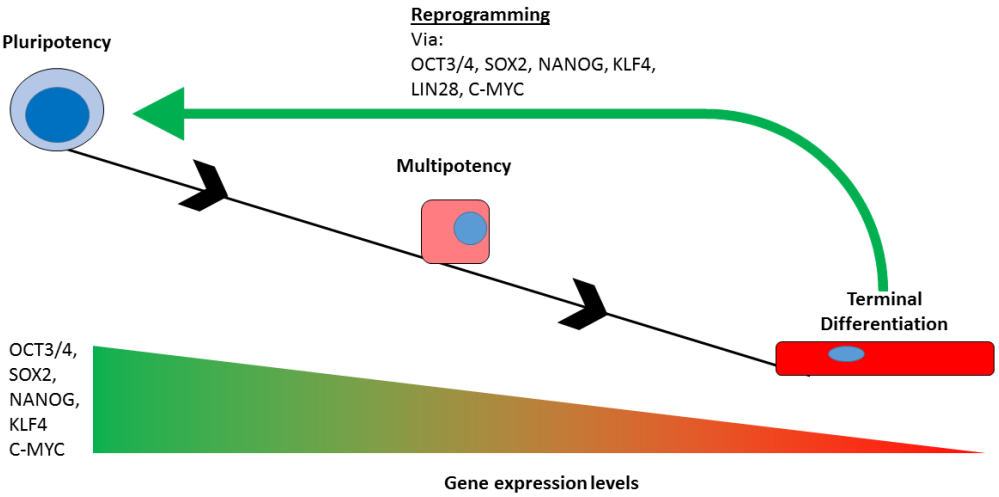


Figure 1-5 - Schematic outlining the principles of iPSC generation
This schematic outlines the principles involved in iPSC generation. The initially pluripotent cell is able to move towards a more specialised and terminally differentiated cell type, in doing so it downregulates the pluripotency related genes such as OCT3/4, NANOG and SOX2. Ultimately with the use of plasmid or viral vectors these factors can then be reintroduced and the pluripotency machinery switched back on.

1.3.3 Cell sources

Initial hiPSC generation was performed using fibroblasts as a result of their ease of isolation and genetic modification (Wakayama et al, 1998; Cowan et al, 2005; Park et al, 2008). However given the high incidence of SNPs due to mechanical abrasion and UV exposure which fibroblasts possess (Takeda et al, 2008) alternatives have been sought. Alternatives which have successfully been used to generate hiPSCs include apidocytes (Qu et al, 2012), renal epithelial cells (Zhou et al, 2011), hepatocytes (Liu et al, 2010) and dental pulp cells (Yan et al, 2010).

1.3.4 Reprogramming factors

The first reports of reprogramming of somatic cells back to a pluripotent state used the transcription factors OCT4, SOX2, C-MYC and KLF4 (Takahashi et al, 2007). A further protocol was published using lentivirus to deliver OCT4, SOX2, NANOG and LIN28 (Yu et al, 2007). Although other factors have been successfully used since, such as L-MYC (Nakagawa et al, 2010) and GLIS1 (Maekawa et al, 2011), these remain the key factors for induction of pluripotency.

1.3.4.1 OCT4

Octamer-binding transcription factor 4 (OCT4) is a master regulator of pluripotency which is expressed by early embryo and germ line cells, embryos which are negative for OCT4 do not express pluripotency when they reach the blastocyst stage and can only differentiate to the extraembryonic trophoblast lineage (Schöler et al, 1990; Nichols et al, 1998). OCT4 is the product of the *OTF3* gene and there have been three isoforms of OCT4 reported, OCT4A, OCT4B and OCT4B1 (Wang et al, 2010). However only OCT4A has been reported to be necessary for maintenance of pluripotency, this isoform shares 87% amino acid sequence identity with the mouse Oct4 (Shi and Jin, 2010). OCT4 null homozygous embryos die as a result of the embryos being unable to implant in the uterine wall (Kehler et al, 2004).

1.3.4.2 SOX2

Sex determining region Y-box 2 (Sox2) is a key regulator of pluripotency in hPSCs as it acts co-operatively with OCT4 and NANOG (Zhang and Cui, 2014). Sox2 is thought to act as a supporting factor to Oct4 expression, as models have shown that Sox2-null mESCs are able to rescue their pluripotent phenotype with overexpression of OCT4 (Matsui et al, 2007).

1.3.4.3 NANOG

NANOG is commonly referred to, along with OCT4 and SOX2, as one of the master regulators of pluripotency as its mRNA is found in pluripotent mouse and human ES cells but not in the differentiated cells from these lines (Chambers et al, 2003). NANOG deficient inner cell mass (ICM) is unable to generate epiblast and is only able to generate parietal endoderm like cells while NANOG deficient hESCs are unable to maintain pluripotency and instead differentiate to extraembryonic endoderm lineage (Mitsui et al, 2003).

1.3.4.4 KLF4

Although KLF4 was required in the initial reprogramming using retroviruses (Takahashi et al, 2007) it was replaced by a combination of LIN28 and NANOG in the original reprogramming using lentivirus (Yu et al, 2007). One of the major roles in KLF4 is thought to be its interaction with OCT4 and SOX2 upstream of NANOG as these factors together are able to turn on

NANOG, a key regulator of pluripotency (Chan et al, 2009). KLF4 has previously been reported as a suppressor of p53 (Rowland et al, 2005). This could explain its role in hiPSC generation as tumour suppressing gene p53 has been shown to suppress the generation of hiPSCs from somatic cells (Hong et al, 2009). Consequently it was reported that a knockdown of p53 could improve the efficiency of hiPSC generation by up to 100 fold, although it could not replace the introduction of KLF4 (Zhao et al, 2008).

1.3.4.5 C-MYC

C-MYC is a known transcription factor which is responsible for driving a whole gene network which controls the regulation of cell growth and proliferation thus its dysfunction can lead to oncogenesis and its inclusion in reprogramming methodologies has been cautioned should the generated cells be used in clinical applications (Okita et al, 2007; Beroukhim et al, 2010; Muller et al, 2016). Unlike the master regulators it is possible for cells to maintain a pluripotent state without the expression of C-MYC (Fagnocchi and Zippo, 2017). Interestingly it has been shown that sustained activation of C-MYC in hESCs results in apoptosis and differentiation further demonstrating the delicate balance these reprogramming factors exhibit in maintaining pluripotency (Sumi et al, 2007). As such there has been much research into the generation of iPSCs without the inclusion of C-MYC and it has been reported that hiPSC generation is possible by using L-MYC as an alternative factor (Okita et al, 2013).

1.3.4.6 LIN28

LIN28 is known to be an essential component of the process of nucleogenesis in early embryonic development (Vogt et al, 2012). The let-7miRNAs have been shown to suppress the expression of pluripotency related genes and LIN28 has been shown to block this miRNA (Ramachandran et al, 2010; Zhang et al, 2016). The role of LIN28 in hiPSC generation appears to be similar to that of p53 inhibition, indeed it has been shown that LIN28 overexpression does not necessarily increase the efficiency of reprogramming but can accelerate the kinetics of the process (Hanna et al, 2009). The overexpression of LIN28 has been shown to inhibit the ability of PSCs to survive at clonal densities as a result of increased levels of differentiation and a decreased rate of cell division (Darr and Benvenisty, 2009). The role of LIN28 is thought to be in directing the fate of hESCs as opposed to their self-renewal (Darr and Benvenisty, 2009). These data correlate with the initial use of LIN28 in hiPSC generation which reported

that LIN28 was not required for reprogramming or stable expansion of newly derived hiPSC clones (Yu et al, 2007).

1.3.5 Integrative reprogramming methods

1.3.5.1 Retrovirus

Retroviruses consist of two copies of a single stranded RNA genome containing *gag, pol* and *env* sequences, for packaging and replication, which are surrounded by a glycoprotein structure known as an envelope (Kurian et al, 2000; Somia and Verma, 2000). Retroviruses go through two distinct life cycles, the initial infection and integration of the viral cDNA is the first and the second is the expression of the viral genes (Nisole and Saib, 2004).

The first successful reprogramming of mice/human somatic cells to a pluripotent state was performed using retroviral vectors (Takahashi and Yamanaka, 2006; Takahashi et al, 2007). The seminal work in the field used Moloney murine leukaemia virus (MMLV)-based retrovirus vector and the transgenes contained within this were driven by 5'MMLV long terminal repeat (LTR) promoter (Takahashi et al, 2007; Shao and Wu, 2010). The reactivation of retroviral promoters has been shown to cause tumorogenicity in murine models when c-Myc is turned back on, this was overcome by producing miPSCs which were generated in the absence of c-Myc, although this was successful it resulted in a major reduction in the efficiency of reprogramming (Aoi et al, 2008; Nakagawa et al, 2008; Shao and Wu, 2010). The starting cell type is important when using retrovirus as it is only able to infect actively dividing cells and reprogramming efficiencies can vary based on which somatic cell type is used as reprogramming efficiencies of up to 100 fold greater have been reported using keratinocytes in comparison to fibroblasts (Aasen et al, 2008; Shao and Wu, 2010).

Integration of the retrovirus was initially believed to occur following a random pattern however further investigation appears to indicate that the MMLV derived retroviruses favour integration near transcriptional regulatory sites, this phenomenon was not observed in other viruses such as Simian Immunodeficiency Virus (SIV) and Human Immunodeficiency Virus (HIV) (Hematti et al, 2004; Recchia et al, 2006; Ambrosi et al, 2008). Given the inability of retroviruses to infect non-dividing cells and their propensity to integrate near gene regulatory sites an alternative method was sought.

1.3.5.2 Lentivirus

Lentiviruses are a subclass of retroviruses which are able to infect both dividing and non-dividing cells unlike retroviruses, therefore giving them greater applications in cell therapy (Shao and Wu, 2010). Lentiviruses have been shown to exhibit a superior efficiency in modifying cells when compared to MMLV retroviruses (Park, 2007).

Initial reports using lentivirus to generate iPSC demonstrated reprogramming efficiencies in the region of 0.01%, this was comparable with the retrovirus efficiencies at the time (Yu et al, 2007; Blelloch et al, 2007). Although lentiviral vectors also randomly integrate into the genome reports have indicated that these integrations show less propensity to occur at sites which may result in oncogenesis than retroviruses (Cattoglio et al, 2007). Lentiviral vectors used in human cells have been adapted in order to render them replication deficient, therefore these vectors are able to infect cells but will not be able to replicate after infection (Shao and Wu, 2010).

It has been reported that although lentiviral vectors are silenced the process is inefficient in iPSCs and there remains the potential for them to be reactivated after differentiation to certain lineages or even to prevent differentiation entirely (Brambrink et al, 2008; Stadtfeld et al, 2008b; Galat et al, 2016). Although lentivirus is able to infect both dividing and non-dividing cells, and is less likely to integrate at key regulatory sites than retrovirus is, the presence and continued expression of viral transgenes can inhibit the differentiation potential of the iPSC lines generated.

1.3.5.3 Inducible/Excisable viral vectors

Given the delicate balance of temporal control over the expression of viral transgenes and its effect over maintenance of pluripotency and differentiation capacity, the potential to induce transgene expression or excise it when convenient was an attractive proposition. iPSC reprogramming has successfully been achieved using excisable cassettes without any loss in reprogramming efficiency when using the same lentiviral vector with and without loxP excision sites (Sommer et al, 2009; Sommer et al, 2010). In addition to the cre/loxP system it has also been shown that the PiggyBac transposon/transposase system can be used to generate hiPSCs (Kaji et al, 2009). Although the reprogramming efficiency and kinetics remained the same, there was a marked increase in the differentiation potential of the hiPSCs which had been generated after excision (Sommer et al, 2010).

Another method to control the expression of viral transgenes is to create an inducible lentiviral vector, such a method has been successfully used to create hiPSCs by inducing the activity of the vector when the cells are cultured in the presence of the drug doxycycline (DOX) (Hockemeyer et al, 2008; Maherli et al, 2008). Using the inducible system it is possible to greatly increase reprogramming efficiency by first collecting hiPSCs and then differentiating these to an easy to culture cell type such as fibroblasts, and as these will contain the DOX-inducible transgenes a so called "second reprogramming" occurs, this has been shown to generate up to 3% reprogramming efficiency which massively improves upon standard retroviral or lentiviral methodology (Hockemeyer et al, 2008; Maherli et al, 2008).

Despite the improvements in reprogramming efficiency and differentiation potential which were achieved using inducible/excisable systems there remained limitations. In the case of excisable systems it has previously been estimated that the efficiency of excision using the cre/loxP system ranges from 20%-99.4% suggesting incomplete excision which may not make it an ideal option in iPSC generation strategies (Jasinskiene et al, 2003). When using the PiggyBac transposon system there remains the risk that after excision the genes can be reintroduced by reintegration (Wang et al, 2008). In the case of the inducible system the integrated transgenes are never removed merely silenced by the lack of DOX in the culture medium and in the case of the incomplete excision some transgenes will remain integrated into the host genome, due to the nature of random integrations there remains the possibility for gene disruption (Banasik and McCray Jr, 2010). Such limitations of integration dependant reprogramming methods necessitated the requirement for non-integrative reprogramming technologies.

1.3.6 Non-Integrative reprogramming methods

1.3.6.1 Sendai virus

Sendai virus (SeV) is a negative strand RNA virus belonging to the *paramyxoviridae* family (Li et al, 2000). Sendai virus replicates in the cytoplasm, unlike other RNA viruses, and doesn't go through the DNA phase of replication, meaning it is unable to integrate into the host's genome (Li et al, 2000). SeV has been shown to be non-pathogenic to humans and able to infect a broad range of hosts (MacArthur et al, 2012). Sendai viral vectors have been considered for use in clinical studies for gene therapy in cystic fibrosis (Yonemitsu et al, 2000), critical limb ischaemia (Masaki et al, 2001) and in vaccine delivery (Takeda et al, 2008). F-protein deficient

SeV vectors were developed to reduce cytotoxicity and prevent replication of the virus while still generating high level of exogenous gene expression (Li et al, 2000).

The first published use of SeV involved insertion of the Yamanaka factors to an F-protein deficient, non-transmissible SeV vector which would allow high level exogenous gene expression without the risk of integration (Fuskai et al, 2009). Reprogramming efficiency of SeV was shown to be 1% which demonstrated comparable reprogramming efficiency to standard lentiviral and retroviral vectors of the time (Fusaki et al, 2009).

Although the Sendai virus vectors cannot integrate into the genome it is possible that the virus will persist in the hiPSCs after reprogramming, this has been combated by the introduction of temperature sensitivity within the plasmids (Ban et al, 2011). This temperature sensitive mutant plasmid has successfully been used to generate hiPSCs and then been removed by temperature shift after hiPSC purification (Ono et al, 2012).

1.3.6.2 Episomal plasmids

Initial reports of episomal reprogramming to hiPSCs using oriP/EBNA-1 episomal vectors which expressed OCT4, SOX2, NANOG, LIN28, c-Myc, KLF4, and SV40LT yielded efficiencies of between 0.0003-0.0006% (Yu et al, 2009). Improvement of this method with the addition of a MEK inhibitor PD0325901, a GSK3b inhibitor CHIR99021, and a TGF-b/Activin/Nodal receptor inhibitor A- 83-01 demonstrated a reprogramming efficiency of 0.0021%, representing ~70 fold increase on the initial method (Yu et al, 2011). Knockdown of p53 has resulted in improved reprogramming efficiency, however given the role of p53 knockdown in cancer and the genomic instability a knockout would create, a transient knockdown was sought (Hong et al, 2009). Subsequently it was reported that the introduction of TP53 shRNA to episomal plasmids was able to improve reprogramming efficiency up to 0.028% (Okita et al, 2011). Furthermore the efficiency of iPSC generation is improved three fold by replacing C-MYC with L-MYC, L-MYC is also less oncogenic than C-MYC (Nakagawa et al, 2010).

1.3.6.3 Adenovirus

Adenovirus is a non-integrating virus which is able to infect both dividing and non-dividing cells (Shao and Wu, 2010). Adenovirus was shown to be effective in reprogramming mouse fibroblasts to a pluripotent state with a maximum efficiency of 0.001% with the resulting miPSCs being free of adenoviral DNA and possessing an ability to differentiate to all three

germ layers (Stadtfeld et al, 2008). It was reported that human fibroblasts could be induced to reprogram to hiPSCs, although this study showed that adenovirus required multiple transductions in order to reprogram the cells but did so at an improved efficiency of 0.0002% (Zhou and Freed, 2009). Although adenoviral vectors are able to infect dividing and non-dividing cells and generate iPSCs without integration there remains very low reprogramming efficiency which can only be improved by the addition of small molecules, the lack of efficiency in using this method limits it routine use in generating iPSCs (Shao and Wu, 2010). It has been suggested that the reason for the limited reprogramming efficiency when using adenoviral vectors is as a result of poor temporal expression of the reprogramming factors leading to a failure of the cell to switch on the endogenous pluripotency machinery (Stadtfeld et al, 2008; Rao and Malik, 2012)

1.3.6.4 Protein delivery

Generation of hiPSCs using purified protein has also been reported previously. Four reprogramming proteins, OCT4, SOX2, KLF4 and C-MYC, were fused with 9R, a cell penetrating peptide (CPP), which delivered the proteins to somatic cells (Kim et al, 2009). However this method required six one week cycles of protein treatment and hiPSC colonies were not observed until around 8 weeks of treatment, making it over twice as long as traditional retroviral or lentiviral methods (Kim et al, 2009). Moreover the method itself delivered a relatively low reprogramming efficiency of 0.001% (Kim et al, 2009). When using purified protein delivery there is a requirement for a large quantity of pure protein in this method and the proteins must be added on more than one occasion (Robinton and Daley, 2012). In addition to the introduction of protein this method also requires the addition of valproic acid (VPA), a histone deacetylase inhibitor (HDAC) inhibitor, which has been shown to increase reprogramming efficiency (Huangfu et al, 2008b; Zhou et al, 2009).

1.3.6.5 RNA delivery

Modified-RNAs encoding the four canonical Yamanaka factors, KLF4, c-MYC, OCT4 and SOX2 were previously transfected into somatic cells using a cationic lipid based transfection reagent to induce reprogramming, LIN28 was also added to improve efficiency (Warren et al, 2010). The transfection efficiency of this process was reported to be 50-80%, suggesting an efficient delivery system (Warren et al, 2010). This system eliminates the possibility of genomic

integration by delivering RNA rather than viral or DNA based vectors. However this process required the design of modified RNA and the presence of B18R, an interferon inhibitor, in the medium to block the cells innate immune response (Warren et al, 2010). Furthermore this method required repeated daily transfections and was reported to generate hiPSCs at an efficiency of 0.2% which was lower the more commonly used integrating methods at the time (Warren et al, 2010).

1.4 Cardiac development and *In Vitro* differentiation

1.4.1 *In Vivo* cardiac development

After fertilisation, the zygote is enclosed in an acelluar envelope termed the zona pellucida. The developing embryo will then undergo multiple rounds of cellular division before compacting and forming a ball of cells which is known as a morula. This morula will then develop into a blastocyst which occurs by the formation of a cavity in the centre of the morula termed the blastocoel. On one side of the blastocoel is a mass of cells termed the inner cell mass (ICM), which will form the embryo, and on the other side is a layer of cells known as the trophoblast which will form the extra embryonic tissue (Hardy et al, 1989; Ingber, 2006).

The heart is formed from mesodermal tissues which first become evident in the embryo during gastrulation which occurs in the third week of prenatal development in humans (Moorman et al, 2003). The developing heart is comprised of four major embryonic regions; primary heart field, secondary heart field, cardiac neural crest and proepicardium (Martinsen and Lohr, 2005).

The migration of heart precursors to the ventral midline in order to form the cardiac crescent is a part of the gastrulation process whereby heart and head mesendoderm migrates the node and primitive streak towards the cranial region of the developing embryo (Harvey, 2002; Moorman et al, 2003). This migration is driven by signalling from *Fgf8* (Sun et al, 1999) and *MesP1* and *MesP2* (Kitajima et al, 2000). The primitive streak is formed by day 15 of human development and the initial mesodermal cells which migrate through this region are destined to become the heart, forming the primary heart field (Martinsen and Lohr, 2005). This specification of the primary heart field is driven by FGF, BMP and WNT which ultimately activate the cardiac specific transcription factors such as - *NKX2-5, GATA4, and TBX5*, and chromatin remodelling protein SMARCD3 (BAF60c) (Lopez-Sanchez and Garcia-Martinez, 2011; Kelly et al, 2014).

After initial migration of primary heart field cells to form the cardiac crescent a second wave of migration brings established cardiac progenitor cells, which in turn form the developing heart tube, these cells are guided to the correct location by a gradient of fibronectin (DeHann et al, 1963; Harvey, 2002). As embryogenesis continues, the process forms what is termed the heart tube which is formed in the shape of a Y (Moorman et al, 2003). The stem of this Y shaped heart tube will form the definitive left ventricle while the arms form the primary atrial component of the heart, however reports suggests that there is insufficient evidence that all components of the heart are present at this stage in the Y shaped heart tube (De la Cruz et al, 1991; Moorman et al, 2003). The developing heart tube then undergoes a process known as looping which is often described as the first example of asymmetry in the developing embryo (Moorman et al, 2003). This looping of the developing heart leads to a ventricular loop which features inflow and outflow tracts (Moorman et al, 2003). During the looping process the secondary heart field undergoes epithelial to myocardial transition and proliferates to increase the number of cardiomyocytes in the outflow tract (Martinsen and Lohr, 2005). Due to the looping process the chambers of the heart become defined by day 28 of human development (Martinsen and Lohr, 2005). The second heart field is marked by the expression of *Isl1* (Burridge et al, 2012).

The next stage in heart development is the formation of the cardiac chambers, by this stage the atrial and ventricular components of the heart are seen as distinct regions which are separated by the atrioventricular canal (Moorman et al, 2003). The four different chambers of the heart display different gene expression profiles which is thought to affect their morphological properties (Small and Kreig, 2004). The atrial chambers are formed from the same cells that exist in the primary tube of the developing heart and are driven to create left-right asymmetry under the control of *Pitx2* (Harvey, 2002). After the specification and segmentation of the chambers within the heart the cardiac neural crest cells, which are neither first nor secondary heart field cells, remodel the cardiac vasculature to ensure that all blood flow directly into the right atrium (Martinsen and Lohr, 2005). The final contributors to heart development are the proepicardial cells which are vital in making up the coronary vasculature (Martinsen and Lohr, 2005). These cells are distinct from other heart cells in that they are derived from the splanchnopleuric mesoderm cells and migrate to the heart tube around day 22-28 of human heart development, before looping has occurred (Martinsen and Lohr, 2005).

Overall the process of cardiac development is heavily dependent on the production of mesoderm which is induced by NODAL signalling in the proximal epiblast during murine cardiomyogenesis at day 5 of development (Figure 1.6) (Burridge et al, 2012). This NODAL signalling drives the formation of mesoderm which is characterised by the appearance of the transcription factor BrachyuryT (Kattman et al, 2011). NODAL signalling results in sustained expression of BMP4 which in turn activates Wnt3 signalling pathway (Burridge et al, 2012). This BMP4 and NODAL activation is then restricted at embryonic day 5.5 in the mouse by the action of Dkk1, which antagonises WNT3 and Lefty1, while Cer1 antagonises NODAL (Burridge et al, 2012). Subsequently at around E5.75 Wnt signalling induces the expression of both BrachyuryT and Eomes which are markers of mesoendodermal lineage. This mesoderm formation is then patterned to a more specific subtype, in the cardiomyocyte this involves Fgf4 and FgF8 which are expressed in the primitive streak (Burridge et al, 2012). MESP1 is a master regulator of cardiac development and its activation is induced by both brachyury and Eomes (Costello et al, 2011; David et al, 2011). MESP1 drives cardiac specification by its interaction with DKK1 which is able to inhibit the Wnt signalling pathway (David et al, 2008). After the specification of cardiac lineage differentiation the roles of the signalling pathways Wnt and NOTCH change from driving mesoderm formation to maintenance of the cardiac progenitor cell (CPC) population (Oyang et al, 2007; Kwon et al, 2009).

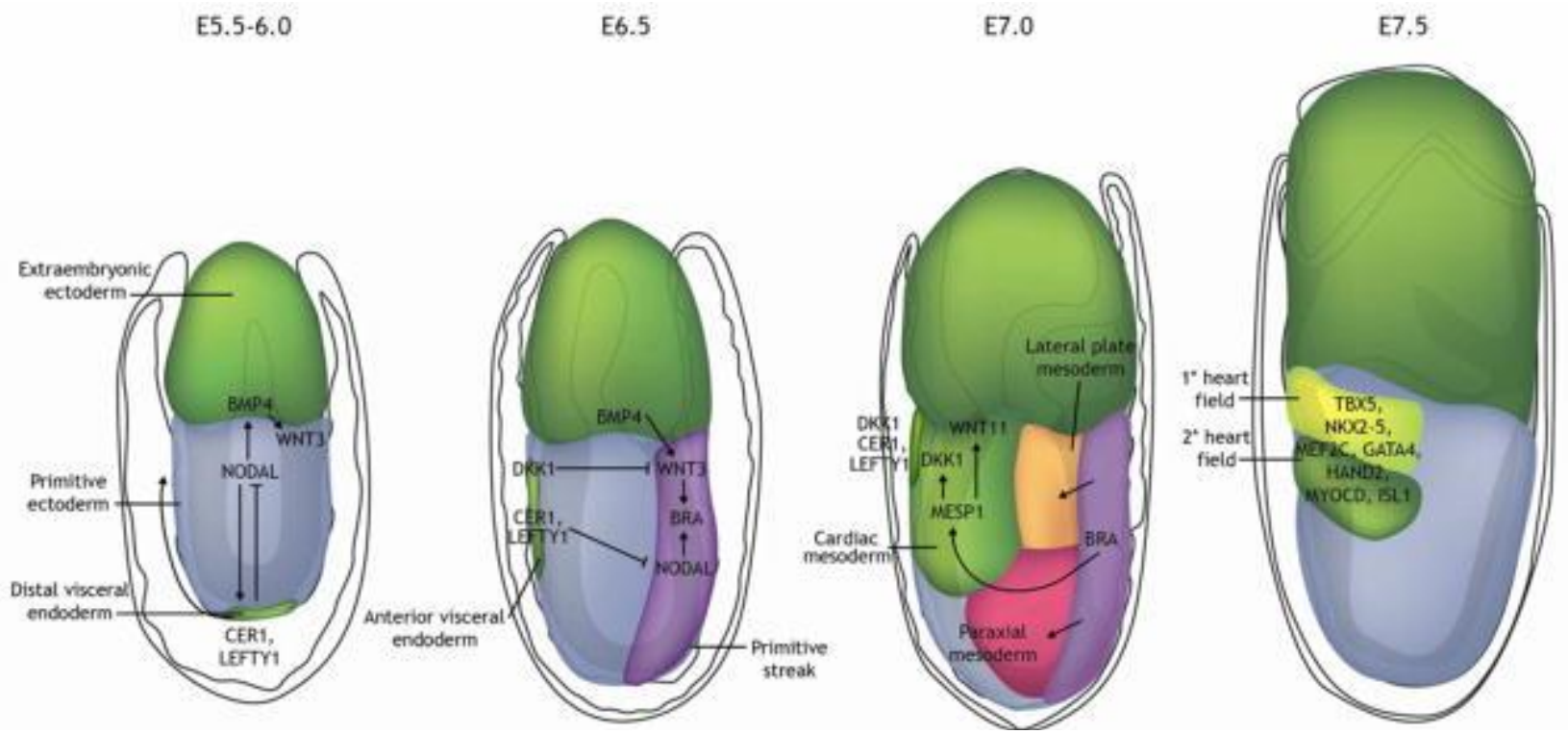


Figure 1-6 - The mouse as a model for cardiogenesis

A - Formation of the primitive streak signals the start of gastrulation. Anterior primitive ectoderm cells then undergo an epithelial to mesenchymal transition (EMT) and migrate through the primitive streak and settle between the primitive ectoderm and the visceral endoderm. B – The cells which sit in the proximal portion of the primitive streak form the extraembryonic mesoderm, mid-primitive streak and the embryonic tissues such as heart and blood. C – Cardiac progenitors progress laterally then ventrally around both sides of the embryo becoming lateral plate mesoderm which forms the first heart field. The lateral plate mesoderm then delaminates to form splanchnic mesoderm which makes the second heart field. D – The FHF form the cardiac crescent whereas the SHF forms medially to the crescent. FHF forms the linear heart tube and what later becomes the left ventricle whereas SHF cells proliferate and join the FHF resulting in rightward looping of the cardiac tube which ends up with a segmented structure creating the 4 heart chambers (Burridge et al, 2012).

1.4.2 Generation of cardiomyocytes from hPSCs *In Vitro*

The use of PSCs in order to generate a specific cell type of interest *de novo* has been a fascinating tool for researchers since the original derivation of mESCs (Evans and Kaufman, 1981). The original generation of human cardiomyocytes from hESCs (Itskovitz-Eldor et al, 2000) sparked interest in using this technology to model human cardiac disease and potentially generate human cardiomyocytes for autologous or allogenic transplantation (Figure 1.7). Described below are the main methodologies to generate cardiomyocytes from hPSCs.

1.4.2.1 Embryoid body formation

Differentiation of hPSCs can be performed using embryoid body (EB) formation using techniques such "forced aggregation" whereby cells are seeded into ultra-low attached v-bottom 96-well plates and centrifuged (Ng et al, 2005). Using this method it was reported to be possible to generate EBs of consistent size and shape which were able to generate derivatives of all three germ layers when hPSCs were exposed to pro-differentiation conditions (Ng et al, 2005). However using EB based methods to generate cardiomyocytes initially demonstrated low efficiencies of around only 21.5% (Segev et al, 2005). Further investigation of the "forced aggregation" system demonstrated that EBs could be formed in standard v-bottom 96-well plates but that there was a high degree of interline variability (Burridge et al, 2007). Cardiac differentiation using EB formation was improved further and demonstrated the capability of generating cardiomyocytes at efficiencies of up to 64-89% across multiple hESC and hiPSC lines (Burridge et al, 2011b).

1.4.2.2 Monolayer differentiation

An alternative method of generating cardiomyocytes from hPSCs is monolayer directed differentiation. This method has many benefits over EB formation in that it removes the complex diffusional barriers present in EBs and also saves time as it does not require the multiple replating steps common in EB methods (Mummery et al, 2012). Furthermore monolayer differentiation has been shown to generate up to 100 cardiomyocytes for every 1 input pluripotent cell (Burridge et al, 2014) in comparison to less than 1 cardiomyocyte for every input pluripotent cell using EB methods (Burridge et al, 2007). In addition to the increased yields reported for this monolayer method there was also an increase in overall

culture purity with reported efficiencies of 80-95% for all cell lines tested (Burridge et al. 2014). Therefore it has been demonstrated that monolayer directed differentiation can increase yield, reduce labour time whilst producing high purity cardiomyocytes.

1.4.2.3 Bioreactor differentiation

Bioreactor culture has been investigated for generation of hiPSC-CMs at very high yields for clinical applications. Some initial concerns regarding this methodology were that cells are likely to aggregate in suspension preventing homogenous diffusion of nutrients and growth factors. (Azarin and Palecek, 2010). Furthermore bioreactor systems can form gradients of temperature, pH and other factors within the system increasing variability of differentiation (Azarin and Palecek, 2010). Agitation of the culture may limit some of the problems noted but would also result in shear forces which could cause cell damage and apoptosis (Cimetta et al, 2009). Indeed these shear forces have been shown to maintain subpopulations of transiently pluripotent cells in mESCs (Shafa et al, 2011). However bioreactor differentiation has more recently been reported to be capable of producing ~$8x10^7$ cells with a reported purity for cTnT of 80% from a starting population of $2x10^7$ hiPSCs, representing 3.2 cardiomyocytes for every 1 input hiPSC (Matsuura et al, 2012). Further improvements have recently led to a study reporting 100% beating cardiac spheroids at purity of ~90% in only 10 days, this study reported an input of $2x10^7$ cells but did not specify yield (Fonoudi et al, 2015). Therefore bioreactor culture represents an attractive source for scalable production of cardiomyocytes.

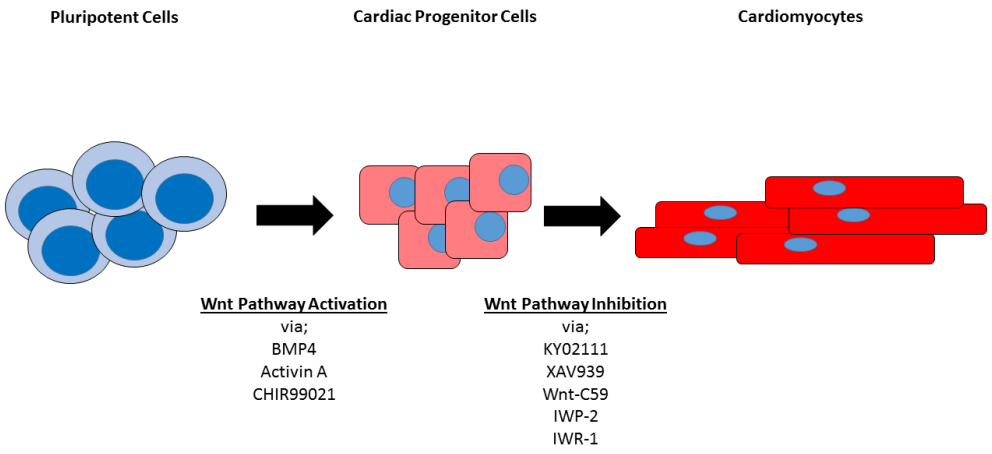


Figure 1-7 - Schematic outlining the principles of In Vitro cardiac differentiation

The process of *in vitro* cardiac differentiation enables the generation of hPSC-CMs when required to enable phenotyping of cardiac disease and drug screening protocols. Traditionally this process requires the initial activation of the Wnt signalling pathway to induce mesoderm before this pathway is inhibited in order to drive the specification of cardiac mesoderm, thus generating cardiomyocytes. These processes can be performed using growth factors or small molecules. This processs will be discussed further in chapter 3.

1.5 The current landscape of hiPSCs in disease modelling

1.5.1 Cardiomyocyte phenotyping

1.5.1.1 Voltage

1.5.1.1.1 Patch clamp electrophysiology

Patch clamp electrophysiology allows the measurement of the electrical activity of a cell in one of four configurations – cell-attached, whole-cell, inside-out and outside- out (Figure 1.8) (Zhao et al, 2009).

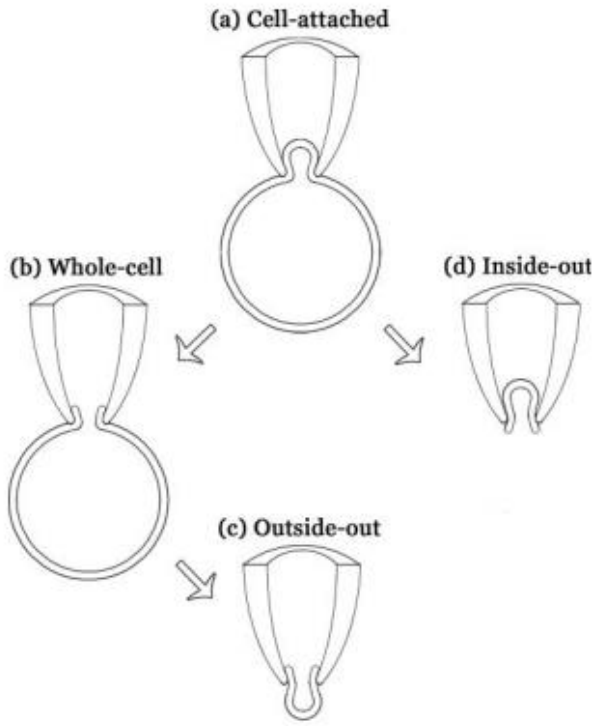


Figure 1-8 - The four configurations of patch clamp electrophysiology
A – The cell-attached configuration whereby the cell is sucked into the tip but not broken. B- The whole-cell configuration whereby the membrane of the cell is broken to provide a continuous seal with the inside of the pipette. C – The outside-in configuration which is achieved by pulling the pipette away while in whole-cell mode. D – The inside-out configuration which is achieved by pulling the pipette away from the cell while in cell-attached mode (Zhao et al, 2009).

The whole-cell patch clamp configuration is the most commonly used as it provides electrical and physical continuity between the intracellular space and the inside of the pipette (Zhao et al, 2009). This process allows the voltage of the cell to be held, or clamped, enabling access to the ion channels within it (Zhao et al, 2009). Given the low throughput of manual patch clamp electrophysiology, around 10-15 data points a day (Farre and Fertig, 2012), the potential to automate this system remains attractive. Such automated systems have traditionally been used with HEK and CHO lines overexpressing ion channels, however a recent report highlighted the utility of these systems in assessing pharmacology in hiPSC-CMs (Rajamohan et al, 2016). However there are some limitations to the automated platforms in that they operate best with highly expressed and stable cell lines, meaning transient lines are unable to be patched in such a way (Long and Li, 2012). Furthermore the randomised shapes of primary cardiomyocytes do not accommodate the random nature of this platforms ability to load cells, requiring extremely high purities to ensure other cell types are not preferentially patched (Long and Li, 2012).

Patch clamp electrophysiology remains the gold standard for cardiomyocyte electrophysiological analysis due to the ability to manipulate both voltage (voltage clamp) and

current (current clamp) which can both be held and maintained in whole-cell mode allowing in depth investigation of the cells' electric properties (Kaestner et al, 2015). Despite this, patch clamp electrophysiology has some drawbacks. The cardiomyocytes must be in single cell format therefore they are not acting in concert with neighbouring cells as would be the case *in vivo*, this has been demonstrated to change cardiomyocyte behaviour (Matsa et al, 2011). Furthermore to achieve a seal on the cardiomyocyte the cell must be mechanically patched, this ruptures the cell membrane (Kaestner et al, 2015). In addition to this the information collected during patch clamp only relates the area of the cell which has been patched and makes no reference to spatial differences across the rest of the cardiomyocytes membrane (Kaestner et al, 2015). Perhaps the most limiting drawback of patch clamp electrophysiology is the labour intensive nature of the procedure, in addition to requiring a highly skilled operator (van Meer et al, 2016).

1.5.1.1.2 Microelectrode Array

While patch clamp electrophysiology can analyse cardiomyocytes at the single cell level microelectrode array (MEA) systems analyse the electrical properties of cardiomyocytes at the population level as clusters (Pradhapan et al, 2013). The MEA system operates by embedding extracellular electrodes in the surface of the dish in which the cardiomyocytes are cultured, from this it is able to detect a partial recapitulation of the cardiac action potential which is termed a field potential (Meyer et al, 2004). MEAs measure the change in the electrical potential of cells by using electrodes on the surface of the dish, however an alternative to this is to use electrodes which are able to penetrate the cell membrane and act as a pseudo patch clamp, the limitation of this system is that the seals formed are generally poor (van Meer et al, 2016).

1.5.1.1.3 Cell Permeable Fluorescent Voltage Indicators

Voltage sensitive dyes are fast-response fluorescent probes which are able to detect changes in the membrane potential of cells (van Meer et al, 2016). Imaging of electrical properties of cells using optical dyes has been reported in the literature with publications using Di-4-ANEPPS (Burridge et al, 2011; Ren et al, 2011) and FluoVolt (Asakura et al, 2015; Bedut et al, 2016). The main benefit of voltage sensitive dyes is that the ease with which they can be used compared to patch clamp electrophysiology. FluoVolt is a commercially available voltage

sensitive dye which has been validated as a phenotyping tool against a panel of reference pharmacological compounds. hiPSC-CMs were stained using FluoVolt and exposed to lidocaine, nifedipine, dofetilide and ivabradine, exhibiting the expected responses to these drugs of known action (Bedut et al, 2016).

1.5.1.1.4 Genetically Encoded Voltage Indicators

The use of genetically encoded voltage indicators (GEVI) remains a relatively new and unexplored field in hiPSC-CM phenotyping. However it has previously been shown that GEVIs can detect changes in voltage when tested in HEK cells, this novel voltage sensing protein was termed ArcLight (Jin et al, 2012). ArcLight has subsequently been used in hiPSC-CMs where it was demonstrated to be able to detect the action potentials of the hiPSC-CMs and was used in a screen to assess toxicity of drug compounds (Leyton-Mange et al, 2014). Ultimately though it appears that GEVIs have not yet reached the level of development which has been achieved using genetically encoded calcium indicators (GECIs) (Kaestner et al, 2014).

1.5.1.2 Calcium

1.5.1.2.1 Cell Permeable Fluorescent Calcium Indicators

Cell permeable fluorescent dyes are a well-established technique to image the calcium handling properties of cardiomyocytes, these dyes fall into two categories – ratiometric and non-ratiometric (van Meer et al, 2016). Ratiometric dyes are able to account for the level of bound and unbound calcium, thus enabling an absolute calcium concentration to be calculated (van Meer et al, 2016). In contrast to this, non-ratiometric dyes are only able to reflect changes in the cytosolic calcium concentration and thus are more susceptible to variations based on cell size, access of dye to the cell and amount of calcium which is loaded (van Meer et al, 2016). The use of cell permeable dyes can enable the simultaneous mapping of both voltage and calcium enabling a more in-depth investigation of hiPSC-CM response to drug exposure (Lee et al, 2012). The utility of intracellular calcium labelling dyes has been demonstrated in toxicity screening in cardiomyocytes as well as hepatocytes (Grimm et al, 2015). However this technique is not without limitations, it is known that the photostability of calcium permeable labels is suboptimal and they are able to result in cytotoxicity (Shinnawi et al, 2015).

1.5.1.2.2 Genetically Encoded Calcium Indicators

As a result of the issues outlined above the generation of genetically encoded calcium indicators (GECI) enables the measurement of high quality optical signals over longer time periods than is possible using fluorescently labelled dyes (Shinnawi et al, 2015). GECIs possess a number of advantages of the use of cell permeable membrane indicators in that they enable cell specific Ca^{2+} mapping as they are driven by a chosen promoter and the stable expression of the fluorescent indicator allows analysis over days or weeks, a vital factor when investigating chronic conditions (Kaestner et al, 2014). However the major downside of GECIs remains the extended time and cellular manipulation required to generate these stably expressing lines as well as improving biocompatibility (Kaestner et al, 2014).

1.5.2 hPSC-Cardiomyocyte structure

There remains distinct differences in the structural properties of hPSC-CMs and native adult cardiomyocytes. Typically adult cardiomyocytes exhibit a rod like structure with an aspect ratio of greater than 5:1 (Denning et al, 2016). In addition to this they possess highly aligned sarcomeres with a longitudinal alignment and display the ultrastructural properties of Z-discs, I-, H-, A- and M-bands (Denning et al, 2016). Adult cardiomyocytes also show bi- or poly-nucleation in greater than 30% of cardiomyocytes and have a well-developed sarcoplasmic reticulum as well as invaginations known as t-tubules (Denning et al, 2016). In contrast to these properties hPSC-CMs are round and angular shaped and typically have an aspect ratio of less than 3:1 (Denning et al, 2016). Furthermore they possess highly chaotic sarcomeric alignment and typically only contain the ultrastructural properties of Z-discs and I-bands, unlike adult cells they are found to be devoid of H-, A- and M- bands (Denning et al, 2016). Predominantly they are mononucleated and exhibit variable responses to drugs such as caffeine and thapsigargin, indicating a poorly developed sarcoplasmic reticulum (Denning et al, 2016). Despite these limitations it has been reported that prolonged culture of hPSC-CMs is able to result in some level of structural maturation. Prolonged culture of hPSC-CMs up to 180 days in culture resulted in the appearance of more sarcomeric alignment and the presence of Z-, A-, H-, and I-bands, notably M-bands did not appear until 360 days in culture and their gene expression levels remained lower than in native adult cardiomyocytes (Lundy et al, 2013; Kamakura et al, 2013).

1.5.3 hPSC-Cardiomyocyte gene expression

Reports regarding gene expression in hPSC-CMs have shown that in hPSC-CMs the dominant isoforms of Myosin Heavy Chain (MYH) is *MYH6* and there is also a prominent expression of *TNNI1* (cTnI) (Denning et al, 2016). However this is in direct contrast to adult cardiomyocytes where *MYH7* and *TNNI3* are the dominant isoforms, indicating a switch of these during the development process (Denning et al, 2016). It has been reported that prolonged culture of hPSC-CMs results in a 14-fold increase in *MYH7* expression levels (Lundy et al, 2013). Furthermore hPSC-CMs rely heavily on both glucose and lactose to provide energy for the cell in comparison to adult cardiomyocytes which use oxidative phosphorylation and fatty acids as a substrate for energy (Kim et al, 2013; Denning et al, 2016). Moreover the mitochondria is thought to occupy up to 40% of the cell volume in adult cardiomyocytes but this is not observed in hPSC-CMs were the figure is lower and the mitochondria are confined to perinuclear locations (Schaper et al, 1985; Denning et al, 2016). Reports have shown that gene expression profiles vary in hPSC-CMs which are cultured for prolonged periods, with expression of *SERCA2A* increasing (Lundy et al, 2013).

1.5.4 hPSC-Cardiomyocyte electrophysiology

Mature adult cardiomyocytes are electrically quiescent as a result of the I_{k1} current which provides a low inward rectifying K^+ current maintaining the cardiomyocytes resting potential at around -85mV (Denning et al, 2016). However the I_{k1} current is either absent or only functional to low levels in hPSC-CMs, giving them the automaticity usually reserved for pacemaker cells (Yang et al, 2014). Reports have suggested that the level of I_{k1} activity in hPSC-CMs is around 4 times lower than in adult cardiomyocytes (Ma et al, 2011). Furthermore the presence of I_{ks} current has recently been called into question (Christ et al, 2015). Previous studies have indicated that I_{ks} is present in some hPSC-CMs but not in all hPSC-CMs, having been demonstrated in around 31% of hPSC-CMs in one study (Ma et al, 2011). However only 53% of native left ventricular adult cardiomyocytes displayed measurable I_{ks} current when analysed for their electrophysiological properties *in vitro* (Virag et al, 2001). The investigation of I_{kr} current in hPSC-CMs has indicated that the current is active and plays a role comparable to that which it plays in native adult cardiomyocytes (Hoekstra et al, 2012). Analysis of I_{kr} blockade using E4031 has demonstrated that this manipulation will cause an increase in the APD of hPSC-CMs (Itzhaki et al, 2011a; Ma et al, 2011; Matsa et al, 2011; Lahti et al, 2012). There remains limited understanding regarding the specific role of the ATP-sensitive K^+ current

in hPSC-CMs, however this current is functional as evidenced by reports which showed its pharmacological activation could decrease APD in hPSC-CMs (Itzhaki et al, 2011a; Matsa et al, 2011). I_f is reported to be present at higher expression levels in hPSC-CMs than in native adult ventricular cells and this is thought to play a role in the spontaneous depolarisations of hPSC-CMs (Ma et al, 2011; Synnergren et al, 2012).

1.5.5 hPSC-Cardiomyocyte calcium handling

Reports surrounding the calcium handling of hPSC-CMs have indicated that despite the poor structural properties of these cells and the underdeveloped sarcoplasmic reticulum hPSC-CMs do cycle calcium and use it in the EC coupling process (Itzhaki et al, 2011). Furthermore these reports state that calcium influx occurs via the LTCC and this leads to increased activation of the RYR2 which results in calcium induced calcium release from the sarcoplasmic reticulum, a vital component of efficient EC coupling in adult cardiomyocytes (Itzhaki et al, 2011; Nunes et al, 2013). However, the U-shaped calcium transient wave seen when analysing calcium transients of hPSC-CMs indicates that a slow or immature calcium induced calcium release is being exhibited by such cardiomyocytes (Lee et al, 2011). Interestingly the calcium cycling within hPSC-CMs has been improved by culturing on micro-grooved substrates indicating that calcium handling in the cell can be improved by manipulation of hPSC-CM environment (Rao et al, 2013). Furthermore prolonged culture of hPSC-CMs was shown to demonstrate that upstroke and downstroke velocities of calcium transients were quicker in older hPSC-CMs, perhaps suggesting improved performance of calcium induced calcium release and reuptake by SERCA (Lundy et al, 2013). However taken as a whole it is highly likely that the immature calcium handling phenotype observed in hPSC-CMs is due to their highly unorganised sarcomeres and a lack of t-tubules which affect the spatial and temporal effects of calcium handling (Gherghiceanu et al, 2011; Lundy et al, 2013). The role of the NCX is vital in removing Ca^{2+} from the cytosol of the cell during relaxation, the absolute value of Ca^{2+} removed by the NCX appears to increase as time in culture increases however what remains constant is the relative contribution to Ca^{2+} extrusion NCX plays in comparison to SERCA (Hwang et al, 2015).

1.5.6 Long term culture of hPSC-CMs *In Vitro*

Prolonged culture of hPSC-CMs aims to mimic the natural process of cardiomyocyte maturation which occurs in humans, although this process requires 6-10 years *in vivo* (Peters

et al, 1994). Prolonged culture of hPSC-CMs for up to 3 months has been shown to increase the developmental maturation of the ion channel currents; I_{to}, I_{k1}, I_f, I_{cal} as well as the transient inward and outward rectifying K^+ currents (Sartiani et al, 2007). Changes in beat rate during long term culture appear to exhibit variable response as some reports have indicated an increase, whereas others have indicated a decrease (Földes et al, 2011; Hazeltine et al, 2012). Reports have shown a loss of viability in older hiPSC-CMs meaning day 30 were the oldest tested in some studies indicating that prolonged cell culture may not be a viable option in all cases (Hwang et al, 2015). As mentioned in Section 1.5.2 the appearance of M-bands in the hPSC-CM structure occurs after around 1 year in culture (Kamakura et al, 2013), this limits the effectiveness of long term culture as a maturation tool.

1.6 CRISPR/CAS9 as a genome editing tool

Clustered regularly interspaced short palindromic repeats (CRISPR) are part of an RNA mediated adaptive immune system found in bacteria and archaea (Weidenheft et al, 2012). The system enables bacteria and archaea to recognise the DNA of foreign pathogens and amount an immune response to induce a double stranded break in the foreign pathogen's DNA (Doudna and Charpentier, 2014).

1.6.1 History of CRISPR

The first evidence of the CRIPSR system was demonstrated in the late 1980's when a group researching the *iap* enzyme in *E. coli* discovered a series of 29 nucleotide repeats downstream of the gene (Ishino et al, 1987). The interesting discovery with regards to these repeats was that they were interspaced with 5 intervening 32 nucleotide sequences which were not repetitive (Ishino et al, 1987; Hsu et al, 2014). The first evidence that CRISPR/Cas9 was an adaptive immune system was demonstrated in 2007 by showing that CRISPR spacers dictated the target specificity whereas the Cas enzymes were responsible for control of the spacer acquisition and for phage defence (Barrangou et al, 2007). Further investigation in the *S. thermophilus* showed that the Cas9 protein was able to be harnessed as part of the CRISPR system to cleave DNA (Garneau et al, 2010).

In order to harness the potential of this CRISPR system for genome editing studies the Cas9 could not simply cleave foreign DNA, it must be guided to an area of interest. It was shown that by forming an RNA chimera - termed the guide RNA (gRNA) - of trans-activating crRNA

(tracrRNA) and CRISPR RNAs (crRNA), Cas9 protein could be directed to a specific location in the genome inducing a double stranded break in the DNA (Jinek et al, 2012). The gRNA binds to a specific site in the genome and recognises the protospacer adjacent motif (PAM) site of the DNA, which contains the sequence NGG (Jinek et al, 2012). Such PAM sites do not limit the scope of this technology as they are found roughly every ~8bp in the genome (Cong et al, 2011). The gRNA requires 20 nucleotides which bind with the target DNA sequence as longer gRNAs have been shown to be trimmed at the 5' end *in vivo* (Ran et al, 2013; Hendel et al, 2015). However more recent research has suggested that reducing the size of the gRNA to 17-18 nucleotides can greatly enhance specificity (Fu et al, 2014). By inducing these double stranded breaks in the DNA at site-specific locations, it is possible to induce changes in the DNA by providing the cells with a template, such as plasmid DNA or a single stranded oligonucleotide, to repair themselves using homology directed repair (HDR) (Ran et al, 2013).

The first example of this system being used in mammalian cells was reported in 2013 whereby two reports demonstrated that the Type II CRISPR system could be manipulated to edit the genome (Cong et al, 2013; Mali et al, 2013). In the work by Mali the gRNA was delivered as a crRNA-tracrRNA fusion transcript driven by U6 polymerase III promoter (Mali et al, 2013). Taken together this system enables the editing of the mammalian genome via Cas9 inducing a double strand break in DNA when guided to an appropriate location by a gRNA (Figure 1.9).

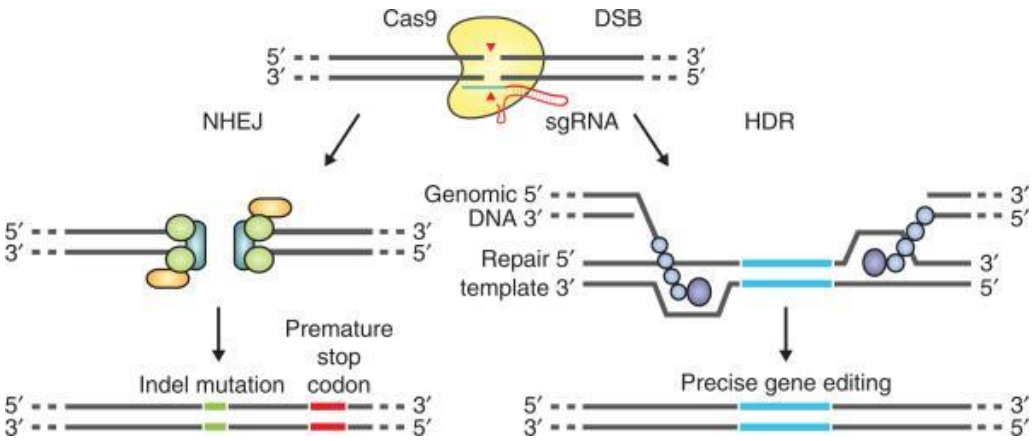


Figure 1-9 - Using CRISPR to edit the genome
This schematic illustrates how the CRISPR/Cas9 system can be used to edit the genome. The sgRNA and Cas9 protein form a complex which is guided to a precise site in the genome by the complementary binding of the sgRNA. Once the sgRNA has bound to its complementary site the Cas9 protein recognises the PAM sequence, this induces DNA cleavage and the inducement of a double strand break. The DNA can then be repaired by two mechanisms – non homologous end joining, resulting in an indel and gene disruption or homology directed repair which lead to precise gene editing. Image from (Ran et al, 2013).

1.6.2 The CRISPR system and its use in human cells

This adaptive immune response occurs in three stages. The first stage is termed adaptation and in this stage the bacteria/archaea insert new spacers into the CRISPR locus to be used for recognition later (Rath et al, 2015). The second stage is termed the expression stage and during this process the *Cas* genes transcribe the CRISPR into what is known as a long precursor CRISPR RNA (pre-crRNA) before this is matured into a crRNA (Rath et al, 2015). The final stage is the interference stage whereby the bacteria/archaea destroy the invading pathogen by the action of the crRNA and the Cas proteins (Rath et al, 2015). Adjacent to the CRIPSR system is the *Cas* gene family, to date up to 45 families of *Cas* genes have been demonstrated to exist, *Cas1* and *Cas2* are the only ones that are conserved across all CRISPR systems (Jansen et al, 2002; Haft et al, 2005; Swarts et al, 2012; Waddington et al, 2016).

There are three categories of CRISPR system (Figure 1.10), common amongst all of them is the activity of the *Cas1* and *Cas2* genes which are believed to play a vital role in the spacer integration during the development of adaptive immunity in bacteria and archaea (Makarova et al, 2011). The Type I CRISPR/Cas System is characterised by the presence of cas3, this protein features both helicase and DNase domains (Sinukas et al, 2011; Rath et al, 2015). Type I systems all feature a Cascade-like complex which binds to the crRNA and locates the target sequence in the genome (Rath et al, 2015). The Type II CRISPR/Cas System encodes *Cas1* and *Cas2* in addition the Cas9 protein and occasionally Cas4 (Rath et al, 2015). In this type of CRISPR system the Cas9 protein is responsible for processing the crRNA and can cleave the DNA when crRNA and tracrRNA are present (Rath et al, 2015). The Type III CRISPR/Cas System is less established and contains the Cas10 protein which operates an unknown function in the system (Rath et al, 2015). Unlike Type I and Type II systems, which are only able to target DNA, the Type III system has been shown to be able to target RNA (Rath et al, 2015). The Type II system has only been found to this stage in bacteria unlike the Type I and Type III systems which have been shown in both bacteria and archaea (Makaorva et al, 2011).

The Cas9 protein is responsible for the cleavage of DNA in the Type II CRISPR system and the Cas9 protein is characterised by two nuclease domains - RuvC and HNH (Hsu et al, 2014). Investigation of the structure of Cas9 in the model species *S pyogenes* revealed that the protein is bilobed with a nuclease lobe and a target recognition lobe (Nishimasu et al, 2014). The target recognition lobe is essential of the binding of gRNA and to the DNA of the target sequence, on the other hand the nuclease lobe contains the RuvC and HNH domains (Nishimasu et al, 2014). Furthermore the nuclease lobe contains a C-terminal domain which

maintains a responsibility for interacting with the PAM site, an NGG, in the endogenous sequence which is vital in initiating DNA cleavage (Nishimasu et al, 2014). To this stage only Type II CRISPR system has been demonstrated to be useful in genome editing (Li et al, 2016).

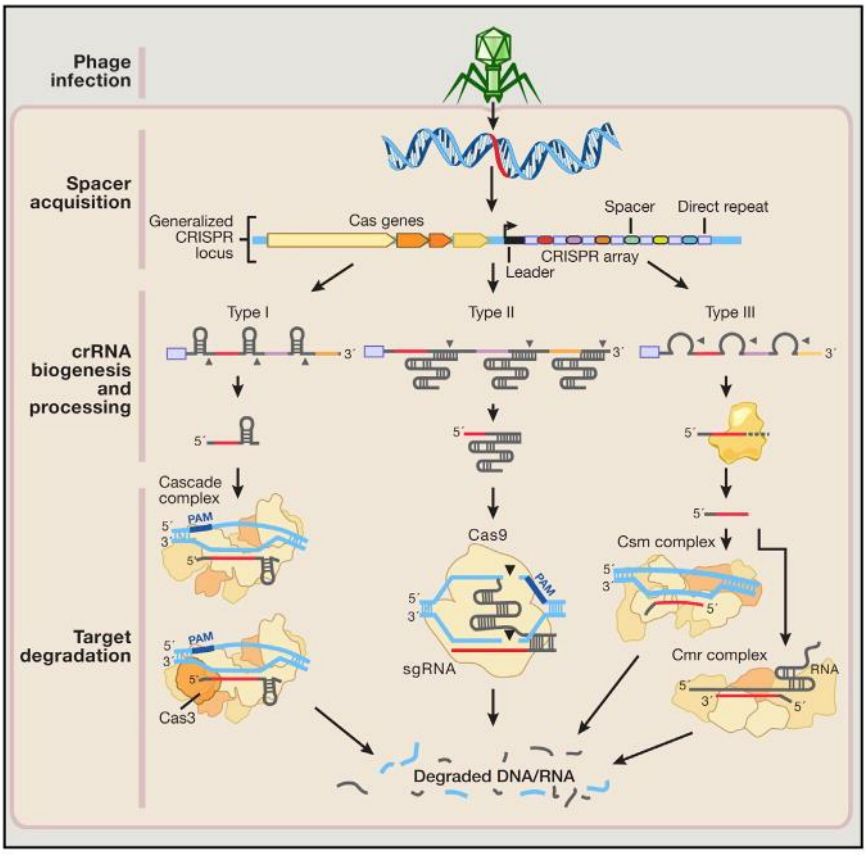


Figure 1-10 - The mechanisms of immunity in the different CRISPR systems
The first step in the CRISPR immune response is the infection of the bacteria by a phage, Cas enzymes then acquire spacers from the exogenous sequence and insert them into the CRISPR locus of the prokaryotic genome in what is known as acquisition. The final step of the immune response is crRNA biogenesis and processing when the RNA transcript is matured and seeks the foreign pathogen for degradation, the method of maturation varies depending on the specific CRISPR system. Type I and III CRISPR systems both use multiprotein interference modules to recognise the target. In type I CRISPR, the Cascade complex is loaded with a crRNA molecule and it is this which recognizes target DNA. The Cas3 nuclease is then recruited to the Cascade-bound R loop resulting in degradation of the foreign DNA. In type III CRISPR, crRNAs associate either with Csm or Cmr complexes which bind and cleave DNA. The Type II system is unique in that it can also degrade RNA. The type II system requires only the Cas9 nuclease to degrade DNA which is complementary to its dual guide RNA consisting of a crRNA-tracrRNA hybrid (Hsu et al, 2014).

Initial testing of this system in human cells was performed to introduce GFP to HEK cells showing that GFP^+ cells were evident only ~20 hours after transfection (Mali et al, 2013). The CRISPR system has been highlighted as potentially improving upon the use of siRNA in large scale genetic screens (Wang et al, 2014; Shalem et al, 2014). Use of the CRISPR/Cas9 system in hiPSCs has been reported to yield gene disruption efficiencies of up to 25% as well as targeting efficiencies of up to 10% (Byrne et al, 2014). Studies in human hematopoietic stem/progenitor cells (HSPCs) have demonstrated that by either delivering a single gRNA to

HSPCs which are expressing Cas9 or a RNA ribonucleoprotein (RNP) to induce cleavage and a single stranded oligonucleotide as a repair template can yield homology directed repair of up to 20% (Gundry et al, 2016). There is a clear appeal for genome modification to treat genetic diseases, to that end β-thalassemia is a common condition worldwide caused by a mutation in the human hemoglobin beta (*HBB*) gene (Xie et al, 2014). This mutation was corrected in hiPSC demonstrating that footprint free genome editing was possible and paving the way for such technology to be expanded further (Xie et al, 2014). More recently hiPSCs were generated from patients suffering from β-thalassemia and subsequently corrected using CRISPR/Cas9 then injected into murine models, this technique demonstrated expression of *HBB* in the mice which had received injections and perhaps more importantly did not result in tumour formation (Ou et al, 2016).

1.7 Thesis rationale and objectives

hPSC-CMs have been used to demonstrate the appropriate pharmacological response to a variety of compounds including those which modulate ion channels and β-adrenoceptor agonists (Rajamohan et al, 2013). Furthermore hPSCs have been used extensively to model diseases *in vitro*, faithfully recapitulating the *in vivo* diseased phenotype of conditions such as LQTS1 (Moretti et al, 2010), LQTS2 (Matsa et al, 2011), CPVT (Fatima et al, 2011), Duchenne Muscular Dystrophy (DMD) (Dick et al, 2011), Alzheimer's Disease (Yagi et al, 2011) and Parkinson's Disease (Seibler et al, 2011) to name a few. Therefore the use of hPSC-CMs can increase knowledge regarding disease state and inform whether drugs exhibit efficacy in treating a specific condition.

As described in Section 1.1.2.1, LQTS remains a serious condition which can be deadly when left untreated. Moreover even for those who are diagnosed and treated a considerable subset of this population will not respond to standardised therapy as it is suboptimal and treats the symptoms, increased heart rate, and not the disease, increased repolarisation time. With regards to CPVT there remains much of the disease which needs to be elucidated, given the spatial and temporal effects which modulate efficient calcium handling it is possible that hPSC-CMs may not recapitulate these calcium handling properties *in vitro*. In addition to this the prevalence of the CPVT phenotype in the Purkinje fibres may necessitate the study of the disease in this specific subset of cardiomyocytes, however current differentiation methodologies are as yet unable to generate specific subtypes. Given these considerations in this thesis it was decided to use the LQTS2 disease model to test a variety of drug compounds

on the LQTS2-hiPSC-CM to assess the effect these compounds exert on APD and therefore QT interval. In addition, the CPVT disease model will be used to assess the functional properties of calcium handling in hiPSC-CMs when compared to an unrelated healthy control and to a CRISPR/Cas9 genetically corrected CPVT-hiPSC line. Taken together these aims will seek to improve understanding of the disorders and elucidate whether the limitations of calcium handling maturity affect the ability to model CPVT *in vitro*.

To achieve this the following objectives were set;

1 – Generate hiPSC lines using non-integrating techniques from a starting cell population which improves the ease of sample collection. [Chapter 3]

2 – Generate high quality and high purity hiPSC-CMs using directed methods of cardiomyocyte differentiation. [Chapter 3]

3 – Generate LQTS2-hiPSC disease model which will be differentiated to cardiomyocyte lineage. These LQTS2-hiPSC-CMs will then be characterised to assess their electrophysiological properties to establish if they recapitulate the disease phenotype *in vitro*. [Chapter 4]

4 - If these LQTS2-hiPSC-CMs are able to accurately recapitulate the LQTS2 phenotype *in vitro* then a panel of potentially therapeutic compounds will be tested to assess their effect on action potential duration and therefore QT interval. [Chapter 4]

5 – Generate CPVT-hiPSC disease model which will be differentiated to cardiomyocyte lineage. In addition to this a CPVT-WT-hiPSC line will be generated using CRISPR/Cas9 genome engineering technology to provide an isogenic control therefore increasing the mechanistic understanding behind the disease through subsequent phenotyping assays. [Chapter 5]

6 – To assess the functional calcium handling properties of hiPSC-CMs using a hiPSC-CM panel which will include CPVT-hiPSC, CPVT-WT-hiPSC and an unrelated healthy control hiPSC line. By achieving this it will be established whether there are functional differences in calcium handling in the diseased CPVT-hiPSC line [Chapter 5]

2 Materials and Methods

2.1 General cell culture techniques

All cell culture was performed in standard biological safety class II vertical laminar flow cabinets under sterile conditions. Cabinets were cleaned before and after use with 70% industrial methylated spirit (IMS). Cells were cultured in a humidified incubator at 37°C with an atmospheric CO_2 of 5%.

2.1.1 Derivation of starting cell populations

2.1.1.1 Derivation of fibroblasts

Dermal fibroblast cell cultures were prepared from excess skin removed from the patient during an operation, informed consent was given by the patients. Skin samples were transported from the clinic into the laboratory in TRANSPORT medium (Table 2.1) and washed three times in the same, after which they were transferred into bacterial-grade Petri dishes. Here, using sterile forceps and scalpels, the adipose and epidermal tissue was removed and the remaining sample cut into 1mm pieces. The cut tissue was digested, first with 2.5% trypsin for 20 minutes, and then with 1mg/ml collagenase IV for 90 minutes, both at 37^{o}C. The digested cells were spun down at 200xg for 5 minutes, plated in FIB medium (Table 2.1) and grown for 2-3 weeks until confluent, with medium changes every 3-4 days. Once confluent, 1ml of spent medium was analysed for mycoplasma contamination. When declared mycoplasma-negative, cells were then expanded and cryopreserved.

2.1.1.2 Derivation of renal epithelial (RE) cells from urine

Urine was collected and the cells harvested according to published procedures (Zhou et al, 2011) with informed consent from healthy volunteers. Briefly; urine samples were aliquoted into 50ml tubes and centrifuged at 400g for 10 minutes before all pellets collected, centrifuged at 400g for 10 minutes again, and seeded into 1x well of a 12-well plate coated with gelatin. RE cells were cultured in RE Proliferation Medium which is a commercially available kit from Lonza which contains REGM BulletKit and RE cell basal medium (Lonza; CC-3190).

2.1.1.3 Derivation of endothelial progenitor cells (EPC) from blood

Derivation of EPCs from blood samples were carried out according to the published protocol (Geti et al, 2012) with informed consent from healthy volunteers. Briefly, 40ml of blood was collected and mixed with 4ml sodium citrate and diluted 1:1 with DPBS (Ca^{2+} and Mg^{2+} free). 10ml of this solution was then added to tubes containing 8ml ficoll (BD; 362780). These samples were then centrifuged for 35 minutes at 400g at room temperature. EPCs were then isolated using a plastic transfer pipette to carefully remove the thin translucent layer between transparent supernatant and red blood cells and seeded into collagen coated T75s. EGM-2MV (Lonza; CC-3202) medium was changed every 2-3 days.

2.1.1.4 Derivation of dental pulp cells from teeth

Dental pulp cell cultures were prepared from whole tooth samples, after informed consent was given by the patients. Whole teeth were transported dry to the laboratory. The teeth were washed in 70% IMS to ensure sterility. Teeth were then thoroughly dried and crushed with a vice to expose the dental pulp. The crushed tooth was digested with 1mg/ml collagenase IV for 90 minutes at 37^{o}C. The digested cells were spun down at 200xg for 5 minutes, plated in FIB medium supplemented with 1x penicillin/streptomycin and 1x fungizone, and grown for 2-3 weeks until confluent, with medium changes every 3-4 days. Once confluent, 1ml of spent medium was analysed for mycoplasma contamination. From here on, cells were expanded and cryopreserved. The second method of extracting cells from teeth was to place the tooth in a flask which was pre-coated in Matrigel in FIB medium. Medium was then changed on this flask every 3-4 days. From here on, cells were expanded and cryopreserved.

2.1.2 Culture of human fibroblasts

Human dermal fibroblasts were cultured as a monolayer in T25 flasks with no additional substrate coating. Cells were maintained in FIB medium (Table 2.1). Cell medium was changed every 2-3 days and cells were passaged at around 90% confluence to avoid over growth. When cells were passaged cell medium was removed and the flask washed in 5ml PBS. This was then aspirated and 500µl of 0.05% Trypsin added to cells. The flask was then incubated at 37^{o}C and at 5% CO_2 for 2 minutes. Gentle mechanical bashing of the flask aided the dislodging of cells before 9mL of serum containing medium was added to quench action

of trypsin. This suspension was then centrifuged at 200g for 5 minutes at room temperature. Supernatant was then discarded and cells resuspended in an appropriate volume of fresh culture medium and then seeded into a fresh T25. If cells were required at a specific density counting was carried out using a haemocytometer.

2.1.3 Culture of human induced pluripotent stem cells (hiPSC)

Human induced pluripotent stem cells were routinely cultured as a monolayer in Matrigel coated T25s. Cells were maintained in commercially available Essential 8 medium (Thermo Fisher) or our in-house Essential 8 medium. Cell medium was changed daily and cells were passaged every 3-4 days to maintain healthy cultures.

When passaging hiPSCs for routine maintenance cell medium as aspirated and the flask washed in 5mL PBS. This was then removed and 1ml 0.5mM EDTA/TrypLE (Thermo Fisher) added to the flask which was then incubated at 37^{o}C and 5% CO_2 for 2-5 minutes. After this EDTA/TrypLE was aspirated off carefully to avoid dislodging cells. The flask was then subject to mechanical force to dislodge cells. Fresh Essential 8 medium was then used to resuspend the cells which were then seeded into a fresh Matrigel coated culture vessel. During the passaging process cells were seeded into fresh Essential 8 supplemented with 10µM Y27632.

2.1.3.1 Cryopreservation and recovery of hiPSC

Cells were dissociated from culture vessel as described in Section 2.1.3. Cells were resuspended in Essential 8 + 10% DMSO. This solution as then added to cryovials and incubated in a Mr Frosty at -80^{o}C overnight. A Mr Frosty contains isopropanol and reduces the temperature of the cells by around 1^{o}C per minute. The following day cryovials were transferred from the Mr Frosty to a liquid nitrogen tank. To thaw cells which had previously been cryopreserved cryovials were removed from liquid nitrogen and heated at 37^{o}C in a waterbath until the liquid had thawed. This was then added to a universal tube and Essential 8 medium was then added dropwise. This was then centrifuged at 160g for 5 minutes at room temperature. Supernatant was then discarded and cells resuspended in an appropriate volume and seeded into fresh culture vessels in Essential 8 medium supplemented with 10µM Y27632.

2.1.4 Tri-Lineage differentiation test

hiPSCs were seeded into wells of a 96 well plate at a final seeding density of 16,700 cells/well and incubated at 37°C. Differentiation was induced at 24 hours post seeding for endoderm and 72 hours post seeding for ectoderm and mesoderm induction. To induce differentiation, E8 was aspirated from the wells and replaced with ectoderm induction medium, endoderm induction medium or mesoderm induction medium A differentiation medium components are shown in Table 2.1. For ectoderm induction medium was changed every 24 hours for 6 days. For endoderm induction medium was changed every 24 hours for 3 days. For mesoderm induction medium was changed to mesoderm induction medium B after 48 hours and cells fixed 2 days later.

2.1.5 Differentiation of hiPSCs to cardiomyocytes

2.1.5.1 ABKYX method

hiPSCs were seeded into an appropriate culture vessel and allowed to reach >90% confluence while being maintained in Essential 8 medium. Once this confluence had been reached medium was changed to StemPro34 (Thermo Fisher) supplemented with 1ng/ml Matrigel overlay and 1ng/ml BMP4. The following day medium was changed to fresh StemPro34 with 5ng/ml BMP4 and 8ng/ml Activin A. Cells were cultured at 37°C and 5% CO_2 for 48 hours. Medium was then changed to RPMI B27 –insulin supplemented with 10nM KY02111 and XAV939. Cells were then incubated at 37°C and 5% CO_2 for 48 hours. Medium was then changed to RPMIB27 supplemented with 10nM KY02111 and XAV939 and incubated at 37°C and 5% CO_2 for 48 hours. After this cells were cultured routinely in RPMIB27 with medium changes every 2-3 days.

2.1.5.2 CDM-CW method

hiPSCs were seeded into an appropriate culture vessel and allowed to reach >90% confluence while being maintained in Essential 8 medium. Once this confluence had been reached medium was changed to CDM3 supplemented with 4µM CHIR99021. Cells were then incubated for 48 hours at 37°C and 5% CO_2. After this the medium was changed on the cells to fresh CDM3 supplemented with 2µM WntC59. The cells were again incubated

for 48 hours at 37°C and 5%CO_2. Medium was then changed to RPMIB27 and changed every 2-3 days.

2.1.5.3 Dissociation of cardiomyocytes

Cardiomyocyte monolayers were dissociated between day 14-18. Medium was removed and cells were washed with HBSS -Ca^{2+} -Mg. Collagenase supplemented with 30µM BTS,10µM Y-27632 and 1µM HEPES and was then added to the cells and these were incubated at 37^oC and 5% CO_2 for 4 hours. Mechanical force was applied to the flask to dislodge cells and medium was then collected and placed in a universal tube. Equal volume of RPMI + 12µg DNase/ml was added to the cell suspension and this was then centrifuged at 100g for 15 minutes. Supernatant was then aspirated and cells resuspended in 10ml RPMI and counted using a haemocytometer. Cells were then either seeded into fresh culture vessels for continued cell culture or frozen in heat inactivated-Hyclone FBS + 10% DMSO.

Table 2-1 - Medium component table

Medium Name	Medium Components	Concentration
Serum Free Medium	1X DMEM Base 0.5M Galactose 100mM sodium pyruvate	97% 2% 1%
FIB Medium	1X DMEM Base FBS NEAA L-glutamine β-mercaptoethanol	78% 20% 1% 1% 100µM
TRANSPORT Medium	HBSS (10x) H_2O Pen/Strep Fungizone	10% 88% 1% 1%
Ectoderm Induction Medium	1x Advanced DMEM:F12 (Base) Lipid concentrate L-glutamine Human Transferin Insulin β-mercapto-ethanol SB431542 Dorsomorphin	98% 1% 1% 7.5µg/ml 14µg/ml 100µM 10µM 1µM
Endoderm Induction Medium	1x RPMI-1640 (Base) 1x B27 serum free supplement CHIR98014 IDE1	98% 2% 1µM 10µM
Mesoderm Induction Medium A	1x RPMI-1640 (Base) Ascorbic Acid rh Human Albumin CHIR99021	100% 213µg/ml 500µg/ml 4µM
Mesoderm Induction Medium B	1x RPMI-1640 (Base) Ascorbic Acid rh Human Albumin WNT-C59	100% 213µg/ml 500µg/ml 2µM
Column Buffer	H_2O HBBS (10x) Sodium Bicarbonate FBS	85% 10% 100µl 5%
In-house E8	DMEM F12 + L-Glutamine + HEPES Ascorbic Acid Insulin Transferrin Sodium Selenite FGF2 TGFβ1 Heparin Sodium Salt	99% 1% 20µg/ml 5µg/ml 14µg/ml 100ng/ml 2ng/ml 100ng/ml

2.2 Reprogramming technologies

2.2.1 Sendai virus reprogramming

Primary cells were plated in one well of a six well plate at a density of $2x10^5$ per well. The following day three tubes containing the viral vectors contained in the CytoTune2.0 kit (Thermo Fisher) were taken from -80°C freezer and thawed briefly in a waterbath at 37°C. A calculated volume of virus from each tube was then added to 3ml of fibroblast medium which had been prewarmed to 37°C. Spent medium was aspirated using plastic pipette and the new medium, containing virus was added to the cells. This was incubated at 37°C with 5% CO_2 overnight. The following day medium was changed to 3ml of fresh fibroblast medium and this was repeated until the cells reached ~80% confluence. At this point medium was removed and cells washed in 3ml PBS. This was then aspirated and 500µl 0.05% trypsin was added to the well, this was incubated at 37°C for up to 2 minutes. 500µl FIB medium was then added to the well and this 1ml was mixed and then added to 4ml of FIB medium in a universal tube. The mixture was then centrifuged at 200g for 5 minutes. Supernatant was removed and cells resuspended in 3ml of Essential 6 medium supplemented with 100ng/ml bFGF. Three 35mm dishes were prepared with vitronectin-peptide and the cells were added to these at a 1:3 dilution. Medium was changed daily with fresh E6 + FGF added until the emergence of established colonies at which time the medium was changed to Essential 8 medium. Following this medium was changed daily until colonies had reached a size ready for isolation. Isolation was performed using either; manual dissection, MACS purification or serial passage with 0.5mM EDTA.

2.2.2 Episomal reprogramming

Fibroblasts were harvested and counted using trypsin as described previously. $1x10^6$ of these primary cells were then resuspended in P3 buffer (Lonza). These cells were then added a tube containing three episomal plasmids; pCXLE0hOCT3/4-shp53-F (Addgene #27077), pCXLE-hUL (Addgene #27080), pCXLE-hSK (Addgene #27078) with 1µg of each plasmid. These cells + plasmids were then mixed and added to a cuvette and electroporated using the Amaxa 4D electroporation system program CM-100. After electroporation the cells were incubated at 37^oC and 5% CO_2 for 5 minutes. Subsequently the cells were resuspended in fresh E6 medium + 100ng/ml FGF and then plated onto vitronectin-peptide coated 35mm dishes and incubated at 37^oC for 24 hours. After this time they were maintained in E6 medium + 100ng/ml FGF, changed daily, until the emergence of colonies, at this stage medium was changed to E8.

2.2.3 GET mediated delivery

Fibroblasts were harvested and counted using trypsin as described previously in Section 2.1.3. $2x10^5$ of these primary cells were then plated into 1 well of a 6 well plate coated with vitronectin-peptide. The next step was to prepare the GET Peptide (FGF2B) and the plasmids as illustrated below;

Two tubes were made as displayed in the table below (volumes below were per well of 6-well plate):

Tube A	Tube B
100ul Optimem	100ul Optimem
3.4ul FGF2B	0.55ul pCXLE0hOCT3/4-shp53-F
	0.59ul PCXLE HSK
	0.67ul PCXLE HUL

The tubes were allowed to complex for 5 mins at room temperature and then combined before being incubated for a further 15 mins at room temperature. The mix was then added onto the cells which were then incubated at 37°C for 24 hours before medium was changed to E6+ 100ng/ml bFGF. Medium was then changed daily until the emergence of colonies at which stage the medium was changed to E8.

2.2.4 Purification of hiPSC colonies after reprogramming

2.2.4.1 Magnetic Activated Cell Sorting (MACS)

Cells were harvested using 1ml of TrypLE and incubated at 37°C for 2 minutes. These cells were then suspended in 9ml of E8 and centrifuged at 300g for 5 minutes. The supernatant was removed and the cell suspension resuspended in 500µl of cold column buffer. 2.5µl of PE conjugated Tra-1-81 antibody was then added to the suspension which was wrapped in foil and incubated at 4°C for 20 minutes. After this incubation 2.5ml of cold column buffer was added to the solution and the cells were centrifuged at 300g for 5 minutes.

Supernatant was carefully aspirated and cells were resuspended in 80µl of cold column buffer, 20µl of anti-PE microbeads were then added to this solution. The tube was then again wrapped in foil and incubated at 4°C for 15 minutes. After this incubation 2ml of cold column buffer was added to the solution and the cells centrifuged at 300g for 5 minutes. During this centrifugation a MACS column was placed into the MACS magnet and a 7ml bijou tube left below it. This column was equilibrated with 500µl cold column buffer. The cell pellet was then resuspended in 500µl cold column buffer, added to the column and allowed to pass through it by gravity. The column was then washed in 500µl cold column buffer three times. The column was then removed from the magnet and 1ml of cold column buffer added into the column this was then ejected using a plunger into a fresh tube and centrifuged at 300g for 5 minutes. After centrifugation the supernatant was aspirated and the pellet resuspended in 1ml E8 and added to a fresh 35mm dish or a T25 depending on pellet size.

2.2.4.2 Manual dissection

During the reprogramming process hiPSC colonies emerge within a population of fibroblasts. To isolate these colonies a stem cell knife was used to cut the hiPSC colony out. This colony was then transferred to a 48 well plate to continue expansion.

2.2.4.3 Serial passage

Serial passage of cells to purify a reprogramming heterogeneous population of cells begins by adding 500µl of 0.5mM EDTA to a 35mm dish which contains a heterogeneous population. This is then incubated at 37^{o}C for 4-5 minutes before the EDTA is carefully removed. The flask/plate is then flushed using E8 medium and the cells reseeded into a fresh Matrigel coated T25. This process is continued for 3-5 passages after which time a pure population should be observed.

2.3 Human induced pluripotent stem cell characterisation

2.3.1 Fixing cells

Cells were fixed using 4% paraformaldehyde. Medium was removed from cells which were then washed in PBS. Cells were predominately fixed whilst in 96 well plate format therefore 100µl PBS was added then aspirated from the wells using a multichannel pipette. 100µl of 4% paraformaldehyde was then added to the cells and this was incubated at room temperature for 15 minutes. After this the paraformaldehyde was then removed and the cells washed twice with 100µl PBS. Cells were then stored with 100µl PBS per well at 4°C for up to two weeks.

2.3.2 Immunostaining

Cells were plated in flat bottomed 96 well plates at a density of 10-20,000 cells per well. Medium was changed after 24 hours and cells were fixed at 48 hours. Fixing was performed as described in Section 2.3.1. Details of the dilutions and antibodies used can be found in Table 2.2. Cells were first washed in PBS using 200µl per well. If cells were to be stained for nuclear markers then they were then incubated for 10 minutes at room temperature in 200µl of 0.1% Triton X-100, this was not carried out on cells which would be stained for surface markers. Cells were then washed in 0.1% PBS-Tween three times using 200µl per well each time. Cells were then blocked using 10% species block made up in PBS, species being that which the secondary was raised in. 200µl was added to each well and this was incubated for 1 hour at room temperature. This was then aspirated and cells washed twice using 200µl 0.1% PBS-Tween. After this washing step cells were incubated in 50µl of primary antibody made up in 1% species block. Plates were wrapped in parafilm and left at 4°C overnight. The following day the primary antibody was aspirated and the cells washed three times using 200µl of PBS-Tween per well. This step included a five minute wash on a shaker. This was then aspirated and the cells treated with 50µl secondary antibody made up in 5% species block, this was incubated on a shaker at room temperature for 1 hour while plate was covered in foil. Secondary antibody was then removed and cells washed three times in 200µl 0.1% PBS-Tween, these washes also include one 5 minute was on a shaker at room temperature. Cells were then stained for DAPI by adding 50µl of DAPI in PBS to each well and incubating at 4°C for 15 minutes. This

was then removed and cells washed twice with 200µl of 0.1% PBS-Tween then once in PBS. A list of antibodies used in this thesis is shown in Table 2.2.

2.3.3 Flow cytometry

Cells were harvested using the TrypLE method detailed in Section 1.1.3. $1x10^6$ cells were counted and washed in PBS before being centrifuged at 160g for 5 minutes. The cells were then fixed by resuspending in 4% paraformaldehyde; these were incubated at room temperature for 15 minutes. Cells were then centrifuged again for 5 minutes at 160g. The pellet was then washed in PBS once before being stained using the antibodies and concentrations detailed in Table 2.2. hiPSCs were incubated with PE-conjugated antibodies at room temperature for 1 hour. These cells were then centrifuged at 200g for 5 minutes and washed in PBS before being centrifuged at 200g for 5 minutes again and resuspended in PBS.

2.3.4 Karyotype analysis

Cells were split and ~48 hours later were incubated with 100ng/ml of Karyomax Colcemid (Thermo Fisher) for 1 hour at 37°C. This medium was then collected and cells washed in 5ml PBS which was also collected. Cells were then harvested using TrypLE as described in 2.4 and centrifuged at 160g for 5 minutes. Pellet was then resuspended in 8ml of hypotonic solution, this was added dropwise while cells were vortexed. This solution was then incubated at room temperature for 20 minutes. Cell suspension was then centrifuged at 300g for 5 minutes. The cell pellet was then resuspended in 8ml of fixing solution and centrifuged at 300g for 5 minutes. This process was repeated three times. After the third fixing step the cells were then resuspended in 500µl fixing solution and sent for G-Band chromosomal analysis.

2.3.5 Calculation of population doubling times

hiPSCs were seeded at the density of $1x10^6$cells per T25 flask. The hiPSCs were then harvested using TrypLE and counted every 48 hours for a total of 5 passages. The doubling time was calculated as shown below:

Cumulative population doubling (CPD) per passage:

$$\frac{\Sigma \log10(\text{fold increase in cell count.per passage})}{\log10}$$ (2)

Table 2-2 - Antibody table

Antibody	Supplier	Dilution Used
OCT4	Santa Cruz: SC-5279	1:50
SOX2	R & D Systems: AF2018	1:200
NANOG	R&D systems: AF1997	1:200
SSEA4	R&D systems ; MAB1435-SP	1:200
SSEA3	R&D systems ; MAB1434-SP	1:200
TRA-1-81-PE Conjugated	eBioscience; 12-8883-82	1:100
SSEA4-PE Conjugated	eBioscience; 12-8843-42	1:100
SSEA1-PE Conjugated	eBioscience; 12-8813-42	1:100
Cardiac Troponin T	Santa Cruz; SC-20025	1:200
Cardiac α-actinin	SIGMA: A7811	1:200
PAX6	SantaCruz: SC-81649	1:100
SOX1	R&D: AF3369	1:100
SOX17	R&D: AF1924	1:100
FOXA2	Millipore: 07-6333	1:500
MESP1	Abcam: AB129387	1:100
ISL1	Abcam: AB86472	1:1000
AlexaFlour Goat Anti-Mouse 488	Invitrogen: A32723	1:1000
AlexaFlour Donkey Anti-Goat 488	Invitrogen: A11055	1:1000
AlexaFlour Goat Anti-Rat 647	Invitrogen: A21247	1:1000

2.4 Molecular biology techniques

2.4.1 Genomic DNA extraction

Extraction of genomic DNA from cells was performed using DNeasy Blood and Tissue Kit (Qiagen) following manufacturers protocol. Briefly, cells were pelleted at 300g for 5 minutes and resuspnded in 200µl PBS and 20µl of proteinase K was added to the cells. This suspension then had 200µl of Buffer AL added to it and was mixed by vortexing, this was then incubated at 56°C for 10 minutes. After this incubation 200µl of 100% ethanol was added to the suspension and this was mixed by vortexing. The solution was then all added to a DNeasy Mini Spin column placed in a 2ml collection tube and centrifuged at 6000g for 1 minute. The collection tube was then discarded and the column placed in a fresh one. To the column was

added 500µl of Buffer AW1 and the column was then centrifuged at 6000g for 1 minute. The collection tube was then discarded and the column placed in a fresh one. To the column was added 500µl of Buffer AW2 and the column was then centrifuged at 20,000g for 3 minutes. Finally the column was placed in a 2ml microcentrifuge tube and 50-100µl of molecular grade H_2O was added, this was then centrifuged at 6000g for 1 minute. DNA was then nanodropped to ascertain yield and quality.

2.4.2 Polymerase Chain Reaction (PCR)

Standard reaction mixes and thermal cycling conditions are detailed below. These protocols were used as standard but in some cases required optimisation to improve results. Primers used are stated in the relevant results section and were designed using Primer3 software and purchased from Sigma. Reactions were carried out using Phusion Polymerase (NEB).

Per Reaction:

Reagent	Volume
Phusion 10X Buffer	10µl
10mM dNTP mix	1µl
Forward Primer (10µM)	2.5µl
Reverse Primer (10µM)	2.5µl
Phusion Polymerase	0.5µl
Template DNA (100-200ng)	1µl
H_2O	32.5µl
Total	**50µl**

Thermal Cycling Conditions

Stage	Time	Temperature	
Initial Denaturation	**2 minutes**	**98°C**	
Denaturation	**30 seconds**	**98°C**	**35 Cycles**
Annealing	**30 seconds**	**55-65°C**	
Elongation	**60-90 seconds**	**72°C**	
Final Elongation	**10 minutes**	**72°C**	

2.4.3 Restriction digests

Restriction digests were carried out as diagnostic tools to ascertain that a plasmid contained the correct inserts. All enzymes used in this thesis were purchased from NEB. All incubations took place for 1 hour or overnight in an orbital incubator using the following reaction;

Component	Volume
10x Reaction buffer	1µl
Template	1µl
H_20	8µl
Total	10µl

Samples were analysed using DNA gel electrophoresis.

2.4.4 DNA gel electrophoresis

Agarose was dissolved in TAE buffer at an appropriate concentration depending on application, routinely this was between 1-2%. This was heated to dissolve the agarose and cooled slightly before the addition of Ethidium Bromide and the gel was then poured into an appropriate tray. Samples were mixed with 6x Blue loading dye (NEB) and ran at between 40-100V depending on band size and application. Samples were run alongside an appropriate DNA ladder, either 100bp or 1kb, (NEB). Bands were then visualised using Fujifilm LAS-1000CCD camera.

2.4.5 Gel extraction

Gel extractions were performed using Qiagen QIAquick Gel Extraction Kit (Qiagen; 28704) following manufacturer's guidelines. Briefly, to extract DNA from a gel the band was first cut out using a sharp scalpel and weighed. 3 volumes of Buffer QG were then added to 1 volume gel (100mg gel = 100µl). This was then incubated at 50°C for 10 minutes, vortexing every few minutes to aid dissolution. After this 1 gel volume of isopropanol was added and the suspension added to a QIAquick spin column with a provided 2ml collection tube. This was centrifuged at 17,900g for 1 minute. The flow-through was then discarded and 500µl of Buffer QG added and then centrifuged at 17,900g for 1 minute again. Flow-through was discarded and 750µl of PE Buffer added to the column which was centrifuged at 17,900g for 1 minute. The column was then placed in a fresh 1.5ml microcentrifuge tube and 20-50µl of molecular grade H_2O added, this was then centrifuged at 17,900g for 1 minute. Yield and quality of DNA extracted was analysed using nanodrop.

2.4.6 Transformation of competent bacteria

One Shot® TOP10 chemically competent *Escherichia coli* (*E. coli*) (Invitrogen, Life Technologies) were used as hosts in these experiments, and transformations were performed as per the manufacturer's protocols. Briefly, a vial of One Shot® was thawed on ice and 1-5µl of plasmid was added to the vial. This was then incubated on ice for 30 minutes. The bacteria were then heat shocked at 42°C in the waterbath for 30 seconds and then incubated in a bucket of ice water for 2 minutes. After this process 250µl of SOC medium was added and the bacteria were incubated at 37°C for 1 hour while shaking at 250rpm in an orbital incubator. This bacteria was then plated out onto prewarmed agar plates supplemented with the appropriate antibiotic and spread. These plates were then incubated at 37°C overnight. Bacterial colonies were then picked and grown overnight in 3ml Luria broth (LB) at 37°C. These plasmids were analysed using diagnostic digests and plasmid sequencing.

2.4.7 Small scale DNA preparation

Small scale DNA purification was carried out using Wizard® *Plus* SV Minipreps DNA Purification System (Promega) with 1-3ml of transformed *E. coli* from overnight culture in LB medium. Bacteria were harvested by centrifugation at 6,000g for 5 minutes. Cell pellets were then thoroughly resuspended in 250µl of Cell Resuspension Solution. To this, 250µl of Cell Lysis Solution was then added and the tube inverted 5 times to mix. 10µl of Alkaline Protease Solution was then added and the tube inverted 5 times, this was then incubated at room temperature for 5 minutes. After this incubation 350µl of Neutralisation Solution was added and this was inverted 5 times to mix the suspension before it was centrifuged at top speed for 10 minutes. The clear lysate from the spin was then decanted into a Spin Column and this was centrifuged at top speed for 1 minute. Flow-through was then discarded and 750µl of Wash Solution added to the column which was then centrifuged at top speed for 1 minute. This step was then repeated using 250µl of Wash Solution. The tube was then centrifuged again for 2 minutes at top speed to remove any residual solution in the column. The spin column was then transferred to a 1.5ml microcentrifuge tube and 100µl of molecular grade H_2O was added to the column, this was then centrifuged at top speed for 1 minute. The extracted plasmid was analysed using a nanodrop to determine quality and yield.

2.4.8 Large scale DNA preparation

Large scale DNA preparation as performed using NucleoBond® Xtra EF (Machery Nagel). Colonies were picked from agar plates and cultured overnight in 5ml of LB media. The following day 100µl of this was added to 100ml of fresh LB medium, containing the appropriate antibiotic and cultured overnight at 37°C in a shaking incubator. This 100ml was then centrifuged at 6000g for 10 minutes at 4°C. The resulting pellet was resuspended in 8ml of Buffer RES-EF, vortexing if necessary to ensure a thorough resuspension. To this suspension was added 8ml of Lysis Buffer and the tube was inverted 5 times to mix before being incubated at room temperature for 5 minutes. During this time a NucleoBond® Xtra Column with inserted filter was equilibrated with 15ml of equilibration buffer. After the 5 minutes incubation 8ml of Neutralisation Buffer was added to the tube which was then inverted 5 times to mix and incubated on ice for 5 minutes. The crude lysate was then added to the column filter and allowed to pass through by gravity, once this was complete, 5ml of filter wash buffer was added and allowed to pass through by gravity. After this step the filter was removed and 35ml of endotoxin free wash buffer is added and allowed to pass through the column by gravity. Once this step had been completed 15ml of wash solution was added to the column and this was allowed to pass using gravity flow. The column was then placed in a centrifuge tube and 5ml of elution buffer added. To this eluted plasmids was added 3.5ml of room temperature isopropanol and this mixture was thoroughly vortexed then centrifuged at 15,000g for 30 minutes. The supernatant was then removed and the pellet washed in 2ml of endotoxin free 70% ethanol before being centrifuged at 15,000g for 15 minutes. Supernatant was then removed and pellet allowed to air dry at room temperature. The pellet was then reconstituted in 100-200µl of endotoxin free H_2O. Analysis of the quality and yield of the plasmid was performed using a nanodrop.

2.4.9 PCR purification

PCR products were purified using QIAquick® PCR Purification Kit (QIAGEN) following manufacturer's protocol. Briefly, 5 volumes of PB buffer were added to 1 volume of PCR product and mixed. This was then added to a QIAquick column in a collection tube and centrifuged at 17,900g for 1 minute. Flow-through was then discarded and column placed back into the same tube, 750µl of Buffer PE was then added to the column and this was centrifuged at 17,900g for 1 minute. Flow-through and collection tube were then discarded and column was placed in a fresh 1.5ml microcentrifuge tube, 20-50µl of molecular grade H_2O

was then added to the column and this was centrifuged at 17,900g for 1 minute. The eluted DNA was then analysed for quality and yield using a nanodrop.

2.4.10 RNA extraction

Total RNA was extracted from hiPSC-CMs cells using the RNeasy Mini (QIAGEN: 74104) kits following the manufacturer recommended protocol. To ensure high yields of good quality RNA, first extraction was done on cell samples that were freshly harvested. RNA was eluted in 30µl of dH_2O, quantified using a NanoDrop ND1000 spectrophotometer and stored at -80^oC for future use. RNA was considered to be of adequate quality if it showed a single absorption peak at 260nm and if its A260/A280 value was between 1.8 and 2.2. All experiments included an RNA negative control to check for RNA/DNA contamination of the RNA extraction agents.

2.4.11 cDNA synthesis

cDNA was synthesised using the First Strand cDNA synthesis kit (GE Healthcare: 27-9261-01) following the manufacturer recommended protocol. Once reverse transcribed, the cDNA solution was made up to a final volume of 100µl in dH_2O, and stored at -20^oC for future use. All experiments included a cDNA negative control (no RNA template) and a Reverse Transcriptase - RT negative control (no reverse transcriptase enzyme). The former would help check for RNA/DNA contamination of the cDNA synthesis reagents while the latter would check for gDNA contamination of the RNA template.

2.5 CRISPR/Cas9 genome engineering

2.5.1 Oligonucleotide method

Transfection of cells with Cas9 RNP and oligos was carried out with a Nucleofector 4D (Lonza). A single cell suspension was prepared by harvesting cells using TrypLE (Thermo Fisher) as described in Section 2.1.3. An aliquot of the cell suspension was counted and $8x10^5$ cells were resuspended in of 100µl Amaxa P3 Primary Cell buffer (4D-Nucleofecter X Kit L; Lonza). Cas9 RNP was pre-assembled *in vitro* in a sterile tube by adding 2 µl recombinant Cas9 protein (10 µg/ul; ToolGen) to 2µl (7-10 µg/ul) of *in vitro* transcribed gRNA and incubated at room temperature for 10 minutes. After this 10 minute incubation, 6µl (500pmol in PBS) of ssODN, 4µl of Cas9 RNP, and 100µl of cells were mixed, transferred to a cuvette, and nucleofected according to the manufacturer's instructions (Lonza) using electroporation program CA-137.

The cells were then plated in to one well of a Matrigel coated 6-well plate in E8 medium supplemented with 10µM Y-27632. These cells were then incubated at 37°C and 5% CO_2 for 24 hours. After this the media was changed to E8 and 48 hours after nucleofection the cells were harvested for analysis and clonal expansion.

2.5.1.1 *In Vitro* RNA synthesis

To generate a purified gRNA, *in vitro* RNA synthesis was carried out as follows:

Initially a double stranded template was required, this was generated by the reaction shown below:

Component	Volume
Top Primer	10µl
Bottom Primer	10µl
X5 High Fidelity Phushion Buffer	20µl
10mM dNTPs	2µl
H_2O	57µl
Total	99µl

The above reaction was incubated at 96°C for 3 minutes, after this 1µl of Phusion polymerase was added to the tube and this was incubated at 72°C for 60 seconds. Following this the mixture was PCR purified and eluted in 100µl.

The *in vitro* reaction was performed according to the reaction shown below:

Component	Volume
T7 10X Reaction Buffer	2µl
T7 ATP Solution (75mM)	2µl
T7 CTP Solution (75mM)	2µl
T7 GTP Solution (75mM)	2µl
T7 UTP Solution (75mM)	2µl
Template DNA (From reaction above)	2µl
T7 Enzyme Mix	2µl
H_2O	6µl
Total	20µl

The reaction was then incubated for ~4 hours at 37°C after which 1µl of Turbo DNAse I was added to the tube which was then incubated at 37°C for a further 15 minutes. This was then purified on the Ambion Mega Columns per manufacturer's guidelines.

2.5.1.2 *In Vitro* test of Cas9 protein activity

Assessment of the activity of Cas9 protein was carried out as follows.

Component	Volume
Cas9 (500ng/µl)	1µl
gRNA (100ng/µl)	1µl
X10 NEB Reaction Buffer	2µl
H_2O	13µl
Total	17µl

The above reaction was then incubated at room temperature for 10 minutes to allow a complex to form of gRNA and Cas9 protein. To the above mix, 3µl of DNA template (~300ng) was added. This was then incubated at 37^{o}C for 1 hour. Analysis of this was carried out by gel electrophoresis.

2.5.2 PiggyBac transposon method

Targeting construct, Cas9 plasmid and gRNA plasmid were transfected into the hiPSCs using Amaxa 4D nucleofector. Plasmids were added at a ratio of 1:1:1 with 1µg of each being transfected into the cells. 1x10^{6} cells were harvested as described previously (Section 1.1.3) and resuspended in room temperature P3 buffer. This mix of cells in buffer was then added to a tube containing the plasmids and this was mixed before being added to a fresh Amaxa cuvette. Cells were then transfected using an optimised protocol and incubated in the cuvette at 37°C and 5% CO_2 for 5 minutes. Cells were then seeded into fresh 6 well plate with 2ml of prewarmed E8 medium containing 10µM Y27632. The following day medium was changed daily until the cells reached confluence. At this stage cells were split at a ratio of either 1:6 or 1:3 into a fresh 6 well plate and maintained for up to 48 hours. At this stage puromyocin selection began and cells were maintained in puromyocin (0.3µg/ml) for up to one week. During this time colonies began to emerge and these were then collected, mixed and added to a T25. These cells were then seeded at density of ~2x10^{5} per well of a 6 well plate. Medium was changed the following day and cells were then transfected with transposase plasmid using GeneJammer as a transfection reagent. These cells were then maintained in the 6 well plate for 3-4 days before being seeded at a density of ~2x10^{5} in a 6 well plate for Ganciclovir selection. Ganciclover selection was carried out for up to 4 days with 10nM added to the well. After this time hiPSCs were cultured in E8 medium and allowed to expand as clones before being picked and expanded for analysis.

2.5.2.1 Gibson assembly

The following sample mix, shown below, was prepared on ice.

Component	Volume
Total amount of fragments	0.2-1 pmols = Xµl
Gibson Assembly Mastermix	10µl
H_20	10 - X
Total	20µl

After this the samples were then held at 50°C for 60 minutes. At this stage samples were ready for transformation. It was also possible to store samples at -20°C at this stage.

2.5.2.2 Ligation of gRNA into gRNA plasmid

Two complementary oligonucleotides which contain the gRNA sequence were annealed together by mixing equimolar concentrations of each together and heating to 95°C for 5 minutes in a heat block. The tube was then allowed to cool to room temperature overnight. The product was then ligated into a pU6 plasmid via sticky end ligation. The pU6 plasmid was digested using BsaI and this was purified from an agarose gel after gel electrophoresis. The annealed product with overhangs complementary to the pU6 plasmid was ligated in by the reaction described below:

Component	Volume
10x T4 Buffer	2µl
pU6 Plasmid (25µg)	4.2µl
Insert (45µg)	12.8µl
T4 Ligase	1µl
H_2O	6µl
Total	20µl

The above reaction was incubated at room temperature for 2 hours before being heat inactivated at 65°C for 10 minutes. At this stage the plasmid is ready for transformation.

2.6 CellOPTIQ assays

2.6.1 Voltage based assay

hiPSC-CMs were seeded into Matrigel coated 96-well plates at a density of $5x10^5$ cells per well. These hiPSC-CMs were then incubated at 37°C and 5% CO_2 for 48 hours to allow cells to

recover. In order to image the voltage properties of the hiPSC-CMs they were dyed using FluoVolt (Thermo Fisher; F10488). Media was removed from wells and serum free media (SFM), the components of which are found in Table 2.1, containing FluoVolt (PartB: 5µl /ml, PartA: 0.5µl /ml) was added, these cells were incubated at 37°C and 5% CO_2 for 30 minutes. After the 30 minute incubation medium was removed and the hiPSC-CMs washed once with serum free medium before 100µl of fresh SFM was added to wells. These plates were then incubated at 37°C and 5% CO_2 for 15 minutes to allow the hiPSC-CMs to equilibrate. At this stage cells could then be visualised. For drug treatment a basal recording was taken before 20 µl of drug added to the well, all drugs were dissolved in DMSO and added to the cells with a 0.1% DMSO concentration. After this addition the hiPSC-CMs were incubated at 37°C and 5% CO_2 for 30 minutes before a second measurement was taken.

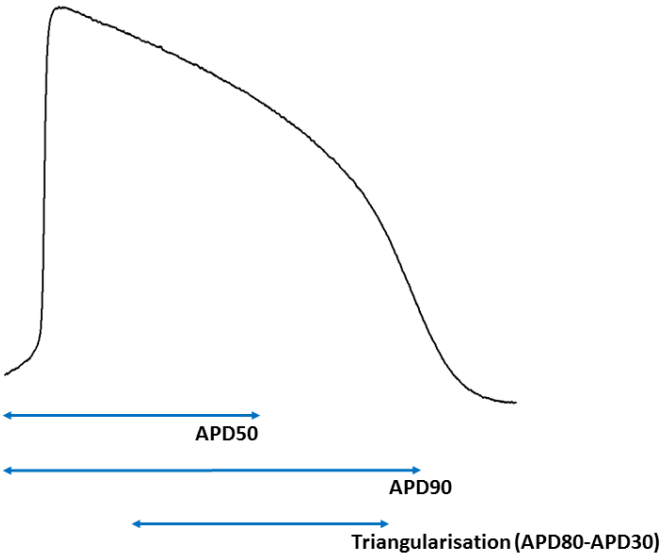


Figure 2-1 - Parameters assessed in voltage traces
Representative action potential trace which highlights the parameters assessed in this thesis

To assess the voltage properties of the hiPSC-CMs in this thesis three key parameters were assessed (Figure 2.1). The first was APD50 which accounts for the time taken for the action potential to reach 50% of its duration, the second was APD90 which accounts for the APD to reach 90% of its length. APD50 allows investigation of the initial repolarisation or phase 2 of the APD while APD90 allows investigation of the second stage of repolarisation and corresponds to phase 3 of the action potential. The final parameter assessed is repolarisation time which is the APD80-APD30, this is a measure of the time taken for the cell to repolarise

and covers the time when both I_{ks} and I_{kr} will be dominant in repolarising the cardiomyocyte. A list of the drugs used in these assays is shown in Table 2.3. Traces are normalised within the CellOPTIQ software.

2.6.2 Calcium based assay

hiPSC-CMs were seeded into Matrigel coated 96-well plates at a density of $5x10^5$ cells per well. These hiPSC-CMs were then incubated at 37°C and 5% CO_2 for 48 hours to allow cells to recover. In order to image the voltage properties of the hiPSC-CMs they were dyed using Fura2-AM (Thermo Fisher; F1201). Media was removed from wells and serum free media containing 4µM Fura2-AM was added, these cells were incubated at 37°C and 5% CO_2 for 30 minutes. After the 30 minute incubation medium was removed and the hiPSC-CMs washed once with serum free medium before 100µl of fresh SFM was added to wells. These plates were then incubated at 37°C and 5% CO_2 for 15 minutes to allow the hiPSC-CMs to equilibrate. At this stage cells can then be visualised. For drug treatment a basal recording was taken before 20 µl of drug added to the well, all drugs were dissolved in DMSO and added to the cells with a 0.1% DMSO concentration. After this addition the hiPSC-CMs were incubated at 37°C and 5% CO_2 for 30 minutes before a second measurement was taken.

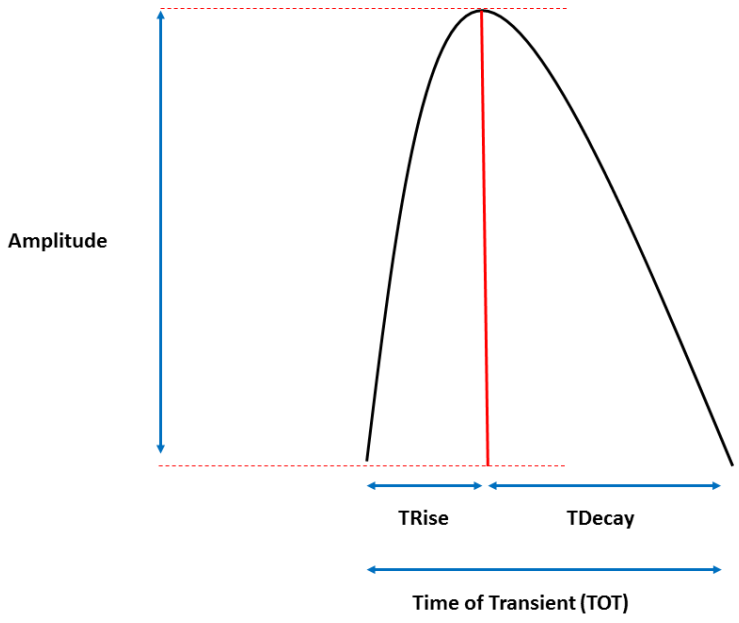


Figure 2-2 - Parameters assessed in calcium traces
Representative calcium transient trace which highlights the parameters assessed in this thesis

To assess the calcium handling properties of hiPSC-CMs in this thesis four different parameters were assessed (Figure 2.2). The first is TRise which accounts for the time it takes for the

transient to reach its peak, here the two key factors are the calcium influx through the LTCC and efflux from the SR into the intracellular space. The second parameter is TDecay this is the time for the calcium to be extruded from the intracellular space either by the NCX or taken back into the SR by the SERCA pump. The third parameter is the time of transient (TOT) this is the time for the whole process to occur. The final parameter to be assessed is amplitude, the amplitude demonstrates the amount of calcium in each transient. A list of the drugs used in these assays is shown in Table 2.3. Traces are normalised within the CellOPTIQ software.

2.7 Statistical analysis

All statistical analyses carried out within this thesis were performed using Graphpad Prism software. All numbers are displayed as mean ± standard deviation, unless otherwise stated. Details of statistical tests carried out are reported in the relevant sections. Statistical significance is represented by stars. Four stars denotes $p<0.0001$, three stars denotes $p<0.001$ but not <0.0001, two stars denotes $p<0.01$ but not <0.001 and one star denotes $p<0.05$ but not <0.01. Electrophysiological data and calcium transient data are disaplyed as box and whisker plots as shown in Figure 2.3.

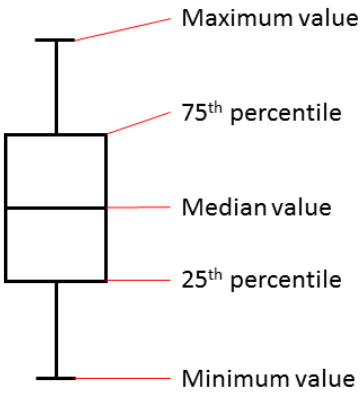


Figure 2-3 - Box and whisker plot
Box and whisker plot showing the median value along with the upper and lower percentiles. This graph also displays the minimum and maximum value. This plot shows the dispersion and skewness over the data.

Table 2-3 - Drug table

Drug	Supplier	Product Code	Dissolved in:
Ryanodine	Tocris	1329	DMSO
Thapsigargin	Sigma	T9033-1MG	DMSO
Xestospongin C	Tocris	1280	DMSO
ORM-10103	Sigma	SML0972-5MG	DMSO
Telmisartan	Sigma	T8949-10MG	DMSO
GW0742	Sigma	G3295-5MG	DMSO
NS1643	Sigma	N0663-5MG	DMSO
Ginsenoside RG3	Sigma	SML0184-5MG	DMSO
ML277	Sigma	SML0524-5MG	DMSO
Minoxidil	Sigma	M4145-100MG	DMSO
Nicorandil	Sigma	N3539-50MG	DMSO
Isoprenaline	Sigma	I5627-100G	H_2O

3 Chapter 3 – Generation and characterisation of hiPSC-and their differentiation to cardiomyocytes

3.1 Introduction

To achieve the aims of this project tissue samples from patients with cardiac channelopathies were obtained. These samples were then reprogrammed to hiPSCs by reactivation of cells' endogenous pluripotency using plasmids or viral vectors to introduce pluripotency genes. These hiPSCs would then be differentiated to cardiomyocytes and ultimately used as tools to study the patient's phenotype *in vitro* using both voltage and calcium sensitive fluorescent dyes. This chapter describes the process of selecting the most appropriate method of both generating hiPSCs and differentiating these to cardiomyocytes.

3.1.1 Identifying a starting cell population for hiPSC generation

3.1.1.1 Fibroblasts

Fibroblasts are routinely used to generate hiPSCs as a result of their robustness and ease of use in cell culture (Park et al, 2008). Furthermore they are amenable to genetic modification as illustrated by experiments which reprogrammed both murine and human fibroblasts using somatic cell nuclear transfer and cell fusion techniques (Wakayama et al, 1998; Cowan et al, 2005). Skin samples are able to be harvested by skin punch biopsy or by the removal of excess skin during a surgical procedure such as the implantation of a pacemaker. Skin samples can be stored at 4^{o}C in physiologically buffered saline for up to two weeks (Dambrot et al, 2013). However, although obtaining a sample during surgery is possible most skin samples are still collected by punch biopsy. This is an invasive procedure which can be painful potentially dissuading patients from providing a sample (Lai et al, 2011). Therefore in this thesis, cells isolated from teeth, blood and urine were tested as potential alternative starting samples. A more thorough list of alternative starting samples reported in the literature can be found in Table 3.1.

3.1.1.2 Teeth

Dental pulp from teeth and gingival tissue from the gum represent a promising cell source for reprogramming with reported efficiencies of between 0.002 - 0.1% when reprogrammed using

a lentiviral vector system (Yan et al, 2010). Milk teeth naturally fall out during childhood with most children having all their adult teeth by age 12-14 according to the American Dental Association. Teenagers commonly have adult teeth removed due to overcrowding in the mouth and adults may undergo extraction if a wisdom teeth has become impacted. When extraction is performed some gum may remain attached to the tooth which has previously been successfully used for iPSC generation using both murine (Egusa et al, 2010) and human samples (Wada et al 2010). In this thesis no gingival tissue was made available after tooth extraction.

3.1.1.3 Blood

Blood has previously provided cells amenable to reprogramming with an efficiency of 0.002-0.005% when using retroviral vectors (Meng et al, 2012). Blood samples can be obtained from both patients and blood banks. It has been reported that hiPSCs can be generated from $CD34^+$ haematopoietic progenitor cells (HPCs) which are found in both mobilised and non-mobilised blood (Loh et al, 2009; Ye et al, 2009). However there is a relatively rarity of HPCs, estimated to be only several hundred per ml of blood, in non-mobilised peripheral blood (Saito et al, 2006). In order to boost this number granulocyte-colony stimulating factor (G-CSF) can be injected into the patient prior to blood sample collection, however this has been reported to have potentially detrimental effects to the patient (Anderlini et al, 2009). Endothelial progenitor cells (EPC) represent a potentially more accessible cell type found readily in the blood with little manipulation required and these have been reported to be amenable to reprogramming using a retroviral vector system with an efficiency of 0.22% (Geti et al, 2012).

3.1.1.4 Urine

Urine sample collection is a simple process which takes advantage of a naturally occurring and necessary bodily function. Multiple cell types have previously been identified in urine, such as: urothelial cells (Rahmoune et al, 2005), epithelial like cells (Dörrenhaus et al, 2000) and a subpopulation of urinary cells which exhibit multidifferentiation potential (Zhang et al, 2008). One potential drawback of using urine as a starting sample is the scarcity of cells present within it as only 2,000-7,000 cells are reported to be extruded in the urine daily (Rahmoune et al, 2005). Cells which have been isolated from urinary samples have been shown to be

amenable to reprogramming with efficiencies between 0.1 - 4% when using retroviral vectors (Zhou et al 2011).

Therefore we sought to establish cell cultures from skin, teeth, blood and urine samples in order to derive starting cell populations which would provide us with the resources to produce hiPSCs.

Table 3-1 - - List of different cell types used to generate hiPSCs

Cell Source	Method Used	Factors Delivered	Reprogramming Efficiency
Fibroblasts	Sendai virus Retrovirus Lentivirus	OCT3/4, SOX2, KLF4 and C-MYC (OKSM) or OKS OCT3/4, SOX2, LIN28 and NANOG (OSLN)	1% (Fusaki et al, 2009) 0.001-0.01% (Takahashi et al, 2007) 0.01-0.1% (Yu et al, 2007)
Keratinocytes	Retrovirus	OKSM or OKS	1% (Aasen et al, 2008)
Renal epithelial cells	Retrovirus	OKSM	0.1-4% (Zhou et al, 2011)
CD34+ Blood Cells	Lentivirus	OS	2% (Meng et al, 2012)
Umbilical cord blood cells	Inducible lentivirus	OKSM	0.1% (Wang et al, 2013)
Peripheral mononuclear blood cells	Sendai virus Sendai virus	OKSM OKSM	Not reported (Cardano et al, 2016) Not reported (Marcatili et al, 2016)
Adipocytes	Episomal reprogramming	OKSM	0.006% (Qu et al, 2012)
Nasal epithelial cells	Sendai virus	OKSM	0.1% (Ono et al, 2012)
Dental pulp cells	Lentivirus	OKSM/OSLN	0.1% (Yan et al, 2010)
Marrow mesenchymal cell	Retrovirus	OKSM or OK	Not reported (Park et al, 2008)
Hepatocyte	Retrovirus	OKSM	0.1-0.2% (Liu et al, 2010)
Urine derived cells	Sendai virus Sendai virus	OKSM OKSM	Not reported (Afzal et al, 2016) Not reported (Sochacki et al, 2016)
Lymphocytes	Sendai virus	OKSM	Not reported (Saito et al, 2016)
Blood erythroid cells	Episomal reprogramming	OKSM and BCL2L.1	Not reported (Bhatt et al, 2016)
Lymphoblast	Episomal reprogramming	OSLN L-MYC p53 shRNA	Not reported (Schroter et al, 2016)
Lymphoblastoid cell lines	Episomal reprogramming	OCT3/4, SOX2, KLF4, L-MYC, LIN28 and murine p53DD	0.005-0.02% (Kumar et al, 2016)

OKSM = OCT3/4, KLF4, SOX2 and C-MYC
OSLN = OCT3/4, SOX2, LIN28 and NANOG

3.1.2 Choosing a non-integrative reprogramming strategy for hiPSC generation

The initial reports of hiPSCs generation used integrating retroviruses (Takahashi et al, 2007) and lentiviruses (Yu et al, 2007; Blelloch et al, 2007). However in order to progress the field towards clinical- or GMP-grade hiPSCs there remains a necessity to minimise the risk of integration of reprogramming transgenes. Various techniques have since been tested including: non-integrative adenoviral vectors (Stadtfeld et al, 2008b), excisable viral cassettes (Soldner et al, 2009; Yusa et al, 2009), episomal vectors (Yu et al, 2009; Okita et al, 2011), Sendai virus (Fusaki et al, 2009; Ban et al, 2011) and the direct delivery of either RNA (Warren et al, 2010) or protein (Zhou et al, 2009). A list of reprogramming strategies can be seen in Table 3.2. Most non-integrative techniques exhibit reprogramming efficiency rates of ~0.0001-0.001% which are up to 1000 fold lower than the more successful integrative methods. However two non-integrative methods which exhibited potential to be used as replacements for integrating methods were; Sendai virus which was reported to yield reprogramming efficiencies of up to 1% (Fusaki et al, 2009) and episomal plasmid reprogramming which was reported to be able to achieve ~0.028% reprogramming efficiency (Okita et al, 2011). Therefore in this project both of these methods were tested to ascertain their robustness for routine use to generate hiPSCs.

Table 3-2 - List of different reprogramming methods used to generate hiPSCs

Method	Efficiency	Advantages	Limitations	References
Retrovirus	0.001-4%	• Moderate efficiency	• Can only infect dividing cells	(Takahashi et al, 2007; Park et al, 2008; Zhou et al, 2011)
Lentivirus	0.01-0.1%	• Can infect dividing and non-dividing cells • Inducible/excisable	• Tumorigenic • Transgene silencing can be incomplete	(Yu et al, 2007; Ebert et al, 2009; Sommer et al, 2009; Sommer et al, 2010)
Zinc Finger Nucleases	0.02%	• Targeted integration	• Genomic integration	(Ramalingham et al, 2013)
Adenovirus	0.0001-0.0018%	• Non-integrative	• Large vector size to deliver	(Stadtfeld et al, 2008b; Okita et al, 2008; Zhou and Freed, 2009; Weltner et al, 2012)
Episomal Plasmid	0.0003-0.028%	• Replicates in episome • Non-integrative	• Low efficiency • Potential for integration	(Yu et al, 2009; Okita et al, 2011)
Sendai Virus	0.01-1%	• RNA based • Non-integrative	• Expensive	(Fusaki et al, 2009; MacArthur et al, 2012)
Purified Protein	0.001%	• DNA-free • Non-integrative	• Repeated and long term transfections • Low efficiency	(Zhou et al, 2009; Kim et al, 2009a)
RNA delivery	0.2%	• DNA-free • Non-integrative	• Repeated and long term transfections • Need to suppress cells innate immune response.	(Warren et al, 2010)
Minicircle DNA	0.005%	• Small constructs • Xeno free • Non-integrative	• Requires multiple transfections	(Narsinh et al, 2011)

3.1.2.1 Sendai virus

Sendai virus replicates in the cytoplasm and therefore is unable to integrate into the host's genome (Li et al, 2000). Sendai virus has been shown to be non-pathogenic to humans and able to infect a broad range of hosts (MacArthur et al, 2012). F-protein deficient Sendai virus vectors were developed to reduce cytotoxicity and prevent replication of the virus while still generating high level of exogenous gene expression (Li et al, 2000). In this thesis Sendai viral vectors were obtained as a commercially available kit (Thermo Fisher) which were produced using previously published protocols (Fusaki et al, 2009; Ban et al, 2011). The CytoTune2.0 kit (Thermo Fisher) contains three separate vectors termed; KOS, hC-MYC and hKLF4, details of these vectors can be found in Table 3.3. Briefly, the kit contains a polycistronic vector expressing OCT3/4, SOX2 and KLF4 as well as two other vectors which each express C-MYC and KLF4. The presence of the third vector containing KLF4 is to compensate for the potentially lower expression of KLF4 in the polycistronic vector as it is the third gene to be expressed (Mizuguchi et al, 2000).

Table 3-3 - Sendai virus vectors used to generate hiPSCs

Vector	Factor	GenBank ID
CytoTune 2.0 KOS	Human Klf4 Human Oct3/4 Human Sox2	BC029923.1 NM_002701.4 NM_003106.2
CytoTune 2.0 hc-Myc	Human c-Myc	K02276.1
CytoTune 2.0 hKlf4	Human Klf4	BC029923.1

3.1.2.2 Episomal plasmids

Initial reports of episomal reprogramming to hiPSCs using oriP/EBNA-1 episomal vectors which expressed OCT4, SOX2, NANOG, LIN28, c-Myc, KLF4, and SV40LT yielded efficiencies of between 0.0003-0.0006% (Yu et al, 2009). Improvement of this method with a cocktail of small molecules detailed in Section 1.3.6.2 improved the efficiency of reprogramming to 0.0021%, representing ~70 fold increase on the initial method (Yu et al, 2011).

It was reported that a knockdown of p53 could improve the efficiency of hiPSC generation by up to 100 fold (Zhao et al, 2008). Subsequently it was reported that the introduction of TP53 shRNA to episomal plasmids was able to improve reprogramming efficiency up to 0.028% (Okita et al, 2011).

As a result of this it was decided in this project to use the episomal plasmids used in Okita and colleagues report from 2011 as these had given the highest reported efficiency of reprogramming.

3.1.2.3 Peptide mediated reprograming

Generation of hiPSCs using purified proteins with CPPs is described in Section 1.3.6.4. Delivery of biologically active cargo using CPPs can mean delivering vast quantities of peptide with exceptionally high charge, this in turn can cause cytotoxicity (Dixon et al, 2015). By fusing a membrane-docking peptide to heparin sulfate glycosaminoglycans (GAGs) with a protein transduction domain (PTD) Dixon et al reported the creation of the GAG-binding enhanced transduction (GET) system. Initial characterisation of this system showed that it was able to synergistically improve the efficiency of PTD-tagged biologically active cargo delivery (Dixon et al, 2015). Furthermore it was demonstrated that this GET system was able to deliver pSIN GFP plasmid to human mesenchymal stem cells at an efficiency >60%, comparable with delivery using lipofectamine 2000 (Dixon et al, 2015). The GET system was demonstrated to be able to deliver NANOG to mESCs cultured in the absence of LIF, by rescuing the cells pluripotent phenotype (Dixon, et al, 2015).

Initial tests in our lab were unable to generate hiPSCs using the GET peptide system to deliver purified proteins. However due to the extensive range of cargo delivered previously using the system including; enzymes, transcriptions factors, magnetic nanoparticles and nucleic acids (Dixon et al, 2015) it was decided to test the efficiency of the system in delivering episomal plasmids to somatic cells in order to induce reprogramming.

3.1.2.4 Feeder and xeno free reprogramming

This thesis sought to demonstrate a more defined methodology by adopting a feeder and xeno free reprogramming approach, such approaches have been shown to reduce efficiency of reprogramming to between 0.01-0.04% when using Sendai virus (MacArthur et al, 2012). MEF feeder layers are often used during reprogramming as they are the substrate which generates the greatest efficiency irrespective of reprogramming method (MacArthur et al, 2012). However, due to their undefined nature using MEF feeder layers represents a risk of contamination within the culture, particularly of mycoplasma which can affect cellular growth, phenotype and karyotype (Villa-Diaz et al, 2013). In addition to this the use of xenogenic

components in hPSC culture hinders the ability to use hPSCs in the treatment of conditions in humans (Villa-Diaz et al, 2013).

Therefore in this thesis vitronectin-peptide was used as a substrate during the reprogramming process and commercially available defined and xeno-free Essential 6 and Essential 8 media were used to maintain the cells. However as these cells were purely generated for *in vitro* analysis Matrigel was routinely used as a substrate during standard hiPSC culture after the reprogramming process was complete.

3.1.3 Choosing a method to differentiate hiPSCs to cardiomyocytes

Differentiation of hPSCs to generate cardiomyocytes *in vitro* was described in Section 1.4.2. Differentiation of hPSCs can be performed using embryoid body (EB) formation, using techniques such "forced aggregation" and has been demonstrated to be capable of generating cardiomyocytes at efficiencies of up to 64-89% across multiple hESC and hiPSC lines (Burridge et al, 2011b).

An alternative method of generating cardiomyocytes from hPSCs is monolayer directed differentiation which removes the complex diffusional barriers present in EBs and also saves time as it does not require multiple replating steps (Mummery et al, 2012). Furthermore monolayer differentiation has been shown to increase the number of cardiomyocytes generated per input cell compared to EB formation (Burridge et al, 2007; Burridge et al, 2014). In addition to the increased yields reported for this monolayer method there was also an increase in overall culture purity with reported efficiencies of 80-95% for all cell lines tested (Burridge et al. 2014). Therefore it has been demonstrated that monolayer directed differentiation can increase yield, reduce labour time whilst producing high purity cardiomyocytes.

Bioreactor culture has been investigated for generation of hiPSC-CMs at very high yields for clinical applications. Some initial concerns regarding this methodology were that cells are likely to aggregate in suspension preventing homogenous diffusion of nutrients and growth factors in addition to gradients of temperature and growth factors. (Azarin and Palecek, 2010). However bioreactor differentiation has more recently been reported to be capable of producing ~$8x10^7$ cells with a reported purity for cTnT of 80% from a starting population of $2x10^7$ hiPSCs, representing 3.2 cardiomyocytes for every 1 input hiPSC (Matsuura et al, 2012). Further improvements have recently led to a study reporting 100% beating cardiac spheroids

at purity of ~90% in only 10 days, this study reported an input of $2x10^7$ cells but did not specify yield (Fonoudi et al, 2015). More recent reports of spinner culture flasks have indicated that yields as high as $2x10^9$ can be achieved when differentiations are performed in a suspension culture (Chen et al, 2015). Therefore along with monolayer differentiation, bioreactor culture represents an attractive source for scalable production of cardiomyocytes.

As a result of this it was decided in this project to test different monolayer methods to ascertain which would reliably and robustly differentiate our hiPSCs to cardiomyocytes. The first method that was tested in this project for monolayer cardiomyocyte differentiation was an in-house developed method termed ABKYX, named due its use of Activin A and BMP4 in the initial differentiation step before using KY02111 and XAV939 in the second step, a timeline of its key steps can be found in Figure 3.1. This method begins with a BMP4 preconditioning step and a Matrigel overlay which has been shown to improve cardiomyocyte differentiation by enhancing epithelial to mesenchymal transition (EMT) (Zhang et al, 2012). Differentiation is initiated by the growth factors BMP4 and Activin A which drive mesoderm specification by activation of the Wnt signalling pathway (Xu et al, 2011). The second stage of cardiac differentiation is to pattern the mesoderm towards cardiac mesoderm, in the ABKYX method this is achieved by inhibiting the Wnt pathway using two small molecules, KY02111 and XAV939 (Minami et al, 2012; Wang et al, 2011). This block of the Wnt pathway is maintained for 96 hours, initially in the absence of insulin before being performed in the presence of insulin. This is performed as insulin has been demonstrated to prevent cardiomyocyte formation between day 2-4 of differentiation (Burridge et al, 2011).

The second method tested in this project was the CDM-CW method developed in Stanford and published in 2014 (Burridge et al, 2014). This method uses a more defined culture medium, CDM3, which only contains RPMI, rhalbumin and ascorbic acid. This stripped down nature of the culture medium is thought to result in less interfering factors during the differentiation process (Burridge et al, 2014). This method applies the same principles as the ABKYX method by seeking to activate the Wnt signalling pathway before inhibiting the pathway later in the process to pattern the cells to cardiac mesoderm. CDM-CW achieves this by activating the Wnt signalling pathway using the small molecule CHIR99021, a GSK3B inhibitor. This activation is maintained for the initial 48 hours before the Wnt signalling pathway is blocked using the small molecule Wnt-C59, this block is maintained for the subsequent 48 hours. After this the cells are maintained in CDM3 medium for routine maintenance.

Two hybrid methods of these cardiac differentiation protocols were also tested. As a result of the cost associated with the ABKYX method alternatives were sought which aimed to make use of the procedures used in the CDM-CW method. Both Hybrid methods sought to incorporate the preconditioning step from ABKYX to improve the robustness of the CDM-CW protocol. Initially this preconditioning was performed in E8 medium and latterly it was tested in CDM3.

The aim of testing these methods was to ascertain which was able to achieve the greatest robustness in generating high purity cardiomyocyte cultures reproducibly both across the same cell line and multiple cell lines in our lab.

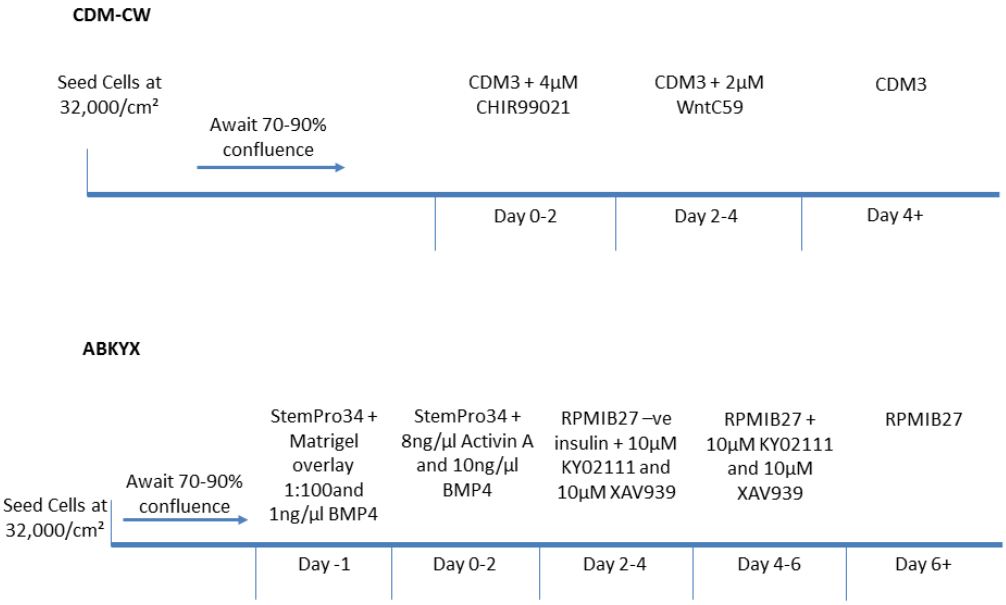


Figure 3-1 - Schematic representation of the two main differentiation methods tested

Figure showing the key steps involved in cardiac differentiation using the two main methods tested. The CDM-CW method features the addition of small molecules at day 0 and day 2 before longer term maintenance is performed in defined and xeno free CDM3 medium. The ABKYX method requires an initial preconditioning step with BMP4 and a Matrigel overlay before addition of growth factors, BMP4 and Activin A, at day 0. On day 2 two small molecules, KY02111 and XAV939, are added in the absence of insulin. On day 4 KY02111 and XAV939 are added in the presence of insulin. After Day 6 the cells are maintained in RMPIB27

3.1.4 Chapter aims and objectives

The aim of this chapter was to ascertain the most reliable starting sample type which would enable the isolation of somatic cells from patients for use in reprogramming to hiPSCs. Secondly after the establishment of a preferred starting sample and cell type three different

methods of hiPSC generation would be tested to ascertain which most reliably produced hiPSCs in our lab. From this these hiPSCs would then be differentiated to cardiomyocytes in order to use them in downstream assays to ascertain the patient's phenotype *in vitro*. For this to be successful it would first be necessary to establish which differentiation method worked most reliably and efficiently in our hands to generate cardiomyocytes of high purity across multiple cell lines. To achieve these aims the following objectives had to be met:

1. Obtain donor or patient skin, teeth, blood and urine samples and attempt to isolate cells from these.
2. Test the efficiency and stability of reprogramming using Sendai virus and episomal reprogramming both via electroporation and via the GET peptide delivery system.
3. Assess the quality of the produced hiPSC lines generated using Sendai virus and compare these against previous lentiviral produced lines made in our lab.
4. Assess the efficiency and reproducibility of the CDM-CW and ABKYX differentiation methods to ascertain which method more reliably generated cardiomyocytes of a high purity across multiple cell lines.

3.2 Results

3.2.1 Generating hiPSCs using previously established methods

In order to assess the effectiveness and robustness of any new hiPSC generating protocol it was first required that a control method was established. Use of lentivirus containing the Thomson factors; OCT4, SOX2, NANOG and LIN28 (termed OSNL), was the previously established method in our lab. This approach had been used to reprogram skin fibroblasts from Duchenne muscular dystrophy (DMD) (Dick et al, 2013) and Long QT Syndrome (LQTS) patients (Matsa et al, 2011). In these instances fibroblast-like cells, derived by differentiating the hESC line HUES7, were used as an 'easy to reprogram' control sample. These cells were termed Hfib and were reprogrammed with lentiviral OSNL to demonstrate hiPSC colonies could be successfully produced both in my hands and with the reagents available in the lab when I started my PhD.

This process entailed transducing Hfib cells with streptavidin-conjugated viral particles in the presence of polybrene at an MOI of 10 as detailed previously (Dick et al, 2013). These cells were then replated in MEF conditioned medium supplemented with FGF at 48 hours post transduction onto mitomycin-C inactivated MEF feeder layers. Medium changes were performed daily until day 25-30. The result, which can be seen in Figure 3.2, was that over a 25 day period colonies of hiPSCs emerged within the culture, these were characterised by defined cell borders, high cytoplasm to nucleus ratio and a loss of the spindle-like morphology typical of fibroblasts. The developing hiPSCs were isolated using MACS with TRA-1-81 as a marker for pluripotency, they were passaged using 0.05% trypsin and were subjected to basic pluripotency assessment after 10 passages. This showed that the derived Hfib-hiPSC-Lenti line displayed the morphology typical of pluripotent cells. In Figure 3.2 the cultures were stained for LIN28, REX1, SSEA4 and TRA-1-81; the more typical pluripotency markers OCT4, NANOG and SOX2 were not used as these were encoded by the lentiviral vectors and it has been shown that transgene expression can persist in hiPSC using this approach (Park et al, 2008).

Finally *in vitro* differentiation capacity was assessed by inducing embryoid body (EB) formation by aggregating 3,000-10,000 cells per well into V-bottom 96-well plates. These EBs were transferred to U-bottom plates on day 10 at a density of 1 EB per well. On day 30 these EBs were then fixed and stained for markers of all three germ layers. This staining demonstrated that portions of the EBs expressed alpha fetoprotein (AFP), α-actinin and β-III-tubulin which are representative for endoderm, mesoderm and ectoderm germlayers respectively (Abe et

al, 1996; Garcia et al, 2006; Dráberová et al, 2008). The results of this staining can be found in Figure 3.2.

Therefore this demonstrated that in my hands, HUES7 derived fibroblast-like cells could be used as a positive control for hiPSC reprogramming and were adopted in future tests described in this chapter for comparable pluripotency analysis.

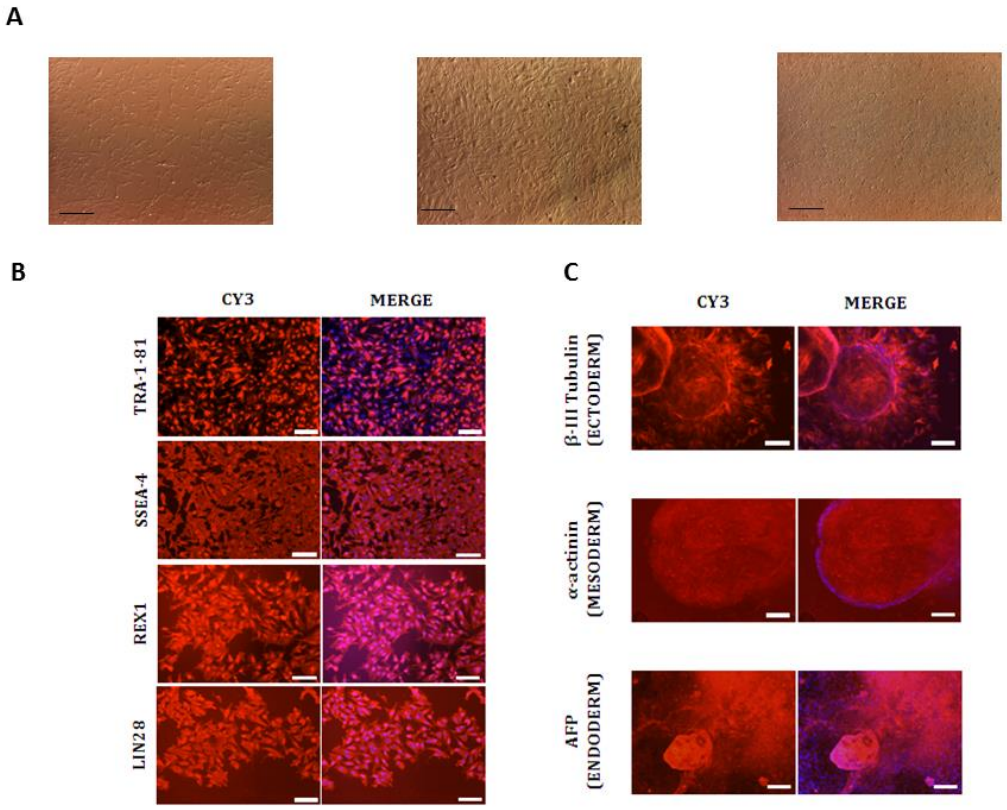


Figure 3-2 Generating hiPSC lines using lentivirus as a delivery mechanism

A – Brightfield images through the reprogramming process starting with Hfib (left), Hfib 13 days after transduction (Centre) and purified Hfib-hiPSC-Lenti line cultured in MEF conditioned medium (right). B – Pluripotency quantification of lentiviral derived hiPSC lines. Images show cells are expressing the markers TRA-1-81, SSEA4, REX1 and LIN28 which are all markers indicative of pluripotency. Images on the left show CY3 staining and images on the right show CY3 merged with DAPI to stain for nuclei. C – Analysis of true pluripotency to show that this lentiviral derived Hfib-hiPSC-Lenti line is able to differentiate to all three germ layers. This image shows that the cells express β-III-Tubulin which is a marker of ectoderm (top), α-actinin which is a marker of mesoderm (middle) and AFP which is a marker indicative of endoderm formation (bottom). The images on the left hand side show CY3 staining for the markers in question while the images on the right side show CY3 staining merged with DAPI to identify nuclei. All scale bars represent 100µm. Pluripotency analysis in this figure was performed by Dr Divya Mirrington.

3.2.2 Establishing the efficiency of transduction and reprogramming using non-integrative methods

The transduction of Sendai virus into fibroblasts had not previously been tested in our lab. There have been some concerns of cytotoxicity during transduction with Sendai virus vectors (Beers et al, 2015). Therefore a Sendai viral vector expressing GFP was used to test the efficiency of transduction and to monitor the cell growth over a 72 hour period to ascertain any toxicity. Three fibroblasts cell lines; WeBr (LQT1), ReBl (LQT2) and SaDe (LQT1), were transduced with commercially available Sendai viral GFP vector at an MOI of 5. A list of lines used and generated in this thesis can be found in Table 3.4. This was transduced into $2x10^5$ cells which were incubated at 37°C for 24 hours. Fluorescent image recordings were taken at 24, 48 and 72 hours for GFP and for hoescht live cell stain, the results of which can be seen in Figure 3.3. Percentage of cells expressing GFP was shown to be 15.09±3.79% at 24 hours, 43.77±5.58% at 48 hours and 50.28±4.96% at 72 hours. This accounts for a significant increase between 24 and 48 hours ($p<0.05$, n=3, paired t test) however the increase between 48 and 72 hours was not found to be significant ($p=0.23$, n=3, paired t test), these data are displayed in Figure 3.3. The total number of cells was found to increase by 17.66±15.54% from 24 to 48 hours, this was not found to be significant ($p=0.32$, n=3, paired t test). The total cell number was found to decrease by 3.44±2.96% from 48 to 72 hours, this was also not found to be significant ($p=0.09$, n=3, paired t test). These data indicate that Sendai virus can transduce cells to a high efficiency and does not appear to exhibit any serious cytotoxic effects based on viral backbone

Table 3-4 - List of patient samples reprogrammed during this study

Cell Line	Gender	Disease State	Gene	Mutation	AA Change
PhiCr	F	LQTS1	KCNQ1	C1986G	Tyr662X
SaDe	F	LQTS1	KCNQ1	G686A	Gly229Asp
ReBl	F	LQTS2	KCNH2	G1681A	Ala561Thr
ZoTh	F	LQTS1 LQTS2	KCNH2 KCNQ1	E130K A341E	Glu44Lys Ala114Glu
CP1	M	CPVT	RYR2	C6737T	Ser2246Leu
ReBl MAT	F	Asymptomatic carrier	KCNH2	G1681A	Ala561Thr
ReBl PAT	M	Healthy	N/A	N/A	N/A
BT2	F	Healthy	N/A	N/A	N/A

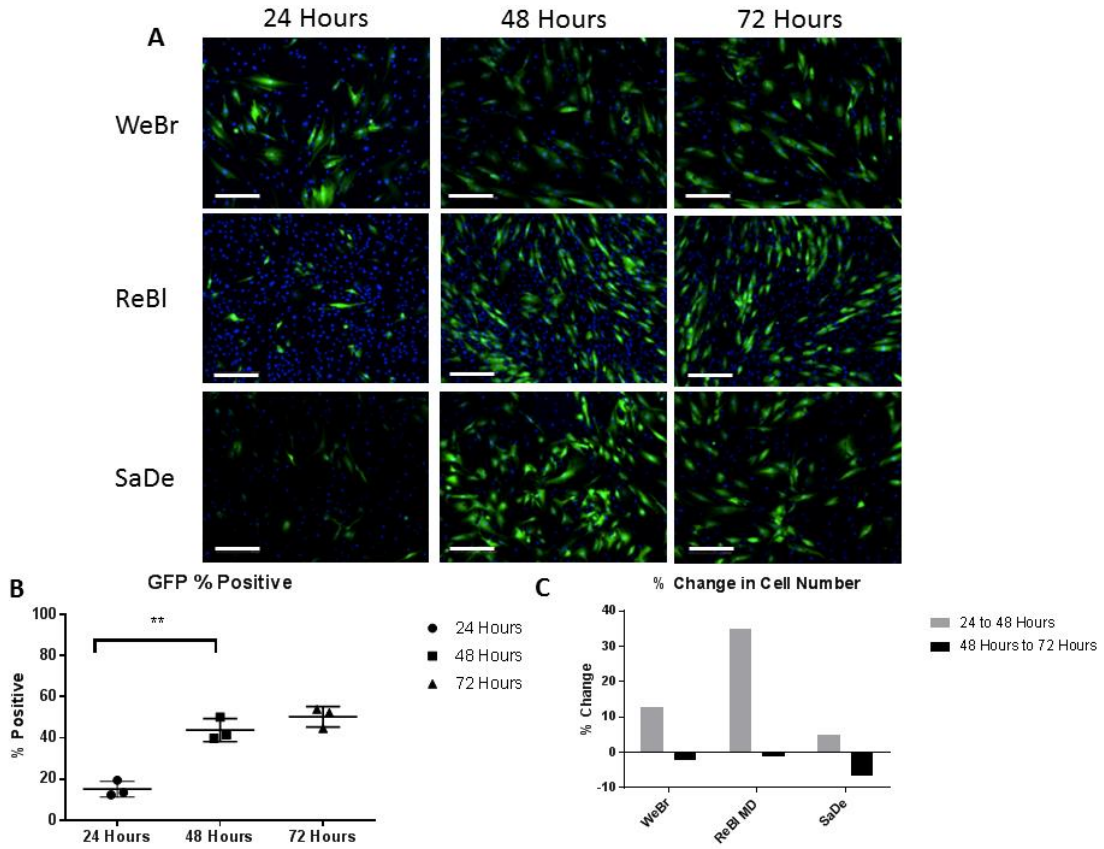


Figure 3-3 Assessment of GFP transduction efficiency using Sendai virus vectors as a delivery vehicle

A – Representative images showing GFP expression for three different fibroblast lines over a period of 72 hours images were obtained using filter for Alexa488 and show expression of GFP merged with DAPI to stain for nuclei. The number of cells expressing GFP was then calculated as a percentage of the total number of cells as assessed by DAPI staining B – Distribution plot showing the increase in GFP expression as a % of total cell number in our three cell lines over a period of 72 hours. Mean % of cells expressing GFP was 15.09±3.79 (24 hours), 43.77±5.58 (48 hours and 50.28±4.96 (72 hours). Change in GFP expression between 24 and 48 hours is significant ($p<0.05$, n=3, paired t-test). Change in GFP expression between 48 and 72 hours does not increase significantly ($p=0.23$ n=3, paired t-test). C – Bar chart showing % change in cell number between 24 - 48 hours and 48 – 72 hours. Average % change in cell number was found to be 17.66%±15.54 from 24 to 48 hours, this was not significant ($p=0.32$, n=3, paired t-test). Cell number was noted to decrease by 3.44%±2.96 between 48-72 hours. This was not deemed significant $p=0.32$, n=3, paired t-test).

Non-integrating reprogramming methods typically demonstrate lower reprogramming efficiency than integrating retroviral and lentiviral methods (Schlaeger et al, 2015). However the risk of random integrations into the genome disrupting cell phenotype and behaviour (Kang et al, 2015) has necessitated the need for more robust and efficient non-integrating methods. Reports in the literature have shown that Sendai virus and episomal reprogramming are able to robustly produce hiPSCs with efficiencies of up to 0.04% using feeder free conditions (MacArthur et al, 2012). Therefore in this project commercially available Sendai virus was compared with episomal reprogramming using previously published plasmids (Okita et al, 2011) delivered using electroporation and the GET peptide system in an attempt to establish a robust and reliable system in our lab.

Three Sendai viral vectors (KOS, hC-MYC and hKLF4) were added to culture medium at MOIs of 5:5:3, per manufacturers guidelines, and transduced into $2x10^5$ cells which were then incubated at 37^{o}C overnight, medium was then changed until the cells reached confluence at which time they were passaged using 0.05% trypsin and plated onto vitronectin-peptide coated 35mm dishes. After this time they were maintained in E6 medium + 100ng/ml FGF, changed daily, until the emergence of colonies between day 10-14. Sendai virus was able to generate hiPSCs from all three fibroblast lines tested (ReBl, ReBl PAT, Hfib) at an efficiency of 0.51%±0.05 (n=3) as measured by ALP staining for hiPSC colonies, these data can be seen in Figure 3.4.

Three episomal plasmids; pCXLE0hOCT3/4-shp53-F (Addgene #27077), pCXLE-hUL (Addgene #27080), pCXLE-hSK (Addgene #27078), were nucleofected into $1x10^6$ cells using the Amaxa 4D electroporation system program CM-100. These cells were then plated onto vitronectin-peptide coated 35mm dishes and incubated at 37^{o}C for 24 hours. After this time they were maintained in E6 medium + 100ng/ml FGF, changed daily, until the emergence of colonies at day 14, at this stage medium was changed to E8. Episomal reprogramming using Amaxa nucleofection was found to generate hiPSC colonies in all three fibroblast lines tested (ReBl, ReBL PAT, Hfib) at an efficiency of 0.004%±0.006 (n=3) as measured by ALP staining for hiPSC colonies, these data can be seen in Figure 3.4.

Finally the same episomal plasmids were transfected into $2x10^5$ cells in a 6 well plate using the GET system. These cells were then incubated at 37^{o}C for 24 hours before medium was changed to E6 medium + 100ng/ml FGF. Medium was then changed daily until the emergence of colonies which occurred at day 21. Episomal reprogramming using the GET system was found to generate hiPSC colonies in all fibroblast lines tested (ReBl, ReBl PAT, Hfib) at an

efficiency of 0.0219%±0.028 (n=3) as measured by ALP staining for hiPSC colonies, these data can be seen in Figure 3.4.

Sendai virus was found to be significantly more efficient than both electroporation ($p<0.05$, n=3, paired t test) and GET peptide ($p<0.05$, n=3, paired t test) delivery of episomal plasmids. There was found to be no significant difference between the reprogramming efficiency when using episomal plasmid between electroporation and GET peptide delivery ($p=0.35$, n=3, paired t test). These data indicate that although all methods tested were able to generate hiPSCs, Sendai virus did so at the greatest efficiency and was chosen as the reprogramming method of choice going forward.

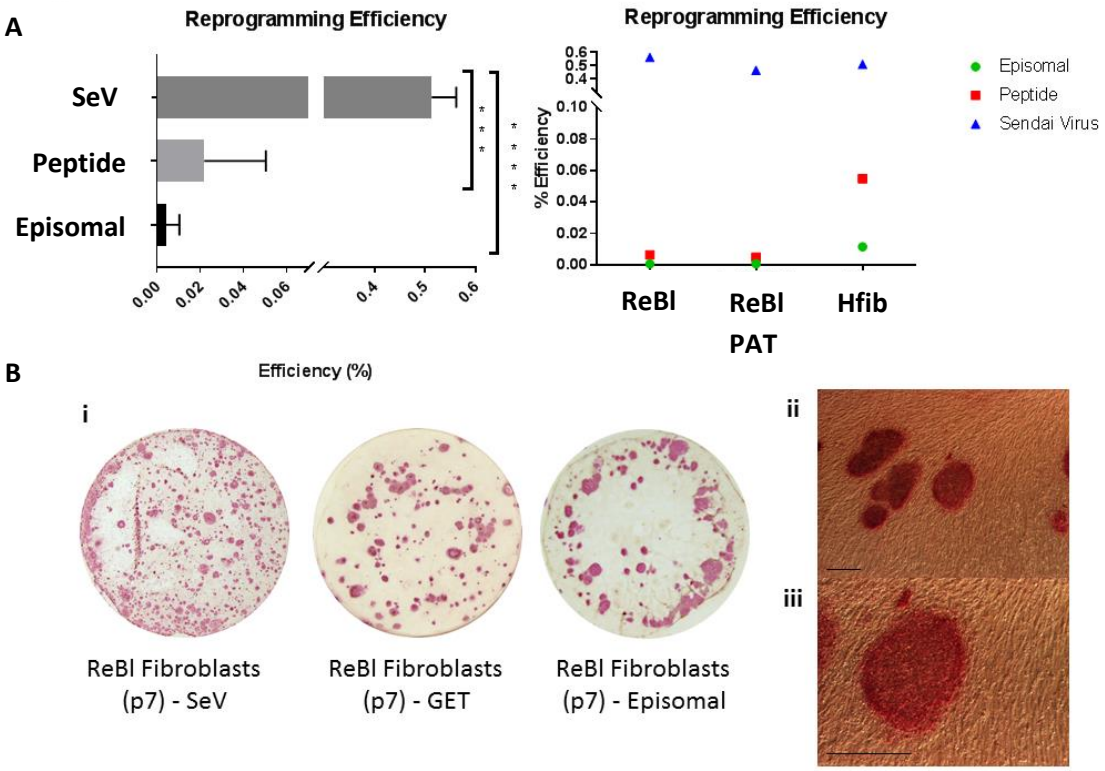


Figure 3-4 Assessment of reprogramming efficiency using different methods of vector delivery

A – Bar graph displaying the reprogramming efficiencies for fibroblasts transduced with SeV and reprogrammed with episomal plasmids either by electroporation or GET peptide delivery. There was found to be no significant difference in reprogramming efficiency between GET peptide and electroporation of episomal plasmid ($p=0.79$, $n=3$, One way ANOVA, Tukeys Multiple Comparisons). However there was found to be a significant improvement in reprogramming efficiency between Sendai virus and electroporation of episomal plasmid ($p<0.05$, $n=3$, One way ANOVA, Tukeys Multiple Comparisons). Sendai virus was also significantly more efficient than GET peptide based delivery ($p<0.05$, $n=3$, One way ANOVA , Tukeys Multiple Comparisons). B – i – Overview of 3 wells of a 6-well plate after alkaline phosphatase (ALP) staining to assess pluripotent colonies. Each colony which stained positive for ALP was counted and this number divided by the initial starting number of somatic cells to calculate the reprogramming efficiency. In these representative images all cell lines had been reprogrammed using Sendai virus. ii – Image of colonies which had emerged and stained positive for ALP where scale bar = 100µM. iii - This image shows a colony which has stained positive for ALP where scale bar = 100µM. ALP staining carried out by Dr James Dixon.

3.2.3 Derivation of starting cell populations from different tissue samples

In order to assess which tissue type would be the most appropriate to obtain routinely in the future it was first necessary to test which ones yielded success most often.

Skin fibroblast samples were obtained from two female donors, LiHa (LQT3) and ClAl (LQT3), during surgery to implant an ICD in each patient. A sample of roughly around 5-10mm was obtained and transported on ice to the lab immediately. Samples were processed according to the procedure described in Section 2.1.1. Briefly; subcutaneous fat and hypodermis were removed from the samples using a scalpel. Skin was then cut into pieces roughly $1mm^3$ in size and enzymatically dissociated using 2.5% Trypsin at 37^oC. Colonies emerged over the following 7-14 days in both samples collected and medium was changed every other day during this process, the results of this can be observed in Figure 3.5. After the cells reached confluence they were passaged into 1x T75 and medium changed every other day before being cryopreserved for future use.

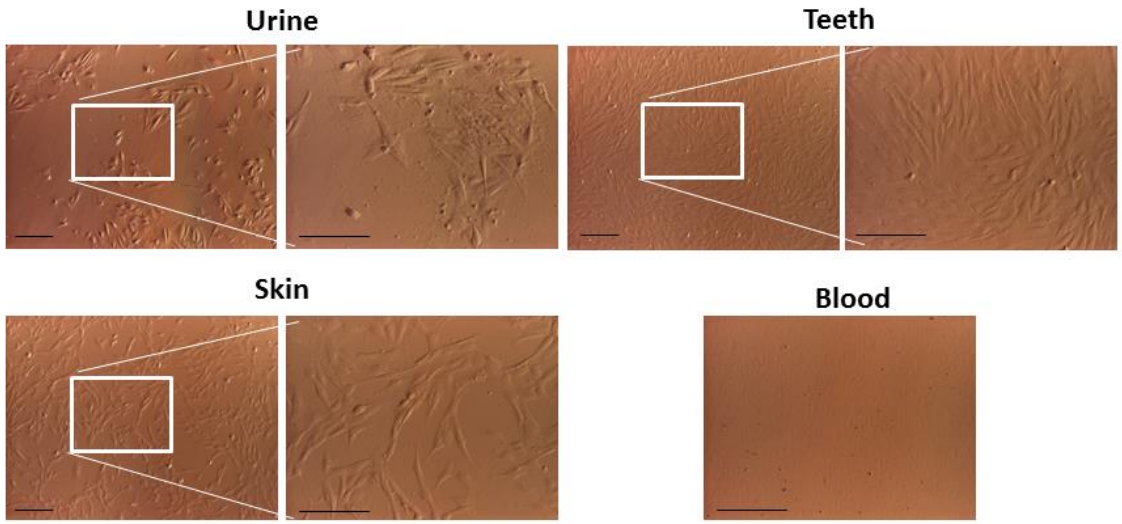
Teeth were obtained from 2 healthy donors, both teenage boys, and processed immediately. Both samples were molar milk teeth extracted by dentists and were used with informed consent of the patients. Attempts to crack teeth using a vice were initially unsuccessful, the first sample was crushed and seeded into a T75 culture flask coated in Matrigel, this did not yield any cells after 14 days in culture and was discarded. Due to the difficulty in cracking the tooth to access dental pulp an alternative was sought. Previous reports showed explants of teeth samples were able to derive starting cell populations (About et al, 2000). Therefore the second sample was processed by simply placing the tooth in a T75 flask containing fibroblast medium which had been coated in Matrigel. Cells were evident after 2-3 days in culture, the results of this are shown in Figure 3.5. This flask was contaminated on day 5 and no characterisation the cells was able to be carried out. Due to time pressure in this project no further attempts were made to derive starting cell populations from tooth samples.

One blood sample was collected from a healthy donor around midday. Sample volume was 40ml which was 20ml less than the amount recommended based on published protocol (Geti et al, 2012). Samples were processed according the procedure described in Section 2.1.3. Briefly, blood is mixed with sodium citrate and inverted, in tubes containing 8ml of ficoll and samples are centrifuged at 400g for 35 minutes. EPCs are then isolated using a plastic transfer pipette to carefully remove the thin translucent layer between transparent supernatant and red blood cells. Medium was changed on the flask every other day up until day 14 at which point the flask was discarded with no evidence of any adherent cells, as shown in Figure 3.5.

Due to time pressure no further attempts were carried out to derive starting cell populations from blood samples.

Urine was collected and the cells harvested according to published procedures (Zhou et al, 2011). Briefly; samples were aliquoted into 50ml tubes and centrifuged at 400g for 10 minutes before all pellets collected, centrifuged at 400g for 10 minutes again, and seeded into 1x well of a 12-well plate coated with gelatin, as described in Section 2.1.4. Urine samples were collected from three donors; two healthy and one carrying LQTS3 mutation (ClAl). Samples were collected around midday on day of donation and amounted to between 100-470ml, only the mid-stream of urine was collected, the initial dense stream was discarded. Medium was changed on the plates every other day and the emergence of colonies was observed at day 2-4, the results of which can be seen in Figure 3.5. This was successfully performed on one occasion. At this stage the experiment was abandoned due to the relative lack of success in generating starter cultures from urine samples and fibroblasts were chosen as the preferred cell type going forward.

A



B

Somatic cell source	Advantages	Limitations	Number of attempts	% success
Urine	Easily obtainable (Zhou et al, 2012)	Low number of cells extruded in urine daily (Zhou et al, 2012)	10	10%
Skin	Established (Takahashi et al, 2007; Yu et al 2007)	High mutation load (Takeda et al, 2008), painful	2	100%
Teeth	Low mutation load (Takeda et al, 2008)	Difficult sample to obtain, especially in adults	2	50%
Blood	Low mutation load, easy access (Geti et al, 2012)	Must be immediately processed	1	0%

Figure 3-5 Isolation of primary cells from human somatic tissue for the purposes of reprogramming

A - Brightfield images of p1 primary cell cultures derived from urine, skin and teeth. No cultures were successfully derived from blood as a starting sample. These somatic cells are all characterised by their long spindle like morphology and low nucleus to cytoplasm ratio. The image for blood empty well as no cells were adherent. B – Table describing the advantages, limitations and ease of derivation of primary cell cultures from different starting somatic cell sources. Urine was successful in 10% (n=10) of attempts compared with 100% success for skin samples (n=2) and a 50% success rate for teeth (n=2). In this study blood was successful in 0% of cases (n=1). Scale bars represent 100µm

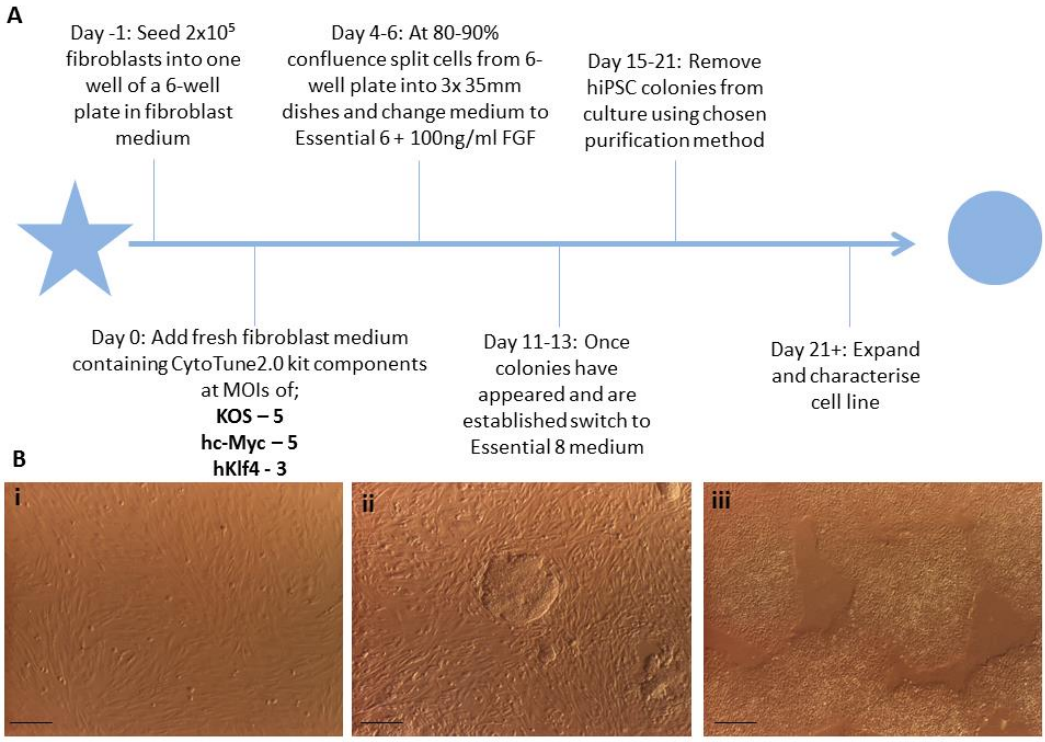


Figure 3-6 Sendai Virus-mediated hiPSC reprogramming
A - Schematic representing the reprogramming procedure with a timeline illustrating the steps during the process. B – Brightfield images showing the morphological changes observed during the reprogramming process i – Initial fibroblast starting cells exhibiting long and spindle like morphology. ii – Presence of long and spindle like cells in this culture are the fibroblasts which haven't undergone the reprogramming process. The colony in the middle of the image exhibits clear and defined edges around its border with more spherical and compact cells within it. iii – This images shows a purified hiPSC line after reprogramming and these cells are characterised by their high nucleus to cytoplasm ratio, tightly clustered colonies and defined cell borders. Scale bar = 100µm.

3.2.4 Pilot reprogramming of control fibroblasts like cell line using Sendai virus

To assess the quality of the hiPSC lines generated using Sendai virus in our lab it was decided to reprogram a control line as had previously been performed using lentivirus to ensure Sendai generated comparable hiPSCs. Hfibs were reprogrammed according to the protocol described in Section 2.3.1, a schematic of which is shown in Figure 3.6, this line was hence described as Hfib-hiPS-SeV. Putative hiPSC colonies were first noted between day 12-14 and the cells ready for purification on day 21. Purification was performed using MACS and the cells expanded up until passage 15 when characterisation was performed. Immunocytochemistry was undertaken to assess the presence of the pluripotency associated transcription factors OCT4, SOX2 and NANOG. In addition to this two pluripotency associated surface markers, SSEA3 and SSEA4, were also stained for. The Hfib-hiPS-SeV line demonstrated high expression of all pluripotency related transcription factors and both pluripotency related surface markers, as shown in Figure 3.7. This expression was not seen on Hfib cells, which were originally reprogrammed to generate Hfib-hiPS-SeV. In order to quantify the level of hiPSC purity in the

Hfib-hiPS-SeV cultures flow cytometry was undertaken for the pluripotency related surface markers TRA-1-81 and SSEA4, in addition to this the differentiation marker SSEA1 was used as a negative control. Hfib-hiPS-SeV cells were found to be 89.3% positive for TRA-1-81 and 97.2% positive for SSEA4 when gated against a negative cell type control, namely Hfibs, these data can be seen in Figure 3.7. Only 1.52% of cells stained positive for SSEA1 when gated against a negative cell type control. Based on these data it was concluded that Hfib-iPS derived using Sendai virus was comparable in terms of pluripotency with previous Hfib-hiPS-Lenti in our lab. Therefore Sendai virus reprogramming was used to generate the hiPSC lines required for this project.

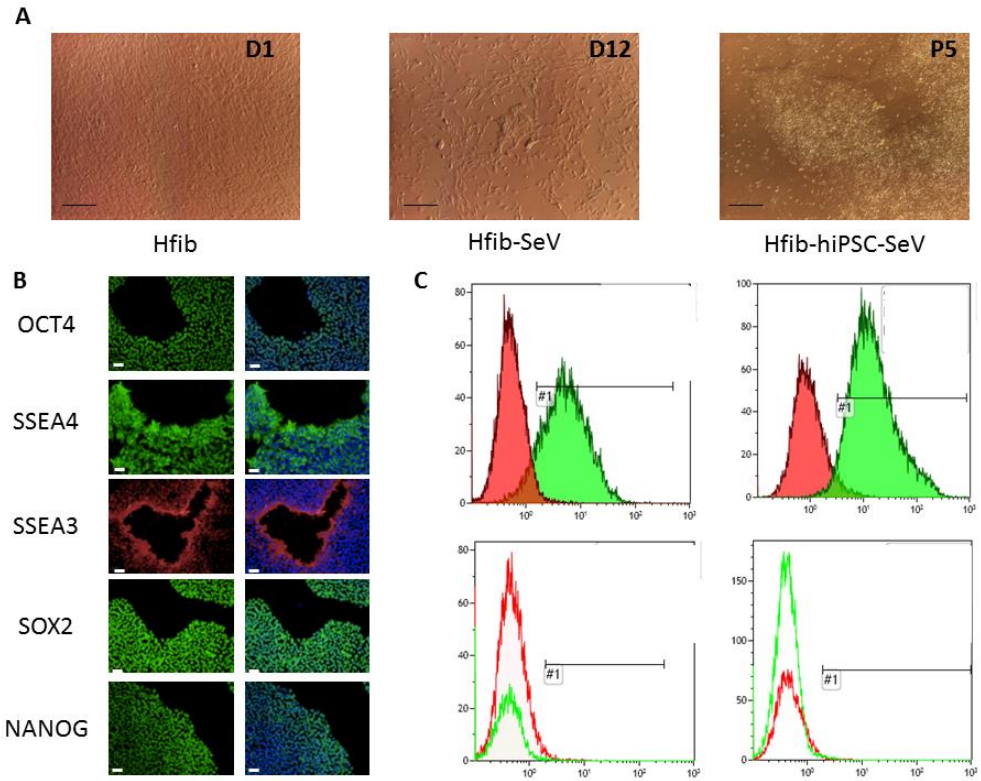


Figure 3-7 Assessing effectiveness of Sendai virus to produce viable hiPSC lines in our lab

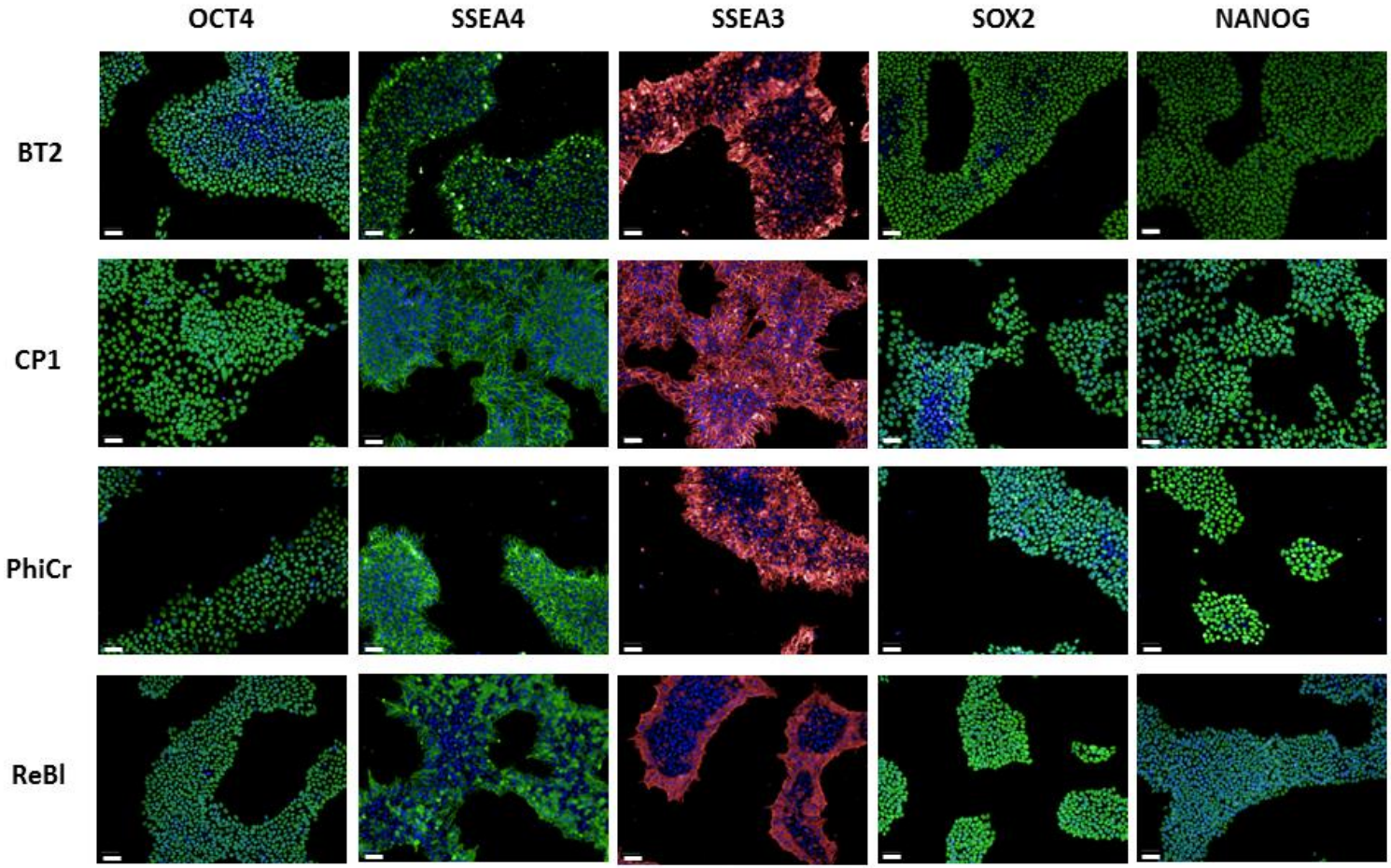
A –Brightfield images through the reprogramming process. From initial seeding of HUES7 fibroblasts in a 6 well plate at a density of $2x10^5$ per well at day 1 post transduction (left) to the emergence of putative hiPSC colonies within the fibroblast cultures at day 10-12 (centre) and the establishment of purified hiPSC lines which are cultured routinely in Essential 8 medium with little to no spontaneous differentiation at passage 5. Scale bars represent 100µm. B – Immunofluorescence analysis of the Hfib-iPSC-SeV line showed that there was clear expression of OCT4, SOX2, SSEA4 and NANOG images on the left show positive staining for Alexa488 (Showin Alexa488 channel) with images on the right showing Alexa488 merged with DAPI to identify cell nuclei. In addition to this there was also clear expression of SEEA3 with the image on the left showing Alexa647 (shown in DRAQ5 channel) staining and on the right showing Alexa647 staining merged with DAPI to identify cell nuclei. Scale bars =50µm.C – Flow cytometry analysis of the newly derived Hfib-iPSC-SeV line showed that these cells expressed TRA-1-81 at a % positive of 89.3%, n=1 and SSEA4 at a % positive of 97.2%, n=1 but only expressed SSEA1 which is a marker of differentiation at a % positive of 1.52%. These cells were compared to a negative cell type control, in this case HUES7-fibs. The positive gate for staining was set not higher than 5% of the negative sample.

3.2.5 Generation of hiPSCs using Sendai virus

Fibroblasts were collected from patients who suffered from either LQTS1, LQTS2 or CPVT. In addition to this some fibroblasts were collected from healthy donors and in one case an asymptomatic carrier with LQTS2 mutation, details of these patients can be found in Table 3.4. These fibroblasts were reprogrammed to hiPSCs using the CytoTune2.0 Sendai virus kit (Thermo Fisher) as described in Section 2.2.1. Putative hiPSC colonies were identified by their defined borders exhibiting a cobblestone-like morphology, a high cytoplasm to nucleus ratio and the loss of the spindle like process with characterise the morphology of fibroblast like cells. These hiPSC colonies began to emerge at day 10-14 post transduction. After purification these hiPSC lines were maintained in the commercially available defined medium E8 on Matrigel coated surfaces.

These putative hiPSC colonies were then tested to ascertain they were exhibiting true 'stem cell' phenotype. Regular monitoring of the cell morphology was performed using bright-field microscopy, this was done to monitor that the cells remained small and rounded with defined cell borders and a had a high cytoplasm to nucleus ratio as these are all factors indicative of an immature cell type (Oh et al, 2005). Newly derived hiPSC lines were subjected to immunostaining for pluripotency transcription factors OCT4, SOX2 and NANOG as well as pluripotency related surface markers SSEA3 and SSEA4 as shown in Figure 3.8. All lines expressed these markers to high levels, however these markers were found to be absent in Hfib, a HUES7 derived fibroblast like cell type. To quantify the purity of our cultures flow cytometry was performed for the pluripotency related surface markers TRA-1-81 and SSEA4 as shown in Figure 3.9. In addition to this the cells were also stained for SSEA1 which is a marker of differentiation. All cell lines were greater than 88% when gated against a negative cell type control for the surface marker TRA-1-81. Furthermore all lines were greater than 92% with the exception of PhiCr which was recorded as 73.7% positive for SSEA4 staining. All lines were recorded to be <2% positive for the differentiation marker SSEA1, these data can be seen in Figure 3.9. Newly derived hiPSC lines were sent for G-banding karyotype analysis to ensure the lines generated were chromosomally stable, any cells which exhibited more than 10% of the same abnormality within one culture were discarded, these data can be observed in Figure 3.10. All cell lines generated in this project exhibited stable and normal karyotypes in at least one "sub line". Cumulative population doubling times were calculated and these CPDs can be seen in Figure 3.10. These growth rates were comparable to the hESC line HUES7 which has been recorded to have a CPD of 33.5 hours in our lab.

Therefore these data confirm that hiPSC lines derived in our lab using the commercially available CytoTune2.0 kit (Thermo Fisher) were karyotypically stable with growth rates consistent with a control hESC line (HUES7). Furthermore all hiPSC lines derived exhibited high expression levels of pluripotency transcription factors and surface markers assessed by immunocytochemistry which were not observed in fibroblast like control cells. This was confirmed and quantified by flow cytometry for pluripotency related surface markers which showed high purity of the hiPSC cultures. Furthermore the newly derived hiPSC cultures also showed very low expression of a differentiation marker. Therefore the cells generated here were good candidates to be taken forward for use in downstream assays after cardiac differentiation.


OCT4
SSEA4
SSEA3
SOX2
NANOG
BT2
CP1
PhiCr
ReBl

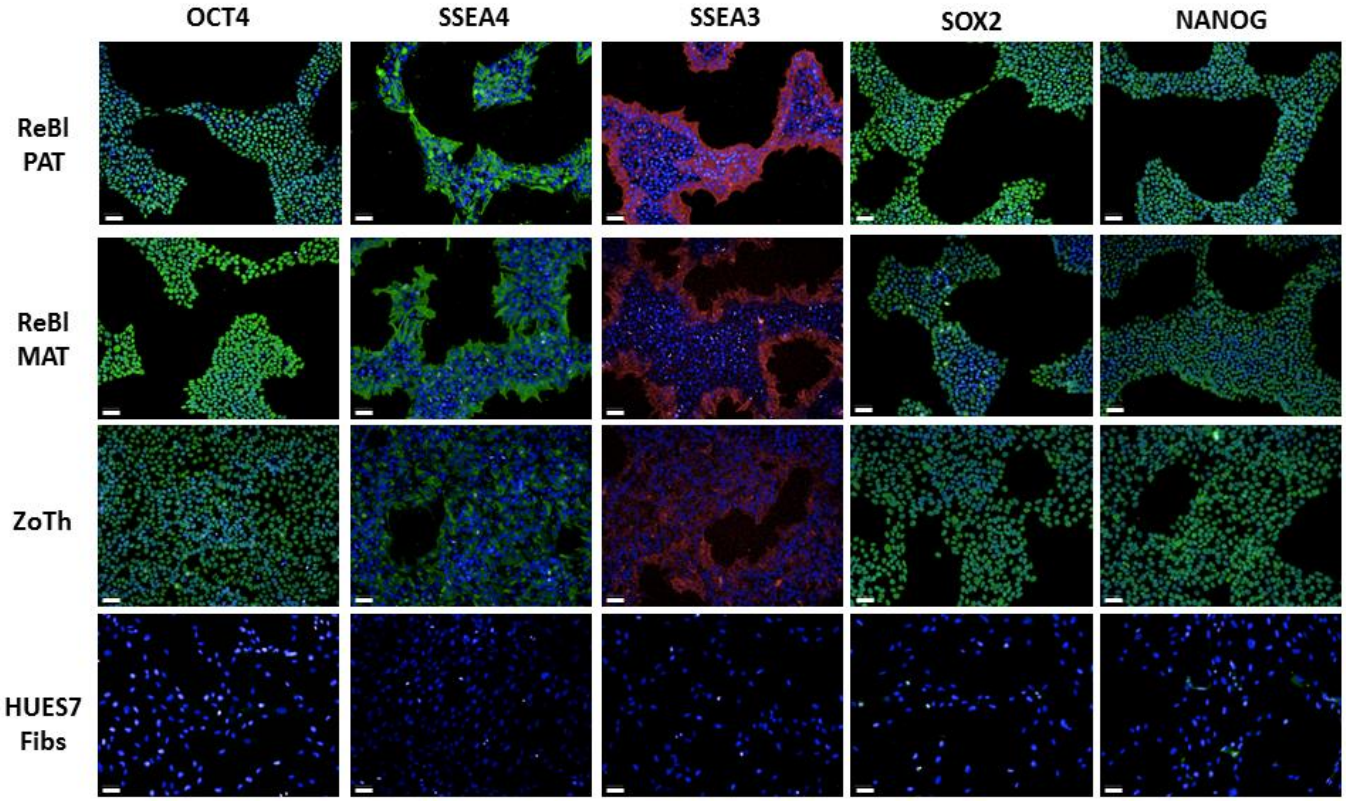
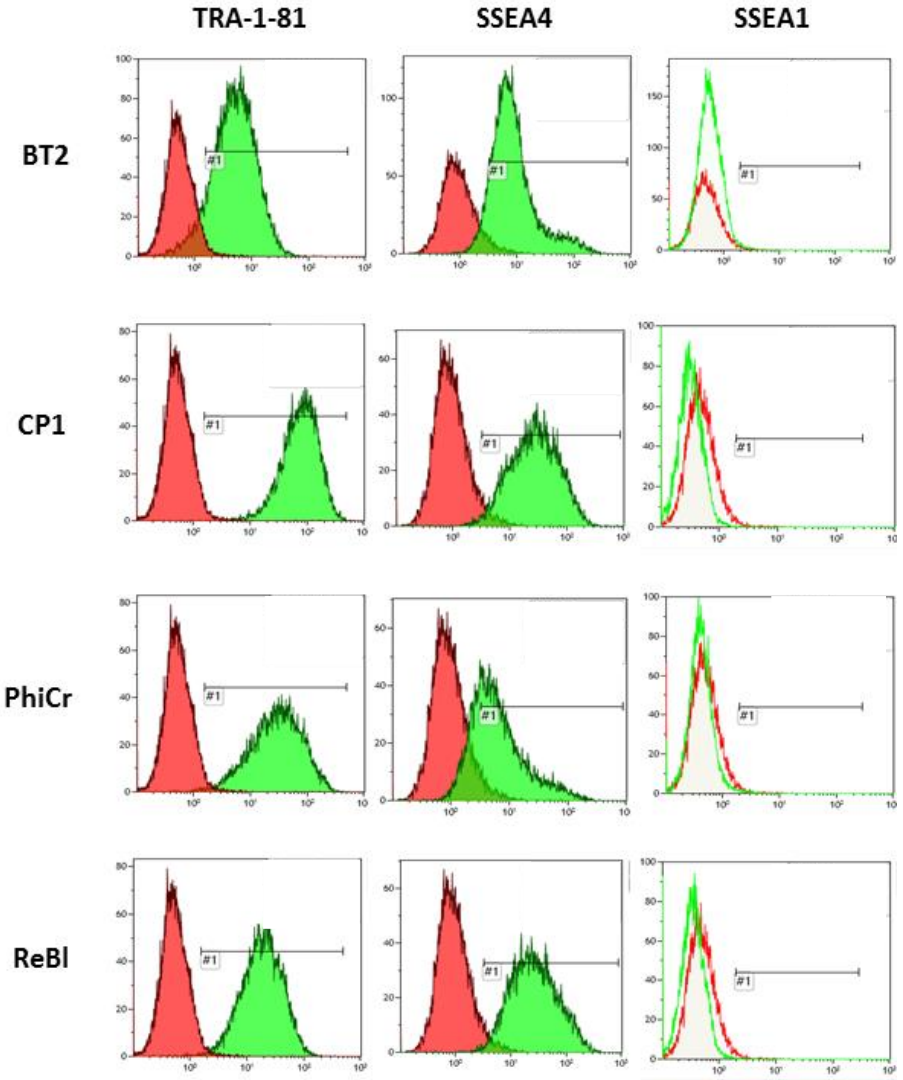


Figure 3-8- Immunocytochemistry analysis of newly derived hiPSC lines

Newly derived hiPSC lines were seeded into 96-well plate format at a density of $1x10^4$ cells per well. These cells were fixed in 4% paraformaldehyde 48 hours after seeding. Cells were stained for markers of pluripotency in this case OCT4, SSEA4, SSEA3, SOX2 and NANOG were used, these are well-established indicators of pluripotency (Adewumi et al, 2007; Li and Belmonte, 2017). Marker expression was captured using the Alexa488 channel (green) or the DRAQ5 channel (red) while the overlay represents a merge of the DAPI (nuclear staining). Scale bars represent 50µm.


TRA-1-81
SSEA4
SSEA1
BT2
CP1
PhiCr
ReBl
#1

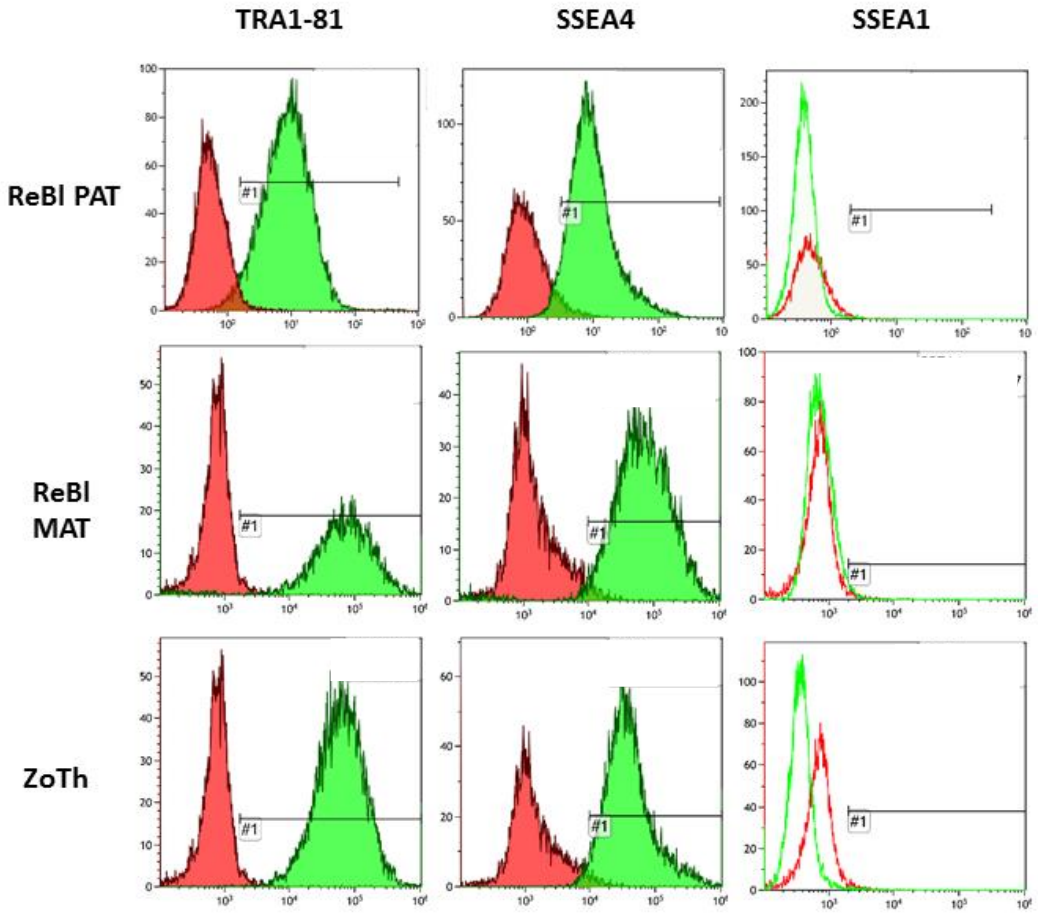
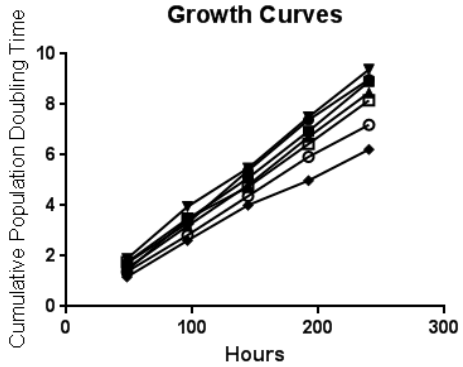


Figure 3-9 - Flow cytometry analysis of pluripotency marker expression in newly derived hiPSCs for quantification

Newly derived hiPSC lines were stained for TRA-1-81 and SSEA4 surface markers which are established markers of pluripotency (Adewumi et al, 2007). In addition to this they were also stained for expression of the surface marker SSEA1 which is an established marker of differentiation (Takahashi et al, 2007). Samples were gated and analysed in comparison to a negative cell type control, in this case Hfibs. The positive gate was set no greater than 5% positive for the negative control. There are no error bars in the graphs as n=1.

A



B

Cell Line	CPD (Hours)
ReBl	26.67
ZoTh	26.94
ReBl MAT	28.33
CP1	25.56
BT2	38.56
PhiCr	33.34
ReBl PAT	29.4

C

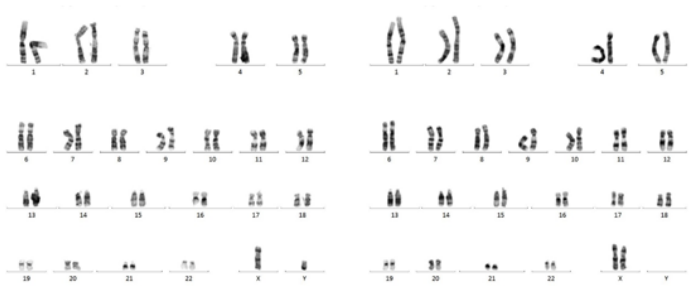


Figure 3-10 - Culture and karyotype assessment of newly derived hiPSC lines

A – Growth curves of newly derived hiPSC lines showing stable rates of growth for our lines which appear to overlap in most cases. The only potential outlier is BT2, this line was discontinued from use in the lab due to the inability to culture in roboflasks for mass cardiomyocyte production. B – Table showing the cumulative population doubling time for the hiPSC lines which were derived in the early stages of this project. C – Representative karyotypes showing 46XY and 46XX karyograms from CP1 and ReBl respectively. G-band karyotyping was carried out by Dr Nigel Smith

3.2.6 Assessing the three germ layer differentiation potential of newly derived hiPSC line ReBl-PAT

A key component in establishing the pluripotency of an hPSC line is to demonstrate it can generate all three germ layers, ectoderm, endoderm and mesoderm (Yu and Thomson, 2008). Traditionally this has been achieved by injecting the hPSC line into an immunodeficient mouse and assessing whether it generates a teratoma (Zhang et al, 2012). In this thesis it was decided to use a directed differentiation approach to try and induce the newly generated hiPSC line to differentitate to all three germ layers before quantifying how successful each was. This work was performed by Dr Luke Flatt as part of his doctoral research.

Briefly hPSC lines were harvested and seeded into wells of a 96 well plate at a final seeding density of 16,700 cells/well. For ectoderm and mesoderm differentiation was induced 72 hours after seeding, however for endoderm it was induced 24 hours after seeding. This process is described in Section 2.1.5.

ReBl-PAT-hiPSC was able to successfully form all three germ layers showing positive staining for markers of ectoderm (SOX1 and PAX6), endoderm (SOX17 and FOXA2) and mesoderm (MESP1 and ISL1) as shown in Figure 3.11. Quantification of this staining was performed using DAPI as a counter stain to assess number of cells and calculating the percentage positive population in each differentiation condition. ReBl-PAT-hiPSC was able to form ectoderm to an efficiency of 64.2%±2.1%, endoderm to an efficiency of 87.6%±6.5% and mesoderm to an efficiency of 68.2%±5.8%.

These data indicate that ReBl-PAT-hiPSC line generated by SeV is able to generate cells from all three germ layers therefore indicating that it displays true pluripotency and providing further confidence in the SeV reprogramming method.

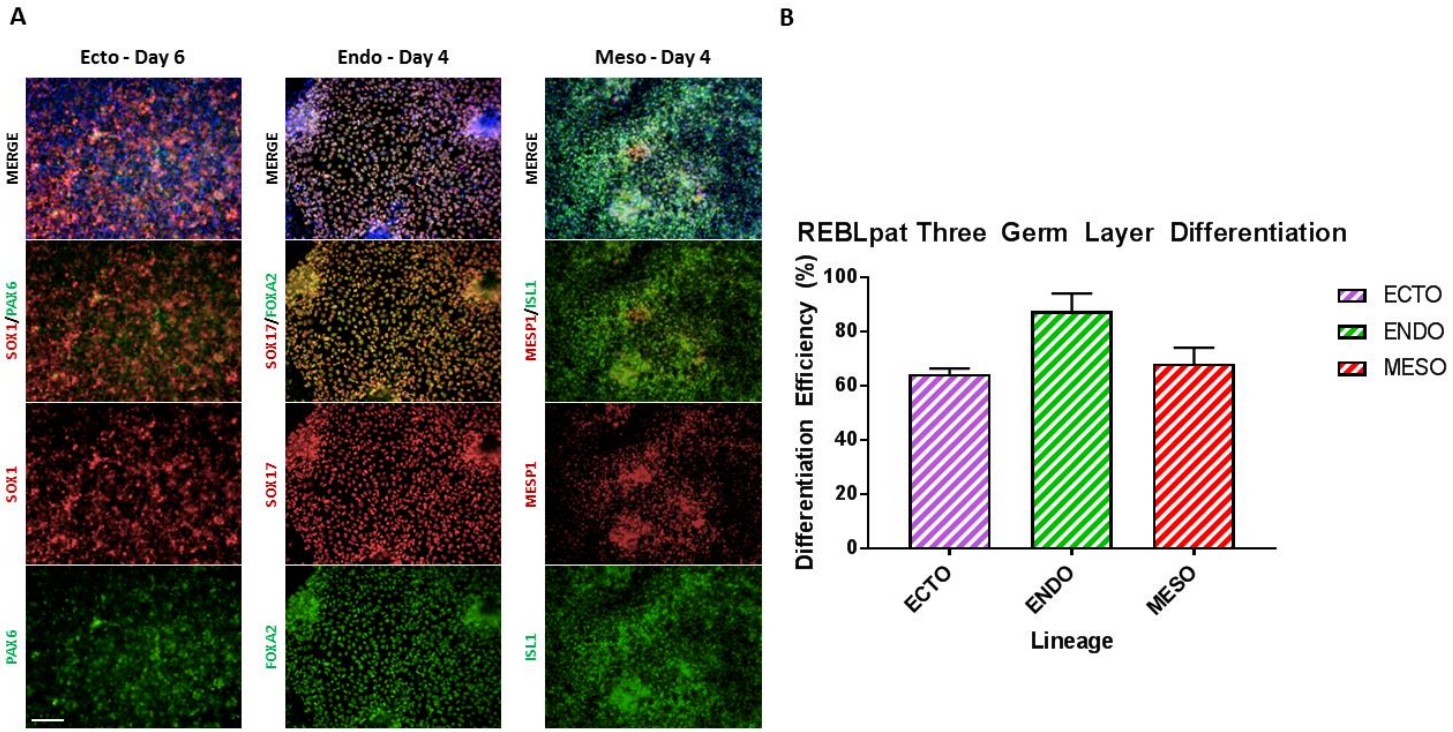


Figure 3-11 - Assessing the ability of newly generated hiPSC line to generate derivatives of all three germ layers

A – Immunocytochemistry images which display the marker expression of ReBI-PAT after tri-lineage differentiation. Immunocytochemistry image to assess the presence of markers of ectoderm differentiation (left). The top image shows a merge of SOX1, PAX6 and DAPI. SOX1 is visualised through the DRAQ5 channel and PAX6 is visualised through the Alexa488 channel. ii) The top image shows a merge of SOX17, FOXA2 and DAPI. Immunocytochemistry image to assess the presence of markers of endoderm differentiation (centre). SOX17 is visualised through the DRAQ5 channel while FOXA2 is visualised through the Alexa488 channel. iii) The top image shows a merge of MESP1, ISL1 and DAPI. Immunocytochemistry image to assess the presence of markers of mesoderm differentiation (right). MESP1 is visualised through the DRAQ5 channel while ISL1 is visualised through the Alexa488 channel. B – Graph displaying the percentage of cells which stained positive for both markers indicating a differentiation efficiency. Scale bars are 100µm, this staining and analysis was carried out by Dr Luke Flatt.

3.2.7 Assessing method for hiPSC purification after reprogramming

Purification of hiPSC during the reprogramming process can be performed using MACS to sort cells which are positive for a marker of pluripotency such as TRA-1-81 (Dick et al, 2011). However previous hiPSC lines generated in our lab using lentivirus with MACS for purification required multiple rounds of purification thereby indicating that the process was less than optimal. During the process of generating the hiPSC lines described in Section 2.2.4. attempts were made to generate 'sub-lines' of these hiPSC lines using different purification techniques to ascertain if high quality pluripotent lines could be generated using two alternative methods described in Section 2.2.4.

Manual dissection (MD) is the process by which individual putative hiPSC colonies are mechanically dissociated by cutting with a stem cell knife before being replated in a 48-well plate and expanded as a monoclonal culture. Serial passage (SP) is the process whereby fibroblasts and putative hiPSC colonies are enzymatically passaged using 0.5mM EDTA and reseeded leading to a purified culture over 3-5 passages. hiPSC lines generated using each of these three different purification methods were then tested to ascertain their level of pluripotency and their genomic stability.

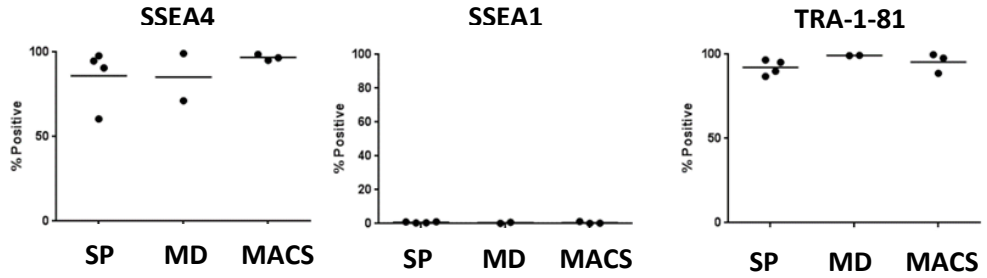
Two hiPSC lines were able to be derived using MD (ReBl, PhiCr) both of these lines were found to be karyotypically stable and exhibited positive staining for pluripotency markers TRA-1-81 and SSEA4 >70% as shown by flow cytometry. In addition they showed differentiation marker SSEA1 staining <1%. These data can be seen in Figure 3.12.

Six lines were purified using SP (BT2, ReBl PAT, PhiCr, ReBl, ZoTh, ReBl MAT) of these all were found to have stable and normal karyotypes. In addition to this these lines expressed pluripotency related surface markers SSEA4 and TRA-1-81 >85% in all cases except PhiCr (63.7%) and SSEA1 expression in <2% in all cases. These data are shown in Figure 3.12

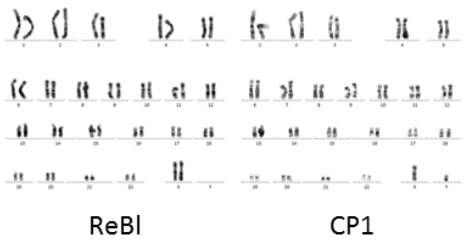
Five lines were purified using MACS (Hfib-hiPS-SeV, ReBl, CP1, SaDe, PhiCr) of these five lines three were found to carry karyotype abnormalities in greater than 10% of the metaphase cells analysed and were discarded from use. The abnormalities can be seen in Figure 3.12. Despite this genomic instability MACS purified hiPSC lines which did not express karyotype abnormalities were analysed for their pluripotency. These genomically stable lines expressed pluripotency related surface markers SSEA4 and TRA-1-81 >85% and expressed the differentiation marker SSEA1 <1% in all cases. These data are shown in Figure 3.12.

These findings led to the conclusion SP or MD lines carried lower risk of karyotype abnormality than using MACS. There was no difference observed in the purity of the hiPSC lines. However monoclonal lines were preferred for downstream use in gene targeting and therefore MD was chosen as the first option for all newly derived hiPSC lines with SP used as a backup option.

A



B



C

Method	Number of Samples	Normal Karyotype	Abnormal Karyotype	% of Abnormal Karyotypes
Manual Dissection	2	2	0	0
Serial Passage	6	6	0	0
MACS	5	2	3	60

D

Cell Line	Abnormality	% Cells Affected
SaDe MACS	46,XX,t(11;12)(p11.2;q13),der(21)t(1;21)(q1;p1)	40%
PhiCr MACS	46,XX,der(20)t(1;20)(p1;q13)	73%
Hues7 iPS MACS	47,XY,+12 (12/30	40%

Figure 3-12 - Assessing the effect of method of purification on hiPSC pluripotency and quality

A - Pluripotency analysis based on % positive cells expressing pluripotency markers SSEA4 and TRA-1-81 as well as the differentiation marker SSEA1 as quantified using flow cytometry data. The % of cells expressing the differentiation marker SSEA1 is also shown. B – Representative karyogram images showing the ReBl cell line with 46XX phenotype (left) and CP1 showing the 46XY phenotype (right). C - Assessing the karyotypical stability of lines based on method of purification. Lines purified by manual dissection were all karyotypically normal at between passage 15-20. The same is true of the lines generated using serial passage of which 6 were derived and all 6 were karyotypically normal at between passages 15-20. 5 lines were derived using a MACS method of purification, of these 3 were found to contain karyotype abnormalities making the line unusable in this study, this accounted for 60% of the lines generated. D – Table showing the specific karyotype abnormality which was present in each of the three MACS lines.

3.2.8 Assessing the loss of reprogramming vectors in the newly derived hiPSCs

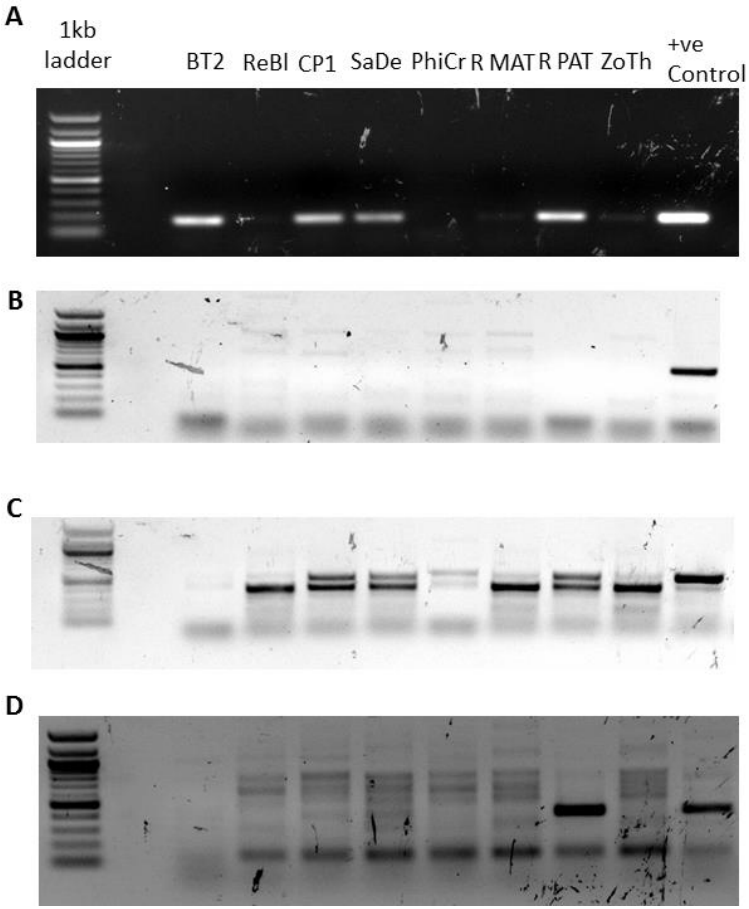
The use of non-integrating reprogramming methods aims to eliminate the integration of viral transgenes which can persist and lead to genomic instability and introduction of single nucleotide polymorphisms (SNPs) (Beers et al, 2015). The vectors contained within the CytoTune2.0 reprogramming kit used in this project act within the cytoplasm and do not enter the DNA phase of replication, thus eliminating the risk of integration. However the length of time which the vectors persist within the cell can still vary. The primers in Table 3.5 were obtained from Thermo Fisher and are recommended for use in detecting SeV vectors. As these vectors are proprietary there is no way of displaying where in the vector the primers bind.

Initial tests were carried using the primer pair which detects the presence of the SeV backbone. It was demonstrated that BT2, CP1, SaDe and ReBl PAT, representing 75% of the lines generated, still exhibited presence of at least one vector after passage 10. Further analysis was carried out to ascertain specifically which vector remained present. No lines showed the presence of the KOS vector. However the C-MYC vector was detected in 37.5% of the lines tested, namely CP1, SaDe and R PAT. Finally the KLF vector was detected in one sample, ReBl PAT, meaning it was detected in 12.5% of the cell lines analysed. The gel images from these experiments are shown in Figure 3.13

It is not established if the presence of these vectors within these cells has any effect on cell behaviour, to this point no issues regarding pluripotency or differentiation potential have been identified. As a result of this no further action was taken with regards to this at this stage.

Table 3-5 - Primer sequences to check for presence of CytoTune2.0 vectors

Target	Primer Sequence	Product Size
SeV	Forward: GGA TCA CTA GGT GAT ATC GAG C Reverse: ACC AGA CAA GAG TTT AAG AGA TAT GTA TC	181bp
KOS	Forward: ATG CAC CGC TAC GAC GTG AGC GC Reverse: ACC TTG ACA ATC CTG ATG TGG	528bp
KLF4	Forward: TTC CTG CAT GCC AGA GGA GCC C Reverse: AAT GTA TCG AAG GTG CTC AA	410bp
C-MYC	Forward: TAA CTG ACT AGC AGG CTT GTC G Reverse: TCC ACA TAC AGT CCT GGA TGA TGA TG	532bp



Vector	% Lines Retaining Vector
SeV	75
KOS	0
C-MYC	50
KLF4	12.5

Vector Tested	Product size
SeV	181bp
KOS	528bp
C-MYC	532bp
KLF4	410bp

Figure 3-13 - Detecting the presence or absence of the SeV vectors using RT-PCR

RNA was extracted from SeV cell lines and RT-PCR performed using primers recommended by Life Technologies to detect the presence or absence of the SeV vectors. A –Using primer pair to detect all SeV vectors with a product sixe of 181bp, BT2, CP1, SaDe and ReBl PAT show the presence of this vector. B – Using primer pair which is designed to detect the presence of KOS vector with a product size of 528bp, no cell lines showed the presence of this vector. C – Using a primer pair which are designed to detect the hC-MYC vector which gives a product size of 532bp, CP1 SaDe and ReBl PAT showed the presence of this vector. D – Using primer pair to detect the hKLF4 vector which gives a product size of 410bp, ReBl PAT showed the presence of this vector. DNA ladder in all gel images is a 1kb ladder from New England Biolabs.

3.2.9 Using monolayer differentiation methods to generate cardiomyocytes

Generation of cardiomyocytes was a vital component in this project. In order to ascertain how best to generate cardiomyocytes robustly, efficiently and across different cell lines it was decided to test multiple methods to assess which one would be most appropriate to use for the phenotyping and drug testing component of the project. To do this a trial run was completed over a one month span during which four different methods were tested as shown in Figure 3.14. These differentiation methods are explained in detail in Section 2.1.5.

During the trial period it was established that 50% of CDM-CW flasks achieved successful differentiation (n=12). This was compared to 90% of flasks which were treated with the ABKYX method (n=19). Attempts at crossing the two methods into a hybrid proved relatively unsuccessful. Hybrid Method 1 was found to work in 0% of attempts (n=4) and Hybrid Method 2 was found to be successful in 40% of attempts, these data are shown in Figure 3.14. Across cell lines it was demonstrated that CDM-CW was successful in 60% of cell lines tested (n=10). ABKYX was found to be successful in 100% of cell lines tested. Hybrid Method 1 was successful in 0% of cell lines and Hybrid Method 2 was found to be successful in 40% of cell lines. These data are shown in Figure 3.14

These data demonstrated that ABKYX was the method which most readily generated cardiomyocytes across various cell lines in my hands in our lab.

A

Method	Day -1	Day 0	Day 2	Day 4	Day 6
CDM-CW	Essential 8	4µM CHIR99021 in CDM3	2µM WntC59 in CDM3	CDM3	CDM3
ABKYX	1ng/ml BMP4 in Stem Pro34 + Matrigel Overlay	5ng/ml Activin A and 10ng/ml BMP4 in Stem Pro 34	10µM KY02111 + 10µM XAV939 in RPMI B27 -ve Insulin	10µM KY02111 + 10µM XAV939 in RPMI B27	RPMI B27
Hybrid 1	1ng/ml BMP4 in CDM3 + Matrigel Overlay	4µM CHIR99021 in CDM3	2µM WntC59 in CDM3	CDM3	CDM3
Hybrid 2	1ng/ml BMP4 in E8 + Matrigel Overlay	4µM CHIR99021 in CDM3	2µM WntC59 in CDM3	CDM3	CDM3

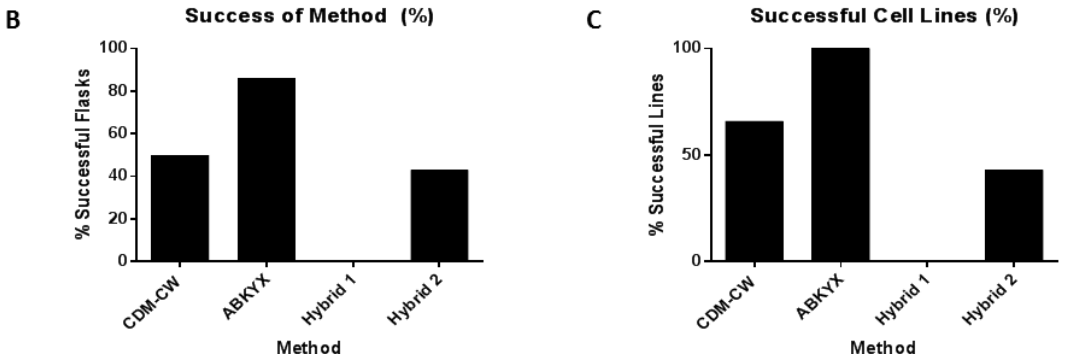


Figure 3-14 - Success of differentiation methods

A - 4 different methods of cardiac differentiation were tested to ascertain if any were able to work more robustly than others. This table illustrates the key steps involved in each procedure. B – Bar graph illustrating the comparison of different differentiation methods and how often they successfully yielded cardiomyocytes CDM-CW was able to successfully yield cardiomyocytes in 50% of cases (n=12). This is in contrast to ABKYX which was able to yield cardiomyocytes in 90% of flasks (n=19). Two hybrid methods were attempted to varying degrees of success, Hybrid method 1 was successful in 0% of cases (n=4) and Hybrid method 2 was successful in 40% of cases (n=10). C – 3/4 methods were found to be transferrable across multiple cell lines with ABKYX working most robustly during this test. CDM-CW was found to work across 60% (n=4) of the cell lines tested. This is in contrast to ABKYX which was able to generate cardiomyocytes in 100% of the cell lines tested (n=4). Hybrid method 2 was successful in only 40% of the cell lines tested (n=4).

When using manual patch clamp in order to assess cardiomyocyte phenotype impure cardiomyocyte populations can be selected for cells which are beating, therefore are cardiomyocytes. However in assays used in this project this was not the case. Using plate readers and fluorescent dyes means that average readings over either the well or field of view are used. Therefore the cardiomyocytes which are being used for these assays must be of a high purity to standardise the process. For this reason it was decided to test the relative purity of the cardiomyocytes using the three methods which had previously given us successful differentiations.

Cardiomyocytes were dissociated after 12-16 days in culture and seeded into 96 well plates at densities of between 40,000-50,000 cells per well. These cells were fixed using 4% paraformaldehyde 48 hours later and stained for cardiac marker alpha-actinin.

ABKYX was demonstrated to show cardiomyocyte differentiation efficiency of 80.94±3.865% n=27, the cell lines used in this test were genetically modified ReBl-PAT hiPSCs – R-GECO hom R12, R-GECO het R2, MYH7 R453C het C11 and MYH7 R453C hom C11. The CDM-CW method was shown to exhibit a cardiomyocyte differentiation efficiency of 60.3±11.2% n=9, the cell lines used in this test were PhiCr-SP, ReBl SP and ReBl MACS. The Hybrid 2 method was demonstrated to exhibit a cardiomyocyte differentiation efficiency of 56.91±11.2% n=9, the cell lines used in this test were PhiCr-SP, PhiCr-MD and BT2-SP. All results in this section are shown as mean ± standard error of the mean (SEM). These results are shown in Figure 3.15

ABKYX did not demonstrate significantly greater efficiency of differentiation compared to CDM-CW ($p=0.08$, n=9, unpaired t test) however it did demonstrate significantly greater differentiation efficiency over Hybrid 2 ($p<0.05$, n=9, unpaired t test). Hybrid 2 and CDM-CW were not found to be significantly different in regards to differentiation efficiency ($p=0.95$, n=9, unpaired t test). This data is shown in Figure 3.15.

Therefore the ABKYX method was found to be the most effective across cell lines in generating successful differentiations and the most reliable in terms of cardiac differentiation efficiency. For these reasons it was used as the standard differentiation method moving forward.

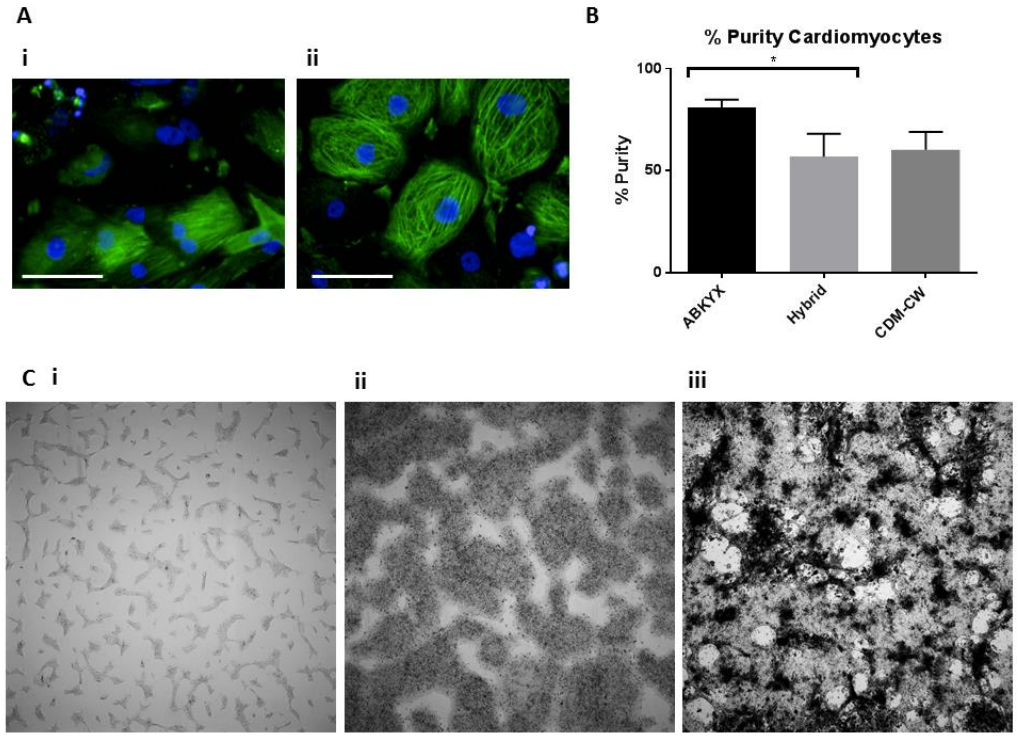


Figure 3-15 - Assessing the quality of the produced cardiomyocytes

A – Representative immunofluorescence images showing the hiPSC-derived cardiomyocytes to be positive for the cardiac markers (A) α-actinin and (B) cTnT. Marker expression was captured using the Alexa488 channel and merged with DAPI (nuclear staining) B – Bar graph illustrating the % purity of cardiomyocytes generated using each method as quantified by assessing number of cells which expressed α-actinin by immunofluorescence. ABKYX was able to generate cardiomyocytes with a relative purity of 80.94±3.865% n=27. Hybrid 2 was able to generate cardiomyocytes with a relative purity of 56.91±11.2%, n=9 and CDM-CW was able to generate cardiomyocytes with a relative purity of 60.3±11.2% n=9. This demonstrated that ABKYX was significantly more efficient than Hybrid 2 ($p<0.05$, n=9, One-way ANOVA, Tukey's Multiple Comparison Test) however ABKYX was not significantly more efficient than CDM-CW ($p=0.08$, n=9, One-way ANOVA, Tukey's Multiple Comparison Test) C – Representative brightfield images through the differentiation process using the ABKYX differentiation method. i – Initial seeding of hiPSC, cells still exhibit a morphology typical of pluripotent cells, namely a high nucleus to cytoplasm ratio and defined cells borders as well as a tendency to cluster tightly together. ii- At this stage hiPSCs are now at a confluence which will be suitable to start the differentiation process, around 80-90%. iii – This is a representative image of cardiomyocytes. There are dense clusters of cells which are connected by others in what resembles a web like monolayer. Cardiomyocyte purity analysis of ABKYX was carried out by Jamie Bhagwan. Scale bars = 50µm.

Effective cryopreservation of cardiomyocytes is a valuable tool in order to enable the generation of frozen banks for large scale drug testing or for maintaining cells at defined ages to improve standardisation of downstream phenotyping assays. However viability of cardiomyocytes after cryopreservation has been reported to be variable in the literature, ranging from 55% to 90% (Xu et al, 2011). Poor viability is problematic in cardiomyocytes as they are a non-proliferative cell type. As a result of this it was decided to test when and how to cryopreserve our cardiomyocytes in order to achieve the greatest efficiency.

Cardiomyocytes were therefore cryopreserved using both Hyclone FBS + 10% DMSO and the commercially available cryopreservation medium CryoStor CS10 (STEMCELL Technologies). Furthermore cardiomyocytes were dissociated using two different methods, a collagenase based method termed UKE and a trypsin based method termed CDS, to ascertain if either related to a reduction in viability post thaw. Full details of the dissociation method can be found in Section 2.1.5.3. Finally cardiomyocytes were frozen at day 14, immediately after the first dissociation or they were dissociated at day 14 then reseeded and given one week of "recovery" time before being dissociated again and cryopreserved at this stage. Viability was assessed according to % of cells staining positive for cell permeable dye propidium iodide (PI).

When HI-FBS was used as a freezing medium post thaw viability was found to be 63.62±17.05% in comparison to 64.26±18.94% when CryoStor CS10 was used, this was not found to be significantly different ($p=0.91$, $n=19$, unpaired t test). These data are presented in Figure 3.16.

Post thaw viability when CDS was used as a method of dissociation was found to be 62.44±19.01% in comparison to 66.52±15.78% when collagenase was used a dissociation method. These were not found to be significantly different ($p=0.48$, $n=14$, unpaired t test). These data are shown in Figure 3.16.

Cardiomyocytes which were cryopreserved at day 14 immediately after first dissociation were found to show a post thaw viability of 68.59±19.37%, this was found to be reduced to 55.98±11.29% when the cells were replated for 7 days before being dissociated again and then cryopreserved ($p<0.05$, $n=14$, unpaired t test). These data are shown in Figure 3.16.

From these data it was decided that routine cryopreservation to create cardiomyocyte banks would be performed using collagenase method of dissociation, cells would be frozen in HI-FBS and this would be performed at first dissociation around day 14 to achieve the maximum post thaw viability.

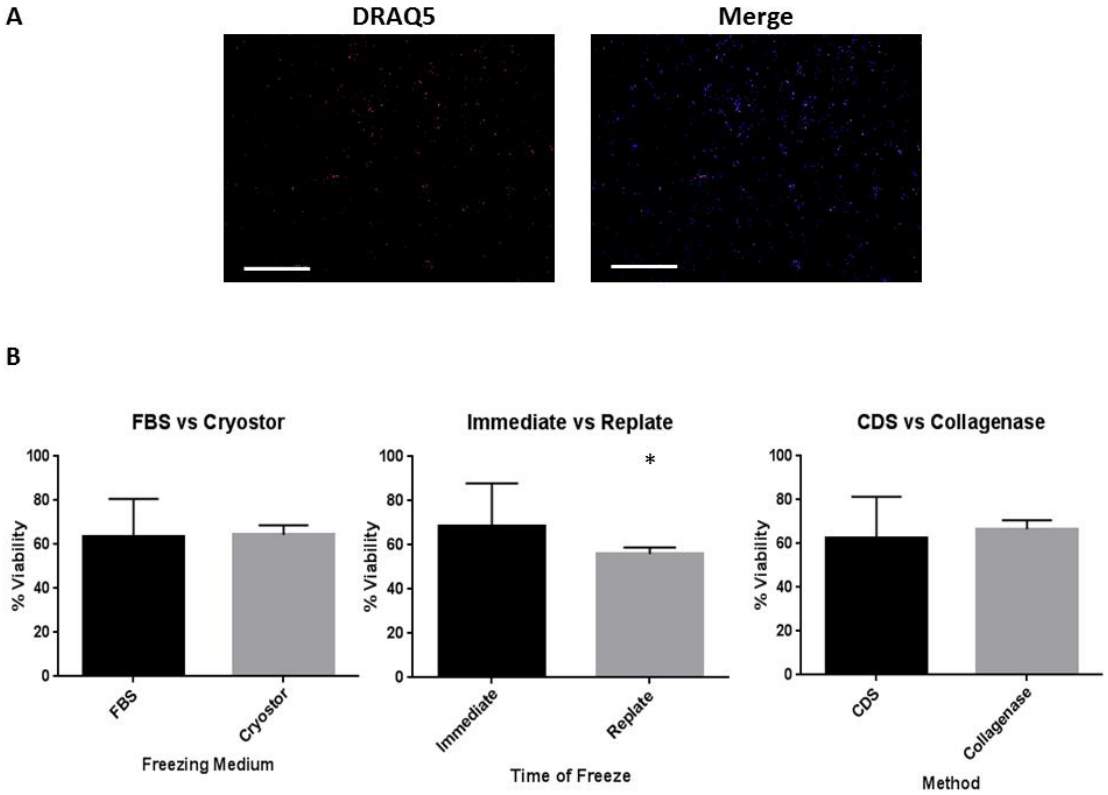


Figure 3-16 - Assessment of cell viability after cryopreservation

A – Representative images of viability staining process. First showing the cells in a 96 well plate format 48 hours after seeding using DRAQ5 channel to capture PI stanining (top). The image second shows the hoescht stain used to show live cells by staining the nucelus blue merged with the image above. Scale bars = 200µm. B – Cells frozen in HI-FBS were found to exhibit a post thaw viability of 63.62±17.05% in comparison to cells frozen in CryoStor CS10 which exhibited a post thaw viability of 64.26±18.94%. This was not found to be a significant difference (n=19, p=0.91, unpaired t test). Cells which were frozen immediately after their first dissociation were found to exhibit a post thaw viability of 68.59±19.37%. This is in comparison to cells which were given 7 days to recover from the initial dissociation which exhibited a post thaw viability of 55.98±11.29%. This was found to be a significant difference (n=14, p=<0.05, unpaired t test).– Cells which were dissociated using UKE were found to exhibit a post thaw viability of 66.52±15.78%. This was compared to cells which were dissociated using CDS which exhibited a post thaw viability of 62.44±19.01%. This was not found to be a significant difference (n=14, p=0.48, unpaired t test).

3.3 Discussion

The seminal reports of hiPSC generation used fibroblasts as a starting cell type (Takahashi et al, 2007; Yu et al, 2007). However alternative starting cell types have been reported in the years since including; lymphocytes (Saito et al, 2016), keratinocytes (Aasen et al, 2008) and hepatocytes (Liu et al, 2010). A more comprehensive list of starting cell types which have been used to generate hiPSCs can be found in Table 3.1. This indicates that generation of hiPSCs can be achieved from a diverse variety of cell types. However in order to choose an optimal cell type a number of factors must be considered. The availability of tissue samples, the ease of isolation of the cells, the ease with which these are able to be genetically manipulated and the efficiency of reprogramming which can be expected are a few factors to consider (Lai et al, 2011).

Fibroblasts are relatively easy to handle *in vitro* and are commonly isolated from skin samples which are able to be stored at 4^{o}C for up to two weeks (Dambrot et al, 2013). This allows samples to be transported to a specialised lab if required. A potential drawback of using skin fibroblasts as a starting cell population is the exposure to mechanical and environmental stresses which can result in significant mutations in these cells (Takeda et al, 2008). This is offset somewhat by the location of skin punch biopsy, which is routinely taken from the upper thigh thus limiting exposure to UV light at least. However, both patients in this study who provided skin did so by consenting to excess skin being taken during surgery for an ICD being fitted, the skin was taken from the chest where it could be argued UV light has ample access. Despite obtaining the samples for this project during surgery, skin punch biopsy is still the most common method of obtaining a skin sample, however this can be off putting to some patients thereby necessitating the investigation of alternatives as has been done in this thesis. However in this study two skin samples were obtained and both generated starting cell populations with relative ease underlining why fibroblasts remain one of the most popular cell types in hiPSC generation.

Supernumerary of teeth is a common reason for dental extraction among adolescents, in adulthood it is not uncommon for wisdom teeth to be removed. An advantage of obtaining cells from dental pulp is that it is insulated within the tooth and is therefore protected from UV damage and microbial contamination (Takeda et al, 2008). A drawback of using dental pulp cells is the relative difficulty in isolating the cells in comparison to isolating skin fibroblasts. The tooth must be cracked open, using a vice, or cut open using a saw. Furthermore if this is successfully achieved there can be little or even no pulp present.

Furthermore the use of dental pulp relies on a tooth being extracted, although wisdom tooth extractions are not uncommon a tooth cannot simply be requested as and when it is required unlike other alternative samples such as blood or urine. In this study attempting to crack or cut the first tooth sample received proved difficult and therefore a change of strategy was employed for the second tooth sample. The initial tooth sample in this study was crushed in a vice and seeded into a Matrigel coated flask but did not result in a successful starting population of cells. The second tooth sample obtained was left in culture medium in a T75 flask and the cells allowed to migrate out, this led to the successful isolation of cells. Unfortunately these became contaminated before any characterisation was possible.

Blood is an attractive source of cells for hiPSC generation as it can readily be extracted from a patient but can also be obtained from blood banks, opening up the potential for large scale stores of histocompatible, allogenic or autogenic hiPSCs for use in therapy. Generation of hiPSC using blood has been established as a reliable starting cell population (Meng et al, 2012; Wang et al, 2013; Bhatt et al, 2016). Initial reports used CD34+ haematopoietic progenitor cells (HPCs) from both mobilised and non-mobilised blood (Loh et al, 2009; Ye et al, 2009). Endothelial progenitor cells (EPCs) are found abundantly in non-mobilised blood therefore avoiding GCSF-stimulation (Geti et al, 2012). These represent a much more attractive and potentially easier to isolate cell type which can be obtained through blood samples which were also shown to be amenable to reprogramming (Geti et al, 2012). In this study 40ml of blood was collected from a healthy donor and this was immediately processed in order to attempt to isolate cells. Unfortunately no cells were observed after 14 days of culture on this occasion, this is potentially due to the volume of blood received as the protocol required 60ml of blood. However low sample volume is unlikely to be a problem in the future using alternative protocols. It has been reported that hiPSCs can be derived using only a pin-prick of blood (Tan et al, 2014). Although blood remains an attractive option as a starting sample no other attempts were made to isolate cells from blood samples due to time pressure during this thesis.

Micturition is a naturally occurring and necessary bodily function which occurs multiple times per day. Although the number of cells found in urine is relatively low, only expected to be a few thousand cells sheared off in the renal system per day (Zhou et al, 2011). However using cells isolated in this way it was previously been shown to be successful in generating hiPSCs at efficiencies reported to up to 4% (Zhou et al, 2011). This reprogramming was reported in a retroviral system however 4% remains among the highest reported hiPSC efficiencies. This is

potentially due to the nature of cells excreted in urine. It has been stated that more terminally differentiated cells can be more difficult to reprogram leading to lower efficiencies (Eminli et al, 2009). Although no characterisation of urine derived cells was possible in this study it has previously been reported that a subpopulation of cells excreted in urine exhibit multidifferentiation potential (Zhang et al, 2008). If this were the case it would serve to increase the attractiveness of urine as a starting sample. In this study urine samples were obtained from two healthy donors, and on one occasion a LQTS3 patient. Overall ten urine samples were obtained over a 3 month period with only one generating a viable starting cell population. A number of factors may be responsible for the lack of success using this method. It is possible that the medium required optimisation or potentially the inexperience of the operator in dealing with urine processing and sample isolation as this was performed in the first 6 months of my PhD. Some potential optimisation experiments would be to test different substrates. Furthermore it may be prudent to test alternative mediums. Attempts at establishing urine as a starting cell population were abandoned due to limited success and time pressure.

Taken together these findings suggest that fibroblasts continue to represent the most robust starting cell population due to the ability to store the samples for up to 2 weeks before processing and their robustness in culture in comparison to other cell types. However the potential for mutations due to environmental stress and UV damage coupled with the potential to dissuade patients from donating samples still indicate an alternative is required. Despite the relative lack of success in this study other studies continue to routinely use blood (Meng et al, 2012; Geti et al, 2012) and urine (Afzal et al, 2016; Sochacki et al, 2016) as stating populations for hiPSC generation and therefore attempts at their isolation should be repeated to optimise this system.

Previous reports of hiPSC generation using SeV have shown up to 1% efficiency using MEF feeder layers (Fusaki et al, 2009). In this project hiPSC generation using SeV is reported at 0.51% using feeder free and xeno free conditions. This is higher than reported efficiencies using SeV in feeder free and defined conditions which have previously been reported between 0.04-0.31% (MacArthur et al, 2012; Yamasaki et al, 2016).

Delivery of episomal plasmids using electroporation has previously been reported to yield efficiencies of between 0.0003-0.028% (Yu et al, 2009; Okita et al, 2011). Although the efficiency reported in this study, 0.004%, falls within the range the plasmids used in this protocol were the same as those used in the work of Okita and colleagues who reported

0.028%, therefore the reported efficiency in this study was lower than anticipated. In this study the plasmids were delivered at 1µg per plasmid as was performed in the literature (Okita et al, 2011). Therefore decreased reprogramming efficiency observed in this study was not the result of variation in the amount of plasmid delivered. It may be the case that further optimisation of the electroporation procedure may be required in order to improve the transfection efficiency. Alternatively it may be genetic and epigenetic factors which result in variable reprogramming efficiency.

Delivery of episomal plasmids using GET peptide delivery system to generate hiPSCs has not been published in the literature previously. This seminal work was able to generate hiPSCs at an efficiency of 0.0219% which is a similar yield to the highest reported efficiency when delivering episomal plasmids to cells via electroporation. The benefit of using the GET peptide system over electroporation is that GET is likely to be more financially advantageous than electroporation and was performed using 5 times less cells in this study. Furthermore GET compares favourably in both transfection efficiency and cell viability compared to widely used transfection reagent, lipofectamine 2000 (Dixon et al, 2015), making it a powerful tool to deliver biologically active cargo to cells.

To conclude, although delivery of episomal plasmids using either electroporation or GET peptide is more financially advantageous than SeV the results of this study found that SeV was able to reprogram fibroblasts at much greater efficiencies. Although there have been some reported concerns regarding toxicity of SeV as a delivery system the optimisation carried out in this study using SeV GFP reporter vector found that there were no adverse effects on the lines tested making SeV the most efficient and robust method tested in this study to generate hiPSCs routinely going forward.

The hiPSC lines generated in this project using SeV compared favourably to previous hiPSC lines generated in our lab using lentiviral mediated transduction. The cells generated in this study expressed multiple markers of pluripotency as assessed by immunocytochemistry and by FACS. In addition to this the majority of the lines generated using SeV exhibited genomic stability with no karyotype abnormalities. Furthermore the average CPD time across all cell lines was found to be 29.8 hours in contrast to previously established CPD for HUES7 of 33.5 hours. These are similar in terms of growth rate, however what must be taken into account is that our new SeV hiPSC lines are maintained in E8 medium whereas previously, the hESC lines HUES7 was maintained in MEF-conditioned medium. Regardless there appears to be a consistent growth rate between the two systems. The newly generated SeV hiPSC lines also

exhibit multi lineage differentiation potential with positive staining for definitive markers of ectoderm, endoderm and mesoderm, this was also shown to be the case with our previously generated lentiviral hiPSC which were also able to form all three germ layers.

Generation of cardiomyocytes using the CDM-CW method yielded success over a one month period in 50% of attempts in 60% of cell lines. This is lower than has been reported in the literature where this method has been shown to generate cardiomyocytes in 100% of cell lines tested, however the robustness of the method is not reported (Burridge et al, 2014). The ABKYX method generated cardiomyocytes in 90% of attempts across 100% of all cell lines tested, illustrating a good degree of robustness across cell lines. In our hands the CDM-CW method required optimisation, the published protocol reports the use of 6µM of CHIR99021 to induce mesoderm formation, this was found to be cytotoxic to most hiPSC lines in our lab and was reduced to 4µM which yielded greater success. The reason for the variation between the methods could be down to a number of factors. It may be the result of genetic and epigenetic variability of hiPSC lines which is thought to be greater than hESC lines as the result of a potential "epigenetic memory" (Kim et al, 2011). This genetic and epigenetic variability has been implicated previously in potentially impacting differentiation potential (Zhang et al, 2009). Optimisation of the concentration of differentiation factors required between different cell lines has been required in our lab previously, albeit using an EB based system. Furthermore the stage of the cell cycle which the cells are in at the initiation of differentiation has been implicated in impacting differentiation potential (Pauklin and Vallier, 2013). Initial screening concentrations of the small molecules used in CDM-CW provided variable results. In this thesis it is unclear why the CDM-CW method proved to be more variable and less reliable than the ABKYX method. The genetic/epigenetic variability of each cell line could potentially be the cause of the variability observed in CDM-CW which was not observed in ABKYX. Although both methods seek to activate the Wnt signalling pathway before later inhibiting it in the differentiation process they achieve this through different means. The CDM-CW method uses GSK3B inhibitor CHIR99021 which acts by upregulating endogenous BMP4 and activing/NODAL signalling (Lian et al, 2012). However this activation may be variable depending on the basal endogenous levels of cytokines in each cell line. The ABKYX method activates the Wnt signalling pathway by introducing exogenous BMP4 and Activin A, therefore acting upstream of CHIR99021, this could be a cause of its increased reliability. Furthermore reports suggest that hiPSCs generated under different conditions leads to variations in cell cycle and DNA replication gene profiles (Chung et al, 2011). This could also be an explanation as to why an in-house developed method generates better results using cell lines generated

in our lab. A further explanation may be the fragile nature of cardiomyocyte differentiation. It is known that the signalling cues required for efficient differentiation must be delivered within what could be considered very tight windows, indeed sustained TGFβ/activing/NODAL, BMP or Wnt signalling which lasts beyond the cardiac mesoderm stage can result in a prohibitive effect in producing cardiomyocytes (Kattman et al, 2011). It remains possible that activation of the Wnt signalling pathway is more robustly achieved using BMP4 and Activin A than CHIR99021. A limitation of this experiment which must be noted is that different hiPSC lines were tested across different methods, in order to fully elucidate whether one method is truly more efficient than the others a more rigorous experiment testing the same cell lines should be performed.

To conclude it appears clear that in our lab, using our reagents the ABKYX method is more reliable and robust than CDM-CW. This is not to suggest that the CDM-CW method does not work but the cell lines generated in our lab appear more reliably differentiated using ABKYX. For this reason ABKYX was the standard differentiation method used going forward.

4 Chapter 4 – Assessing the phenotype of LQTS2 hiPSCs and the effects of pharmacological intervention

4.1 Introduction

The Long QT Syndromes (LQTS) are a group of cardiac channelopathies characterised by an elongation of the QT interval on an ECG alongside T-wave irregularity, ventricular tachycardia and an increased risk of sudden death (Crotti et al, 2008). LQTS2 is the second most common subtype of LQTS and accounts for 30-45% of cases (Schwartz et al, 2012). Models of LQTS2 rely on the use of both animal models and heterologous overexpression systems overexpressing specific ion channels. However these models are often inaccurate as a result of inter-species differences in the cardiovascular system (Rajamohan et al, 2013) and the inability of recombinant systems to accurately model the synergistic relationship between ion channels *in vivo* (Shiba et al, 2009). For example I_{kr} is found at very low levels in murine cardiomyocytes, however is a major determining factor in repolarisation of human cardiac cells (He et al, 2003). Heterologous expression of hERG and analysis of its blockade can lead to a drug such as verapamil being labelled as dangerous as terfenadine when this is not the case *in vivo* (Kramer et al, 2013). These factors necessitate the need for use of hiPSC-based models of LQTS which will help model and understand the pathogenesis of LQTS2 and be used as part of *in vitro* drug assays to identify potentially therapeutic compounds. This chapter describes the use of hiPSC-CMs in this thesis in phenotyping assays which demonstrate their ability to demonstrate functionality and recapitulate the patient phenotype *in vitro*. Furthermore this chapter reports the use of drugs with four different targets, I_{kr}, $I_{katp,}$ PPARδ and I_{ks} agonists, to reduce the APD and therefore the QT interval in LQTS2-hiPSC-CMs.

4.1.1 Long QT Syndrome type 2

LQTS2 is the second most common reported subtype of LQTS, responsible for up to 45% of cases, and is characterised by a defective I_{Kr} α-subunit Kv11.1 coded for by the *KCNH2* gene (Schwartz et al, 2012). The mechanism of this defect can be categorised as class 1 (disruption of channel synthesis) or class 2 (disruption of channel trafficking) and it has been estimated that ~90% of LQTS2-linked missense mutations act via this class 2 mechanism (Smith et al, 2016). The majority of LQTS2 associated cardiac events are triggered by emotional stress which can be induced by auditory stimuli such as an alarm clock sounding or a telephone ringing (Schwartz et al, 2001). Diagnosis of LQTS2 typically follows an episode of syncope or seizures which are not able to be explained by any pre-existing medical condition. The

prolongation of the QT interval coupled with an ECG which shows a notched or bifid T-wave typically confirms the diagnosis (Zhang et al, 2000).

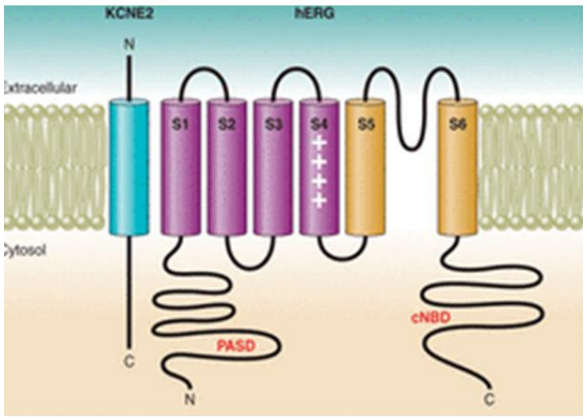


Figure 4-1 - The structure of hERG channel
Schematic displaying the hERG channel. In blue is shown the KCNE2 accessory subunit of the I_{kr} channel complex. This accessory subunit consists of a single transmembrane helix. Shown in purple are the four hERG1 subunits which form the pore-forming alpha subunit of I_{kr} by tetramarisation, the voltage sensing domain is found in this region. S5 and S6 shown here in yellow form the pore domain and are vital in the formation of the K^+ permeation pathway which allows K^+ flow in and out of the cardiomyocyte (Bohen et al, 2017).

4.1.2 Molecular and structural biology of I_{kr} current

The *KCNH2* gene is located on chromosome 7q35-36 and encodes the human ether a go-go-related K^+ channel (hERG) (Warmke et al, 1994), the structure of which is shown in Figure 4.1. hERG is occasionally referred to as hERG1 as there have been two other isoforms discovered however hERG1 remains the dominant isoform in cardiomyocytes (Shi et al, 1997). Functional hERG channels consist of four hERG α-subunits which contribute to the formation of either a hERG1a homomeric channel or a hERG1a/hERG1b heteromeric channel (Jones et al, 2004). The four hERG subunits tetramerize to form the pore-forming subunit of the I_{kr}, hERG1 contains a voltage-sensitive domain and a pore domain while *KCNE2* is considered an accessory subunit of the I_{kr} channel complex consisting of a single transmembrane helix (Bohnen et al, 2017). The S4 transmembrane segments of the hERG contains the primary positively charged amino acid required for voltage-sensing and opening of the activation gate. hERG channels exist in a non-conducting closed state at negative membrane potential and depolarisation of the cell membrane to potentials greater than 60mV induces the hERG channel to open leading to an outward flow of K^+ ions as a result of the electrochemical gradient (Sanguinetti and Tristani-Firouzi, 2006). The gating properties of hERG differs from that of other K_v channels, inactivation is more rapid than activation, thereby reducing outward flow of K^+ ions at depolarised potentials thus prolonging phase 2 of the action potential. Recovery from inactivation occurs quicker than deactivation thereby initiating phase 3 of the

action potential which results in a rapid repolarisation due to K^+ ion efflux (Sanguinetti and Tristani-Firouzi, 2006).

4.1.3 The role of I_{kr} current in cardiac function

In the human heart the delayed rectifier K^+ current which consists of slowly-activating (I_{ks}) and rapidly-activating (I_{kr}) components is a key factor in the duration of cardiac repolarisation and thus the action potential (AP) (Shih, 1994). The cardiac action potential undergoes 4 distinct phases during which repolarisation of cardiac myocytes primarily occurs during phase 3 and is achieved predominantly via the I_{kr} current conducted through hERG channels (Sanguinetti et al, 1995; Trudeau et al, 1995). The dysfunction of the I_{kr} channel results in the reduction of the outgoing K^+ current during phase 3 of the AP resulting in elongation of the action potential duration (APD) (Medeiros-Domingo et al, 2007).

The role of hERG in maintenance of normal cardiac electrical activity is derived from its unusual gating properties where the channel is slowly activated but quickly inactivated (Piper et al, 2005). During the plateau phase of the AP a low amount of current flows through hERG channels. This reflects the fact that the channels are in a state of inactivation. However as the cells begin to repolarise this repolarisation induces a self-perpetuating more rapid repolarisation by increasing the recovery from inactivation of the channel (Roden et al, 2006).

4.1.4 hiPSCs as a model for LQTS2

In hiPSC-CMs the role of specific mutations within the *KCNH2* gene has been studied in a number of reports. Study of the G1681A mutation, which will be investigated in this thesis, demonstrated that hiPSC-CMs from G1681A patients exhibited prolonged APD in comparison to control cell lines, including the patient's asymptomatic mother, when analysed using both single cell manual patch clamp electrophysiology and multi electrode array cluster analysis (Matsa et al, 2011). Furthermore the cardiomyocytes analysed in this report were found to exhibit EADs when stressed using β-adrenergic agonist isoprenaline, these EADs were not observed in control cells (Matsa et al, 2011).

The patient in this study presented at 15 years of age having suffered 11 episodes of syncope in the previous year and was found to exhibit a QTc interval of 571ms (Matsa et al, 2011). This patient was found to carry the LQTS2-autosomal dominant point mutation at *KCNH2* G1681A which causes an alanine to threonine substitution at position 561 of the encoded protein and

is located within the pore-forming region at transmembrane segment S5 (Dausse et al, 1996; Matsa et al, 2011). Mutations in the pore forming region of the protein carry a higher mortality risk than elsewhere (Moss et al, 2002). This may be as a result of the pore domain spanning the S5-S6 transmembrane segments which harbour the K^+ permeation pathway necessary for K^+ ion conduction (Doyle et al, 1998). The location of this mutation and the length of the recorded QTc, 571ms (Matsa et al, 2011), underlie the severity of this patient's phenotype.

4.1.5 Treatment options for LQTS

Treatment for LQTS is vital as mortality rate for symptomatic patients who remain untreated for one year is 21% (Schwartz et al, 2012). The most common form of pharmacological intervention for LQTS patients is β-blockers such as propranolol or nadolol (Crotti et al, 2008). However in the case of LQTS2 patients up to 23% still experience adverse cardiac events despite β-blocker therapy (Priori et al, 2004). In addition to this patients remain at risk if they fail to take their medication regularly. The ineffectiveness of pharmacological intervention usually signals the need for surgical solutions as described in Section 1.1.2.2.

It would be advantageous to improve pharmacological treatments due to the invasive nature of surgical procedures. Previous reports have indicated that APD can be shortened in LQTS patients by increasing K^+ outflow (Antzelevitch and Oliva, 2006; Yazawa et al, 2011; Itzahki et al, 2011). In this thesis four different types of drugs were investigated with regards to their efficacy in reducing the duration of the action potential in LQTS2-hiPSC-CMs. The four types of drugs were I_{katp} activators, I_{kr} activators, PPARδ activators and an I_{ks} activator, the effects of these drugs were then compared to the more standard β-blocker therapy in hiPSC-CMs.

4.1.5.1 I_{katp} Activators

Nicorandil has been reported to act as an I_{katp} opener (Biermann et al, 2011). I_{katp} activators have previously been demonstrated to reduce APD in LQTS2-hiPSC-CMs (Matsa et al, 2011). Studies using nicorandil on LQTS2 hiPSC-CMs have reported a decrease in APD of up to 18% in addition to abolishing spontaneously occurring EADs (Matsa et al, 2011; Liang et al, 2013). This action was further attenuated by delivering nicorandil in the presence of an I_{kr} opener, PD-118057 (Matsa et al, 2011). Nicorandil has recently been reported to act by unblocking the hERG channel (Chen and Zou, 2016). Minoxidil has been shown to reduce APD in enzymatically isolated guinea pig cardiomyocytes without affecting the basal resting membrane potential

(Hayashi et al, 1993). In the time since the publication from Hayashi and colleagues, a search of the literature has shown no reports of its use in human cells for cardiac related diseases, indeed it is more commonly used in hair loss treatments (Varothai and Bergfeld, 2014).

4.1.5.2 I_{kr} Activators

I_{kr} block led to an increase in cellular repolarisation in canine ventricular cells *in vivo* (Volders et al, 2003). Given the role in repolarisation that I_{kr} plays it may be considered intuitive to activate this channel in order to reduce the QT interval in patients who exhibit increased prolongation. NS1643 is a compound which acts by activating I_{kr} and has been shown to reduce APD in ventricular cardiomyocytes of isolated guinea pig hearts (Meng et al, 2013). Furthermore NS1643 was demonstrated to activate I_{kr} in guinea pig cardiomyocytes and reduced the action potential to 65% of control samples (Hansen et al, 2005). NS1643 also suppressed ventricular tachyarrhythmias in a rabbit *in vivo* model (Diness et al, 2008). The mechanism of action for NS1643 has been reported to be that of a partial agonist of hERG channels by reducing their inactivation (Casis et al, 2006). It has been reported that NS1643 shortens the APD in canines and achieves this by interacting with a number of transmembrane currents including I_{ca}, I_{kr}, I_{ks} and I_{to}, the authors speculate that the APD shortening effect in this case is likely related to both inhibition of I_{ca} and enhancement of I_{kr} (Szabo et al, 2011).

Meng and colleagues also analysed the effect of another antiarrhythmic compound, ICA-105574, which exhibited the ability to reduce APD and ameliorate EADs, however this compound was found to have potentially proarrhythmic effects in healthy hearts (Meng et al, 2013). For this reason NS1643 was studied in this thesis for its effect on LQTS2-hiPSC-CMs however ICA-105574 was not due to its potentially negative side effects in healthy patients.

Ginsenoside RG3 (RG3) is extracted from the medicinal plant *Panax ginseng* and is thought to increase nitric oxide production (Wang et al, 2015). Indeed it was demonstrated to be a major determinant of endothelium-dependant nitric oxide mediated relaxation and this was postulated to be achieved through activation of K^+ channels (Kim et al, 1999). In addition to this RG3 was demonstrated to mediate the induction of a persistent current through the hERG channel as well as slowing the channels deactivation in xenopus heterologous expression model overexpressing the hERG channel (Choi et al, 2011). In humans, RG3 is known to activate the *KCNQ1* and *KCNE1* genes leading to increased current in the I_{ks} channel (Choi et al, 2010).

4.1.5.3 Peroxisome proliferator-activated receptor delta (PPARδ) Activators

The hERG channel has been reported to interact with the protein 14-3-3 epsilon which is encoded by the gene *YWHAE* (Kagan et al, 2002). Protein 14-3-3 epsilon is reported to interact with hERG by prolonging the effects of adrenergic stimulation by shielding phosphates from degradation via stabilisation of the PKA-phosphorylated state of the channel (Kagan et al, 2002). Therefore upregulation of protein 14-3-3 epsilon could potentially activate the hERG channel in LQTS2 patients thus increasing the outflow of K^+ ions during repolarisation leading to faster repolarisation in cardiac myocytes. PPARδ has been shown to activate the YWHAE promotor in endothelial cells thus increasing its expression (Brunelli et al, 2007).

The PPARs belong to a nuclear receptor super family of ligand-activated transcription factors and can be subtyped to three isoforms, α, β/ δ and γ, all of which are found in the human heart (Lee and Kim, 2015). A search of the literature has shown no reports of PPARδ agonists being used in LQTS patients either *in vivo* or *in vitro*, however their ability to interact with and potentially upregulate the activity of the hERG channel led to the decision to test two PPARδ agonists in this thesis.

Telmisartan is an angiotension II receptor blocker which has been shown to activate PPARδ receptors in mouse models of skeletal muscle (He et al, 2010; Feng et al, 2011; Li et al, 2013). More recently telmisartan was found to activate the PPARδ pathway in mesangial cells in humans potentially possessing an anti-fibrotic effect (Mikami et al, 2014). Furthermore telmisartan has previously been used to treat hypertensive patients with left ventricular hypertrophy and was found to improve sympathovagal balance and electrical stability in the heart (Galetta et al, 2010). GW0742 is a highly selective PPARδ agonist which has previously been tested in human cancer cell lines and was demonstrated to activate the PPARδ receptor but were not shown to potentiate tumorigenesis (Hollingshead et al, 2007). Traditionally GW0742 has been used as an anti-inflammatory as it has been shown to reduce lung inflammation in mice (Galuppo et al, 2010).

4.1.6 Chapter aims and objectives

The aims of this chapter were to ascertain whether ReBl-hiPSC-CMs (LQTS2), carrying G1681A mutation in *KCNH2*, could recapitulate the phenotype of the patient *in vitro* and be used for an *in vitro* drug screen of compounds which may exert beneficial effects for LQTS2 patients. In order to achieve this both healthy and LQTS2-hiPSC-CMs were tested for their electrophysiological properties using voltage sensitive fluorescent dyes. The initial testing was

to demonstrate that these hiPSC-CMs displayed functionality by their response to drugs of known action. Should these hiPSC-CMs demonstrate functionality they would then be used downstream in an *in vitro* drug assay to assess the effectiveness of drug compounds in reducing QT interval in LQTS2-hiPSC-CMs. These experiments would be carried out by analysis of the APD of the *in vitro* cardiomyocytes as a surrogate for the QT interval. In order to achieve this the following objectives had to be met:

1. Ascertain the functionality of hiPSC-CMs by assessing response to known β-adrenoceptor agonist isoprenaline.
2. Ascertain that the CellOPTIQ platform was able to detect differences in APD between hiPSC-CMs and changes in APD after drug treatment.
3. Assess whether ReBl-hiPSC-CMs exhibit different electrophysiological properties at basal levels in contrast to healthy-hiPSC-CMs.
4. Assess the effectiveness of β-blockers in modulating QT interval in LQTS2 hiPSC-CMs.
5. Assess the effectiveness in comparison to β-blockers of I_{katp}, $I_{kr,}$ PPARδ and I_{ks} agonists in reducing QT interval in ReBl-hiPSC-CMs

4.2 Results

4.2.1 Assessing cellular response to β-adrenergic stimulation

In order to assess that the hiPSC-CMs generated in this thesis displayed functionality it was necessary to ascertain their response to a drug of known action. Isoprenaline (ISO) is a known β-adrenoceptor agonist, exposure to which should result in the hiPSC-CMs increasing their beat rate (Ngeumo et al, 2012). In order to measure beat rate hiPSC-CMs from healthy (ReBl PAT) and LQTS2 (ReBl) patients were loaded with calcium labelling dye Fluo-4. Each calcium transient was considered a surrogate for a beat as calcium transients drive contraction of cardiomyocytes (Bers, 2002). These cells were analysed using the Envision fluorescent plate reader before and after ISO addition.

Beat rate recordings from the Envision platform were taken before and after treatment of ReBl-hiPSC-CMs with 25, 50, 100, 200 or 400nM isoprenaline. As shown in Figure 4.2, only the 400nM treatment led to a significant increase in beat rate (32±8.49bpm vs 109±7.01bpm; $p<0.05$, n=2, paired t test). Beat rate recordings from the Envision platform were taken before and after treatment of ReBl-PAT-hiPSC-CMs with 25, 50, 100, 200 or 400nM isoprenaline. As shown in Figure 4.2, only the 400nM treatment led to a significant increase in beat rate (27±1.41bpm vs 47.95±1.9bpm, $p<0.05$, n=2, paired t test).

Therefore in this experiment both healthy and LQTS2 hiPSC-CMs respond to a drug of known action, ISO, as expected (Ngeumo et al, 2012), by increasing their beat rate. These data provide confidence that these hiPSC-CMs display functionality and respond to drugs of known action *in vitro* appropriately.

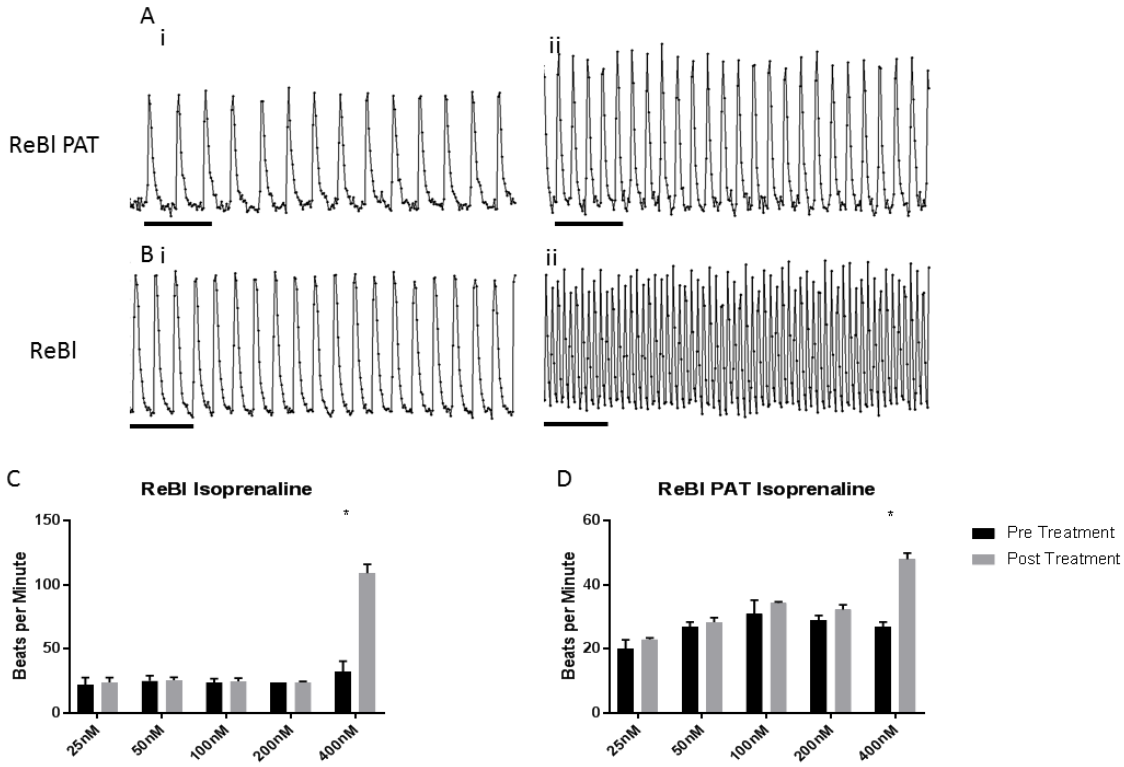


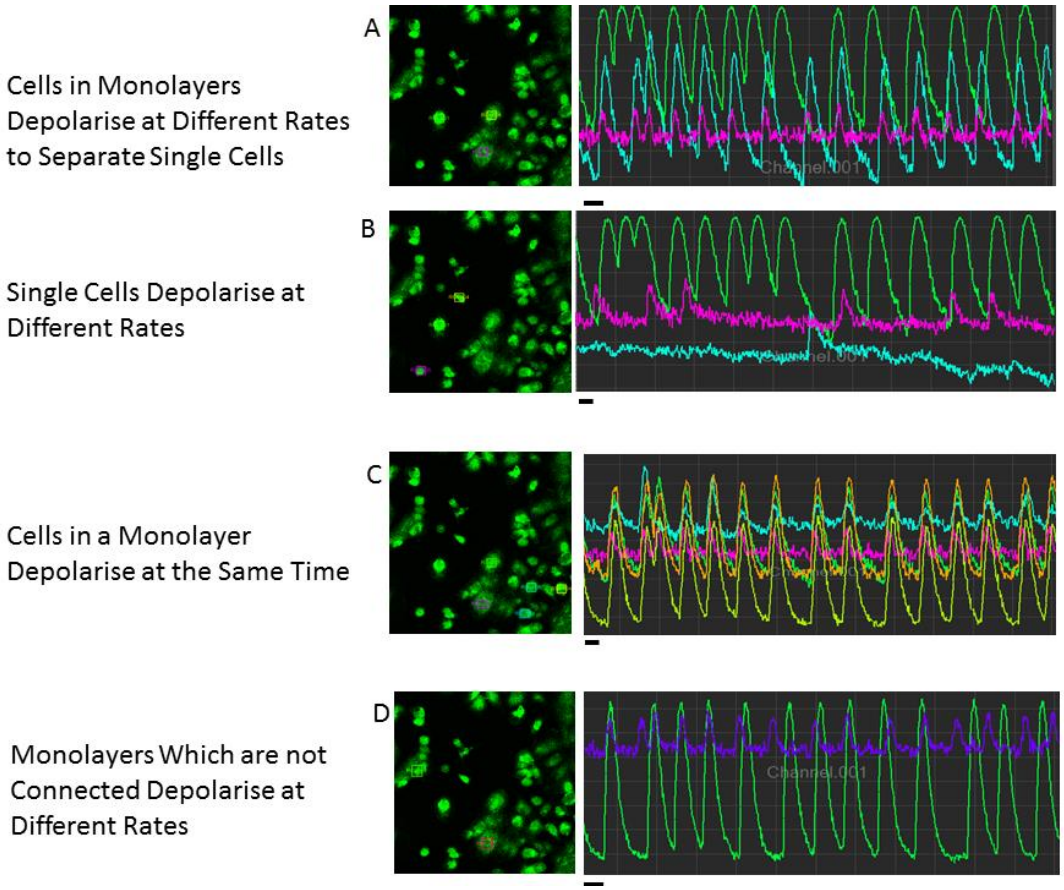
Figure 4-2 - Using the Envision to assess hiPSC-CM response to isoprenaline

A – Envision scans which show calcium transients as detected using Fluo-4 calcium labelling dye for the healthy control cell line ReBl-PAT-hiPSC-CMs. i) Transients detected under basal conditions. ii) These are the transients which were observed after the addition of 400nM Isoprenaline. Scale bar = 5 secs. B - Envision scans which show calcium transients as detected using Fluo-4 calcium label for the ReBl-hiPSC-CMs which carries the G1681A mutation leading to LQTS2. i) These transients were recorded under basal conditions. ii) These are transients which were recorded after the addition of 400nM Isoprenaline. Scale bar = 5 secs. C – Graph showing the beats per minute of ReBl-PAT-hiPSC-CMs before and after treatment with isoprenaline. There were no significant differences between beat rates found for 25nM ($p=0.28$, $n=2$, paired t test), 50nM ($p=0.46$, $n=2$, paired t test), 100nM ($p=0.39$, $n=2$, paired t test), 200nM ($p=0.14$, $n=2$, paired t test), however there was a significant increase observed when the cells were treated with 400nM isoprenaline ($p<0.05$, $n=2$, paired t test). D - Graph showing the beats per minute of ReBl-hiPSC-CMs before and after treatment with isoprenaline. There were no significant differences between beat rates found for 25nM ($p=0.72$, $n=2$, paired t test), 50nM ($p=0.87$, $n=2$, paired t test), 100nM ($p=0.79$, $n=2$, paired t test), 200nM ($p=0.95$), however there was a significant increase observed when the cells were treated with 400nM isoprenaline ($p<0.05$, $n=2$, paired t test).

4.2.2 Assessing the cells behaviour as single cells and monolayers

Traditional electrophysiology analysis of hPSC-CMs has relied on the use of manual patch clamp technology whereby a single cell is patched by a thin glass electrode to elucidate its electrical properties (Matsa et al, 2011). However, while this approach yields high resolution information, it is labour intensive and low throughput. The advent of calcium-sensitive dyes enables analysis of single cells, multi-cellular clusters and monolayers of cardiomyocytes in medium- to high-throughput. Therefore, the purpose of this section was to use realtime confocal optical imaging of calcium transients to evaluate which densities of hiPSC-CMs were most suitable for analysis.

Cardiomyocytes from two hiPSC lines (NCRM5 and CP1) were seeded at different densities to produce single cells and multi-cellular clusters, as well as patches of confluent monolayer (Figure 4.3). hiPSC-CMs were then stained using Fluo-4 calcium sensitive dye, after this staining scans of 60s in duration were used to determine whether beat rate frequency of different areas containing single cells or monolayers. Regions within interconnected monolayers beat in synchrony as shown in Figure 4.3A and 4.3C, whereas there was a high level of beat rate diversity between single cells or uncoupled regions as shown in Figure 4.3A, 4.3B and 4.3D. This confirmed the expectation that coupled monolayers beat in synchrony. Since this was deemed important for reproducibility of data, all further experiments used seeding densities that produced confluent monolayers of hiPSC-CMs.



Cell	Transients
Single Cell 1	14
Monolayer 1A	15
Monolayer 1B	15

Cell	Transients
Single Cell 1	14
Single Cell 2	6
Single Cell 3	1

Cell	Transients
Monolayer 1A	14
Monolayer 1B	14
Monolayer 1C	14
Monolayer 1D	14
Monolayer 1E	14

Cell	Transients
Monolayer 1	13
Monolayer 2	15

Figure 4-3 - - Analysis using confocal microscopy of calcium transients in single cells and monolayers

A –Confocal image with analysis of individual cells within it. Highlighted is one single cell and two separate cells within the same monolayer. Despite similar numbers of total transients there is a lack of synchronous depolarisation. B –Three single cells which are not connected to any cell around them. The data here show that there is no synchrony with regard to triggering of a transient or indeed to how many we expect to see given a set time point. C –5 cells are shown here within a monolayer of cells, it is expected these cells will be electrically coupled (Zhu et al, 2014). The data here show that these cells exhibit the same number of transients and that these transients are triggered synchronously. D – Here we show 2 cells which are within monolayers, previously shown to be synchronous, but not the same monolayer. The data here show that there is no intrinsic rate of calcium transient and that there is no co-ordinated triggering off the transients between these monolayers. Scale bar = 2 secs

4.2.3 Optimisation of the CellOPTIQ platform

In Section 4.2.1 the Envision plate reader was used to assess the response of hiPSC-CMs to isoprenaline treatment. While this platform is able to read fluorescence across an entire well it is incapable of image analysis of single or multiple cells. Therefore the Envision platform is not capable of detecting local changes in calcium or voltage. To carry out this higher level of analysis required the CellOPTIQ platform was used in this thesis. The CellOPTIQ platform is capable of measuring calcium, voltage and contractility of hiPSC-CMs. The machine is able to use non-toxic fluorescent cell dyes to detect rapid (<1μs) changes in voltage at high frequencies (>10 kHz) enabling detection of subtle changes in upstroke kinetics. Furthermore the machine is capable of visualising calcium movement within a cell using a ratiometric dye meaning measurements free from artefacts due to hiPSC-CM movement.

In order to ascertain whether this system would be suitable for the *in vitro* drug assays planned in this thesis it was first required to optimize the system using our cells. A healthy control line (NCRM5) was differentiated to cardiomyocytes and these were seeded in 96 well plate under a variety of different conditions. Cells were seeded onto glass and plastic bottomed 96-well plates which were coated with either Matrigel or vitronectin-peptide. Finally the cells were loaded with either FluoVolt or Di-4-ANEPPS voltage sensitive fluorescent dyes and their signal:noise ratio (S:N) assessed. Di-4-ANEPPS was demonstrated to exhibit a S:N of 4.12±1.69 in comparison to a S:N of 29.46±4.9 when using FluoVolt when coated on standard plastic bottomed 96-well plates coated in Matrigel. This increase was observed to be significant ($p<0.05$, n=4, unpaired t test). Averaged action potential traces and S:N ratios are displayed in Figure 4.4. Replacing Matrigel coating with vitronectin-peptide coating was not found to improve S:N. In addition to this the use of glass-bottomed 96-well plates instead of plastic bottomed 96-well plates did not improve S:N.

These data conclude that the hiPSC-CMs used in this experiment exhibit their optimal S:N, generating high quality recordings, when seeded into plastic-bottomed 96-well plates coated in Matrigel and dyed using FluoVolt. As a result of these findings this was the standard assay layout used going forward.

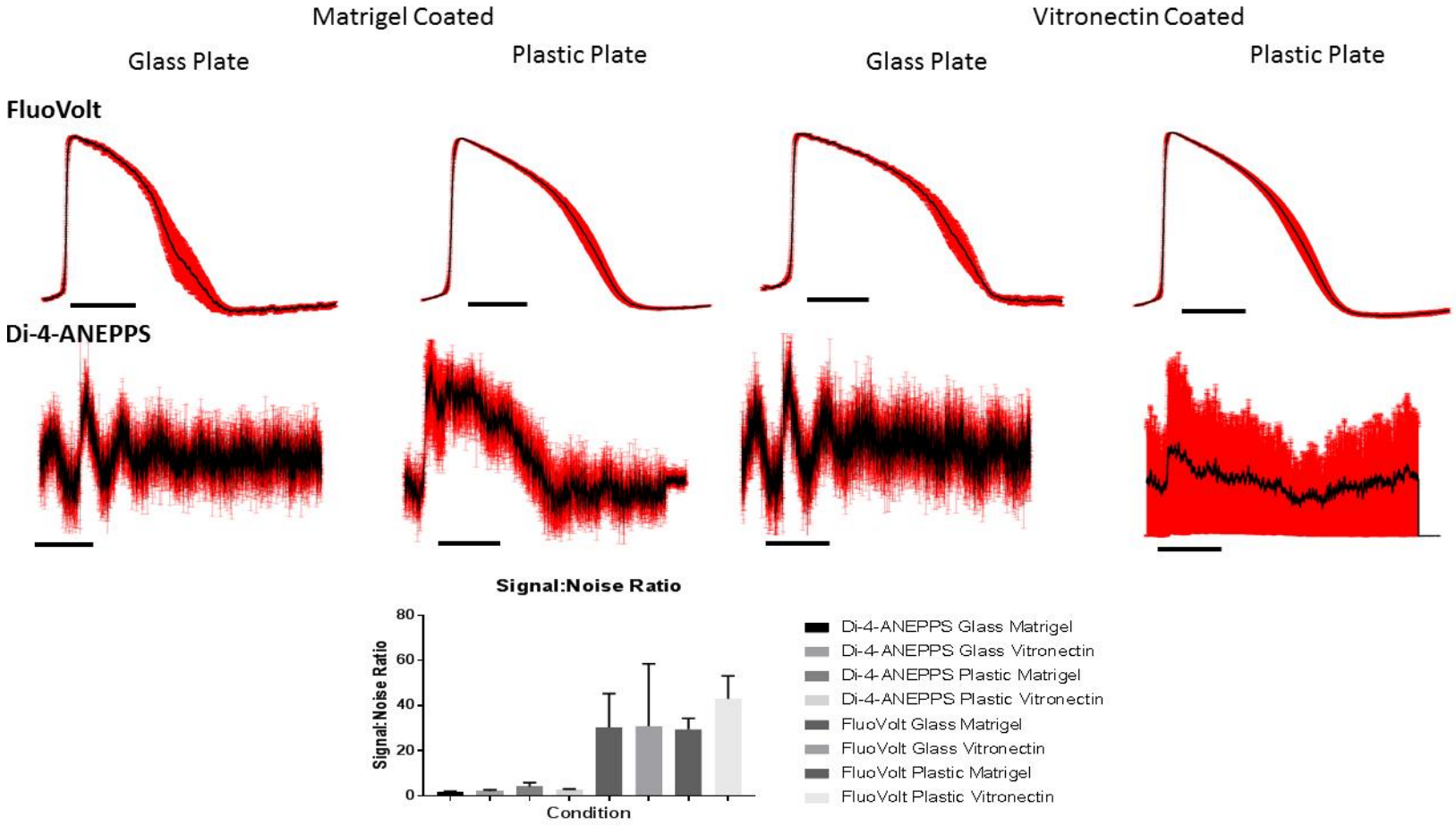


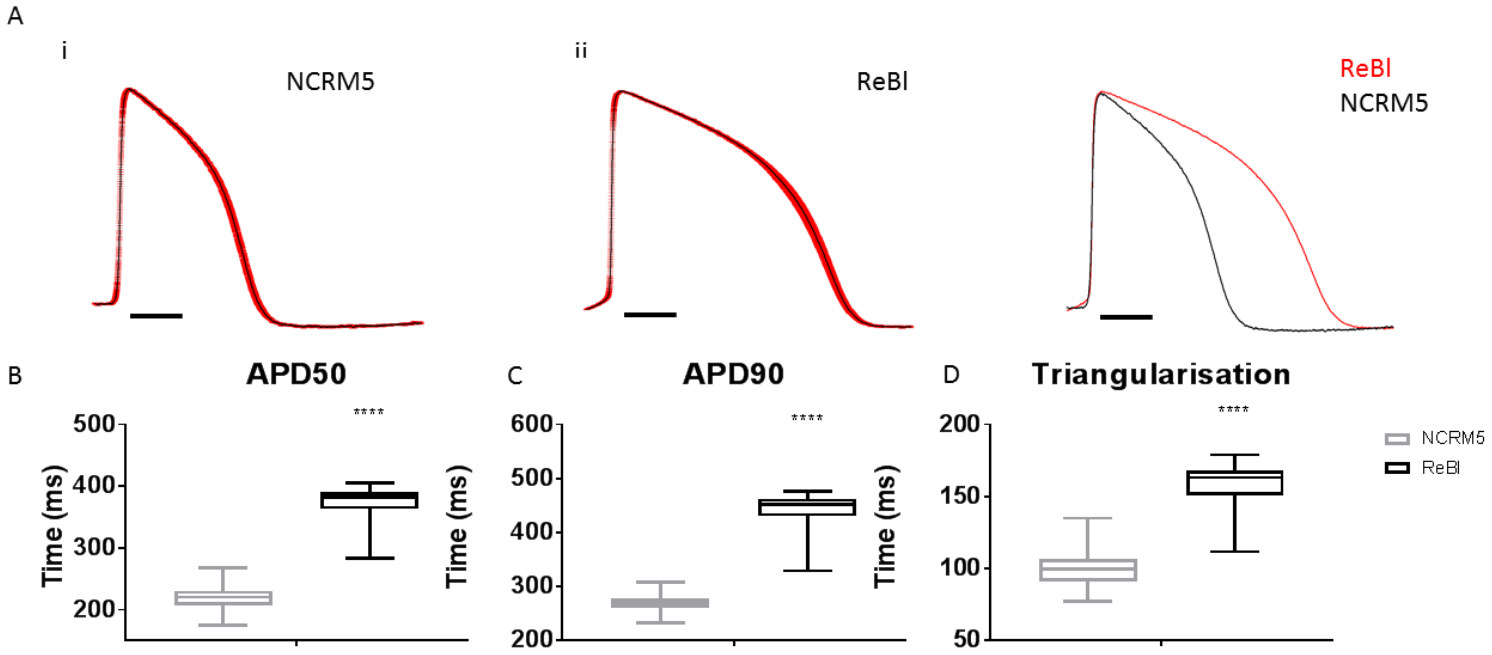
Figure 4-4 - Analysing Signal:Noise ratios of hiPSC-CMs on CellOPTIQ

Action potential data was collected using the CellOPTIQ and voltage sensitive fluorescent dyes, Di-4-ANEPPS and FluoVolt. Here we display averaged action potential traces (n=4) under different conditions. Cells were seeded on either plastic or glass 96-well plates which had been coated with either Matrigel or vitronectin-peptide. S:N ratios were calculated for both voltage dyes. Using Matrigel coated plastic bottomed 96-well plates the S:N for Di-4-ANEPPS was demonstrated to be 4.12±1.69 in contrast to using FluoVolt where a S:N of 29.46±4.9 was observed. This difference in S:N was found to be significant ($p<0.05$, n=4, unpaired t test). Black lines illustrate the average trace and the red lines illustrate the standard error of the mean of the average trace. Scale bar = 100ms.

4.2.4 Assessing LQTS2 phenotype under basal conditions

LQTS2 is characterised by an elongation of the QT interval of the patient which can be observed *in vitro* by recording and analysis of the APD (Matsa et al, 2011). In order to ascertain whether the CellOPTIQ platform could be used to detect an elongated APD in LQTS2-hiPSC-CMs, a healthy control line (NCRM5) and ReBl, which has G1681A mutation in *KCNH2,* were differentiated to cardiomyocytes. These hiPSC-CMs were then seeded to confluence in Matrigel coated plastic bottomed 96-well plates and stained with FluoVolt to assess their action potential characteristics using the CellOPTIQ system.

Figure 4.5 shows cross comparison of cardiomyocytes from NCRM5 and ReBl-hiPSC-CMs. This determined values for APD50 (219.2±2.62 vs 374.08±25.03ms; $p<0.05$, n=40, unpaired t test), APD90 (268.8±2.36 vs 442.56±31.04ms; $p<0.05$, n=40, unpaired t test) and triangularisation (99.97±16.61 vs 158.42±15.16ms; $p<0.05$, n=40, unpaired t test). Thus, by all measures, the diseased cardiomyocytes showed significantly prolonged action potential characteristics relative to the healthy cells and suggests that the ReBl-hiPSC-CMs accurately recapitulate the patient phenotype *in vitro.*



E

Cell Type	APD50 (ms)	APD90 (ms)	Triangularisation (ms)
NCRM5	219.2 ± 2.62	268.8 ± 2.36	99.97 ± 1.61
ReBl	374.1 ± 3.96	442.6 ± 4.91	158.4 ± 2.4

Figure 4-5 - Assessment of the LQTS2-hiPSC-CMs basal APD in comparison to healthy-hiPSC-CM basal APD

A – i) Averaged action potential trace for NCRM5, healthy control, n=48. ii) Averaged action potential trace for ReBl, LQTS2 cell line. n=48. iii) Overlay of ReBl averaged action potential trace with NCRM5 averaged action potential trace showing elongation of the ReBl cell line. B – Graph displaying the APD50 data from NCRM5 cells at basal conditions (219.22±18.14ms) and from ReBl cells at basal conditions (374.08±25.03ms), ReBl cells show a significantly increased APD50 under basal conditions ($p<0.05$, n=40, unpaired t-test). C – Graph displaying the APD90 data from NCRM5 cells at basal conditions (268.77±16.36ms) and from ReBl cells at basal conditions (442.56±31.04ms), ReBl cells show a significantly increased APD90 under basal conditions ($p<0.05$ n=40, unpaired t-test). D – Graph displaying the triangularisation data from NCRM5 cells at basal conditions (99.97±11.13ms) and from ReBl cells at basal conditions (158.42±15.16ms), ReBl cells show a significantly increased triangularisation under basal conditions ($p<0.05$ n=40, unpaired t-test). E – Table displaying mean plus standard deviations of the graphs.

4.2.5 Assessing if the CellOPTIQ can detect changes in APD

Having established that the LQTS2-hiPSC-CMs are able to recapitulate the patient phenotype *in vitro* the next step was to establish whether APD could be altered using pharmacological intervention. In order to achieve this it was first required that it was established whether the CellOPTIQ was able to detect changes in APD after drug exposure. To achieve this an optimisation experiment was set up. Healthy control cell line NCRM5 was differentiated to cardiomyocytes. These NCRM5-hiPSC-CMs were then seeded at $5x10^4$ CMs per well in a plastic bottomed 96-well plate with Matrigel as a substrate. The NCRM5-hiPSC-CMs were then exposed to E4031, a known I_{kr} blocker which should result in increased APD values (Egashira et al, 2012). Basal APD recordings were taken before NCRM5-hiPSC-CMs were incubated with E4031 at 3nM, 10nM and 30nM for 30 minutes on the CellOPTIQ platform. After this incubation APD measurements were recorded again. All changes in AP characteristic were subjected to one-way ANOVA with Dunnett's multiple comparison test and were n=8.

Figure 4.6 shows the NCRM5-hiPSC-CM response to E4031. APD50, APD90 and triangularisation values were observed to significantly increase at 10nM and 30nM of E4031 exposure.

Table 4-1 - NCRM5-hiPSC-CM response to E4031

Condition	APD50 (ms)	SD	% Change	APD90 (ms)	SD	% Change	Triangularisation (ms)	SD	% Change
Basal	219.23	18.14		268.77	16.36		99.97	11.13	
3nM	224.46	16.02	2.39	283.56	14.57	5.50	117.76	8.71	17.80
10nM	250.38	26.63	14.21	327.79	25.89	21.96	156.03	9.51	56.08
30nM	321.26	22.98	46.54	465.3	19.19	73.12	280.04	18.72	180.12

These data indicate that increased concentrations of the known I_{kr} blocker E4031 resulted in increased APD50, APD90 and triangularisation times in the healthy control NCRM5-hiPSC-

CMs. Furthermore these results confirm that the CellOPTIQ is able to readily record change in APD in response to pharmacological intervention.

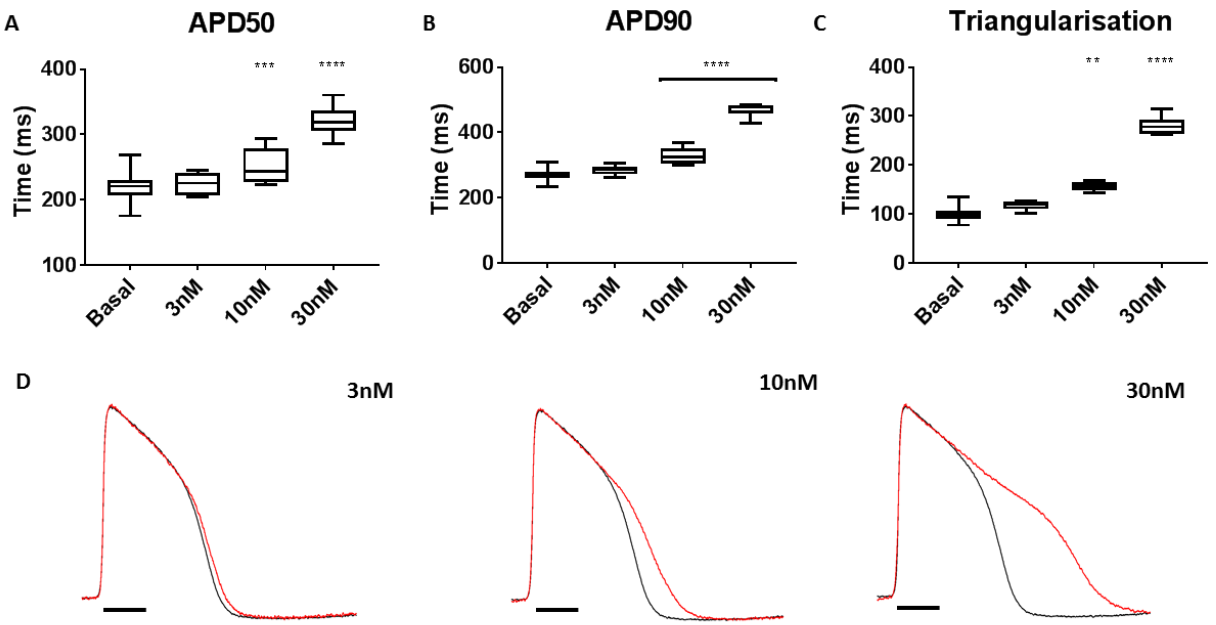


Figure 4-6 - Assessment of NCRM5-hiPSC-CM response to E4031

A – Graph displaying the APD50 values for basal measurement (219.2±18.14ms, n=30) alongside ADP50 measurements for cells after treatment with E4031. 3nM of the drug was found to have no significant effect on the APD50 value of the cells (p=0.91, n=8, Dunnett's multiple comparison test). However 10nM and 30nM were found to significantly increase the APD50 of these cells (p<0.05, n=8, Dunnett's multiple comparison test). B – Graph displaying the APD90 values for the basal measurement (268.77±16.36ms, n=30) alongside APD90 values for the cells after treatment with E4031. 3nM of the drug was not found to have a significant effect on the APD90 value (p=0.13, n=8, Dunnett's multiple comparison test). However 10nM and 30nM did exhibit a significant effect (p<0.05, n=8, Dunnett's multiple comparison test). C – Graph showing the triangularisation values for basal measurement (99.97±11.13ms, n=30) alongside the measurements for cells after treatment with E4031. 3nM, 10nM and 30nM were all found to significantly increase the triangularisation value of the cells (p<0.05, n=8, Dunnett's multiple comparison test). D – Averaged trace data for the action potentials of cells. Starting with basal recording (n=30) and overlaying this trace with averaged trace data from treated cells (n=8) at the concentrations tested. Black line illustrates the average basal trace, the red line indicates the averaged treated trace. Scale bar=100ms.

4.2.6 Assessing LQTS2-hiPSC-CM response to E4031

ReBl-hiPSC-CMs in this thesis have been shown to exhibit increased APD and triangularisation times when compared to healthy control NCRM5-hiPSC-CMs. E4031 is a known blocker of the I_{kr} channel which is defective in our LQTS2-hiPSC line (Medeiros-Domingo et al, 2007; Egashira et al, 2012). In order to ascertain the effect of this block in LQTS2-hiPSC-CM, E4031 was added to ReBl-hiPSC-CMs and incubated for 30 minutes. Recordings of APD were taken under basal conditions and then after the 30 minute incubation. All changes in AP characteristic were subjected to one-way ANOVA with Dunnett's multiple comparison test and were n=8.

Figure 4.7 displays the ReBl-hiPSC-CM response to E4031. These ReBl-hiPSC-CMs demonstrated no significant changes in response to E4031 exposure with regards to APD50. The ReBl-hiPSC-CMs exhibited a significant increase in APD90 at 1µM. ReBl-hiPSC-CM triangularisation time was demonstrated to significantly increase at 1µM.

Table 4-2 ReBl-hiPSC-CM response to E4031

Condition	APD50 (ms)	SD	% Change	APD90 (ms)	SD	% Change	Triangularisation (ms)	SD	% Change
Basal	186.72	25.48		334.24	23.64		233.48	19.36	
10nM	176.4	12.56	-5.53	324.11	19.04	-3.03	231.06	12.74	-1.04
30nM	186.11	22.05	-0.33	328.11	15.16	-1.83	231.23	9.98	-0.96
100nM	180.11	31.06	-3.54	328.04	28.19	-1.85	233.05	22.07	-0.18
300nM	182.45	26.71	-2.29	337.25	25.68	0.90	241.10	24.00	3.26
1uM	191.01	36.28	2.30	362.79	32.25	8.54	266.04	18.47	13.95

Therefore these ReBl-hiPSC-CMs exhibit increased ADP90 and triangularisation time when treated with I_{kr} blocker E4031. However no effect was observed on the APD50 value of these ReBl-hiPSC-CMs. These data indicate that ReBl-hiPSC-CMs exhibit an increased repolarisation time in response to blockade of the I_{kr} channel.

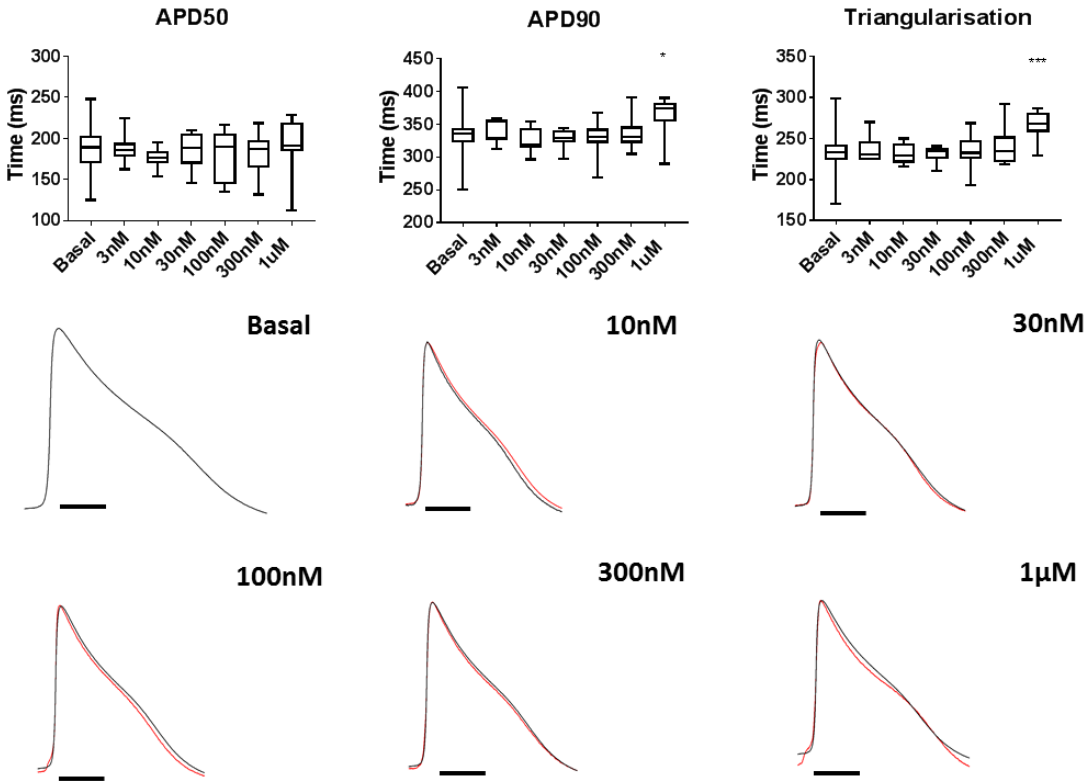


Figure 4-7 - Assessment of ReBl-hiPSC-CM response to E4031

A – Graph displaying the APD50 values measured for basal conditions (186.72±25.48ms) alongside the values measured after treatment with different concentrations of E4031, all changes in AP characteristic were subjected to one-way ANOVA with Dunnett's multiple comparison test and were n=8. 3nM, 10nM, 30nM, 100nM, 300nM and 1uM all showed no significant difference in APD50 ($p>0.05$). B - Graph displaying the APD90 values measured for basal conditions (334.24±23.64ms) alongside the values measured after treatment with different concentrations of E4031. 3nM, 10nM, 30nM, 100nM and 300nM all showed no significant difference in APD90 value in these LQTS2hiPSC-CMs ($p>0.05$). However 1uM ($p<0.05$) was found to significantly increase the APD90 of the cardiac action potential. C - Graph displaying the triangularisation values measured for basal conditions (233.48±19.36ms) alongside the values measured after treatment with different concentrations of E4031. 3nM, 10nM, 30nM, 100nM and 300nM were not shown to have any significant effect on the triangularisation period of these LQTS2 hiPSC-CMs ($p>0.05$). However 1uM ($p<0.05$) was found to exhibit a significant increase on the triangularisation of the cardiac action potential. D - Averaged trace data for the action potentials of cells. Starting with basal recording (n=40) and overlaying this trace with averaged trace data from treated cells (n=8) at the concentrations tested. Black lines indicate the averaged basal trace while the red lines indicate the average treated trace. Scale bar=100ms.

4.2.7 Assessing effect of β-blockers on LQTS2-hiPSC-CM

The standardised mode of therapy for patients suffering from LQTS2 is to prescribe β-blockers (Cho, 2016). However there remain a sizable subpopulation of patients who still experience arrhythmic events despite the use of β-blockers (Priori et al, 2004). In order to ascertain the differential effect of our candidate drugs against more traditional β-blockers, propranolol was tested in this thesis. ReBl-hiPSC-CMs were measured for their basal AP characteristics, after which the ReBl-hiPSC-CMs were incubated for 30 minutes with increasing concentrations of propranolol. After the 30 minutes incubation a second measurement was taken. All changes in AP characteristic were subjected to one-way ANOVA with Dunnett's multiple comparison test and were n=8.

Figure 4.8 shows the ReBl-hiPSC-CM response to propranolol at increasing concentrations of; 3nM, 10nM, 30nM, 100nM, 300nM and 1µM. There was found to be a significant decrease in APD50 at 10nM. No other significant changes in ReBl-hiPSC-CM APD50, APD90 or triangularisation were observed in response to propranolol.

Table 4-3 ReBl-hiPSC-CM response to propranolol

Condition	APD50 (ms)	SD	% Change	APD90 (ms)	SD	% Change	Triangularisation (ms)	SD	% Change
Basal	231.3	38.28		344.82	35.13		209.64	26.16	
10nM	196.39	31.24	-15.09	331.86	20.80	-3.76	222.26	25.00	6.02
30nM	213.79	30.73	-7.57	323.76	33.47	-6.11	200.86	23.01	-4.19
100nM	205	21.66	-11.37	320.64	29.26	-7.01	199.98	23.84	-4.61
300nM	212.88	26.75	-7.96	322.89	23.50	-6.36	191.74	22.58	-8.54
1uM	199.06	33.46	-13.94	321.35	22.15	-6.81	207.15	13.81	-1.19

Therefore these data illustrate that propranolol was not found to cause any significant change in the APD50 values of our ReBl-hiPSC-CMs at most of the concentrations tested. However 10nM did result in a significant reduction in APD50 value in these ReBl-hiPSC-CMs. Incubation with propranolol was not found to lead to any significant alterations in the ReBl-hiPSC-CMs APD90 values. Indeed there was also demonstrated to be no significant difference in the triangularisation time of the ReBl-hiPSC-CMs when incubated with propranolol at any of the concentrations tested. Therefore these data indicate that any beneficial effects of propranolol for LQTS2 patients is unlikely to be related to modulation of the APD

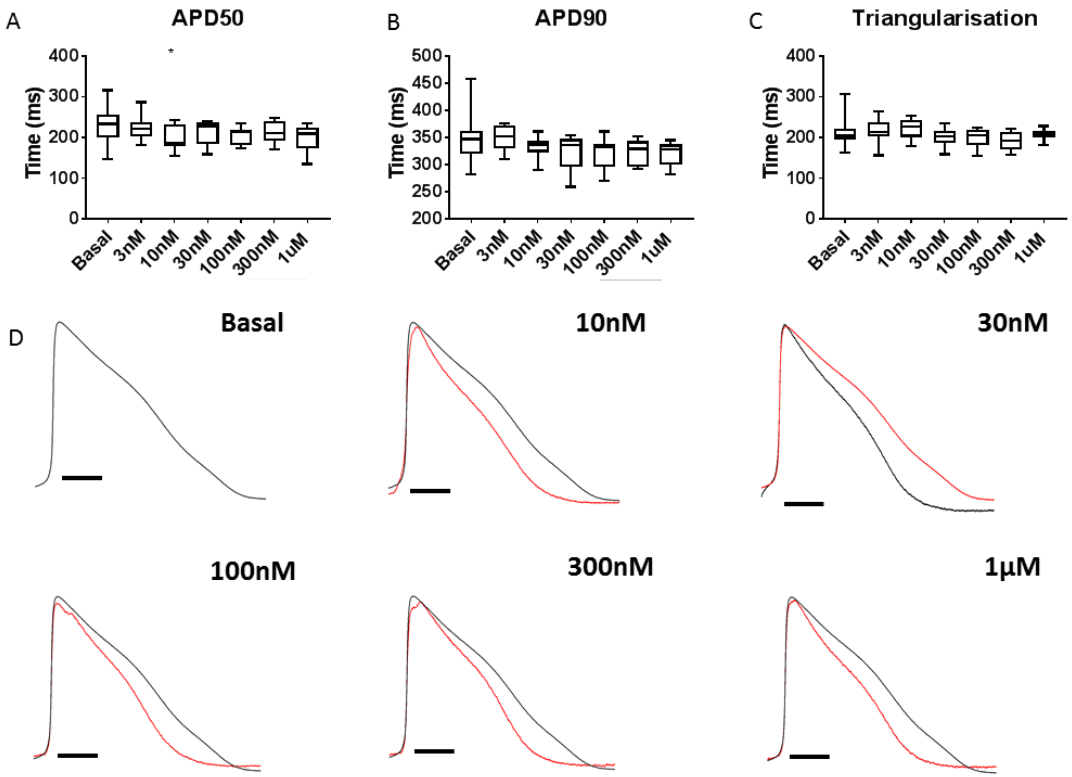


Figure 4-8 - Assessment of ReBl-hiPSC-CM response to propranolol

A – Graph displaying the APD50 values measured for basal conditions (231.30±38.28ms) alongside the values measured after treatment with different concentrations of propranolol, all changes in AP characteristic were subjected to one-way ANOVA with Dunnett's multiple comparison test and were n=8. 3nM, 30nM, 100nM, 300nM and 1uM were all found to exhibit no significant difference on the APD50 of the cardiac action potential ($p>0.05$). 10nM ($p<0.05$) was found to significantly decrease the length of APD50 B - Graph displaying the APD90 values measured for basal conditions (344.83±35.13ms) alongside the values measured after treatment with different concentrations of propranolol. 3nM, 10nM, 30nM, 100nM, 300nM and 1uM were all found to exhibit no significant difference on the APD90 of the cardiac action potential ($p>0.05$) C - Graph displaying the triangularisation values measured for basal conditions (209.64±26.16ms) alongside the values measured after treatment with different concentrations of propranolol. 3nM, 10nM, 30nM, 100nM, 300nM and 1uM were all found to exhibit no significant difference on the triangularisation of the cardiac action potential ($p>0.05$). D - Averaged trace data for the action potentials of cells. Starting with basal recording (n=48) and overlaying this trace with averaged trace data from treated cells (n=8) at the concentrations tested. Black line indicates the averaged trace for basal AP while the red line indicates the average trace for treated AP. Scale bar=100ms.

4.2.8 Assessing effect of I_{katp} agonists on LQTS2-hiPSC-CM

The LQTS2 phenotype is caused by a relative lack of K^+ outflow during phase 3 of the cardiac action potential (Medeiros-Domingo et al, 2007). In order to improve the repolarisation time of cardiac myocytes it would be a prudent strategy to increase the flow of K^+ ions, this may occur through an alternative channel to I_{kr} (Matsa et al, 2011). In this thesis two I_{katp} agonists were tested for their efficacy in reducing APD time and improving the triangularisation time. Nicorandil has previously been shown to reduce APD in LQTS2-hiPSC-CMs (Matsa et al, 2011). However a search of the literature has shown that there are no publications relating to the use of minoxidil in LQTS2 hiPSC-CMs. Basal AP characteristics were measured in ReBl-hiPSC-CMs before these cells underwent a 30 minute incubation with increasing concentrations of either nicorandil or minoxidil (10nM, 30nM, 100nM, 300nM and 1µM). All changes in AP characteristic were subjected to one-way ANOVA with Dunnett's multiple comparison test and were n=8.

Figure 4.9 displays the ReBl-hiPSC-CM response to nicorandil. APD50 and APD90 values for ReBl-hiPSC-CMs were observed to significantly decrease at all concentrations of nicorandil tested. Exposure to nicorandil resulted in a significant decrease in triangularisation time at 300nM and 1 µM.

Table 4-4 ReBl-hiPSC-CM response to nicorandil

Condition	APD50 (ms)	SD	% Change	APD90 (ms)	SD	% Change	Triangularisation (ms)	SD	% Change
Basal	400.38	21.13		485	27.30		185.36	15.42	
10nM	341.3	7.15	-14.76	420.88	10.93	-13.22	167.71	11.07	-9.52
30nM	331.7	12.84	-17.15	411.85	10.65	-15.08	177.10	32.29	-4.46
100nM	338.48	22.59	-15.46	428.55	45.33	-11.64	180.53	34.03	-2.61
300nM	334.59	7.64	-16.43	410.85	9.33	-15.29	161.19	10.63	-13.04
1uM	319.3	12.53	-20.25	393.2	11.30	-18.93	158.90	19.65	-14.27

Figure 4.10 displays the ReBl-hiPSC-CM response to minoxidil. APD50 and APD90 values for ReBl-hiPSC-CMs were observed to significantly decrease at all concentrations tested Triangularisation of ReBl-hiPSC-CMs was found to significantly decrease at; 100nM, 300nM and 1μM.

Table 4-5 ReBl-hiPSC-CM response to minoxidil

Condition	APD50 (ms)	SD	% Change	APD90 (ms)	SD	% Change	Triangularisation (ms)	SD	% Change
Basal	388.59	18.27		471.62	21.60		184.35	12.53	
10nM	345.13	10.55	-11.18	425.16	9.71	-9.85	174.54	14.27	-5.32
30nM	342.01	6.79	-11.99	421.06	11.75	-10.72	173.81	11.77	-5.72
100nM	331.65	6.04	-14.65	409.38	5.93	-13.20	166.21	6.59	-9.84
300nM	326.23	7.12	-16.05	400.55	8.24	-15.07	160.24	8.23	-13.08
1uM	314.68	11.15	-19.02	386.09	13.41	-18.14	153.60	8.55	-16.68

These data indicate that I_{katp} agonists can be used to reduce APD and improve triangularisation in ReBl-hiPSC-CMs. Nicorandil was shown to significantly reduce the APD50 and APD90 times for ReBl-hiPSC-CMs, in addition to this it was also shown to reduce triangularisation times at higher concentrations. Similarly minoxidil was observed to reduce APD50 and ADP90 times at all concentrations tested. Furthermore it was also able to reduce triangularisation time at lower concentrations than nicorandil.

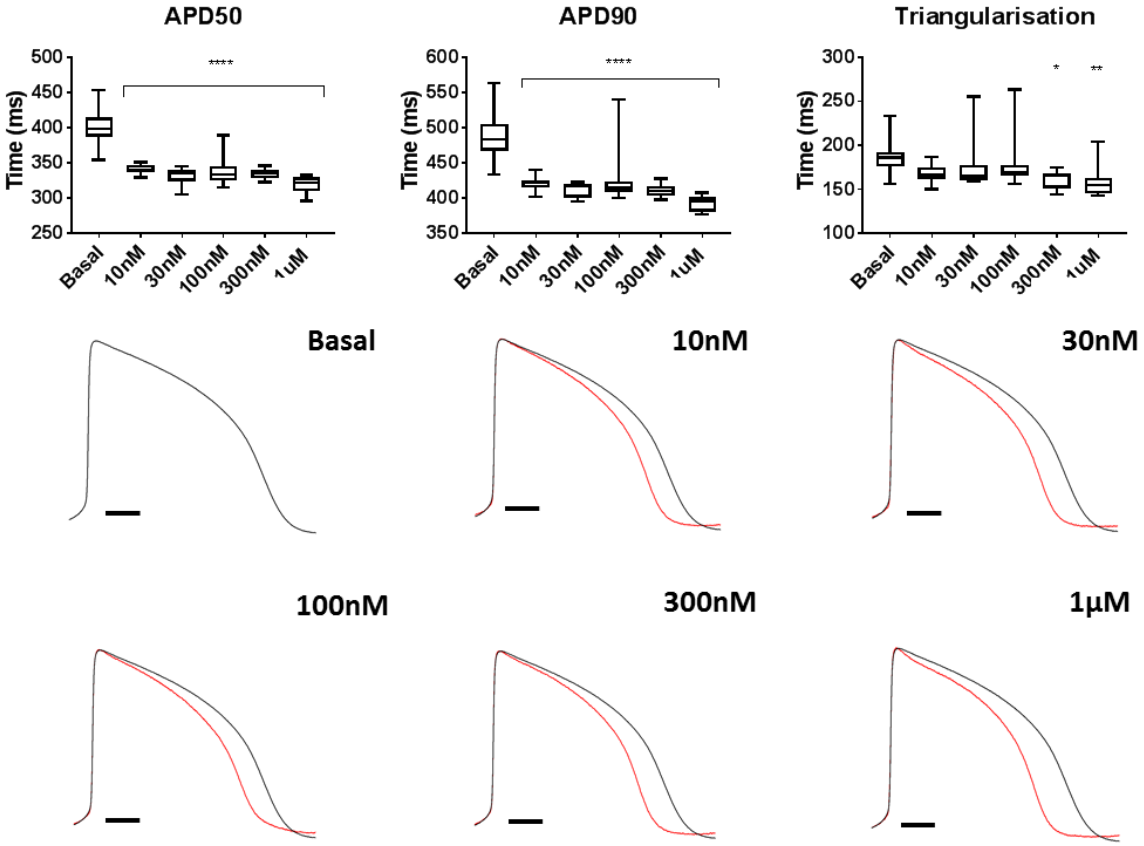


Figure 4-9 - Assessment of ReBl-hiPSC-CM response to nicorandil

A – Graph displaying the APD50 values measured for basal conditions (400.38±21.12ms) alongside the values measured after treatment with different concentrations of nicorandil, all changes in AP characteristic were subjected to one-way ANOVA with Dunnett's multiple comparison test and were n=8. 10nM, 30nM, 100nM, 300nM and 1uM were all found to significantly decrease the APD50 of the cardiac action potential ($p<0.05$, n=8, Dunnett's multiple comparison test). B - Graph displaying the APD90 values measured for basal conditions (485.00±27.3ms) alongside the values measured after treatment with different concentrations of nicorandil. 10nM, 30nM, 100nM, 300nM and 1uM were all found to significantly decrease the APD90 of the cardiac action potential ($p<0.05$). C - Graph displaying the triangularisation values measured for basal conditions (185.36±15.42ms) alongside the values measured after treatment with different concentrations of nicorandil. 10nM, 30nM and 100nM were all shown to exhibit no significant effect on the triangularisation of these hiPSC-CMs ($p>0.05$). However 300nM and 1uM were both found to exhibit a significant decrease on the triangularisation of the cardiac action potential ($p<0.05$). D - Averaged trace data for the action potentials of cells. Starting with basal recording (n=40) and overlaying this trace with averaged trace data from treated cells (n=8) at the concentrations tested. Black lines indicate the averaged basal trace while red line indicate the average treated trace. Scale bar=100ms.

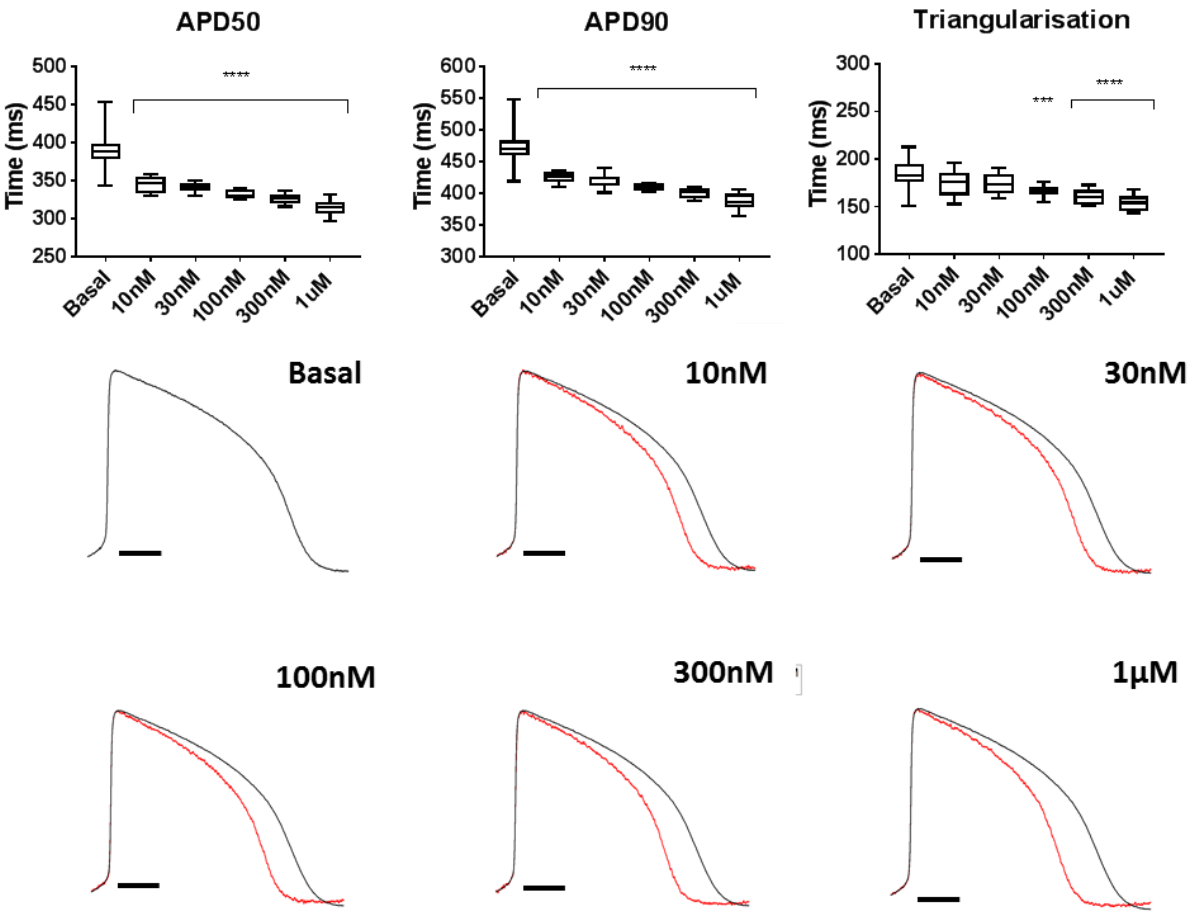


Figure 4-10 - Assessment of ReBl-hiPSC-CM response to minoxidil
A – Graph displaying the APD50 values measured for basal conditions (388.59±18.27ms) alongside the values measured after treatment with different concentrations of minoxidil, all changes in AP characteristic were subjected to one-way ANOVA with Dunnett's multiple comparison test and were n=8. 10nM, 30nM, 100nM, 300nM and 1uM were all found to significantly decrease the APD50 of the cardiac action potential ($p<0.05$). B - Graph displaying the APD90 values measured for basal conditions (471.62±21.6ms) alongside the values measured after treatment with different concentrations of minoxidil. 10nM, 30nM, 100nM, 300nM and 1uM were all found to significantly decrease the APD90 of the cardiac action potential ($p<0.05$). C - Graph displaying the triangularisation values measured for basal conditions (184.35±12.53ms) alongside the values measured after treatment with different concentrations of minoxidil; 10nM and 30nM were both shown to exhibit no significant effect on the triangularisation of these cells ($p>0.05$). However 100nM, 300nM and 1uM were all found to exhibit a significant decrease on the triangularisation of the cardiac action potential ($p<0.05$). D - Averaged trace data for the action potentials of cells. Starting with basal recording (n=40) and overlaying this trace with averaged trace data from treated cells (n=8) at the concentrations tested. Black lines indicate the averaged basal trace while red lines indicte the averaged treated trace. Scale bar=100ms.

4.2.9 Assessing effect of I_{kr} agonists on LQTS2-hiPSC-CM

In LQTS2 the patient phenotype is characterised by a decrease in I_{kr} current as a result of defective hERG channels (Schwartz et al, 2012). However, as some channels remain functional it is prudent to test whether an increase in hERG activation could increase the K^+ outflow in LQTS2-hiPSC-CMs. In this study two I_{kr} agonists were tested to ascertain whether they were able to reduce the APD values for LQTS2-hiPSC-CMs and improve the triangularisation times for the LQTS2-hiPSC-CMs. RG3 is a known agonist of I_{kr} and I_{ks} (Choi et al, 2011). NS1643 is a known agonist of the I_{kr} channel (Durdagi et al, 2012). Basal AP characteristics were measured in ReBl-hiPSC-CMs before these cells underwent a 30 minute incubation with increasing concentrations of either RG3 or NS1643 (10nM, 30nM, 100nM, 300nM and 1µM). All changes in AP characteristic were subjected to one-way ANOVA with Dunnett's multiple comparison test and were n=8.

Figure 4.11 displays the ReBl-hiPSC-CM response to RG3. APD50 and APD90 values for ReBl-hiPSC-CMs were observed to significantly decrease at; 30nM, 100nM, 300nM and 1µM. Triangularisation value for ReBl-hiPSC-CMs was not observed to significantly change at any concentration.

Table 4-6 ReBl-hiPSC-CM response to RG3

Condition	APD50 (ms)	SD	% Change	APD90 (ms)	SD	% Change	Triangularisation (ms)	SD	% Change
Basal	360.05	12.21		429.86	13.62		157.23	9.84	
10nM	360.58	6.16	0.15	427.98	8.75	-0.44	154.18	8.61	-1.94
30nM	346.71	9.53	-3.71	417.29	9.74	-2.92	153.89	12.9	-2.12
100nM	342.71	4.37	-4.82	413.59	4.87	-3.78	154.25	6.9	-1.90
300nM	330.36	21.83	-8.25	406.46	7.25	-5.44	169.03	45.99	7.50
1uM	326.78	8.84	-9.24	395.41	9.95	-8.01	146	5.35	-7.14

Figure 4.12 displays the ReBl-hiPSC-CM response to NS1643. APD50 and APD90 values for ReBl-hiPSC-CMs were observed to significantly decrease at all concentrations tested. Triangularisation value for ReBl-hiPSC-CMs was observed to significantly decrease at; 10nM, 30nM, 300nM and 1µM.

Table 4-7 ReBl-hiPSC-CM response to NS1643

Condition	APD50 (ms)	SD	% Change	APD90 (ms)	SD	% Change	Triangularisation (ms)	SD	% Change
Basal	341.66	17.09		410.82	18.71		153.65	9.05	
10nM	302.4	6.39	-11.49	368.6	7.06	-10.28	142.54	5.87	-7.23
30nM	302.64	8.79	-11.42	367.1	8.79	-10.64	138.11	6.29	-10.11
100nM	294.1	10.91	-13.92	362.1	10.74	-11.86	146.45	17.23	-4.69
300nM	285.78	9.94	-16.36	352.28	10.09	-14.25	142.55	13.42	-7.22
1uM	267.14	5.41	-21.81	327.93	6.20	-20.18	127.83	7.69	-16.80

These data indicate that despite the loss functionality within the hERG channel in ReBl-hiPSC-CMs, exposure to I_{kr} agonists does result in modulation of APD. RG3 was found to significantly decrease the APD50 and APD90 times of the ReBl-hiPSC-CMs. However it was not found to significantly reduce the triangularisation time of these cardiomyocytes. NS1643 was also found to result in significant reduction of APD50 and APD90 time. However unlike RG3 exposure of NS1643 to ReBl-hiPSC-CMs resulted in significant reduction of triangularisation time in all concentrations tested except 100nM.

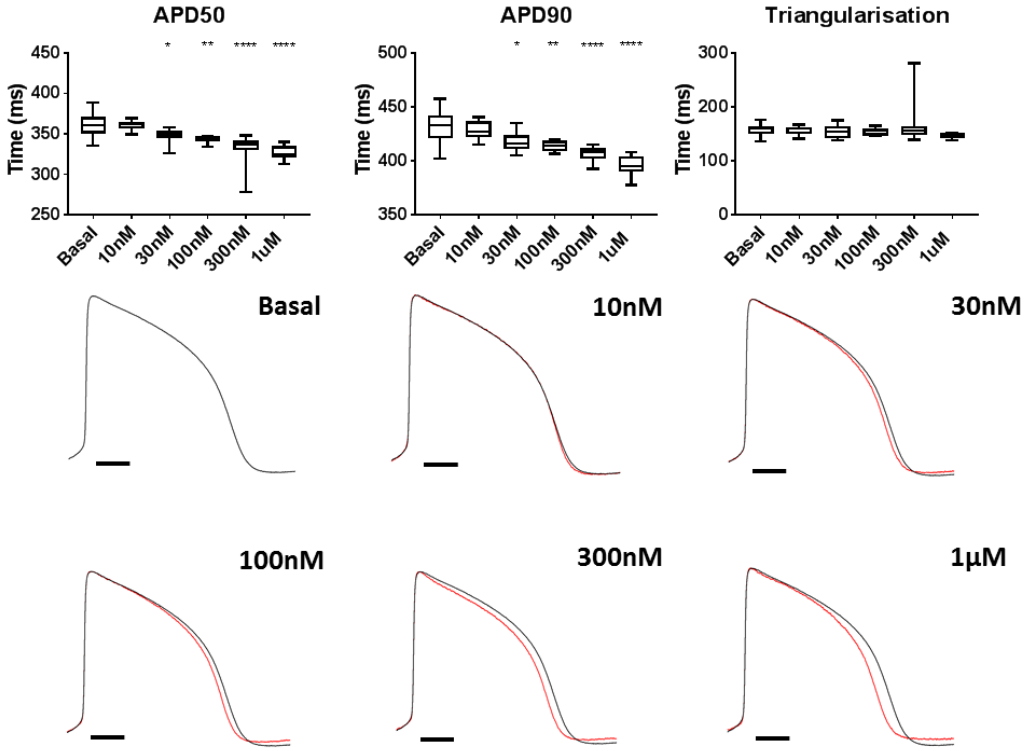


Figure 4-11 - Assessment of ReBl-hiPSC-CM response to RG3

A – Graph displaying the APD50 values measured for basal conditions (360.05±12.21ms) alongside the values measured after treatment with different concentrations of RG3, all changes in AP characteristic were subjected to one-way ANOVA with Dunnett's multiple comparison test and were n=8. 10nM ($p>0.05$) was found to exhibit no significant difference to the APD50. However 30nM, 100nM, 300nM and 1uM were all found to significantly decrease the APD50 ($p<0.05$, n=8, Dunnett's multiple comparison test). B - Graph displaying the APD90 values measured for basal conditions (429.86±13.62ms) alongside the values measured after treatment with different concentrations of RG3. 10nM ($p>0.05$) was found to show no significant difference in the APD90 of the cardiac action potential. However 30nM, 100nM, 300nM and 1uM were all found to significantly decrease the APD90 ($p<0.05$). C - Graph displaying the triangularisation values measured for basal conditions (157.23±9.84ms) alongside the values measured after treatment with different concentrations of RG3. 10nM, 30nM, 100nM, 300nM and 1uM were all found to exhibit no significant difference on the triangularisation ($p>0.05$, n=8, Dunnett's multiple comparison test). D - Averaged trace data for the action potentials of cells. Starting with basal recording (n=40) and overlaying this trace with averaged trace data from treated cells (n=8) at the concentrations tested. Black lines indicate averaged basal traces while red lines indicate averaged treated traces. Scale bar=100ms.

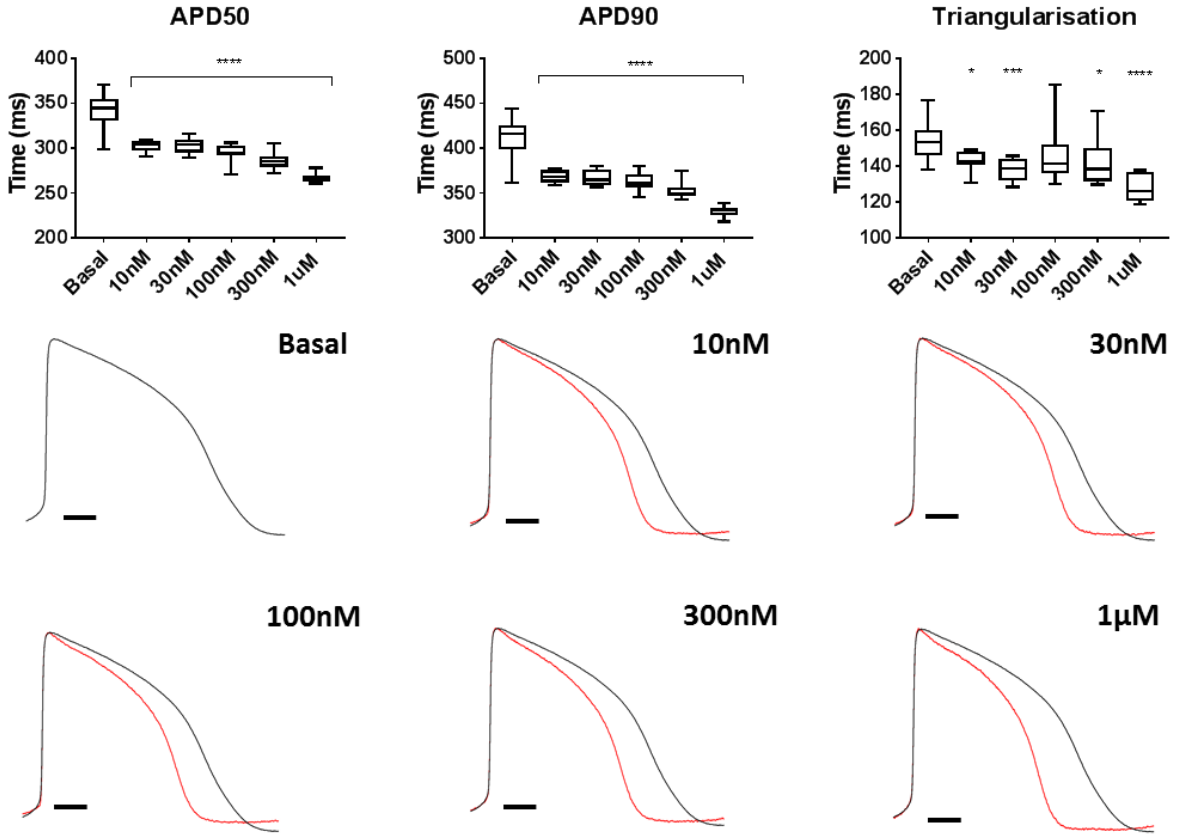


Figure 4-12 - Assessment of ReBl-hiPSC-CM response to NS1643

A – Graph displaying the APD50 values measured for basal conditions (341.66±17.09ms) alongside the values measured after treatment with different concentrations of NS1643, all changes in AP characteristic were subjected to one-way ANOVA with Dunnett's multiple comparison test and were n=8. 10nM, 30nM, 100nM, 300nM and 1uM were all found to significantly decrease the APD50 ($p<0.05$). B - Graph displaying the APD90 values measured for basal conditions (410.81±18.71ms) alongside the values measured after treatment with different concentrations of NS1643. 10nM, 30nM, 100nM, 300nM and 1uM were all found to significantly decrease the APD90 ($p<0.05$). C - Graph displaying the triangularisation values measured for basal conditions (153.65±9.05ms) alongside the values measured after treatment with different concentrations of NS1643. 10nM and 30nM, 300nM and 1uM were found to exhibit a significant decrease on the triangularisation ($p<0.05$). However 100nM ($p>0.05$) was found to show no significant differences in the triangularisation times D - Averaged trace data for the action potentials of cells. Starting with basal recording (n=40) and overlaying this trace with averaged trace data from treated cells (n=8) at the concentrations tested. Black lines indicate averaged basal traces while red lines indicate averaged treated traces. Scale bar=100ms.

4.2.10 Assessing effect of PPARδ agonists on LQTS2-hiPSC-CM

PPARδ agonists are known to activate the hERG pathway through interaction with protein 14-3-3 epsilon (Kagan et al, 2002). Given that I_{kr} agonist are able to reduce APD times and improve triangularisation it is therefore prudent to ascertain whether PPARδ agonists are able to activate hERG and reduce APD and triangularisation times in our LQTS2-hiPSC-CMs. Telmisartan and GW0742 are two PPARδ agonists (Feng et al, 2012; Luquet et al, 2005). Both were used in this thesis to ascertain their effects on ReBl-hiPSC-CMs. Basal AP characteristics were measured in ReBl-hiPSC-CMs before these cells underwent a 30 minute incubation with increasing concentrations of either telmisartan or GW0742 (10nM, 30nM, 100nM, 300nM and 1µM). All changes in AP characteristic were subjected to one-way ANOVA with Dunnett's multiple comparison test and were n=8.

Figure 4.14 displays the ReBl-hiPSC-CM response to telmisartan. APD50, APD90 and triangularisation values for ReBl-hiPSC-CMs were observed to significantly decrease at all concentrations tested.

Table 4-8 ReBl-hiPSC-CM response to telmisartan

Condition	APD50 (ms)	SD	% Change	APD90 (ms)	SD	% Change	Triangularisation (ms)	SD	% Change
Basal	374.08	25.03		442.56	31.04		158.42	15.16	
10nM	336.04	17.48	-10.17	400.55	23.30	-9.49	143.50	13.07	-9.42
30nM	333.58	12.29	-10.83	400.3	18.71	-9.55	150.43	14.22	-5.04
100nM	327.61	6.60	-12.42	392.83	6.69	-11.24	145.80	10.54	-7.97
300nM	316.6	19.85	-15.37	377.9	28.11	-14.61	137.18	15.74	-13.41
1uM	314.61	6.69	-15.90	376.94	11.26	-14.83	138.69	9.61	-12.45

Figure 4.14 displays the ReBl-hiPSC-CM response to GW0742. APD50, APD90 and triangularisation values for ReBl-hiPSC-CMs was observed to significantly decrease at all concentrations tested.

Table 4-9 - ReBl-hiPSC-CM response to GW0742

Condition	APD50 (ms)	SD	% Change	APD90 (ms)	SD	% Change	Triangularisation (ms)	SD	% Change
Basal	374.08	25.03		442.56	31.04		158.42	15.16	
10nM	336.04	17.48	-10.17	400.55	23.30	-9.49	143.50	13.07	-9.42
30nM	333.58	12.29	-10.83	400.3	18.71	-9.55	150.43	14.22	-5.04
100nM	327.61	6.60	-12.42	392.83	6.69	-11.24	145.80	10.54	-7.97
300nM	316.6	19.85	-15.37	377.9	28.11	-14.61	137.18	15.74	-13.41
1uM	314.61	6.69	-15.90	376.94	11.26	-14.83	138.69	9.61	-12.45

These data indicate that despite the loss of functionality within the hERG channel in ReBl-hiPSC-CMs, exposure to PPARδ agonists does result in modulation of APD. Telmisartan was found to significantly decrease the APD50 and APD90 times of the ReBl-hiPSC-CMs. However it was not found to significantly reduce the triangularisation time of these cardiomyocytes at 30nM or 100nM. However concentrations of the drug >300nM did result in significant reduction in triangularisation. GW0742 was also found to result in significant reduction of APD50 and APD90 time. However unlike telmisartan exposure of GW0742 to ReBl-hiPSC-CMs resulted in significant reduction of triangularisation time in all concentrations tested.

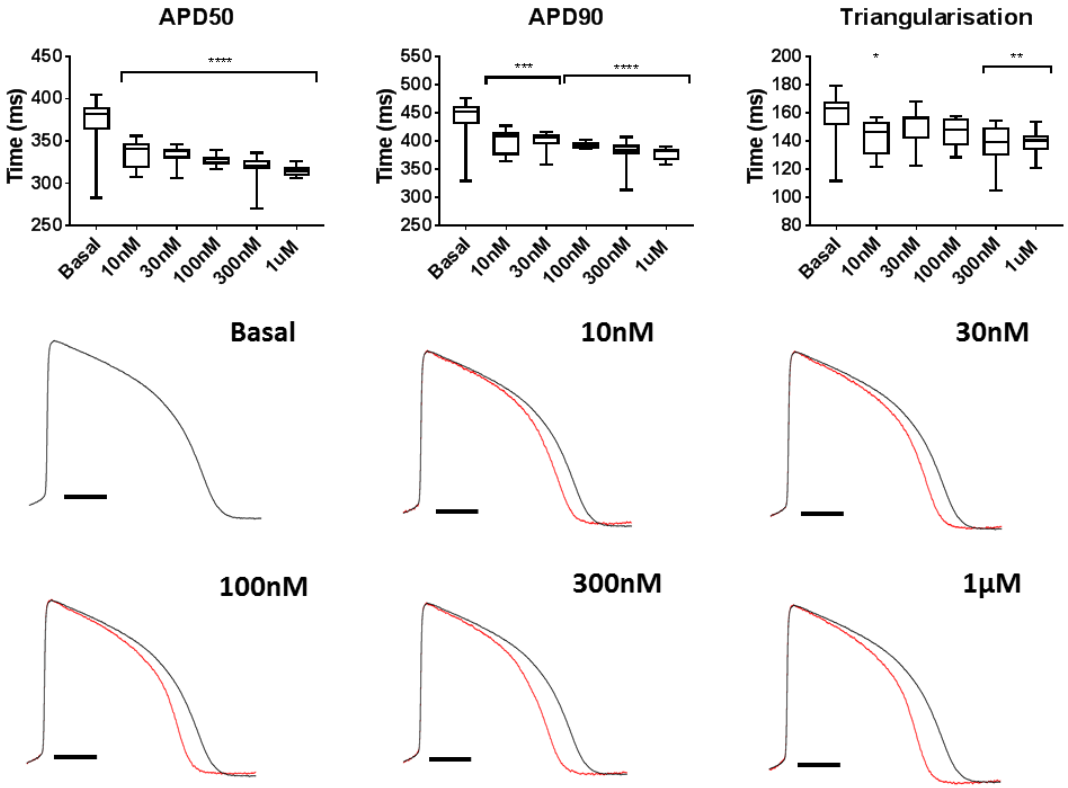


Figure 4-13 - Assessment of ReBl-hiPSC-CM response to telmisartan

A – Graph displaying the APD50 values measured for basal conditions (374.08±25.03ms) alongside the values measured after treatment with different concentrations of telmisartan, all changes in AP characteristic were subjected to one-way ANOVA with Dunnett's multiple comparison test and were n=8. 10nM, 30nM, 100nM, 300nM and 1uM were all found to significantly decrease the APD50 ($p<0.05$). B - Graph displaying the APD90 values measured for basal conditions (442.56±31.04ms) alongside the values measured after treatment with different concentrations of Telmisartan. 10nM, 30nM, 100nM, 300nM and 1uM were all found to significantly decrease the APD90 ($p<0.05$). C - Graph displaying the triangularisation values measured for basal conditions (158.42±15.16ms) alongside the values measured after treatment with different concentrations of telmisartan. 10nM, 300nM and 1uM were all found to exhibit a significant decrease on the triangularisation ($p<0.05$). 30nM and 100nM were found to exhibit no significant difference in triangularisation ($p>0.05$). D - Averaged trace data for the action potentials of cells. Starting with basal recording (n=40) and overlaying this trace with averaged trace data from treated cells (n=8) at the concentrations tested. Black lines indicate averaged basal traces while red line indicate treated traces. Scale bar=100ms.

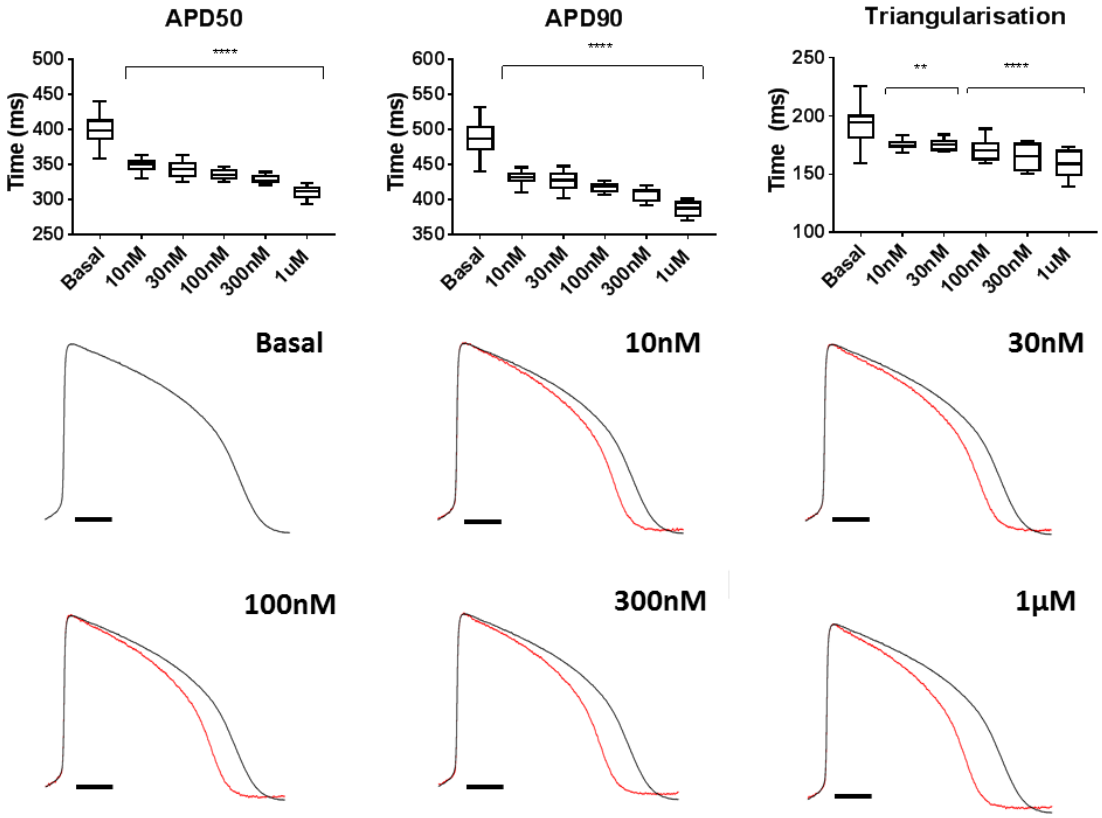


Figure 4-14 - Assessment of ReBl-hiPSC-CM response to GW0742

A – Graph displaying the APD50 values measured for basal conditions (399.7±19.12ms) alongside the values measured after treatment with different concentrations of GW0742, all changes in AP characteristic were subjected to one-way ANOVA with Dunnett's multiple comparison test and were n=8 10nM, 30nM, 100nM, 300nM and 1uM were all found to significantly decrease the APD50 ($p<0.05$). B - Graph displaying the APD90 values measured for basal conditions (486.86±22.9ms) alongside the values measured after treatment with different concentrations of GW0742. 10nM, 30nM, 100nM, 300nM and 1uM were all found to significantly decrease the APD90 ($p<0.05$). C - Graph displaying the triangularisation values measured for basal conditions (191.65±13.43ms) alongside the values measured after treatment with different concentrations of GW0742. 10nM, 30nM, 100nM, 300nM and 1uM were all found to exhibit a significant decrease on the triangularisation ($p<0.05$). D - Averaged trace data for the action potentials of cells. Starting with basal recording (n=40) and overlaying this trace with averaged trace data from treated cells (n=8) at the concentrations tested. Black lines indicate averaged basal traces while red lines indicate averaged treated traces. Scale bar=100ms.

4.2.11 Assessing effect of I_{ks} agonists on LQTS2-hiPSC-CM

I_{ks} and I_{kr} together form the repolarising K^+ current of the heart active during phases 2 and 3 of the cardiac action potential (Shih, 1994). However, there remains some dubiety as to whether the I_{ks} channel is expressed in hPSC-CMs (Virag et al, 2001; Jost et al, 2005; Ma et al, 2011). In this thesis it was decided to use the I_{ks} activator ML277 to ascertain whether it was able to exert a response on ReBl-hiPSC-CMs. Basal AP characteristics were measured in ReBl-hiPSC-CMs before these cells underwent a 30 minute incubation with increasing concentrations of ML277 (3nM, 10nM, 30nM, 100nM, 300nM and 1µM). All changes in AP characteristic were subjected to one-way ANOVA with Dunnett's multiple comparison test and were n=8.

Figure 4.15 displays the ReBl-hiPSC-CM response to ML277. APD50, APD90 and triangularisation values for ReBl-hiPSC-CMs were observed to significantly decrease at; 300nM and 1µM

Table 4-10 - ReBl-hiPSC-CM response to ML277

Condition	APD50 (ms)	SD	% Change	APD90 (ms)	SD	% Change	Triangularisation (ms)	SD	% Change
Basal	224.22	35.05		350.33	32.01		222.82	25.37	
10nM	202.29	34.61	-9.78	342.1	34.26	-2.35	224.03	35.43	0.54
30nM	205	46.62	-8.57	312.98	57.12	-10.66	189.25	30.47	-15.07
100nM	204.56	48.31	-8.77	328.79	53.31	-6.15	214.34	36.09	-3.81
300nM	137.69	32.45	-38.59	223.23	38.01	-36.28	128.09	16.35	-42.51
1uM	128.84	23.99	-42.54	189.11	24.95	-46.02	93.06	15.84	-58.24

These data indicate that ML277, an I_{ks} agonist, was able to result in the decrease of APD50 and APD90 values in ReBl-hiPSC-CMs at concentrations >300nM. Furthermore the drug was

also able to significantly reduce triangularisation at concentrations >300nM. This indicates that there may be a role for I_{ks} in reducing APD in LQTS2-hiPSC-CMs.

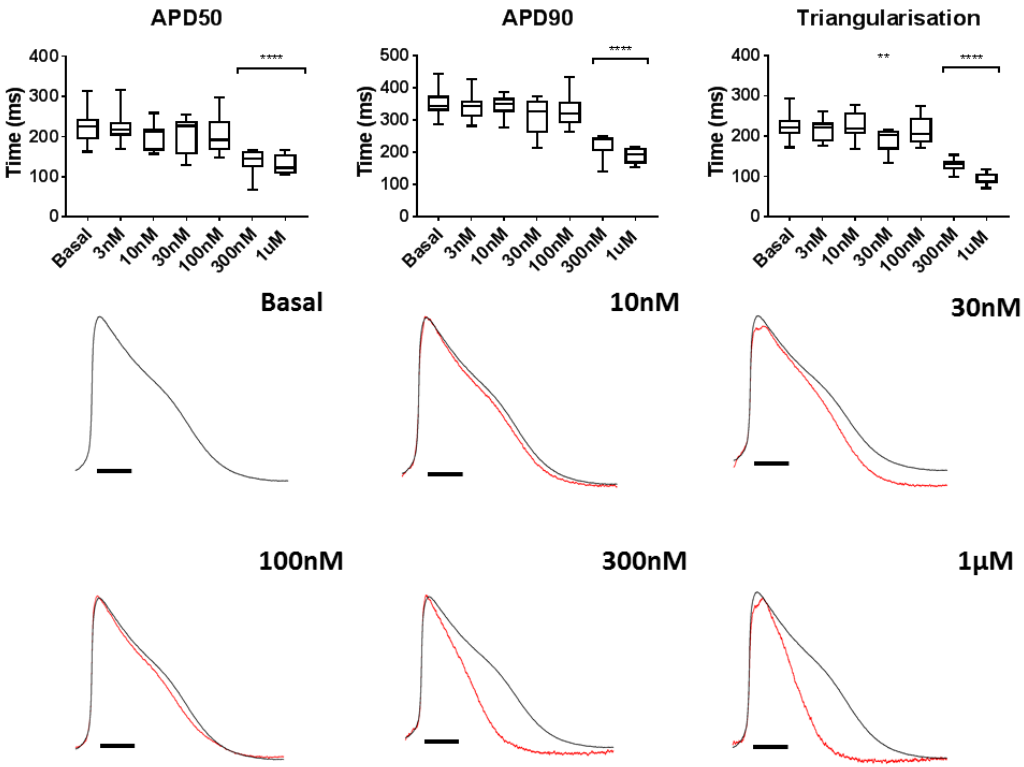


Figure 4-15 - Assessment of ReBl-hiPSC-CM response to ML277

A – Graph displaying the APD50 values measured for basal conditions (224.22±35.05ms) alongside the values measured after treatment with different concentrations of ML277, all changes in AP characteristic were subjected to one-way ANOVA with Dunnett's multiple comparison test and were n=8. 3nM, 10nM, 30nM, 100nM all showed no significant difference in APD50 ($p>0.05$). However 300nM and 1uM were both found to significantly decrease the APD50 ($p<0.05$). B - Graph displaying the APD90 values measured for basal conditions (350.33±32.01ms) alongside the values measured after treatment with different concentrations of ML277. 3nM, 10nM, 30nM, 100nM all showed no significant difference in APD90 ($p>0.05$). However 300nM and 1uM were both found to significantly decrease the APD90 ($p<0.05$). C - Graph displaying the triangularisation values measured for basal conditions (222.81±25.36ms) alongside the values measured after treatment with different concentrations of ML277. 3nM, 10nM and 100nM were shown to exhibit no significant effect on the triangularisation ($p>0.05$). 30nM, and 1uM were found to exhibit a significant decrease on the triangularisation ($p<0.05$). D - Averaged trace data for the action potentials of cells. Starting with basal recording (n=40) and overlaying this trace with averaged trace data from treated cells (n=8) at the concentrations tested. Black lines indicate averaged basal traces while red lines indicate averaged treated traces. Scale bar=100ms.

4.3 Discussion

Using hPSCs to generate cardiomyocytes is a vital component to disease modelling. Initial reports showed that cardiomyocytes could be generated from hESCs which displayed the structural and functional properties of early stage cardiomyocytes (Kehat et al, 2001; Mummery et al, 2002). However hESC-CMs displayed a phenotype that was consistent with fetal cardiomyocytes not adult cardiomyocytes (He et al, 2003; Mummery et al, 2003; Brito-Martins et al, 2008). This issue with hESC-CMs has persisted in cardiomyocytes generated using hiPSC with reports showing gene expression of cardiac genes such as *MYL2, MYH7 and TNNI3* more closely resemble fetal like cardiomyocytes than adult ones (Guo et al, 2011). However, despite this potential limitation reports in the literature have demonstrated that hiPSC-CMs are valuable and useful tools in modelling cardiac diseases such as LQTS1 (Moretti et al, 2010), LQTS2 (Matsa et al, 2011), LQTS3 (Davis et al, 2012), CPVT (Jung et al, 2012) and dilated cardiomyopathy (Sun et al, 2012).

Table 4-11 - Summary of drugs tested on LQTS2 disease model

Drug	Target	Maximum % Reduction in APD50	Maximum % Reduction in APD90	Maximum % Reduction in Triangularisation
Nicorandil	Ikatp agonist	-20.25	-18.93	-14.27
Minoxidil	Ikatp agonist	-19.02	-18.14	-16.68
RG3	Ikr agonist	-9.24	-8.01	-7.14
NS1643	Ikr agonist	-21.81	-20.18	-16.80
Telmisartan	PPARδ agonist	-15.90	-14.83	-13.41
GW0742	PPARδ agonist	-22.28	-20.64	-16.94
ML277	Iks agonist	-42.54	-46.02	-58.24

In this thesis the hiPSC-CMs were tested to assess their response to a drug of known action in order to confirm their functionality. In this case a β-adrenoceptor agonist, isoprenaline and I_{kr} blocker E4031. Both the healthy control hiPSC-CMs and ReBl-hiPSC-CMs exhibited increasesd beat rate in response to isoprenaline. It has previously been reported that isoprenaline results

in a positive chronotropic response in hiPSC-CMs, although the concentration required in this thesis was higher than usually reported (Itzhaki et al, 2011). In addition to this both the healthy control-hiPSC-CMs and ReBl-hiPSC-CMs were shown to increase APD in response to E4031. Taken together these data illustrate the functionality of the hiPSC-CMs generated in this study and provide confidence for their use in downstream assays.

Contemporary models of cardiac diseases typically use patch clamp electrophysiology (Ma et al, 2011; Matsa et al, 2011; Davis et al, 2012; Liang et al, 2013) or multielectrode arrays (MEA) (Matsa et al 2011; Itzhaki et al, 2011; Egashira et al, 2012; Navarrete et al, 2013; Mathur et al, 2015) in order to analyse the electrical behaviour of the cells. However in this study optical dyes and confocal microscopy were used in order to ascertain the AP characteristics of the hiPSC-CMs. Imaging of electrical properties of cells using optical dyes has been reported in the literature previously with publications using Di-4-ANEPPS (Burridge et al, 2011; Ren et al, 2011) and FluoVolt (Asakura et al, 2015; Bedut et al, 2016). This thesis sought to use optical dyes as an alternative to more conventional patch clamp electrophysiology in order to assess the phenotype of the cells in monolayers rather than single cell level whereby the cells are not working in conjunction with their neighbouring cells as would occur *in vivo*. This was considered important as there remains a high degree of variability in the APD characteristics of hiPSC-CMs when analysed using patch clamp electrophysiology. The aim of this thesis was to establish whether this variability could be reduced in order to improve the power of the findings in our downstream experiments. In this thesis it is reported that hiPSC-CMs which are at the single cell level exhibit a high degree of variability in the observed calcium transients. However this variability can be reduced by seeding the cells in a monolayer format. This is intuitive as cells in a monolayer format are likely to be electrically coupled and the monolayer acting in sync, unlike single cells which exhibit no intrinsic behaviour. Furthermore it was shown that different monolayers exhibit different calcium transient behaviours, this indicates that there is unlikely to be intrinsic behaviour of a hiPSC-CM monolayer and none was observed in this thesis. These data indicate that to decrease variability to as low as experimentally possible cells should be analysed in monolayers to allow for electrical coupling (Zhu et al, 2014). In this thesis calcium transients were found to be less variable between monolayers than between single cells.

In this thesis the phenotypic analysis of the hiPSC-CMs was carried out using the CellOPTIQ platform. This platform remains relatively novel and few reports in the literature are yet to cite its use. However it has been shown to detect arrhythmias and changes in APD when cells

are exposed to compounds which modulate the action potential (Hortigon-Vinagre et al, 2016). Optimisation of the CellOPTIQ platform led to the conclusion that Di-4-ANEPPS resulted in a significantly reduced S:N ratio when compared to FluoVolt. This confirms published work which demonstrated an improvement of 5x in S:N when using FluoVolt rather than Di-4-ANEPPS (Watanabe et al, 2016). This is consistent with the findings of this thesis where a 7X increase in S:N was demonstrated. In order to achieve the greatest S:N ratio possible to ensure accurate AP data FluoVolt was chosen as the optical dye to be used in this thesis. In all assays it was decided to maintain as consistent a protocol as possible and therefore Matrigel and plastic bottomed 96-well plates were used due to their routine availability in our lab. Having established that the CellOPTIQ is capable of measuring changes in APD in response to drug exposure the next stage of this thesis was to characterise the LQTS2-hiPSC-CMs generated. Basal AP recordings of healthy NCRM5-hiPSC-CMs lines were compared to basal AP recordings of ReBl-hiPSC-CMs which possess G1681A mutation in *KCNH2*. The data for these hiPSC-CMs indicated clearly that ReBl-hiPSC-CMs exhibited significantly greater APD50 and ADP90 values in addition to exhibiting an increased triangularisation time. These data confirm that the ReBl-hiPSC-CM monolayers used in this study recapitulate previously published data demonstrating increased APD in hiPSC-CMs, with G1681A, when analysed as single cells using patch clamp electrophysiology and clusters of cells using multielectrode array systems (Matsa et al, 2011). This indicates that the ReBl-hiPSC-CMs generated in this study recapitulate the patient phenotype *in vitro*.

Having established the optimum conditions to be used in our CellOPTIQ assays the next step was to establish its efficacy in being used as a tool to identify potentially therapeutic compounds for LQTS2 patients. To demonstrate that they would be suitable for use in an *in vitro* drug testing assay it was required to determine that the machine would be able to detect changes in APD in response to a drug of known action. In this thesis it was clearly demonstrated that control hiPSC line (NCRM5) cardiomyocytes exhibited significantly increased APD50, AP90 and triangularisation in response to exposure to E4031 as expected from the literature (Egashira et al, 2012). This illustrated that the CellOPTIQ was able to measure basal electrophysiological characteristics and then repeat these measurements after drug treatment. The move from manual patch clamp electrophysiology to the CellOPTIQ platform improved the potential output in this thesis from 4-8 data points per day to up to 224 data points per day.

Standardised therapy for LQTS2 patient remains the use of β-blockers and lifestyle changes (Cho, 2016). However up to as many as 23% of LQTS2 patients experience cardiac events despite β-blocker therapy (Priori et al, 2004). In order to improve upon this relatively high rate of failure new pharmacological interventions are required. The aim of this thesis was to contrast the effect of various drug compounds on ReBl-hiPSC-CMs with the effects of β-blocker therapy to ascertain whether these compounds could reduce the APD. In this study propranolol was used as a control drug to assess its effect on ReBl-hiPSC-CMs. The significant effect on APD50 value observed when ReBl-hiPSC-CMs were exposed to 10nM of propranolol was not found to persist at higher concentrations therefore it is likely to be an outlier. This may have been caused by overexposure which was an issue observed on a few occasions as a result of leaving the filter open with the excitation lamp on while a time course was completed. This experiment should be repeated to ensure this is the case. Aside from that result propranolol was not observed to exert any significant effect on APD50, ADP90 or triangularisation time in the ReBl-hiPSC-CMs. This indicates that its role in benefiting LQTS2 patients is not through modulation of the APD. Propranolol has been reported to prevent the chronotropic effect of isoproterenol with no significant effect on beat rate alone, but only in conjunction with isoproterenol (Yokoo et al, 2009; Mandel et al, 2012). Due to time pressure it was not possible to challenge the ReBl-hiPSC-CMs with isoprenaline in the presence of propranolol, however given the available literature this would make a good future experiment in order to further elucidate the role of propranolol in ReBl-hiPSC-CMs. In addition to this, propranolol was only administered to ReBl-hiPSC-CMs in this thesis. Therefore it would be prudent in future to test across a range of cell lines including healthy control hiPSC lines to uncover its response to these hiPSC-CMs. Given the evidence in this thesis propranolol appears to act by mediating any increase to beat rate as opposed to reducing beat rate at basal levels. Furthermore there was no evidence in this thesis or the wider literature that propranolol modulates the AP.

The LQTS2 patient phenotype is characterised by a decrease in K^+ ion outflow during phase 3 of the cardiac action potential (Medeiros-Domingo et al, 2007). A mutation within the pore domain damages K^+ permeation pathway necessary for K^+ ion conduction (Doyle et al, 1998). Therefore it is intuitive that increasing the K^+ ion flow through alternative K^+ channels may benefit the patient. It is reported in this study that use of nicorandil resulted in a significant decrease in the APD50 and AP90 values of the ReBl-hiPSC-CMs at all concentrations tested. In addition to this triangularisation was significantly reduced at concentrations above 300nM. This is in agreement with the published literature regarding the use of nicorandil on LQTS2-

hiPSC-CMs where it has previously been reported that the drug can reduce APD by up to 18% (Matsa et al, 2011). This is consistent with the findings in this thesis which report a maximum decrease in APD50 and APD90 of up to 20% using nicorandil. This thesis also reports that minoxidil resulted in a significant reduction in APD50 and APD90 values at all concentrations tested. In addition to this it also resulted in significant reduction of triangularisation time at concentrations greater than 100nM. This is the first report which comments on the efficacy on minoxidil in reducing APD in hiPSC-CMs. This thesis reports that APD50 and ADP90 can be reduced by around 19% using minoxidil. As mentioned previously this drug is more commonly used in hair loss treatments (Varothai and Bergfeld, 2014). However as it is approved for use there would be less concern regarding the safety of this drug were to be trialled in LQTS2 patients. These data indicate that minoxidil may be more potent in reducing triangularisation than nicorandil, although both appear to possess potent effects on APD. In order to assess this further these drugs should both be tested on a wider panel of LQTS2-hiPSC-CMs. Furthermore these data indicate that activation of the I_{katp} channels can increase K^+ ion flow and lead to a reduction in APD highlighting a potentially beneficial avenue for drug discovery to treat LQTS2 patients.

Increasing the activation of the I_{kr} channels which remain functional in LQTS2 patients is a potentially beneficial avenue to explore. In this thesis the use of RG3 resulted in significant decreases in APD50 and APD90 at all concentrations tested. However there was not found to be any significant change in triangularisation time, which determines the time of repolarisation. Previous reports which used RG3 in LQTS1 and healthy control patient indicated that the drug did not have an effect on the APD (Zhang et al, 2012). The reasons for the discrepancy between this study and Zhangs' may be a result of different hiPSC lines. Genetic variability of these lines may be the cause of the differential effects observed. Furthermore these are different disease models, in this thesis an LQTS2 line was studied, in Zhangs an LQTS1 and healthy control lines were tested. To that end it would be prudent to test a panel of the healthy control lines we have in our lab to ascertain the response to RG3. However a further potential explanation of this discrepancy is experimental design. In Zhangs work the electrophysiology of the cells is assessed by single cell patch clamp at room temperature, they make no reference to CO_2. However in this thesis all drug testing was performed on monolayers at controlled, physiological conditions of 37^{o}C with 5% CO_2. The second I_{kr} agonist investigated in this thesis was NS1643 which was demonstrated to result in significant decreases in APD50 and APD90 values at all concentrations tested. However in contrast to RG3 NS1643 was able to significantly reduce triangularisation time in all

concentrations tested except 100nM. Given its effect at lower and higher concentrations this is likely to be an outlier, caused by overexposure, and should be investigated further. NS1643 has previously been shown to reduce FPD in hiPSC-CMs, although it was required at concentrations as high as 30μM to do so (Zhang et al, 2014). Further reports on NS1643 have indicated its role in reducing the relaxation time of cardiomyocyte tissue constructs (Mannhardt et al, 2016). Taken together these data indicate that activation of the I_{kr} current is sufficient to increase K^+ ion flow in LQTS2-hiPSC-CMs. RG3 was able to potently decrease APD but not improve triangularisation time potentially indicating that despite its APD modulating properties it would not be beneficial in aiding repolarisation in LQTS2 patients. However NS1643 was able to potently reduce APD50 and ADP90 in addition to improving triangularisation, possibly indicating a beneficial effect in LQTS2 patients.

Having demonstrated that activation of the I_{kr} channels was able to modulate APD and improve repolarisation in LQTS2-hiPSC-CMs it was decided to ascertain the potential benefits of activating hERG upstream. PPARδ agonists have not been reported in the literature for their effects in modulating APD. They are more commonly reported to be involved in lipid and glucose homeostasis (Evans et al, 2004). Telmisartan was demonstrated in this thesis to elicit a significant decrease APD50 and ADP90 at all concentrations tested as well as improving triangularisation time at concentrations greater than 300nM. These data indicate that telmisartan is able to modulate the APD of hiPSC-CMs and reduce the time of each action potential. In addition to this the other PPARδ activator tested, GW0742, was also demonstrated to exhibit a beneficial effect. GW0742 significantly decreased APD50, APD90 and triangularisation time in all concentrations tested. Taken together these data provide evidence of the potentially beneficial effect of PPARδ agonists in treating LQTS2 patients. GW0742 is currently not approved but is being investigated for potential therapeutic effects by GlaxoSmithKline. The next step for these drugs will be to test them against a larger panel of LQTS2-hiPSC-CMs as well as healthy controls to further elucidate their APD modulating properties.

$I_{ks,}$ alongside $I_{kr,}$ forms the rapid reactivation current. However there remains a degree of dubiety regarding the expression of KCNQ1 and therefore the I_{ks} current in hiPSC-CMs (Christ et al, 2015). In this study an agonist of I_{ks}, ML277, was tested on the ReBl-hiPSC-CMs in order to ascertain whether activation of I_{ks} could modulate ReBl-hiPSC-CMs APD. ReBl-hiPSC-CMs were demonstrated in this thesis to significantly decrease ADP50, APD90 and triangularisation times in response to exposure to ML277 at concentrations greater than 300nM. These

indicates that activation of I_{ks} can modulate APD and decrease the action potential of ReBl-hiPSC-CMs. However given the dubiety surrounding expression of I_{ks} it would be prudent to analyse this further to ensure there is not an element of nonspecific binding behind this effect as it only occurs at higher concentrations.

To that end it would be worthwhile to assess the effect of ML277 against a panel of hiPSC-CMs, both healthy, LQTS2 and LQTS1. In addition to this ReBl-hiPSC-CMs should be exposed to an I_{ks} blocker, such as chromanol 293b, in order to ascertain if such block has an effect, identifying whether I_{ks} is active and functional in these hiPSC-CMs. The seeding of cells in a monolayer format as opposed to single cell analysis will enable the hiPSC-CMs to electrically couple and may impact on ion channel density or functionality.

To summarise, this chapter has demonstrated that ReBl-hiPSC-CMs are able to accurately recapitulate the patients LQTS2 phenotype *in vitro*. Furthermore it is possible using the CellOPTIQ system to assess the AP characteristics of hiPSC-CMs using voltage sensitive dye FluoVolt and this system can detect changes in APD of hiPSC-CMs in response to drug exposure. This system was used to successfully run an *in vitro* drug assay to identify compounds which may possess beneficial effects for LQTS2 patients yielding positive results in I_{katp}, I_{kr} PPARδ and I_{ks} agonists which should be investigated further.

5 Chapter 5 –Phenotyping a CPVT S2246L mutation in hiPSC-CMs

5.1 Introduction

Catecholaminergic polymorphic ventricular tachycardia (CPVT) is a cardiac channelopathy which inhibits the ability of the cardiac myocyte to appropriately handle calcium, a vital component in the excitation-contraction (EC) coupling process (Cerrone et al, 2007; Roux-Buisson et al, 2012). Studies have demonstrated the expression of RYR2, SR Ca^{2+}/ATPase (SERCA), IP3R2, L-type calcium channel (LTCC) and Sodium-Calcium exchanger (NCX) in hiPSC-CMs using semi quantitative RT-PCR (Itzhaki et al, 2011; Lee et al, 2011). Furthermore functionality of RYR2, SERCA, IP3R and LTCC has also been demonstrated (Itzhaki et al, 2011). However, what remains under addressed is the difference between healthy hiPSC-CMs and CPVT-hiPSC-CMs in their respective functional calcium handling properties. Thus, in contrast to the LQTS model which was used for drug screening, the intention for the CP1-hiPSC-CM in this thesis was to investigate their calcium handling properties. This was achieved by comparing the functionality of CP1-hiPSC-CMs to a CRIPSR/Cas9 genetically corrected hiPSC line (CP1-WT) as well as an unrelated but healthy control hiPSC line, ReBl-PAT.

5.1.1 CPVT

CPVT has up to 5 subtypes which are characterised by mutations in *calsequestrin 2* (*CASQ2*) (Lahat et al, 2001), *CALM1* (Hyegaard et al, 2012), *TRDN* (Roux-Buisson et al, 2012), *TECRL* which exhibits a crossover phenotype between CPVT and LQTS (Devalla et al, 2016) and *RYR2* (Swan et al, 1999). CPVT1 is characterised by a mutation within *RYR2* and it is this subtype which will be discussed in this chapter (Priori et al, 2001). CPVT is characterised by the appearance of a healthy phenotype at rest. However, patients present with symptoms such as bidirectional polymorphic ventricular tachycardia when exposed to adrenergic stimulation brought on by exercise or stress (MacLennan and Zvaritch, 2011; Kim et al, 2014). CPVT is inherited in an autosomal dominant manner and is often caused by mutation in the *RYR2* gene (Swan et al, 1999; Priori et al, 2001). Over 70 mutations have been reported to date in the *RYR2* region, the majority of which cluster to four highly conserved protein domains labelled domains I-IV (Priori and Chen, 2011). However mutations within the *RYR2* gene have only been identified as causative in around 50% of dominantly inherited CPVT cases (Nyegaard et al, 2012). These defects in calcium handling lead to the spontaneous release of calcium from the sarcoplasmic reticulum (SR) during diastole (Roux-Buisson et al, 2012). In turn this increase in cytosolic calcium concentration can trigger DADs which are a risk factor for arrhythmias. This process is particularly enhanced under adrenergic stimulation (Cerrone et al, 2007). The

mechanism for these DADs is by increased cytosolic calcium activating the NCX creating a transient inward current leading to depolarisation (van der Werf and Wilde, 2013).

5.1.2 Molecular and structural biology of RYR2 channel

Three isoforms of *RYR* have been identified in mammals; *RYR1*, *RYR2* and *RYR3*. These genes share ~70% sequence identity and are found in different cell types (Sorrentino and Volpe, 1993). *RYR1* is predominantly found in skeletal muscle (Takeshima et al, 1989), *RYR2* in the heart (Nakai et al, 1990) and *RYR3* is found primarily in the brain (Hakamata et al, 1992). The RYR2 channel has been mapped to chromosome 1q42-43 and the human *RYR2* gene comprises of 105 exons (Tiso et al, 2001). The human *RYR2* gene is primarily translated into a large monomer which comprises an N-terminal domain of ~4500aa and a C-terminal domain of roughly ~500aa (Lanner et al, 2010). It has been predicted using topology models that the C-terminus contains 4-12 membrane-spanning domains (Blayney and Lai. 2010). It has been suggested that the GGIG sequence which is found in one transmembrane loop and conserved across all isoforms of *RYR* may form the pore loop, due to its similarity to the selectivity filter of voltage gated K^+ channels (Du et al, 2001). The C-terminus of *RYR2* is also believed to interact with proteins such as calsequestrin (CASQ), junction and triadin which are important in the regulation of calcium induced calcium release (CICR) (Lanner et al, 2010). The RYR2 channel is a tetramer comprised of four RYR2 polypeptides and four FK506 binding proteins (Marx et al, 2000).

5.1.3 Regulation of cardiac ryanodine receptor

RYR2 activity is regulated by a number of factors including Ca^{2+} and proteins such as protein kinase A (PKA), CASQ, FK506-binding proteins (FKPBs) and Ca^{2+}/calmodulin dependent protein kinase (CaMKII) (Kimlicka and Van Petegem, 2011). One FKBP molecule is bound to each subunit of RYR and this assembly is thought to aid the characteristic of gating as an ensemble rather than stochastically, a vital component of efficient EC coupling (Brillantes et al, 1994; Kaftan et al, 1996; Marx et al, 1998). The regulation of the binding between FKBP12.6 and the RYR channel is achieved by PKA phosphorylation state (Marx et al, 2000). If PKA is phosphorylated then FKBP12.6 becomes dissociated from the channel leading to increased calcium sensitivity (Marx et al, 2000). Reports have indicated that increased expression of CaMKII can lead to higher levels of SR Ca^{2+} leak (Fischer et al, 2013). CaMKII has been shown to increase Ca^{2+} entry via LTCC in murine and rabbit cardiomyocytes (Dzhura et al, 2000).

Furthermore it can influence Ca^{2+} uptake and release from the SR by inducing the phosphorylation of RYR in both heterologous overexpression of RYR in HEK cells and in rabbit *in vivo* models (Wehrens et al, 2004; Currie et al, 2004).

CASQ acts as a sensor of Ca^{2+} for the RYR2 channel, communicating changes in luminal levels of Ca^{2+}, and at basal levels associates with triadin and junction which anchor it to the membrane of the SR (Gyorke et al, 2004; Gaburjakova et al, 2013). The true molecular mechanism of this process remains poorly understood (Gaburjakova et al, 2013). Under normal conditions CASQ2 acts as a suppressor of the RYR2, however an increase in SR levels of Ca^{2+} results in a conformational change of the protein which results in a cessation of its inhibitory effect (Gyorke et al, 2004). Overexpression of CASQ2 has been shown to result in larger calcium transients and spontaneous calcium sparks from isolated heart cells (Terentyev et al, 2003). CASQ2 has also been shown to lengthen the recharging process of the SRs calcium stores thus suggesting a role in maintaining a refractory period after contraction (Terentyev et al, 2003).

Store overload-induced calcium release (SOICR) is the term given to a Ca^{2+} influx-independent and SR Ca^{2+}-dependent release of calcium from the SR stores (Jiang et al, 2004). SOICR suggests the potential for a luminal Ca^{2+} regulatory function of the RYR. Increased luminal Ca^{2+} has been reported to increase the open probability of single RYR2 channels in both canine and sheep models (Sitsapesan et al, 1994; Gyorke et al, 1998). However SOICR remains controversial as any Ca^{2+} which exists in the luminal space of the SR has the potential to activate the RYR as it passes through the cytosol of the cell, a potential mechanism termed “feed-through” activation (Tripathy et al, 1996; Xu et al, 1998). A second hypothesis states that RYR may be activated through the luminal side (Gyorke et al, 1998). Yet another potential explanation is that RYR2 is activated by both SR and cytosolic Ca^{2+} together (Laver, 2007). However assessment of this phenomenon is outwith the scope of this thesis.

5.1.4 Calcium handling in the cardiac myocyte

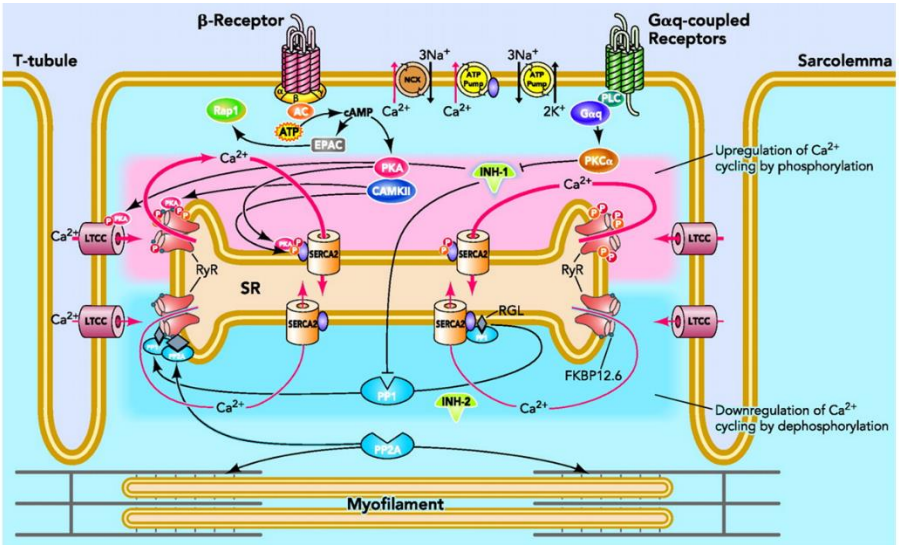


Figure 5-1 - The cardiac calcium cycle

Ca^{2+} enters the cell through LTCC which are found in the invaginations of the cell known as t-tubules. The Ca^{2+} then activates the RYR2 receptor which sits on the SR. This activation leads to Ca^{2+} release from the SR in a process known as calcium induced calcium release (CICR). This CICR is vital in establishing a high concentration of cytosolic calcium which associates with troponin to induce contraction, a key component of the EC coupling. After contraction the Ca^{2+} in the cytosolic space must be removed to allow relaxation and this is achieved by two principal mechanisms: The first and larger component is through the SERCA which transfers cytosolic Ca^{2+} back into the SR in a reuptake mechanism; the second is through the NCX which exchanges Na+ and Ca^{2+} ions across the cell membrane. The amplitude and velocity of the Ca^{2+} transient is regulated by phosphorylation of nodal Ca^{2+} cycling regulators in cardiomyocytes. (Ikeda et al, 2008).

5.1.4.1 The role of L-Type calcium channel

In the cardiac myocyte the L-Type Calcium Channel (LTCC) is the route by which calcium enters the cell and activates the RYR2 receptor on the SR thereby releasing calcium from its store in what is termed calcium induced calcium release (CICR) (Yamakage et al, 2002) (Figure 5.1). In hiPSC-CMs calcium flow through the LTCC is required for calcium transients which are eliminated by its blockade (Itzhaki et al, 2011). In the human heart the pacemaker cells which regulate beat rate are driven by LTCC as they allow spontaneous depolarisation, thus initiating the cardiac action potential in these cells (Guo et al, 2011; Torrente et al, 2016). Calmodulin is an important calcium dependent modulator of LTCC activity promoting either calcium dependent inactivation or calcium dependent facilitation of ionic flow (Zuhlke et al, 1999; Saimi et al, 2002; Saucerman et al, 2008). It has recently been shown that the protein myoscape, which localises to t-tubules, is able to interact with LTCC to modulate calcium current (Eden et al, 2016). Therefore the major role of LTCC in calcium handling is to facilitate Ca^{2+} entry to the cardiomyocyte to initiate the process of CICR.

5.1.4.2 The role of RYR2

RYR2 is known to be important in maintaining calcium homeostasis in the heart and thus is vital in the EC coupling process which underpins the heart's electrical activity (van der Werf and Wilde, 2013). RYR2 is a cation-selective ion channel which is found within the membrane of the SR where it is responsible for inducing the release of calcium from this intracellular storage organelle (Williams et al, 2001). Activation of a single RYR2 leads to a local increase in cytosolic Ca^{2+} release in what is termed a calcium spark (Cheng et al, 1993). These calcium sparks significantly amplify the original Ca^{2+} signal leading to CICR (Lou et al, 2013). *In vivo,* several RYR2 channels are situated on the membrane of the SR closely linked to a t-tubule invagination of the sarcolemma, these form a couplon (Franzini-Armstrong et al, 1999; Brette et al, 2002). This in turn leads to a close association with the LTCC and this spatial association is key in the amplification of the signal which underlies efficient EC coupling in cardiomyocytes (Scoote and Williams, 2002). Inward flow of calcium leads to increased release of calcium from the SR which ultimately reaches a threshold whereby contraction occurs as calcium ions bind to troponin C (Scoote and Williams, 2002). Relaxation of the cardiac myocyte requires the dissociation of calcium from troponin C and its removal from the cytosol which is achieved by the NCX which pumps Ca^{2+} out of the cell and SERCA which returns the calcium to SR stores (Bassani et al, 1994). Therefore the predominant role of the RYR2 is to be the gatekeeper of the SR Ca^{2+} store, initiating its release when activated by Ca^{2+} flow through the LTCC.

5.1.4.3 The role of SERCA

SERCA is a key component in removing Ca^{2+} from the intracellular space and returning it to the stores within the SR, and is estimated to remove up to 70% of the calcium required during relaxation (Bassani et al, 1994; Shigekawa and Iwamoto, 2001). SERCA2 is the key isoform found in cardiac muscle (Frank et al, 2003). The SERCA pump serves two purposes: firstly it induces relaxation of the cardiac muscle by lowering cytosolic Ca^{2+} levels and secondly it restores the Ca^{2+} load within the SR for subsequent muscle contraction (Lipskaia et al, 2010). SERCA is a single polypeptide with a molecular mass of 110kDa which is localised to the SR membrane (Periasamy and Kalyanasundaram, 2007). SERCA is driven by ATP hydrolysis and is able to transport two Ca^{2+} ions for each molecule of ATP hydrolysed (Periasamy and Kalyanasundaram, 2007). SERCA removes Ca^{2+} from the cytosol of the cell by interacting with the protein phospholamban (PLB) which regulates the activity of the SERCA pump (Kranias et al, 2012). PLB inhibits the SERCA pump when in the unphosphorylated state. However when phosphorylated by PKA, this inhibition is relieved leading to an increase in pump activity (Zima

et al, 2014). The major role of SERCA in calcium handling therefore, is to remove calcium from the cytosol which results in muscle relaxation and to refill the SR in order to prepare for the next contraction.

5.1.4.4 The role of NCX

The NCX is a membrane transporter which contains 10 transmembrane helices, with four ion-binding sites specifically for Ca^{2+} and three which likely bind Na^{+} (Liao et al, 2012). NCX is known to transport 3 Na^{+} ions in exchange for 1 Ca^{2+} ion which results in an ionic current (Ottolia et al, 2013). The role of NCX in healthy hearts is to remove the same volume of Ca^{2+} which entered the cell via the LTCC, while SERCA recycles Ca^{2+} from SR (Bridge et al, 1990). The NCX achieves this by exchanging Na^{+} and Ca^{2+} ions across the plasma membrane during Ca^{2+} influx or efflux depending on the electrochemical gradient formed, therefore it is driven by electrical activity (Shigekawa and Iwamoto, 2001). Early in the cardiac action potential process, there is a large influx of Na^{+} to the cells which forms an electrochemical gradient causing the NCX to pump Na^{+} ions out of the cell and Ca^{2+} ions into the cell (Bers, 2002). Furthermore, it has been suggested that calcium influx through the NCX can synergistically amplify the effect of CICR which is driven through the LTCC (Litwin et al, 1998). Although SERCA is more prominent during Ca^{2+} extrusion through its reuptake mechanism than NCX, it has been shown that in the event of inadequate reuptake of Ca^{2+} into the SR, the NCX will increase its activity to increase the amount of Ca^{2+} extruded from the cell (Piacentino et al, 2003). Therefore the NCX plays a dual role in the process of calcium cycling: it can transport Ca^{2+} into the cell in the early phases of the cardiac action potential; but its main purpose is the extrusion of Ca^{2+} from the cell during relaxation of the cardiac muscle.

5.1.4.5 The role of IP3

IP3R is activated by IP3 which is generated by the activation of phospholipase C (Marks, 2000). The role of IP3 in calcium handling in the human heart remains a controversial subject. It has been postulated that IP3 is more functional with regard to calcium cycling in fetal cardiomyocytes but this process is taken over by RYR as cells mature (Rosemblit et al, 1999). However evidence from some studies have indicated that IP3 still plays a major role in controlling intracellular calcium concentrations (Poindexter et al, 2001). Action potentials are not thought to activate IP3 and it is therefore not electrically driven (Kentish et al, 1990). What is more, although IP3 receptors are found in the heart the rate and extent of Ca^{2+} release from

IP3 is thought to be much lower than CICR (Bers, 2002). Indeed, IP3R is thought to be around 50 times less abundant than RYR in the human heart (Moschella et al, 1993). One of the more interesting roles thought to involve IP3 is the propagation of electrical signals in the heart given the abundance of IP3 receptors in the Purkinje fibres (Gorza et al, 1993). IP3 has been shown to play a role in calcium handling in hESC-CMs and hiPSC-CMs (Satin et al, 2008; Itzhaki et al, 2011). Therefore the role of IP3 in calcium handling may be more prominent in hPSC-CMs than in native adult cardiomyocytes due to their immature phenotype.

5.1.5 CRISPR/Cas9 genome engineering to generate isogenic controls

Early genome editing work was carried out using Zinc-Finger Nucleases (ZFNs) and transcription activator-like effector nucleases (TALENS). ZFNs consist of two different domains - a DNA binding and a DNA cleavage domain (Carroll, 2011). ZFNs are able to induce a double strand break (DSB) in the genome at a specific location (Urnov et al, 2010). However ZFNs require laborious screening and optimisation when trying to combine multiple ZFNs to target unique sites in the human genome (Boch, 2011). TALENS are a fusion protein secreted by *Xanthomonas* bacteria and they consist of nonspecific FokI endonuclease and an adaptable TALE DNA-binding domain (Boch and Bonas, 2010; Brookhauser et al, 2017). TALENS contain amino acids in the conserved TALE domain which are termed repeat variable diresidues (RVD). These give the TALEN specificity over where in the genome it will induce a break in the DNA (Boch et al, 2009; Moscou and Bogdanove, 2009). Despite the success of genome editing using TALENS there remain concerns regarding undesired off target effects, which can result in unintended disruption of genes (Grau et al, 2013).

Clustered regularly interspaced short palindromic repeats (CRISPR) are part of an RNA mediated adaptive immune system found in bacteria and archea (Weidenheft et al, 2012). Figure 5.2 below shows a schematic explaining the key processes in CRIPSR/Cas9 targeting. It was shown that by forming an RNA chimera - termed the guide RNA (gRNA) - of trans-activating crRNA (tracrRNA) and CRISPR RNAs (crRNA) that Cas9 protein could induce double strand breaks in the genome at site specific locations (Jinek et al, 2012). The gRNA binds to it complementary site in the genome and recognises the PAM in the endogenous sequence, which contains the sequence NGG (Jinek et al, 2012). By inducing these double stranded breaks in the DNA at site-specific locations, it is possible to induce changes in the DNA by providing the cells with a template, such as plasmid DNA or a single stranded oligonucleotide, to repair themselves using homology directed repair (HDR) (Ran et al, 2013). Plasmid based

targeting using the PiggyBac transposon system has previously been utilised to correct the β-thalassemia mutation in hiPSCs (Xie et al, 2014). The PiggyBac system exhibits benefits over the single stranded oligonucleotide system, which provides a single stranded oligonucleotide as a template for HDR, as it features both positive and negative selection using puromycin and by expressing thymidine kinase (Chen and Bradley, 2000). In this thesis the initial intention was to target CP1-hiPSC using the oligonucleotide method of the CRISPR/Cas9 system. However should this prove unsuccessful, then a plasmid based method using a modified PiggyBac transposon system would be used.

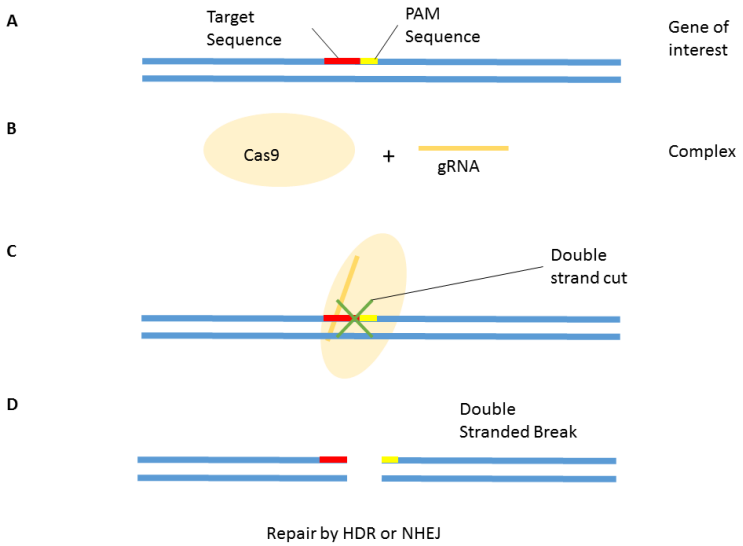


Figure 5-2 - Schematic explaining the CRISPR/Cas9 process
A – The initial selection of gene of interest with an identified gRNA target sequence and a PAM site immediately downstream. The target sequence provides a region in the genome for the gRNA to bind and the PAM site will activate Cas9 protein leading to a double stranded break in the DNA. B – This step is the formation of a single entity of complexed gRNA and Cas9 protein, which is only activated when it recognises a PAM site. The role of the gRNA is to direct the Cas9 to a specific location in the genome. C – When the complex of gRNA and Cas9 protein find the complementary sequence and bind to it, the Cas9 protein is activated and a double strand break is induced in the DNA. D – This double strand break can then be repaired by NHEJ which will likely result in indels or frameshift mutations. Alternatively the cell can use HDR to repair itself, for this a template must be present, in the CRISP/Cas9 genome editing system an oligonucleotide or targeting plasmid will be provided as a template.

5.1.6 Chapter aims and objectives

The genetic variability between cell lines necessitates the generation of isogenic control hiPSC lines using gene editing technology to further explain the role of specific mutations in disease phenotype. This chapter demonstrates the use of CRISPR/Cas9 gene editing technology to correct the S2246L mutation in the *RYR2* gene of the CP1 hiPSC line to create an isogenic control. Furthermore this chapter has assessed a selection of key calcium handling parameters namely TRise, TDecay, amplitude and time of transients (TOT) (Shinnawi et al, 2015) to determine whether they show a differential phenotype in CPVT-hiPSC-CMs when compared to a healthy, unrelated control cell line (ReBl-PAT) and a genetically corrected hiPSC line (CP1-

WT) when different components of the calcium handling machinery are blocked. To achieve this the following aims must be met;

1. Using CRISPR/Cas9 genome editing technology correct the S2246L mutation in the *RYR2* of the CP1 hiPSC line.
2. Assess the basal calcium handling behaviour of both healthy-hiPSC-CMs and CPVT-hiPSC-CMs.
3. Assess the role pharmacological blockade has on the calcium handling machinery in both healthy-hiPSC-CMs and CPVT-hiPSC-CMs.

5.2 Results

5.2.1 Patient history and genetic profile

The patient in this study was a male who presented at 5 years of age with a normal ECG but with a history of syncope and a previous diagnosis of CPVT. A genetic screen on the patient had shown that he carried the autosomal dominant missense mutation *RYR2* c.6737C>T. This mutation causes a substitution of leucine for serine at amino acid position 2246 designating this mutation S2246L and locating it in the cytosolic central domain of the RYR2 protein. Figure 5.3 illustrates the reprogramming process to generate hiPSC from the patient's skin fibroblasts which were obtained during the implantation of an implantable cardiac monitor. The patient provided informed consent and this sample collection was approved by the University of Nottingham Research Ethics Committee (License 09/H0408/74). Figure 5.3 continues by showing genotyping analysis of the affected region in CP1 and in the healthy control hESC line HUES7. CP1-hiPSC contains the heterozygous C/T, using custom designed primers shown in Table 5.1. The HUES7 chromatogram shows a homozygous C, also shown using custom designed primers shown in Table 5.1. Finally Figure 5.3 displays a schematic explaining where in the *RYR2* this mutation is located.

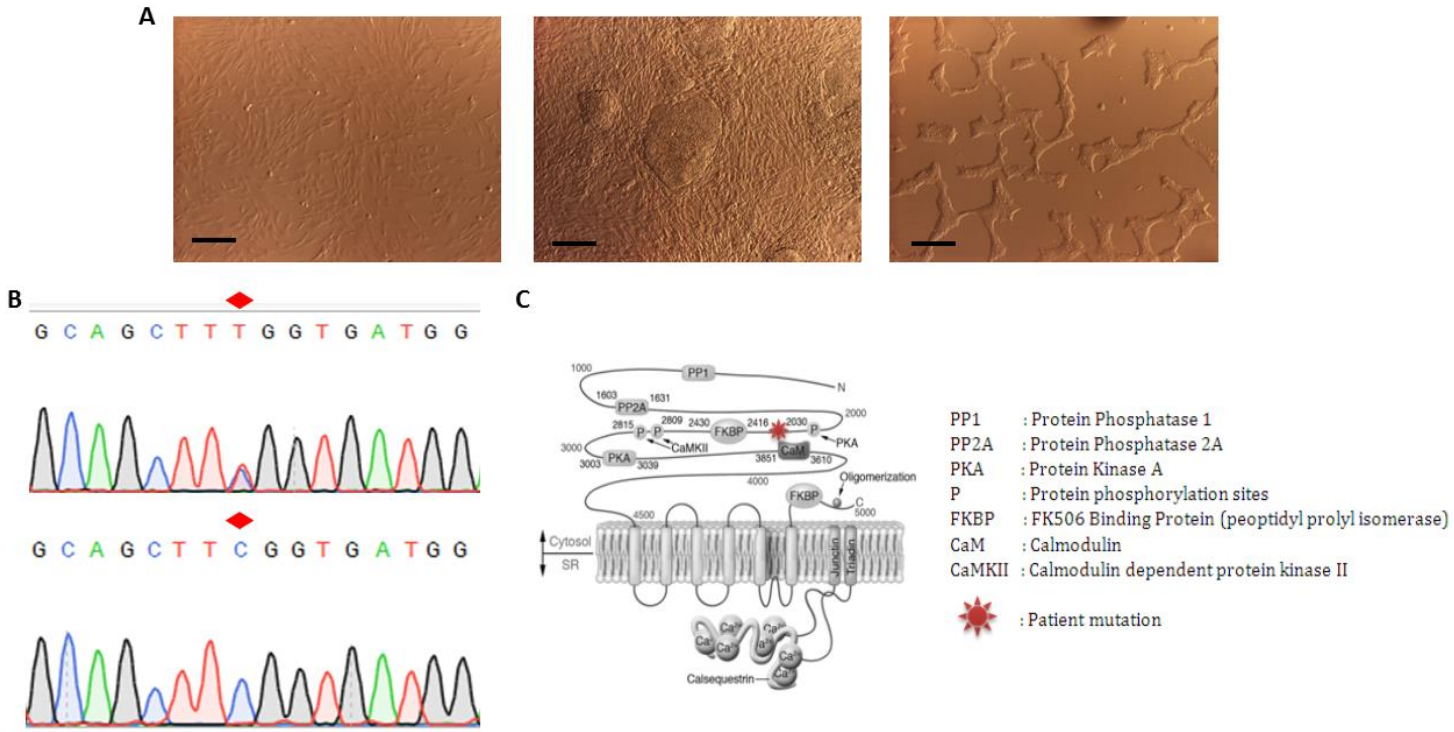


Figure 5-3 - Assessing the CP1 patient genotype

A – Representative images through the reprogramming process of CP1. From the initial seeding of CP1-fibs through to the emergence of putative hiPSC colonies after the addition of SeV. Finally the purified hiPSC line. B – Chromatograms covering the S2246L mutation in CP1 cell line on the top the red diamond indicates the heterozygous mutation. The image on the bottom shows the same region in HUES7 hESC line which features the WT genotype of a homozygous G at position 2246. C – Schematic which displays the predicted structure of the cardiac RYR2, the patient mutation has been highlighted by a red star. The mutation occurs in the cytosolic domain of the *RYR2* and is thought to be primarily involved in inter-domain interactions. Schematic adapted from (Priori and Napolitano, 2005), genotyping of the mutation was performed by Dr Divya Rajamohan.

5.2.2 Targeting CPVT hiPSC with CRISPR/Cas9 using single stranded oligonucleotide method

In order to assess the role of the S2246L mutation in patient phenotype, genome editing techniques were used to alter the mutated base pair. CRISPR/Cas9 was utilised to target the S2246L mutation in the CP1 patient hiPSC line using the oligonucleotide method whereby HDR is facilitated by the introduction of a single stranded oligonucleotide as has previously been demonstrated (Bialk et al, 2015).

Figure 5.4 shows the location of the mutation in exon 44 of the *RYR2* gene. In order to target the CP1-hiPSC line using the oligonucleotide method three components were required. The first was an oligonucleotide of ~100bp to act as a DNA template for HDR. First the CP1-hiPSC line was PCR amplified and sequenced using the custom designed primer pair in Table 5.1. This was performed to detect any SNPs in the genome compared to reference sequence as it was vital that the repair template oligonucleotide retained 100% homology with the endogenous sequence with the obvious exception being the nucleotide being targeted. Two 101bp oligonucleotides were then synthesised by Sigma, one featuring a C (to make the mutated allele WT and correct the genotype) and one featuring a T (to mutate the WT allele and create a double mutant) at the position corresponding to exon 44 c6373 in the *RYR2*. The second component was a gRNA which was designed using the online CRISPR tool developed by MIT (http://crispr.mit.edu/). Using an input sequence of ±100bp from the mutation site the online tool identified potential gRNAs followed by the 5'-NGG PAM sequence. This online tool was also able to predict the specificity and likelihood of off target effects for each gRNA identified. The gRNA was then generated using a commercially available RNA *in vitro* transcription kit (Ambion). The final component was purified Cas9 protein purchased from ToolGene. All three components were nucleofected into CP1-hiPSC using the Amaxa 4D system and programme CA-137.

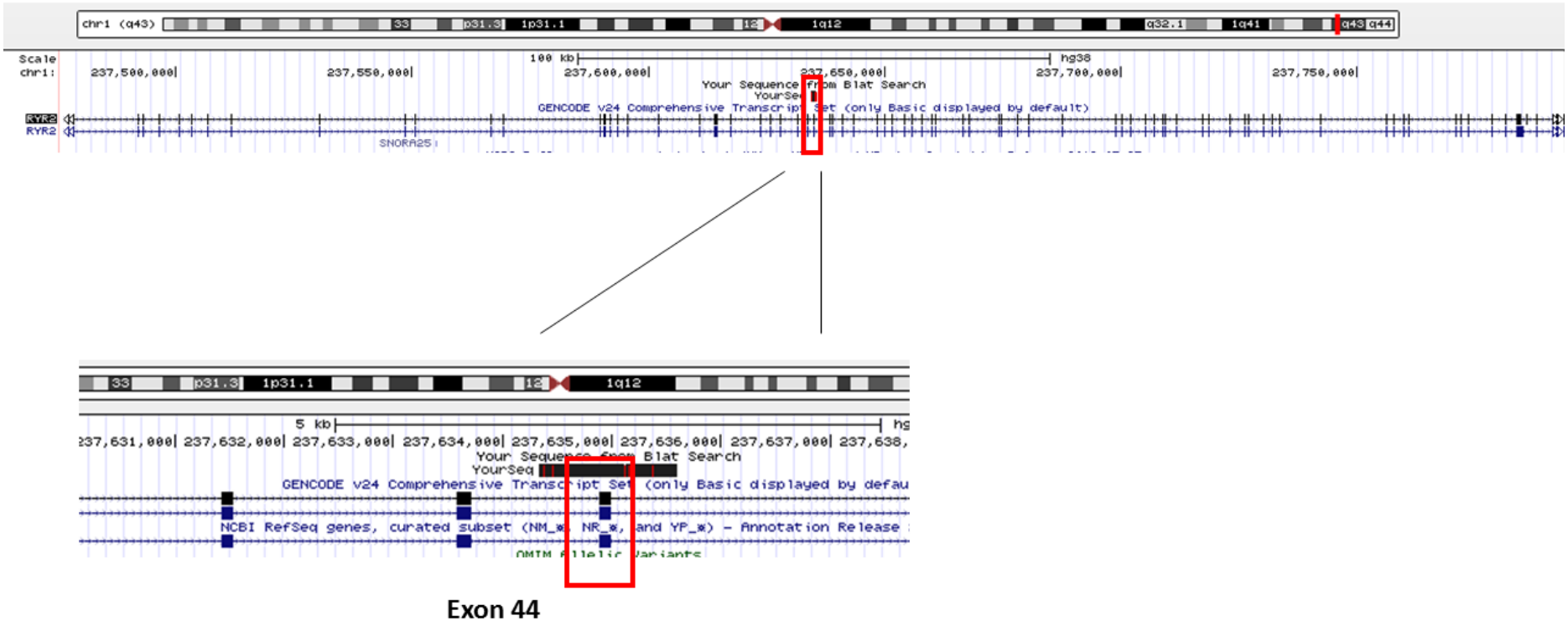
After electroporation CP1-hiPSCs were plated in one well of a 6-well plate coated in Matrigel and 48 hours later these hiPSCs were harvested and plated at clonal density in Matrigel coated 35mm dishes. A small number of cells were removed for gDNA extracted in order to assess whether any targeting had occurred using a restriction digest. In the case of the system used in this thesis a restriction enzyme was removed by silently mutating a C>T, removing the SfcI restriction site from the PCR product generated by the product from the primer pair shown in Table 5.1. These hiPSCs were then grown at clonal density until ready to be collected, using mechanical dissociation, and expanded. After this expansion, cell pellets were collected and gDNA extracted. Using the custom designed primers pair shown in Table 5.1 PCR was

performed to amplify the region around the mutation, these products were then sequenced to assess the extent to which targeting had successfully occurred.

Table 5-1 - Primers used to sequence CP1

Primer Pair	Primer Sequence 5' - 3'	Product Size
CP1 5' Primer	ccccagctatgagaggttca	445bp
CP1 3' Primer	gaacgttggttctccttcca	

A


chr1 (q43)
p31.3
1p31.1
1q12
q32.1
1q41
q43
q44
Scale
chr1:
237,500,000
237,550,000
100 kb
237,600,000
237,650,000
hg38
237,700,000
237,750,000
Your Sequence from Blat Search
GENCODE v24 Comprehensive Transcript Set (only Basic displayed by default)
RYR2
SNORA25
5 kb
237,631,000
237,632,000
237,633,000
237,634,000
237,635,000
237,636,000
237,637,000
237,638,
NCBI RefSeq genes, curated subset (NM_*, NR_*, and YP_*) - Annotation Release

Exon 44

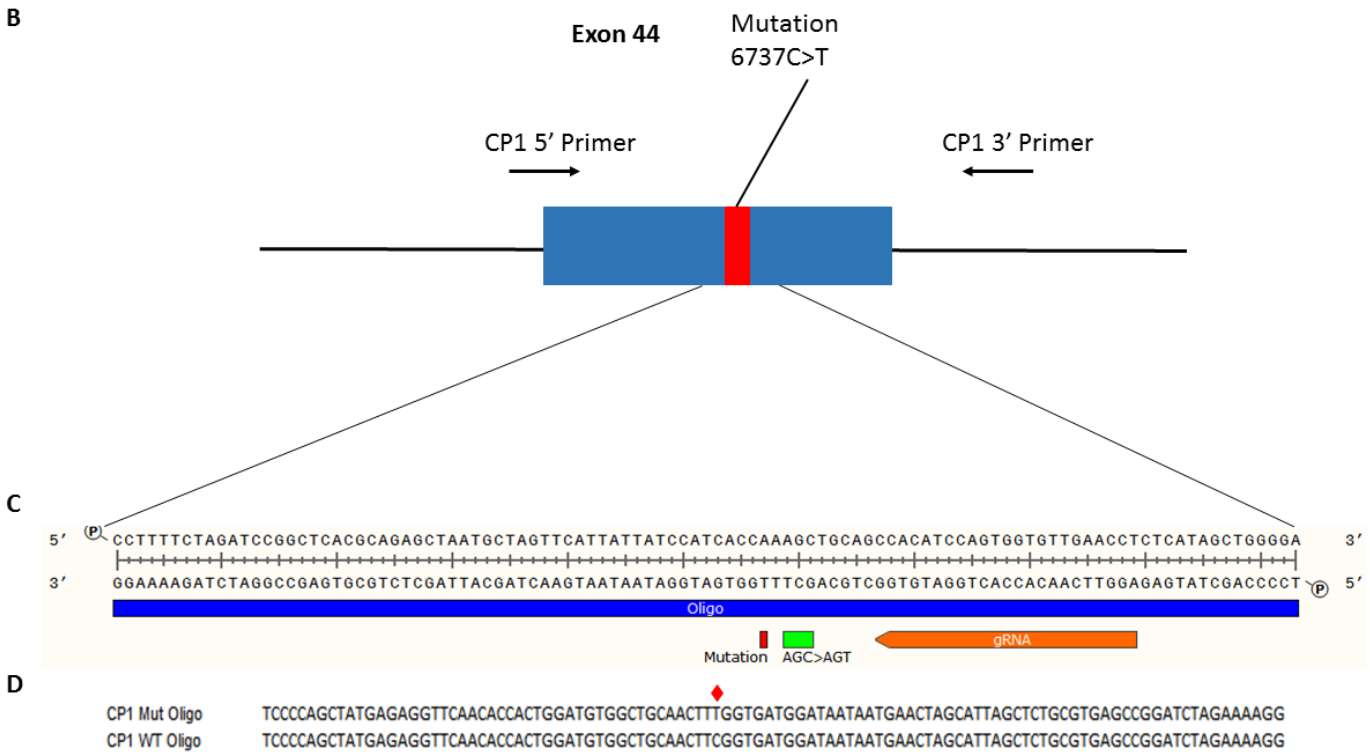


Figure 5-4 - Selecting the tools for the oligonucleotide method of gene targeting using CRISPR/Cas9

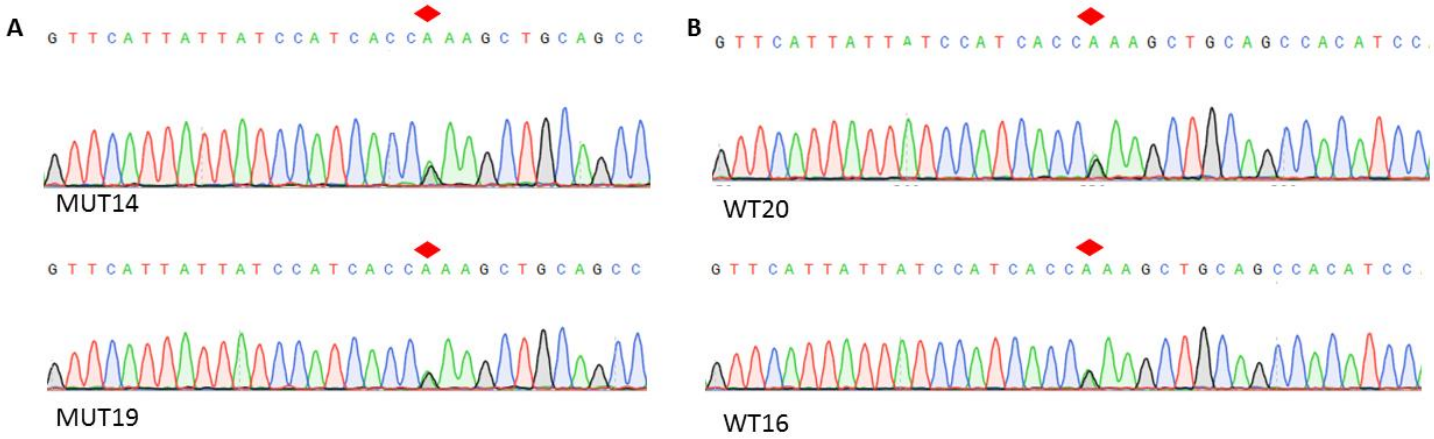
A - Identification of *RYR2* genomic sequence using genome browser (RYR2 NCBI Reference Sequence: NC_000001.11). Using the Blat tool to search for the genomic DNA sequence which was derived from the CP1-hiPSC line identified exon 44. B – Schematic displaying the location of the mutation which is situated in exon 44 of the *RYR2*. This schematic also displays the location of the 5' and 3' sequencing primers used to sequence the genome around the mutation. C – This image shows the 101bp oligonucleotide, synthesised by Sigma, which was provided to the cells as a template for HDR after the initiation of a double strand break by the Cas9 protein. The mutation is highlighted, in the CP1-hiPSC line the mutation is a C>T. Finally there will be a silent mutation(no amino acid change) within the oligonucleotide which removes a unique restriction site from a screening PCR product, thus aiding screening. On this diagram the sequence should be read from 5' to 3' on the bottom strand. D – Two different oligonucleotides were used in this experiment: one was designed to correct the mutant allele to WT (CP1 WT Oligo) and the other is intended to mutate the WT allele to a T, this will result in a homozygous mutation, this is termed CP1 Mut Oligo.

By nucleofecting an oligonucleotide along with a gRNA and Cas9 protein the expectation was that the Cas9 protein would complex with the gRNA and result in a double stranded break (DSB) in the genome at the site to which the gRNA was complementary. The introduction of this DSB would then result in the targeted cell repairing the break through HDR, using the template provided as an oligonucleotide, or by NHEJ which will likely result in a frameshift mutation or an indel.

Figure 5.5 shows the analysis of the targeted clones, 23 of which were assessed by PCR amplification of the region around the mutation using the custom designed primers shown in Table 5.1 and then sequenced. These analyses showed that of the 13 clones which had been targeted with the CP1-WT oligonucleotide to correct the mutated allele, 0% exhibited successful targeting and 0% exhibited indel or frameshift mutations. 10 clones were assessed all of which had been targeted using the CP1-MUT oligonucleotide to mutate the healthy allele with 0% success rate, along with 0% indels or frameshift mutations. The lack of success and noticeable lack of indels or frameshift mutations indicated two potential issues. The first was that the gRNA was not specific enough and therefore was directing the Cas9 protein to a different location in the genome. The second potential problem was that the purified Cas9 protein was not active and therefore no DSBs were being induced.

At this stage a number of colleagues in the lab had noticed a similar lack of successful targeting or indel/frameshifts using the oligonucleotide method. As a result of this it was decided as a lab-wide practice to test the activity of the Cas9 protein used in this thesis as shown in Figure 5.5. This was performed by incubating purified gRNA with Cas9 protein and plasmid DNA from a previously successful targeting experiment in an Eppendorf tube and running the resulting DNA on a gel to assess whether any cleavage of the DNA had occurred. This showed that the Cas9 protein which had been used in this thesis, was not actively cutting compared to Cas9 protein from an alternative supplier (which was actively cutting) and to previous batches from ToolGene which were also actively cutting.

The conclusion therefore was that the lack of successful targeting using this method was a consequence of inactive Cas9 protein. Due to the need to optimise the process and the concentrations of new reagents when using an alternative Cas9 protein supplier, the direction of this experiment was changed and a different system to edit the CP1-hiPSC genome was introduced.



C

Condition	Number of clones	% Positive Targeting	% Indels/Frameshifts
CP1 WT	13	0	0
CP1 MUT	10	0	0

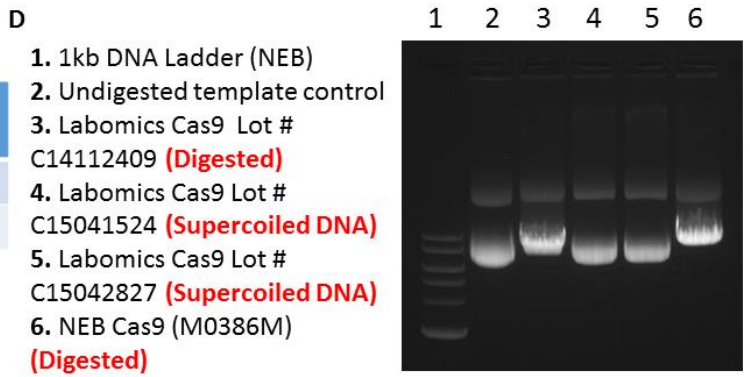


Figure 5-5 - Analysing the success of the oligonucleotide method using CRISPR/Cas9

A – Representative chromatograms of the CP1-Mut targeted cells after sequencing. The red diamond indicates the heterozygous mutation remains at position 2246. B - Representative chromatograms of the CP1-WT targeted cells after sequencing. The red diamond indicates the heterozygous mutation remains at position 2246. C – Table showing the relative success of the targeting using the oligonucleotide method. There were 0% successful targeting events as well as 0% indels or frameshift mutations. Given the scarcity of indels it was suggested that the Cas9 protein was not active. D – A diagnostic digest using control gRNA and gDNA from previously successful CRISPR/Cas9 oligonucleotide targeting. This gel highlights that lane 3 (Labomics Cas9 Lot # C14112409) and lane 6 (NEB Cas9 (M0386M)) result in successful cutting of control DNA. However in lane 4 (Labomics Cas9 Lot #C15041524) and 5 (Labomics Cas9 Lot # C15042827) no cutting was evident suggesting that these lots of CAs9 protein were not active, it was Lot#C15041524 which was used in these experiments. The *in vitro* test of Cas9 protein was carried out by Dr Alexander Kondrashov.

5.2.3 Targeting CPVT hiPSC with PiggyBac transposon method

One of the advantages of the oligonucleotide system is that there is no integration of plasmid DNA which subsequently will need to be excised potentially leaving a footprint which may result in the disruption of gene expression (Liu et al, 2011). However the PiggyBac transposon system has previously been used successfully to modify the human genome “footprint free” (Galvan et al, 2009). Moreoever using a modified version of this system (Figure 5.6) it was possible to introduce two selection steps. The first was to kill any hiPSC not expressing puromycin and which were therefore not targeted during nucleofection and the second was to introduce ganciclovir to the hiPSCs after excision as this will kill any hiPSC expressing thymidine kinase thus killing hiPSCs which had not excised the insert. In this thesis the PiggyBac system was used along with a Cas9 plasmid and a gRNA plasmid meaning the delivery of three plasmids to the cells using nucleofection. Assembly was required to generate the targeting construct plasmid.

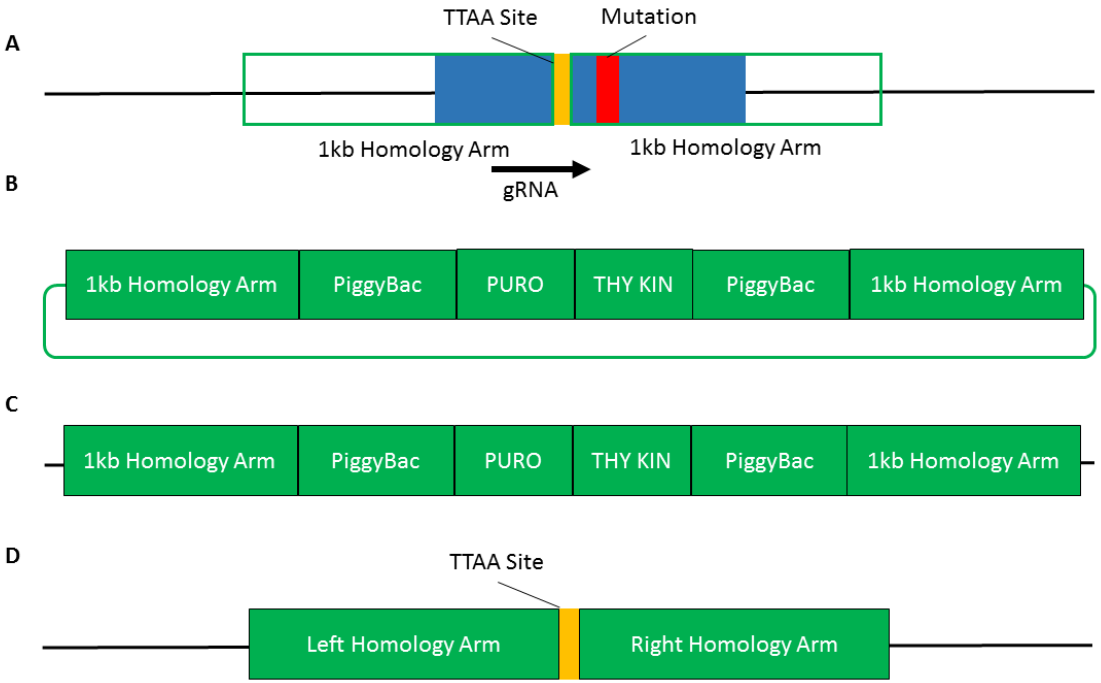


Figure 5-6 - Schematic explaining the PiggyBac method

A – The endogenous genomic sequence. The areas mapped out by the green outline show the 1kb arms of homology on either side of the TTAA site which will be created by PCR amplification of the endogenous sequence from gDNA and incorporated into a targeting plasmid construct. The TTAA site is omitted from the targeting construct as the excision of the PiggyBac will leave a TTAA footprint, by incorporating this into the targeting strategy the method can be considered 'footprint' free as no amino acid or nucleotide changes will be made. The mutation is highlighted in red. The targeting construct will feature the WT nucleotide sequence at this location. Also seen in this section is the gRNA: it should be noted that as the gRNA used in this strategy spans the TTAA site it will not be present in the targeting construct, as the PiggyBac splits the homology arms. This prevents the gRNA plasmid cutting the targeting construct and reducing efficiency B – This is a schematic representing the targeting construct. The targeting construct has a pBluescript backbone and features two key components which will be used in selection. The puromycin resistance cassette allows positive selection by killing any hiPSCs in the culture which have not successfully taken up the plasmid after electroporation. The plasmid also expresses thymidine kinase, this will be used for negative selection after excision as the addition of ganciclovir will kill any cell still expressing the plasmid, leaving only fully excised hiPSC. There are also two 1kb arms of homology flanking the PiggyBac sequence. C – This schematic represents the plasmid components integrated into the endogenous DNA, due to the PiggyBac sequence insertion between the arms of homology the gene will be disrupted while this insertion is in place. D – The left and right homology arms from the targeting construct will remain after excision and this will leave the corrected nucleotide at position c6736.

The targeting construct plasmid was made up of 4 components; a pBluescript backbone, a PiggyBac region containing a puromycin resistance cassette and expressing thymidine kinase, a left arm of homology from the CP1-hiPSC endogenous sequence and a right arm of homology from CP1-hiPSC endogenous sequence. 40bp primers with overhangs between the borders of the 4 components were synthesised by Sigma and used to amplify the homology arms from endogenous CP1-hiPSCs. The PiggyBac sequence with overhangs was amplified from PiggyBac plasmid DNA. These PCR amplifications were performed using custom designed primers which are shown in Table 5.2.

Table 5-2 - 40bp primers used to generate targeting plasmid

Primer Name	5' – 3' Sequence
Backbone > Left Flank	acggtatcgataagcttgattacgtaaaattaaactttaa
PB > Left Flank	gactatctttctagggttaaaatattgagaaaaccgtgaa
Left Flank > PB	ttcacggttttctcaatattttaaccctagaaagatagtc
Right Flank > PB	tgcaccaaccttacttatattTAACCCTAGAAAGATAATCA
PB> Right Flank	TGATTATCTTTCTAGGGTTAaatataagtaaggttggtgca
Backbone > Right Flank	ccgggctgcaggaattcgatcagtaaaggaaacaggaaga

To assemble the targeting plasmid PCR amplification was performed using the custom primers shown in Table 5.2. Figure 5.7 shows a schematic explaining the four different components required to generate the targeting construct plasmid for the CP1-WT plasmid. Figure 5.7 displays gel electrophoresis images showing the left and right arm of homology, 320bp and 1000bp respectively, and the PiggyBac sequence which was 3235bp after PCR amplification using the custom designed primers shown in Table 5.2. These products were extracted from the gel and annealed along with the pBluescript backbone using Gibson assembly. Colonies were then plated on agar plates containing ampicillin and incubated at 37^{o}C overnight. The following day colonies were picked from the agar plates and they underwent a small scale DNA prep as described in Section 2.4.7. In order to assess whether the Gibson assembly had been successful, plasmids were linearized with EcoRI and gel electrophoresis was performed. Of the 16 clones linearised, 8 exhibited the correct product size. Upon sequencing it was demonstrated that all 8 had the right homology arm inserted correctly as shown by sequencing with M13R primer, but only 6 had the left homology inserted correctly, as shown by sequencing with M13F primer. Of the final 6 plasmids which featured the correct size and orientation of the components, all exhibited the nucleotide C at the corresponding mutation point 6737. This suggested that these plasmids would result in a WT phenotype if used in the CP1 hiPSC line. The final plasmid map for the CP1-WT targeting plasmid can be seen in Figure 5.8.

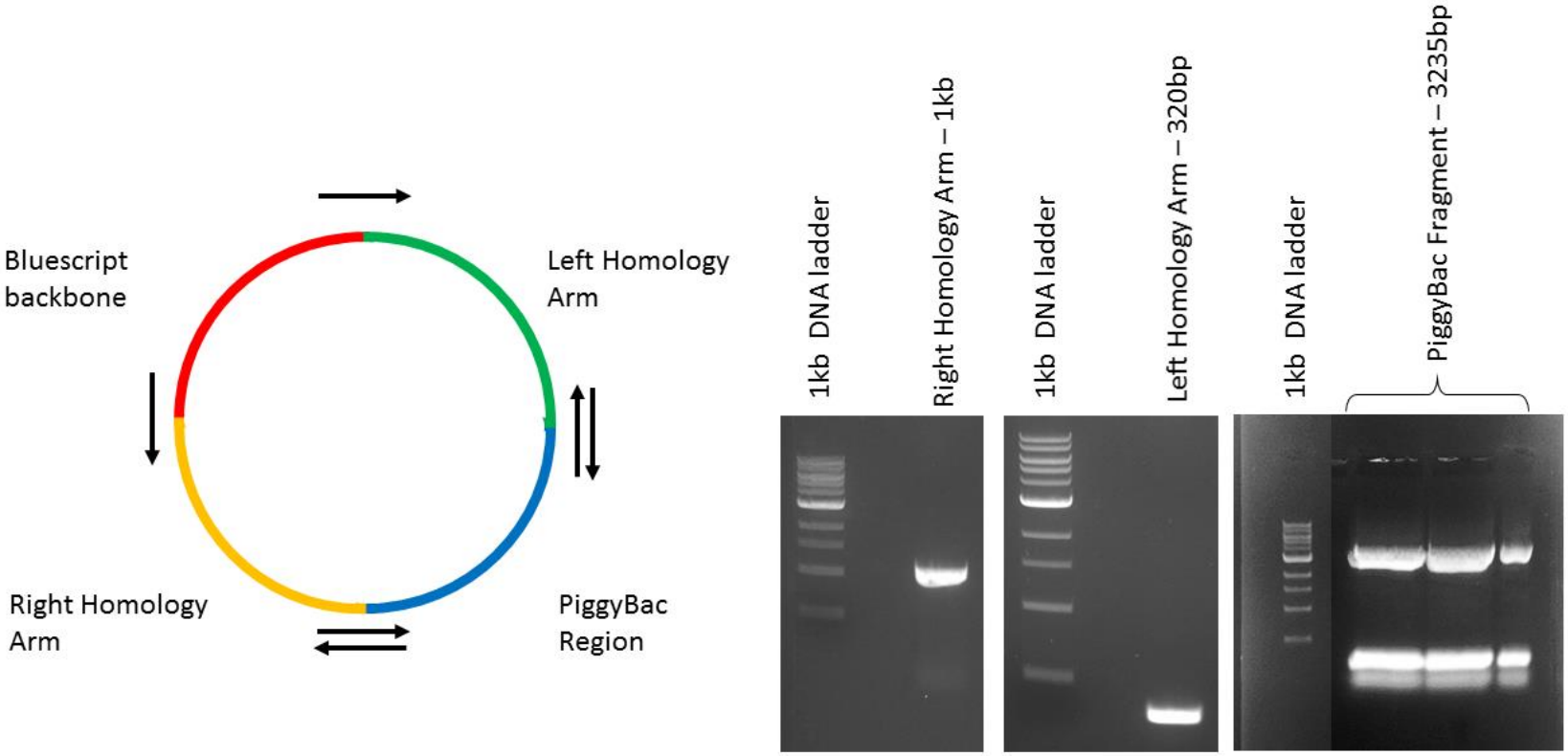


Figure 5-7 - Generating the targeting construct for use in PiggyBac system in CRISPR/Cas9

The generation of a targeting construct required the building of a plasmid form 4 components. The first component was a pBluescript backbone which was generated by digestion using EcoRI (red). The second component was the left homology arm from the CP1 endogenous sequence which resulted in a PCR product of 320bp as shown (green). The third component was a right homology arm from the CP1-hiPSC endogenous sequence which resulted in a PCR product of 1000bp as shown (yellow). The final product was a PigggyBac region which featured a puromycin resistance cassette and expressed thymidine kinase and this resulted in a 3235bp PCR fragment as shown (blue). These PCR products were cut from the gel and purified before being assembled using Gibson assembly. The black arrows indicate the primers described in Table 5.2.

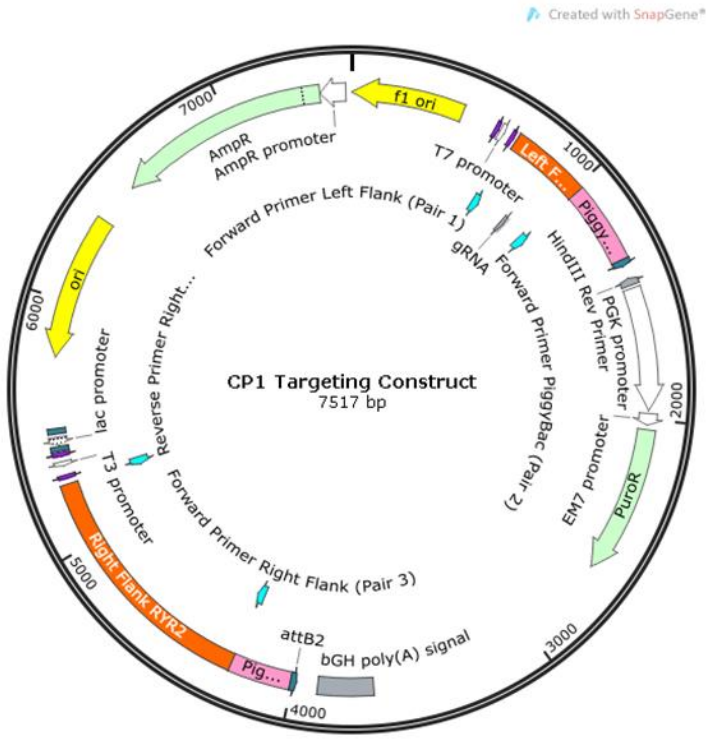


Figure 5-8 - Plasmid maps of CP1 targeting construct

The targeting plasmids used to provide a template for the HDR after the inducement of a DSB in the CP1-hiPSC line. The CP1 targeting construct features puromycin resistance under the control the PGK promoter as well as a change in nucleotide sequence form T>C which will correspond to a change in the sequence of nucleotide position 6737, resulting in a WT genotype. The two arms of homology (orange) are split by the PiggyBac sequence (pink) which will leave a TTAA excision site when removed.

Figure 5.9 shows the generation of the gRNA plasmid. To construct the gRNA plasmid suitable gRNA sequences for targeting *RYR2* were identified using online CRISPR tool (http://crispr.mit.edu/). Using an input sequence of ±100bp from the TTAA site the online tool identified potential gRNAs followed by the 5'-NGG PAM sequence. This online tool was able to predict the specificity and likelihood of off target effects for each gRNA identified. To create the gRNA plasmid gRNA primers shown in Table 5.3 were annealed together and ligated into linearized pU6 plasmid (Dr Bill Skarnes, Sanger Institute). Ligation was aided by the BsaI overhangs at the 5' and 3' end (Figure 5.9). These plasmids were then plated on agar plate containing kanamycin and incubated at 37^{o}C overnight. The following day colonies were picked and were subjected to small scale DNA preparation as described in Section 2.4.7. In total 3 colonies were selected for analysis which was carried out by having the plasmid sequenced using the SP6 primer (5' ATTTAGGTGACACTATAG 3'). All were successfully ligated with the gRNA inserted correctly.

Table 5-3 - Primer pair used to generate gRNA sequence for ligation

gRNA Pair	Sequence 5' – 3'	Product Size
CP1 gRNA	accGattttaaatataagtaaggttgg	27bp
	aaacccaaccttacttatatttaaaat	

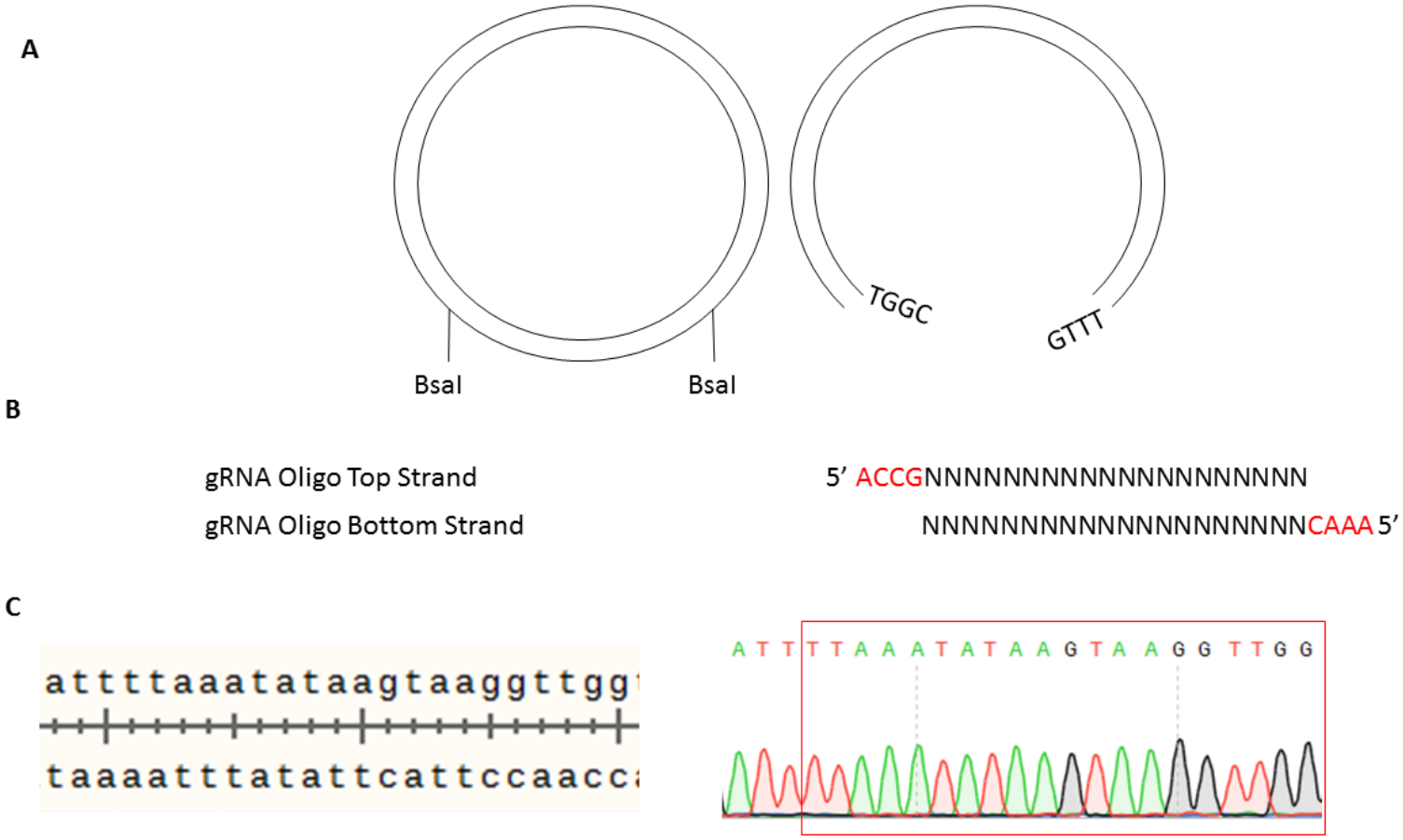


Figure 5-9 - Generation of the gRNA plasmid

This schematic shows the gRNA vector backbone, pU6_BsaI. A – The plasmid is then digested using BsaI to create over hanging sticky ends for subsequent ligation. B – Plasmid now has the pU6 backbone and TGGC and GTTT over hangs. C - The sequenced gRNA after ligation showing the correct sequence.

5.2.4 Optimisation of Amaxa 4D nucleofection

Before nucleofection of the three plasmids required for this method of gene targeting the optimal conditions for nucleofection in hiPSC lines using the Amaxa 4D system were first assessed as shown in Figure 5.10. pSin GFP plasmid was nucleofected into two hiPSC lines using 7 different programmes on the Amaxa 4D system per manufacturers guidelines. These data indicate that DN-100 (86.5±6.5% at 24 hours), DC-100 (59.6±12% at 24 hours) and CA-137 (47.3±12% at 24 hours) were the most efficient programs at all time points. Maximum GFP % was achieved at 24 hours under all conditions. In addition to the efficiency of transfection, the cell number was also calculated in order to assess viability. In this regard CB-150 (6909±1836.32), CD-118 (6024.75±2363.87) and CE-118 (5973.5±1150.25) were shown to have the most cells present at 24 hours. Only two conditions exhibited cell numbers lower than the non electroporated control indicating higher levels of cytotoxicity, CA-137 (4037.75±1209.86) and DN-100 (1908.25±474.69).

These data indicated that DN-100, DC-100 and CA-137 were the most efficient programmes to target hiPSCs despite some cytotoxicity in DN-100 and CA-137.

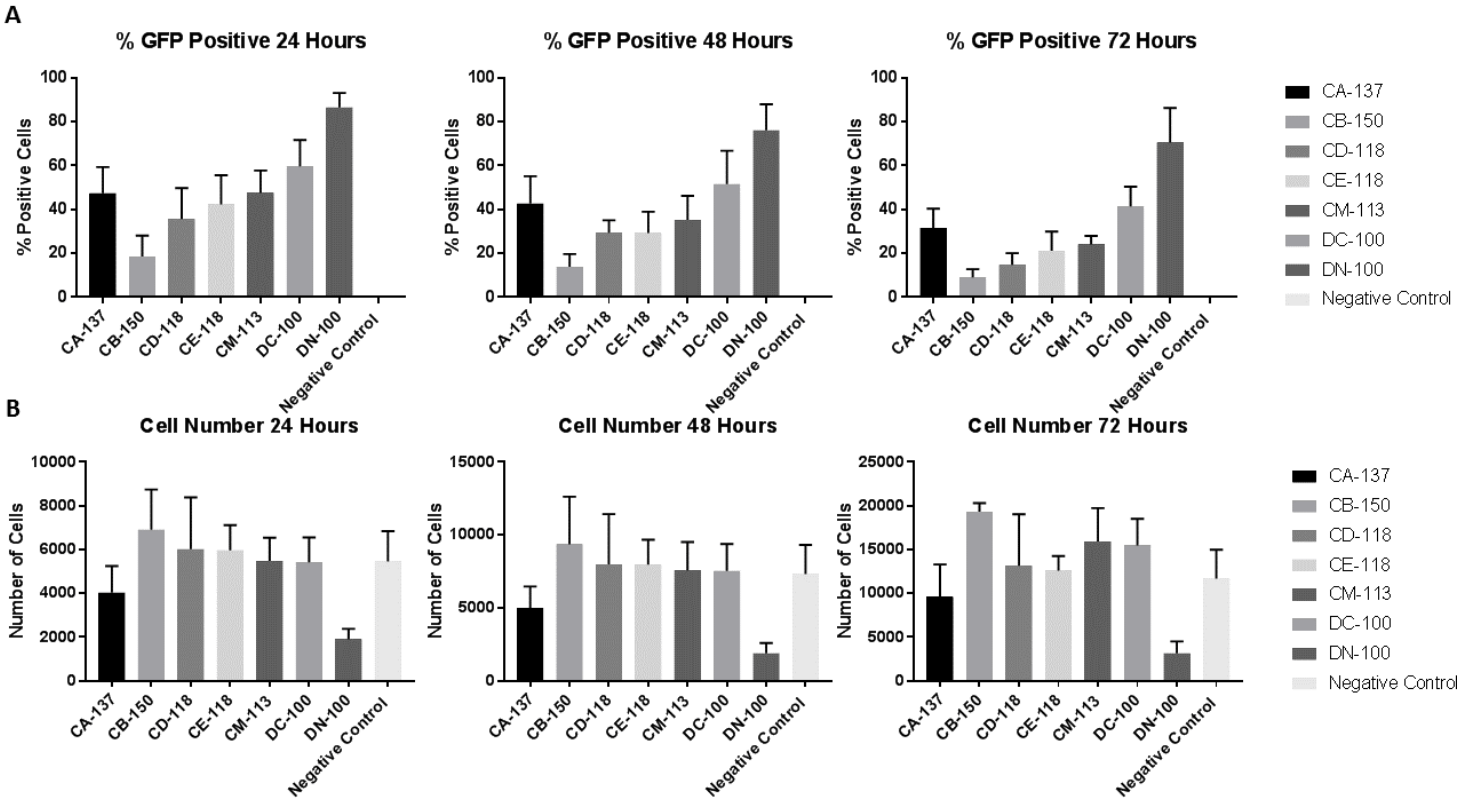


Figure 5-10 - Assessing the optimal conditions of electroporation on the Amaxa 4D system

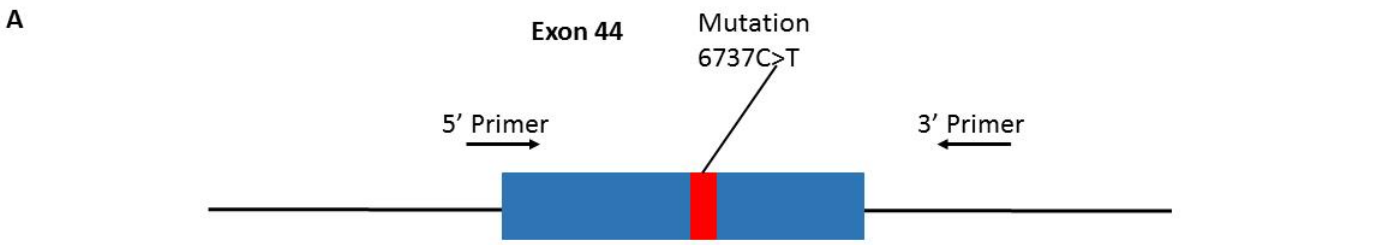
To assess the optimal Amaxa 4D electroporation programme two hiPSC lines were tested. $1.6x10^6$ were harvested in the logarithmic growth phase and resuspended in Amaxa P3 nucleofection buffer with 6.4µg of pmaxGFP vector added. The hiPSC were then equally seeded into 16 different wells in a Cell Line Optimization 4D-Nucleofector X Kit strip before being nucleofected. After nucleofection the strip was then incubated at 37^0C with 5% CO_2 for 5 minutes to allow the hiPSCs to recover. After this the entire contents of each well were resuspended in E8 medium + 10µM Y-27632 and each transferred to 1 well of a 48 well plate. The hiPSCs were then analysed and stained with hoescht at 24, 48 and 72 hours to assess cell count by imaging the cells using the DAPI channel on a confocal plate reader. In addition to this the cell count was used, along with the number of hiPSCs which stained green in the Alexa488 channel, to calculate % positive. A – These graphs display the % of hiPSCs which were positive for GFP using the Alexa488 channel on a confocal plate reader at 24, 48 and 72 hours. B – These graphs show the number of cells present within the well as assessed by hoescht live cell staining in the DAPI channel, n=2.

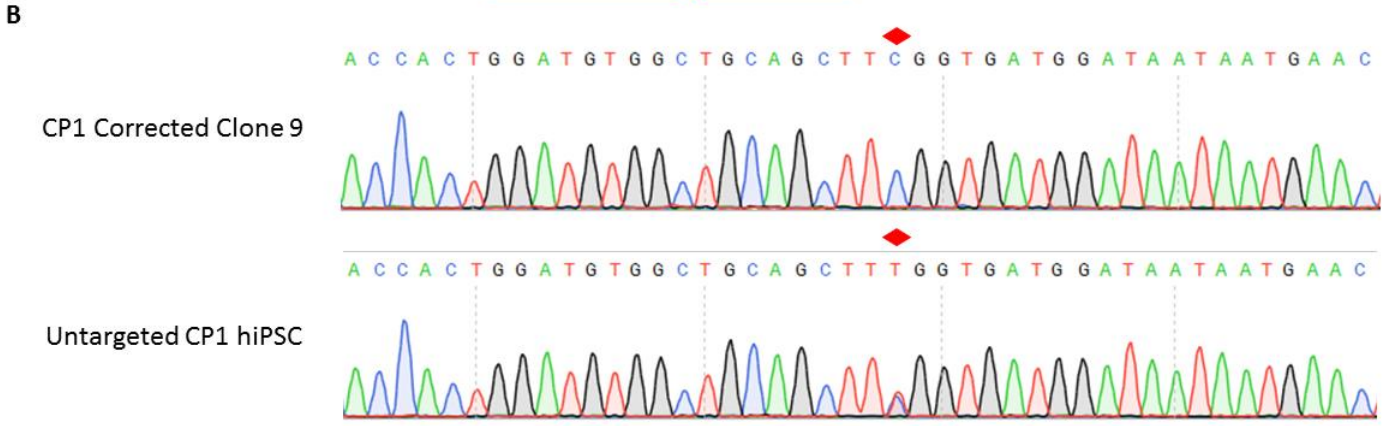
5.2.5 Assessment of targeting using plasmid method

Upon successful nucleofection of the gRNA and Cas9 plasmids the genome will be cut at the site specified by the gRNA design program. As WT Cas9 plasmid was used in this thesis the cut in the genome will be a DSB (Ran et al, 2013). Once this DSB is induced the cell will then repair the break by NHEJ leading to a frameshift mutation/indel. If a template is present then the cell may repair itself by HDR. Successful nucelofection of all three targeting plasmids would create the condition of DSB at the site desired in the genome and the presence of a template for HDR which would correct the mutated base pair.

The hiPSCs targeted in this thesis were left for 24-48 hours to recover from electroporation after which they were passaged to fresh plates and treated with puromycin. After 1 week of puromycin treatment all hiPSCs were harvested and replated before being transfected with 1µg transposase plasmid to excise the PiggyBac sequence. The hiPSCs were then given 24-48 hours to recover from this transfection before being treated with ganciclovir as any hiPSCs in which the PiggyBac insert had not been excised would still express thymidine kinase which converts ganciclovir into a toxic product (Beck et al, 1995). After this process of negative selection clonal hiPSCs were dissociated mechanically (using a stem cell knife) and sequenced using the primers in Table 5.1 to assess whether successful targeting had occurred. Figure 5.11 shows the analysis of the 12 hiPSC clones which were picked, expanded and analysed. Sequence data indicated that 1 of the 12 clones analysed exhibited a corrected phenotype. The others maintained a heterozygous C/G at position 6737.

Therefore the genotype of this hiPSC clone had been altered and from that point it was termed CP1-WT. Further analysis was required to ensure clean recombination of the DNA after excision of the targeting construct with no indels, SNPs or frameshift mutations.





C

Clones Analysed	Positive Clones
12	1 (8%)

Figure 5-11 - Analysing the success of the plasmid method of targeting using CRISPR/Cas9

A - Schematic displaying the location of the mutation which is situated in exon 44 of the *RYR2.* B – Chromatograms which show the sequence around the S2246L mutation in untargeted CP1-hiPSCs and in CP1-targeted WT clone 9. The red diamond indicates the position of the mutation in the CP1 untargeted cells and the position of the corrected homozygous G in the CP1-WT Clone 9 line. C – This table shows the relative targeting efficiency of the protocol used in this thesis. Of the 12 clones analysed after two selection steps 1 was positive giving a targeting efficiency of 8%.

Having successfully altered the T>C at position 6737 in the mutated allele of CP1-hiPSC the next step in characterising this line was to assess the recombination of the homology arms and the TTAA excision site with the endogenous sequence. PCR amplification of the regions of interest was performed using the custom primers shown in Table 5.4. These PCR products were then sequenced to ascertain if there were any indels or frameshift mutations at these locations.

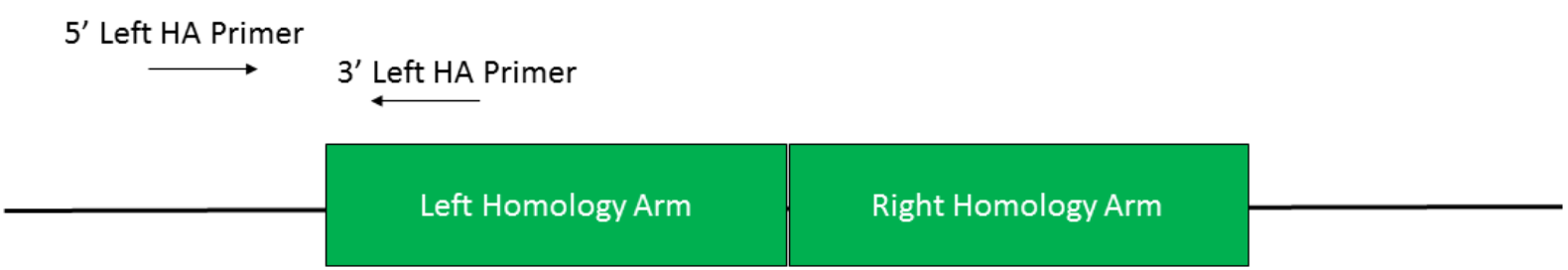
As shown in Figure 5.12 there was clean recombination of the region where the left homology arm and right homology arm were introduced in the initial targeting step. Furthermore the TTAA excision was also recombined cleanly.

These data indicate that no damage to the endogenous DNA had occurred at the introduction or excision site of the plasmids used in this thesis.

Table 5.4 - Primers used to assess if clean recombination had occurred after excision of the PiggyBac

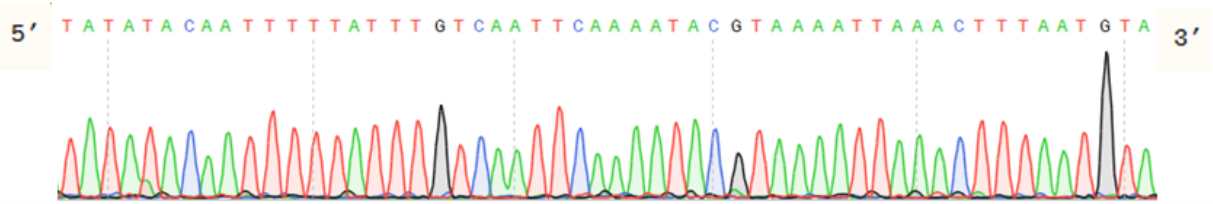
Region to Assess	Primer Pair	Sequence 5' – 3'	Product Size
Left Homology Arm	5' Left HA Primer	ggagtggttggggagatgtt	399bp
	3' Left HA Primer	acctggatcgtgctgtaact	
Right Homology Arm	5' Right HA Primer	catcgtggctctttgtaggc	411bp
	3' Right HA Primer	agtgtctacccagtgctgac	
TTAA Site	5' TTAA Primer	ccccagctatgagaggttca	445bp
	3' TTAA Primer	gaacgttggttctccttcca	

A



Left Homology Arm Sequence

CP1 Corrected Clone 9



NCBI Reference Sequence:
NC_000001.11

5′ tatatacaattttatttgtcaattcaaaatacgtaaaattaaactttaatgta 3′

3′ atatatgttaaaaataaacagttaagttttatgcattttaatttgaaattacat 5′

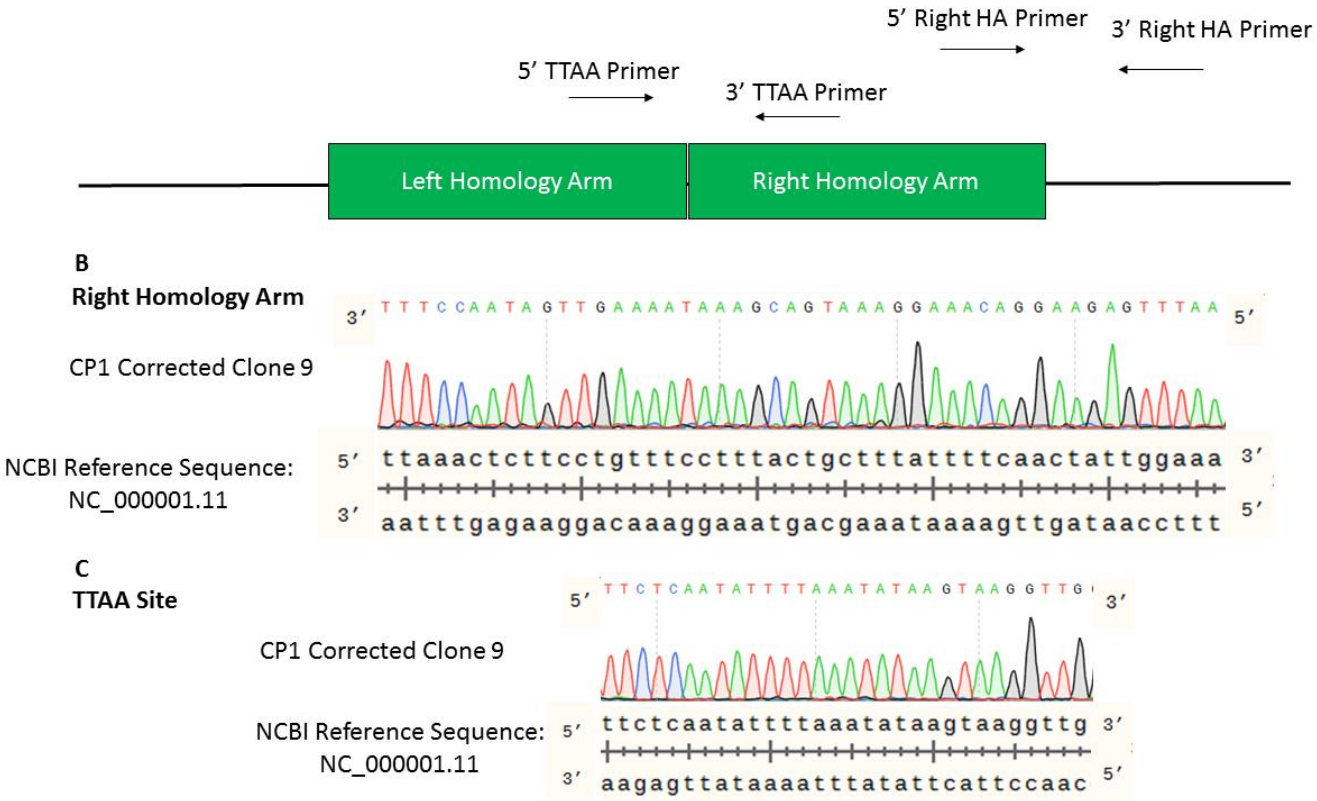


Figure 5-12 - Assessing the left and right homology arms as well as the TTAA site after PiggyBac excision

A – The schematic of the recombined genomic DNA at the site of insertion features the primers used to assess the recombination of the left homology arm. This chromatogram and snapgene file illustrate the sequence of the CP1-WT hiPSC line at the point where the left arm of the targeting construct ends and the endogenous sequence begins. These data indicate clean recombination at the left arm of homology. B - The schematic of the recombined genomic DNA at the site of insertion features the primers used to assess the recombination of the right homology arm. This chromatogram and snapgene file illustrate the sequence of the CP1-WT hiPSC line at the point where the right arm of the targeting construct ends and the endogenous sequence begins. These data indicate clean recombination at the right arm of homology. This reference sequence should be rad 5′ to 3′ on the bottom strand. C - The schematic of the recombined genomic DNA at the site of insertion features the primers used to assess the recombination of the TTAA. This chromatogram and snapgene file illustrate the sequence of the CP1-WT hiPSC line at the TTAA excision point where the plasmid was initially integrated. These data indicate clean recombination at the TTAA site.

5.2.6 Basal calcium handling data for healthy-hiPSC-CMs and CPVT-hiPSC-CMs

To assess whether the differences in basal calcium handling phenotype were observed in hiPSC-CMs it was decided to test four key parameters of the calcium transient; TRise, TDecay, Amplitude and Time of Transients (TOT) (Shinnawi et al, 2015). These parameters were measured in CP1-, CP1-WT and ReBl-PAT-hiPSC-CMs using the CellOPTIQ platform. To achieve this hiPSC-CMs were seeded at $5x10^4$ cardiomyocytes per well in a 96 well plate and dyed using the calcium label Fura2-AM. Measurements were obtained with stable conditions of temperature at 37^{o}C and CO_2 at 5%.

Figure 5.13 shows the basal calcium handling characteristics of the hiPSC-CM panel used in this thesis. All three hiPSC-CMs were analysed for their basal levels of TRise, TDecay, amplitude and TOT. It was observed that ReBl-PAT-hiPSC-CMs exhibit significantly shorter TRise (346.4±20.54ms vs 365.8±20.01ms, $p<0.05$, n=92, Tukeys multiple comparisons test) and significantly shorter TOT (1330±314.7ms vs 1475±297.9ms, $p<0.05$, n=92, Tukeys multiple comparisons test) than CP1-hiPSC-CMs. CP1-hiPSC-CMs displayed a significantly longer TRise time (365.8±20.01ms vs 335.4±16.45ms, $p<0.05$, n=91, Tukeys multiple comparisons test), a significantly larger amplitude (0.26±0.15 vs 0.1±0.06, $p<0.05$, n=91, Tukeys multiple comparisons test) and a significantly shorter TOT (1475±297.9ms vs 1811±604.8ms, $p<0.05$, n=91, Tukeys multiple comparisons test) than CP1-WT-hiPSC-CMs. ReBl-PAT-hiPSC-CMs exhibited a significantly longer TRise time (346.4±20.54ms vs 335.4±16.45ms, $p<0.05$, n=91, Tukeys multiple comparisons test), a significantly shorter TDecay time (458.3±124.5ms vs 502.3±115.7ms, $p<0.05$, n=91, Tukeys multiple comparisons test), a significantly larger amplitude (0.23±0.10 vs 0.1±0.06, $p<0.05$, n=91, Tukeys multiple comparisons test), and a significantly shorter TOT (1330±314.7ms vs 1811±604.8ms, $p<0.05$, n=91, Tukeys multiple comparisons test) than CP1-WT-hiPSC-CMs.

These data indicate that significant differences exist between healthy and CVPT hiPSC-CMs. Furthermore they indicate that there are also significant differences between CPVT-hiPSC-CMs and CPVT-WT-hiPSC-CMs after genetic correction of the hiPSC line. Finally the CP1-WT-hiPSC-CMs exhibit differences to the heathy-hiPSC-CMs indicating genetic variation between hiPSC-CMs.

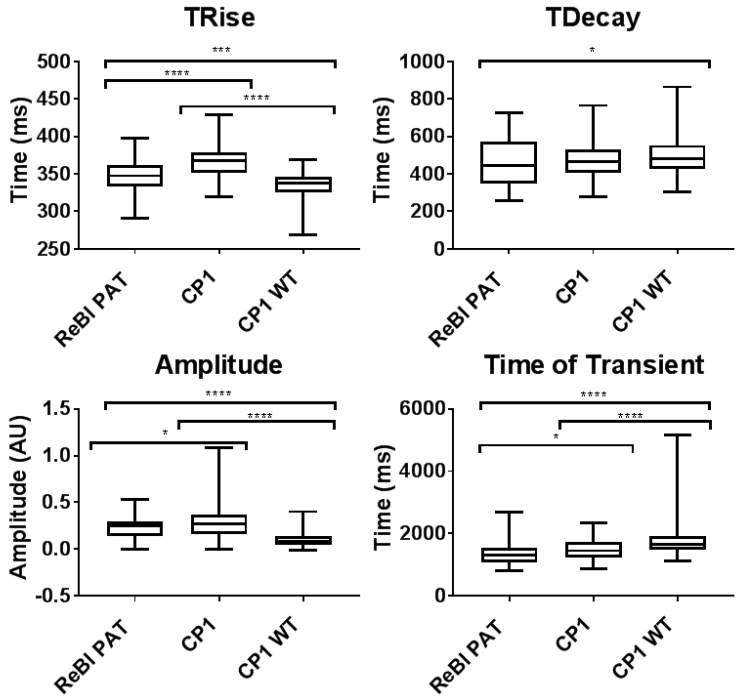


Figure 5-13 - Basal calcium handling characteristics of CP1-, ReBl-PAT- and CP1-WT- hiPSC-CMs

hiPSC-CMs were seeded into Matrigel coated 96-well plates at a density of $5x10^4$ per well to create a confluent monolayer. All hiPSC-CMs in this study were between d30-35 post differentiation. hiPSC-CMs were stained with intracellular calcium label FURA2-AM and transients were recorded on the CellOPTIQ platform. ReBl-PAT-hiPSC-CMs exhibited basal TRise of 346.4±20.54ms (n=92), TDecay of 458.3±124.5ms (n=92), amplitude 0.23±0.10 (n=92) and TOT of 1330±314.7ms (n=92). CP1-hiPSC-CMs exhibited basal a TRise of 365.8±20.01ms (n=96), TDecay of 470.2±89.09ms (n=96), amplitude of 0.26±0.15 (n=96) and TOT of 1475±297.9ms (n=96). CP1-WT-hiPSC-CMs exhibited a TRise of 335.4±16.45ms (n=91), TDecay of 502.3±115.7ms (n=91), amplitude of 0.1±0.06 (n=91) and TOT of 1811±604.8ms (n=91). ReBl-PAT-hiPSC-CMs showed significant difference to CP1-hiPSC-CMs with regards to TRise ($p<0.05$, n=92, Tukeys multiple comparisons test) and TOT ($p<0.05$, n=92, Tukeys multiple comparisons test). CP1-hiPSC-CMs significant difference in TRise ($p<0.05$, n=91, Tukeys multiple comparisons test), amplitude ($p<0.05$, n=91, Tukeys multiple comparisons test) and TOT ($p<0.05$, n=91, Tukeys multiple comparisons test) compared CP1-WT-hiPSC-CMs. ReBl-PAT-hiPSC-CMs exhibited significantly differences in TRise ($p<0.05$, n=91, Tukeys multiple comparisons test), TDecay time ($p<0.05$, n=91, Tukeys multiple comparisons test), amplitude ($p<0.05$, n=91, Tukeys multiple comparisons test), and TOT ($p<0.05$, n=91, Tukeys multiple comparisons test) than CP1-WT-hiPSC-CMs.

5.2.7 Assessment of LTCC blockade in healthy-hiPSC-CMs and CPVT-hiPSC-CMs

The LTCC is a key component of the calcium handling machinery of a cardiomyocyte. Calcium ions flow into the cell through the LTCC and activate the RYR2 leading to CICR from the SR (Yamakage et al, 2002). Nifedipine is a known blocker of the LTCC (Itzhaki et al, 2011) and for this thesis was used to assess the effect that LTCC has on the calcium transient across our hiPSC panel. hiPSC-CMs were seeded into a 96-well plate at a density of $5x10^4$ per well. These hiPSC-CMs were then stained with the intracellular calcium labelling dye Fura2-AM and basal recordings were taken using the CellOPTIQ system. Nifedipine was added at 50, 100 and 1000nM and incubated on the cells for 30 minutes. After this incubation a second recording was taken. To assess changes one-way ANOVA with Dunnett's multiple comparisons test was used to compare treated hiPSC-CMs to basal hiPSC-CMs within the same cell line, n=5.

Exposure to 1000nM stopped calcium transients in all 6 replicates of all hiPSC-CM lines. In addition to this only 1 of 6 CP1-WT-hiPSC wells continued to beat after treatment with 100nM of nifedipine (Figure 5.14). In all hiPSC-CMs TRise, TDecay, amplitude and TOT were assessed after treatment with 50, 100 and 1000nM of nifedipine. In ReBl-PAT-hiPSC-CMs and CP1-hiPSC-CMs TRise was significantly reduced at 100nM. In CP1-WT-hiPSC-CMs TRise was significantly reduced at 50nM.

Having established the response of this hiPSC-CMs panel to LTCC block, the second task was to assess whether there were any differences between CP1-hiPSC-CMs and CP1-WT-hiPSC-CMs in the magnitude of the responses. The percentage change in each parameter was assessed across the hiPSC-CM panel tested to establish if the magnitude of responses varied between cell lines (Figure 5.15). To assess if a significantly different effect was observed unpaired t tests were undertaken. In all cases n=5.

The effect of nifedipine on TRise was significantly smaller between CP1 compared to CP1-WT at 50nM and 100nM. There was a significantly smaller change in amplitude observed in CP1 than CP1-WT at: 50nM and 100nM. There was also a significant difference in the magnitude of effect on TOT between CP1 and CP1-WT at 100nM of nifedipine exposure.

Table 5-4 - Effect of nifedipine on calcium handling mechanics

	Condition	Trise (ms)	SD	% Change	Tdecay (ms)	SD	% Change	Amplitude (au)	SD	% Change	TOT (ms)	SD	% Change
R-PAT	Basal	348.21	18.13		419.92	112.44		0.20	0.12		1294.08	418.62	
	50nM	325.28	21.07	-6.59	487.74	191.74	16.15	0.14	0.09	-28.56	1474.10	382.01	13.91
	100nM	303.04	24.28	-12.97	342.24	105.87	-18.50	0.10	0.07	-51.31	1408.12	695.54	8.81
	1uM	0.00	0.00	-100.00	0.00	0.00	-100.00	0.00	0.00	-100.00	0.00	0.00	-100.00
CP1	Basal	371.80	22.92		492.80	80.85		0.15	0.12		1748.47	320.23	
	50nM	349.28	8.97	-6.06	510.86	121.50	3.67	0.18	0.12	23.63	1558.56	244.08	-10.86
	100nM	317.16	46.82	-14.70	462.28	159.63	-6.19	0.08	0.09	-45.41	2443.16	1855.47	39.73
	1uM	0.00	0.00	-100.00	0.00	0.00	-100.00	0.00	0.00	-100.00	0.00	0.00	-100.00
CP1 WT	Basal	338.33	23.35		555.11	146.89		0.10	0.10		2049.25	945.70	
	50nM	284.74	41.27	-15.84	462.94	169.74	-16.60	0.05	0.05	-51.11	2396.65	1108.33	16.95
	100nM	66.84	149.46	-80.24	95.00	212.43	-82.89	0.02	0.04	-81.64	318.80	712.86	-84.44

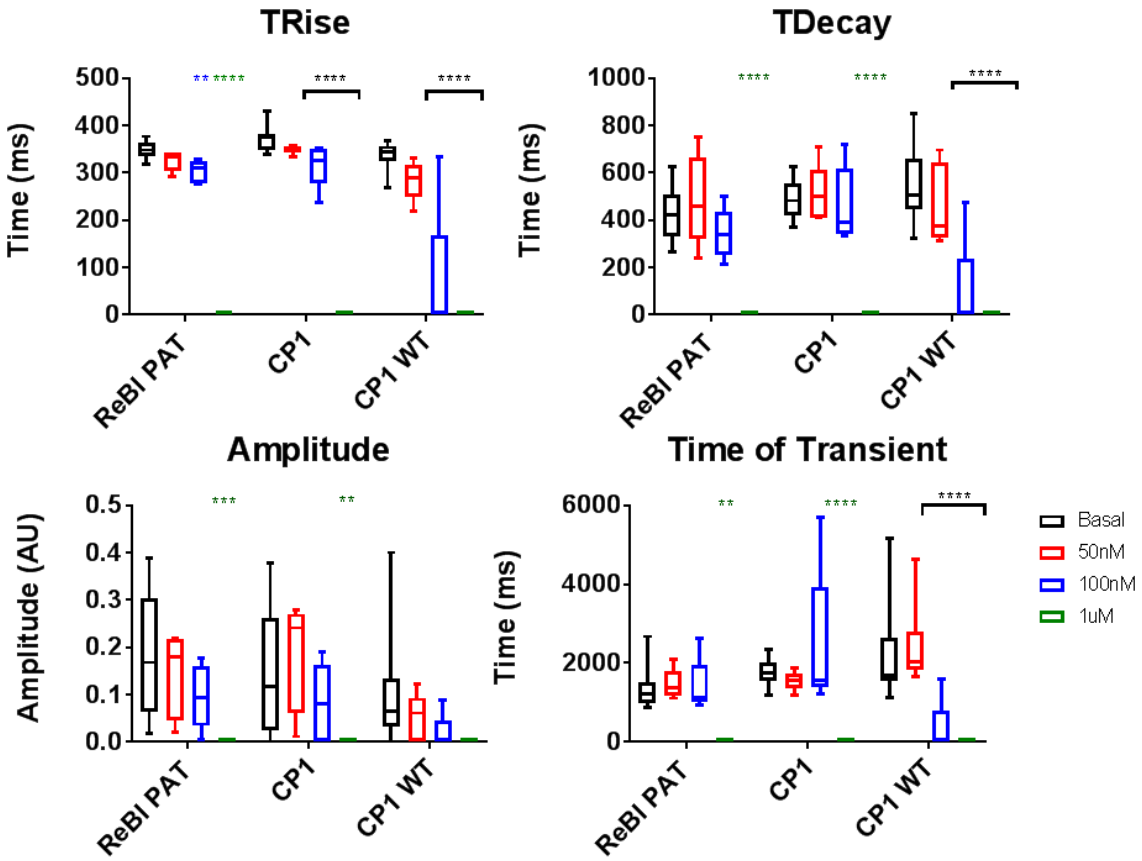


Figure 5-14 - Assessment of hiPSC-CM calcium handling response to LTCC blocker nifedipine

hiPSC-CMs were seeded into Matrigel coated 96-well plates at a density of $5x10^4$ per well to create a confluent monolayer. All hiPSC-CMs in this study were between d30-35 post differentiation. hiPSC-CMs were stained with intracellular calcium label FURA2-AM and transients were recorded on the CellOPTIQ platform. To assess changes one-way ANOVA with Dunnett's multiple comparisons test was used to compare treated hiPSC-CMs to basal hiPSC-CMs within the same cell line, n=5. All hiPSC-CMs ceased beating after the addition of 1µM nifedipine. In the case of CP1-WT-hiPSC-CMs only 1 well out of 6 remained beating after addition of 100nM of nifedipine. Statistical analysis was carried out on each parameter (TRise, TDecay, amplitude and TOT) for each hiPSC-CM line across all concentrations tested to assess if drug exposure resulted in any significant changes. TRise in ReBl-PAT-hiPSC-CMs was significantly altered at 100nM ($p<0.05$) and 1uM ($p<0.05$). TRise in CP1-hiPSC-CMs was significantly altered at 100nM ($p<0.05$) and 1uM ($p<0.05$). TRise in CP1-WT-hiPSC-CMs was significantly altered at 50nM ($p<0.05$), 100nM ($p<0.05$) and 1uM ($p<0.05$). TDecay in ReBl-PAT-hiPSC-CMs, CP1-hiPSC-CMs and CP1-WT-hiPSC-CMs was significantly altered at 1uM ($p<0.05$) or 100nM ($p=0.37$). Amplitude in ReBl-PAT-hiPSC-CMs, CP1-hiPSC-CMs and CP1-WT-hiPSC-CMs was significantly altered at 1uM ($p<0.05$). TOT in ReBl-PAT-hiPSC-CMs, CP1-hiPSC-CMs and CP1-WT-hiPSC-CMs was significantly reduced at 1uM ($p<0.05$). Stars denote significance in the change between basal and treated levels within the same hiPSC-CM line.

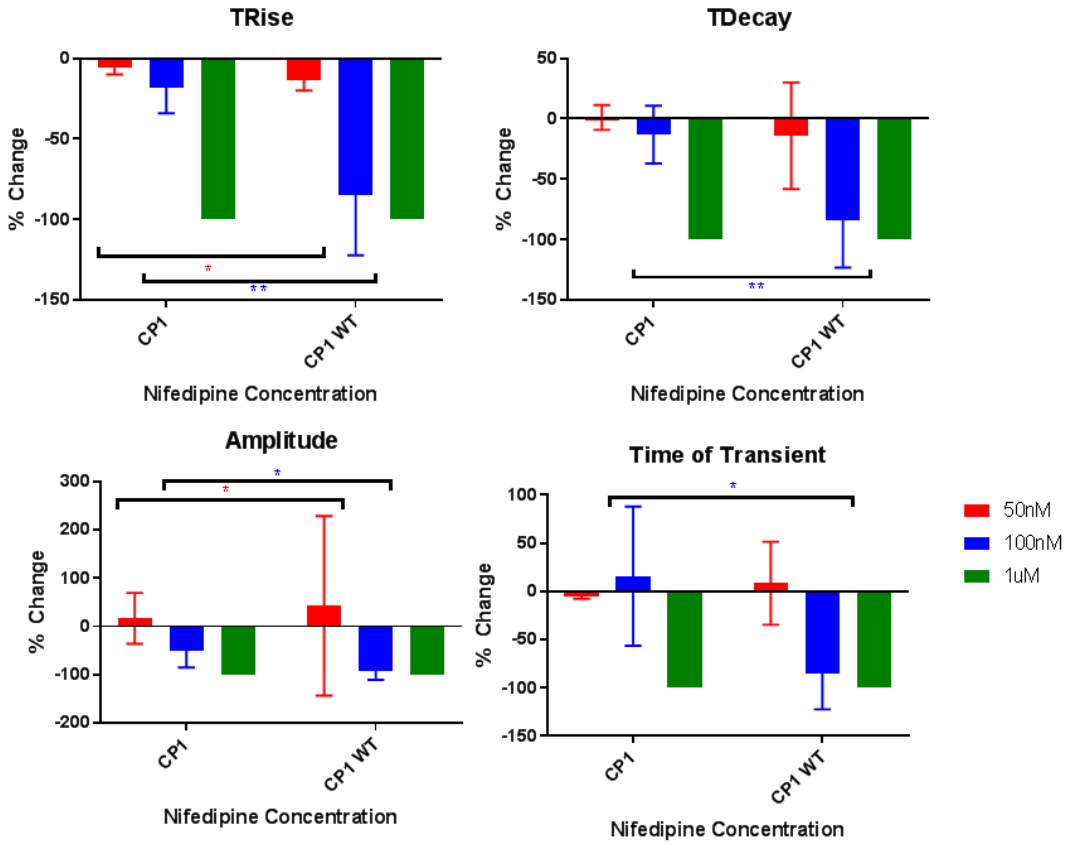


Figure 5-15 - % change in calcium handling parameters between CP1-hiPSC-CMs and CP1-WT-hiPSC-CMs in response to different doses of nifedipine

hiPSC-CMs were seeded into Matrigel coated 96-well plates at a density of $5x10^4$ per well to create a confluent monolayer. All hiPSC-CMs in this study were between d30-35 post differentiation. hiPSC-CMs were stained with intracellular calcium label FURA2-AM and transients were recorded on the CellOPTIQ platform. Calcium transients were completely abolished in both CP1- and CP1-WT-hiPSC-CMs at 1uM. In CP1-WT-hiPSC-CMs 5 of the 6 wells tested in this thesis abolished calcium transients at 100nM of nifedipine. The effect of nifedipine on TRise was significantly different between CP1 and CP1-WT at 50nM (-5.8±4.12% vs -14±5.9%, $p<0.05$, n=5, unpaired t-test) and 100nM (-18.56±15.51% vs -84.69±37.51%, $p<0.05$, n=5, unpaired t-test). The observed difference in magnitude of the effect on amplitude of 50nM (16.76±52.61% vs 42.43±185.5%, $p<0.05$, n=5, unpaired t-test) and 100nM (-50.69±34.1% vs -93.04±17.05%, $p<0.05$, n=5, unpaired t-test) was significant between CP1 and CP1-WT. There was a significant difference in the magnitude of effect on TOT between CP1 and CP1-WT at 100nM of nifedipine exposure (15.83±2.58% vs -84.69±37.5% $p<0.05$, n=5, unpaired t-test). Comparisons within these graphs relate to differences in % change between each cell line when exposed to same concentration of drug.

5.2.8 Assessment of RYR2 blockade in healthy-hiPSC-CMs and CPVT-hiPSC-CMs

Calcium release from the SR is mediated by activation of the RYR by an influx of Ca^{2+} ions through the LTCC (Yamakage et al, 2002; Itzhaki et al, 2011). In CPVT the RYR 'leaks' Ca^{2+} ions into the cytosol of the cell, when excessive Ca^{2+} accumulates here the cell inappropriately attempts to contract (Roux-Buisson et al, 2012). In this study it was decided to block the RYR with the known blocker ryanodine, which is known to activate the receptor at nanomolar concentrations (Buck et al, 1992). In this thesis therefore, concentrations in the range of 10µM-20µM were used, high enough to block the receptor (Lindsay et al, 1994) and to assess the effect on calcium handling behaviour.

hiPSC-CMs were seeded into a 96-well plate at a density of $5x10^4$. These hiPSC-CMs were stained with the intracellular labelling dye Fura2-AM and basal recordings were taken using the CellOPTIQ system. Ryanodine was added at 10, 15 and 20µM and incubated on the cells for 30 minutes. After this incubation a second recording was taken. To assess changes one-way ANOVA with Dunnett's multiple comparisons test was used to compare treated hiPSC-CMs to basal hiPSC-CMs within the same cell line, n=6 (Figure 5.16).

In ReBl-PAT-hiPSC-CMs TDecay was significantly increased at 10µM, 15µM and 20µM. TOT was significantly increased at 10µM, 15µM and 20µM. In CP1-WT-hiPSC-CMs TDecay was significantly increased at 10µM, 15µM and 20µM.

Having established the response our hiPSC-CMs panel to RYR2 blockade the second challenge was to assess whether the magnitude of response was different between CP1-hiPSC-CMs and CP1-WT-hiPSC-CMs (Figure 5.17). To assess if a significantly different effect was observed unpaired t tests were undertaken. In all cases n=6.

Exposure to ryanodine resulted in an effect of a significantly different magnitude on TRise between CP1 and CP1-WT at 15µM and 20µM. Exposure to ryanodine resulted in an effect of significantly different magnitude on TDecay between CP1 and CP1-WT at 10µM and 15µM. There was found to be a significantly larger effect on amplitude on CP1-WT than CP1 when exposed to 10µM of ryanodine.

These data indicate that there are variable responses to RYR2 blockade between CP1-hiPSC-CMs and CP1-WT-hiPSC-CMs.

Table 5-5 - Effect of ryanodine on calcium handling mechanics

	Condition	Trise (ms)	SD	% Change	Tdecay (ms)	SD	% Change	Amplitude (au)	SD	% Change	TOT (ms)	SD	% Change
R-PAT	Basal	354.57	24.96		536.00	136.38		0.24	0.10		1445.53	294.43	
	10uM	343.55	16.15	-3.11	725.67	71.69	35.39	0.22	0.12	-6.85	2157.62	418.01	3.89
	15uM	338.22	19.71	-4.61	746.03	42.88	39.19	0.15	0.06	-37.39	2192.86	374.83	51.70
	20uM	345.95	16.81	-2.43	743.35	20.27	38.68	0.21	0.08	-14.30	1959.02	337.44	35.52
CP1	Basal	359.44	21.11		504.77	120.95		0.26	0.09		1501.75	242.60	
	10uM	377.83	17.74	5.12	580.58	109.30	15.02	0.20	0.09	-21.67	1926.42	578.46	28.28
	15uM	379.88	12.29	5.69	603.50	26.65	19.56	0.20	0.06	-21.11	1902.42	195.20	26.68
	20uM	377.12	8.81	4.92	567.62	63.97	12.45	0.18	0.06	-32.11	1834.37	309.90	22.15
CP1 WT	Basal	333.72	16.52		477.89	97.50		0.08	0.06		1915.21	679.53	
	10uM	333.98	7.97	0.08	757.33	94.71	58.48	0.06	0.04	-28.32	2037.37	472.39	6.38
	15uM	302.67	16.38	-9.30	676.82	126.18	41.63	0.04	0.03	-56.89	2252.20	322.54	17.60
	20uM	309.28	27.43	-7.32	699.08	121.94	46.29	0.06	0.03	-33.96	2054.98	424.48	7.30

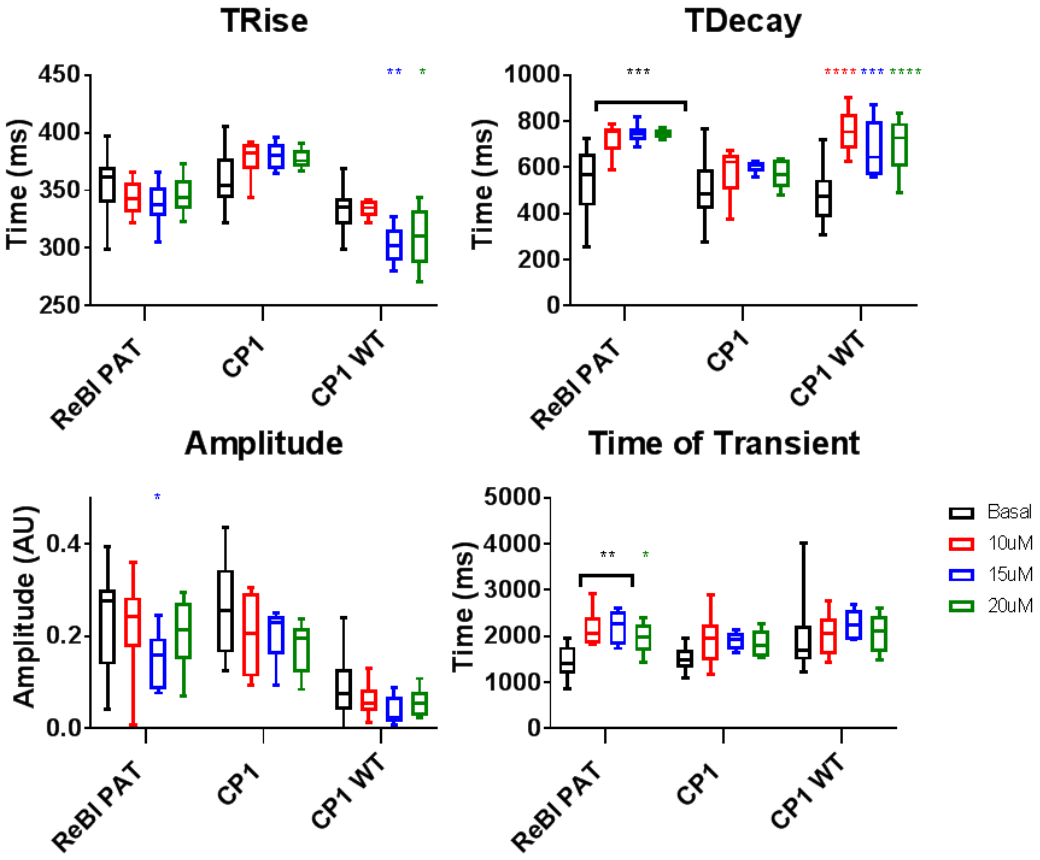


Figure 5-16 - Assessment of hiPSC-CM calcium handling response to RYR2 blocker ryanodine

hiPSC-CMs were seeded into Matrigel coated 96-well plates at a density of $5x10^4$ per well to create a confluent monolayer. All hiPSC-CMs in this study were between d30-35 post differentiation. hiPSC-CMs were stained with intracellular calcium label FURA2-AM and transients were recorded on the CellOPTIQ platform. Statistical analysis was carried out on each parameter (TRise, TDecay, amplitude and TOT) for each hiPSC-CM line across all concentrations tested to assess if drug exposure resulted in any significant changes. To assess changes one-way ANOVA with Dunnett's multiple comparisons test was used to compare treated hiPSC-CMs to basal hiPSC-CMs within the same cell line, n=6. TRise of CP1-WT-hiPSC-CMs was significantly reduced at 15µM ($p<0.05$) and 20µM ($p<0.05$). TDecay of ReBI-PAT-hiPSC-CMs was significantly increased at 10µM ($p<0.05$), 15µM ($p<0.05$) and 20µM ($p<0.05$). TDecay of CP1-WT-hiPSC-CMs was significantly increased at 10µM ($p<0.05$), 15µM ($p<0.05$) and 20µM ($p<0.05$). Amplitude of ReBI-PAT-hiPSC-CMs was significantly decreased at 15µM ($p<0.05$). TOT of ReBI-PAT-hiPSC-CMs was significantly increased at 10µM ($p<0.05$), 15µM ($p<0.05$) and 20µM ($p<0.05$). Stars denote significance in the change between basal and treated levels within the same hiPSC-CM line.

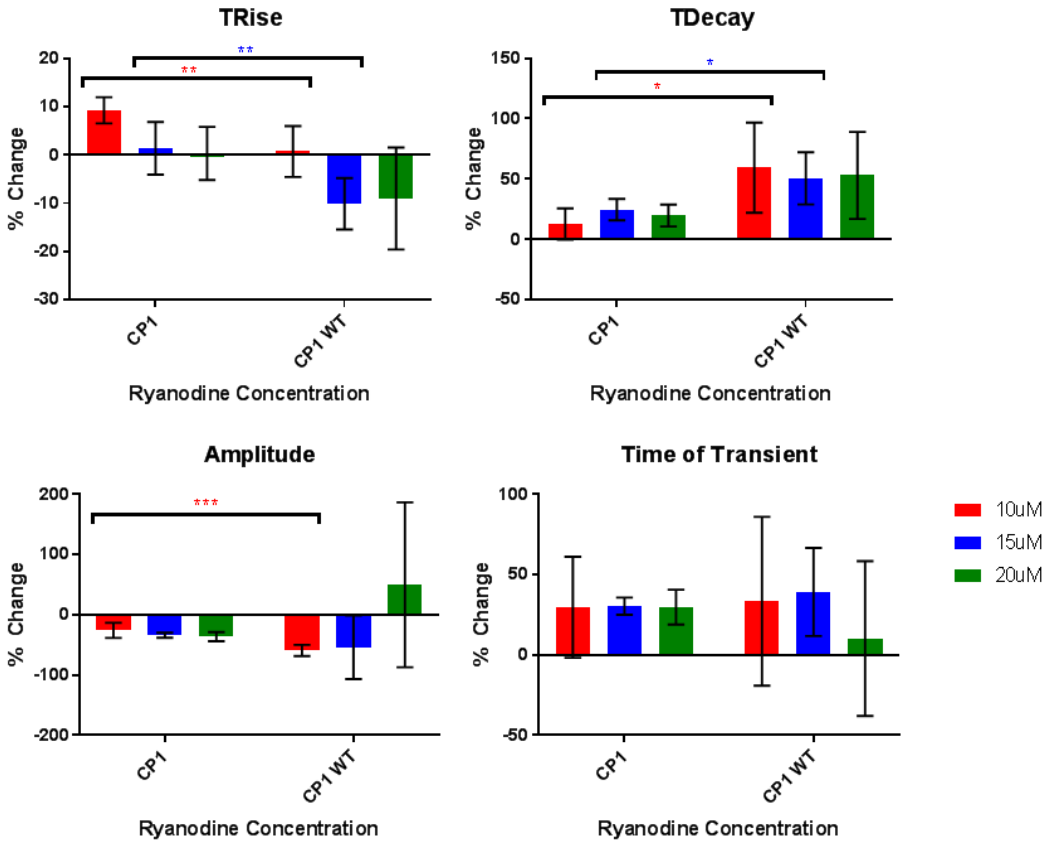


Figure 5-17 - % change in calcium handling parameters across hiPSC-CM panel in response to different doses of ryanodine

hiPSC-CMs were seeded into Matrigel coated 96-well plates at a density of $5x10^4$ per well to create a confluent monolayer. All hiPSC-CMs in this study were between d30-35 post differentiation. hiPSC-CMs were stained with intracellular calcium label FURA2-AM and transients were recorded on the CellOPTIQ platform. Statistical analysis was carried out to assess if there were any significant differences in the magnitude of response of TRise, TDecay, amplitude or TOT between CP1 and CP1-WT. Exposure to ryanodine resulted in a significantly different magnitude of effect on TRise between CP1 and CP1-WT at 15uM (1.39±5.4% vs -10.11±5.34%, $p<0.05$, n=5, unpaired t-test) and 20uM (0.31±5.5 vs -9.03±10.53%, $p<0.05$, n=6, unpaired t-test). Exposure to ryanodine resulted in a significantly different magnitude of effect on TDecay between CP1 and CP1-WT at 10uM (12.85±12.97% vs 59.37±37.32%, $p<0.05$, n=5, unpaired t-test) and 15uM (24.75±8.88% vs 50.66±21.51%, $p<0.05$, n=5, unpaired t-test). There was found to be a significantly larger effect on amplitude on CP1-WT than CP1 when exposed to 10uM of ryanodine (-25.62±12.49 vs -59.02±9.26%, $p<0.05$, n=5, unpaired t-test). Comparisons within these graphs relate to differences in % change between each cell line when exposed to same concentration of drug.

5.2.9 Assessment of SERCA blockade in healthy-hiPSC-CMs and CPVT-hiPSC-CMs

One of the key processes during EC coupling is removal of calcium ions from the cytosol of the cardiac myocyte after contraction (Bassani et al, 1994; Shigekawa and Iwamoto, 2001). This is achieved primarily through two mechanisms, the NCX which accounts for around 30% of Ca^{2+} removal and SERCA which accounts for 70% of Ca^{2+} removal (Bassani et al, 1994; Shigekawa and Iwamoto, 2001). In CPVT there is excessive leakage from the SR which results in Ca^{2+} accumulation in the cytosol (Roux-Buisson et al, 2012). Therefore blockade of the SERCA pump may have a differential effect in CPVT-hiPSC-CMs as compared to healthy controls.

To investigate this hiPSC-CMs were seeded into a 96-well plate at a density of $5x10^4$ per well. These hiPSC-CMs were stained with the intracellular labelling dye Fura2-AM and basal recordings were taken using the CellOPTIQ system. Thapsigargin was added at 10µM, 15µM and 20µM and incubated on the cells for 30 minutes. After this incubation a second recording was taken. To assess changes one-way ANOVA with Dunnett's multiple comparisons test was used to compare treated hiPSC-CMs to basal hiPSC-CMs within the same cell line, n=6 (Figure 5.18).

In ReBl-PAT-hiPSC-CMs the increase in TRise was found to be significant at 15µM and 20µM. TDecay was significantly increased at 10µM, 15µM and 20µM. Amplitude was significantly reduced at 15µM and 20µM. TOT was significantly increased at 10µM, 15µM and 20µM. In CP1-hiPSC-CMs amplitude was significantly increased at 15µM. TOT was significantly increased at 20µM. In CP1-WT-hiPSC-CMs TDecay was significantly increased at 10µM, 15µM and 20µM. TOT was significantly increased at 20µM.

Having established the response of the hiPSC-CMs panel to SERCA block the next question was to assess whether the magnitude of response was different between CP1-hiPSC-CMs and CP1-WT-hiPSC-CMs (Figure 5.19). To assess if a significantly different effect was observed unpaired t tests were undertaken. In all cases n=6. A significantly smaller response was observed in TDecay of CP1 when compared with CP1-WT when exposed to 15uM and 20uM of thapsigargin.

Table 5-6 - Effect of thapsigargin on calcium hanlding mechanics

	Condition	Trise (ms)	SD	% Change	Tdecay (ms)	SD	% Change	Amplitude (au)	SD	% Change	TOT (ms)	SD	% Change
R-PAT	Basal	355.01	10.48		501.35	85.99		0.29	0.07		1453.11	218.41	
	10uM	338.95	12.92	-4.52	674.25	90.57	34.49	0.25	0.08	-12.76	2151.88	422.98	-12.56
	15uM	332.97	7.22	-6.21	683.45	106.60	36.32	0.18	0.05	-39.95	1878.47	698.22	29.27
	20uM	326.40	17.72	-8.06	722.73	99.87	44.16	0.16	0.05	-44.88	2135.90	284.25	46.99
CP1	Basal	363.00	18.19		420.08	51.43		0.19	0.07		1270.66	186.12	
	10uM	375.84	19.96	3.54	496.64	75.66	18.23	0.23	0.21	20.03	1448.47	264.92	13.99
	15uM	366.57	24.39	0.98	475.97	80.07	13.30	0.29	0.16	50.15	1561.00	312.60	22.85
	20uM	362.73	14.40	-0.07	464.15	51.02	10.49	0.26	0.14	36.29	1720.97	662.84	35.44
CP1 WT	Basal	332.54	14.66		501.46	117.86		0.09	0.06		1784.39	432.18	
	10uM	339.32	18.13	2.04	670.97	82.41	33.80	0.05	0.02	-40.67	2375.76	405.04	33.14
	15uM	340.60	10.80	2.42	691.44	18.23	37.88	0.07	0.08	-22.02	1989.74	483.16	11.51
	20uM	344.08	10.79	3.47	636.02	41.92	26.83	0.06	0.05	-26.32	2542.70	359.01	42.50

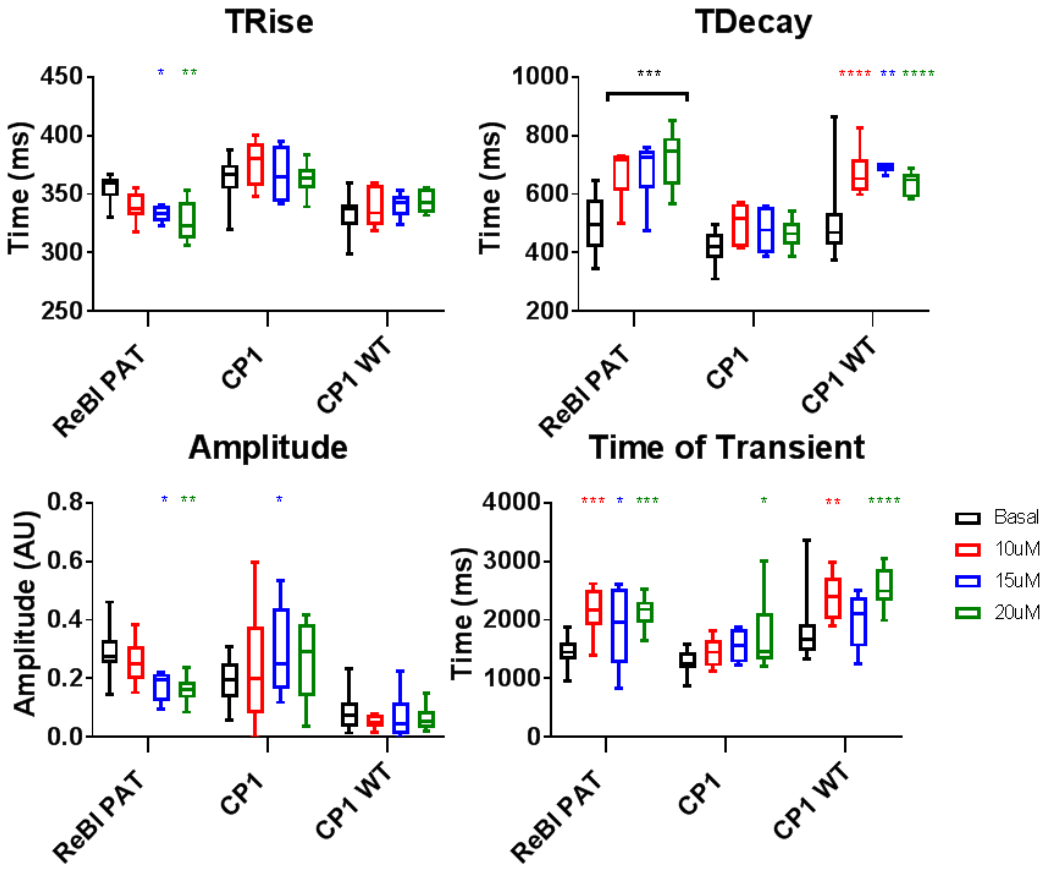


Figure 5-18 - Assessment of hiPSC-CM calcium handling response to SERCA blocker thapsigargin

hiPSC-CMs were seeded into Matrigel coated 96-well plates at a density of $5x10^4$ per well to create a confluent monolayer. All hiPSC-CMs in this study were between d30-35 post differentiation. hiPSC-CMs were stained with intracellular calcium label FURA2-AM and transients were recorded on the CellOPTIQ platform. Statistical analysis was carried out on each parameter (TRise, TDecay, amplitude and TOT) for each hiPSC-CM line across all concentrations tested to assess if drug exposure resulted in any significant changes. To assess changes one-way ANOVA with Dunnett's multiple comparisons test was used to compare treated hiPSC-CMs to basal hiPSC-CMs within the same cell line, n=6. TRise of ReBl-PAT-hiPSC-CMs was significantly reduced at 15µM ($p<0.05$) and 20µM ($p<0.05$). TDecay of ReBl-PAT-hiPSC-CMs was significantly increased at 10µM ($p<0.05$), 15µM ($p<0.05$) and 20µM ($p<0.05$). TDecay of CP1-WT-hiPSC-CMs was significantly increased at 10µM ($p<0.05$), 15µM ($p<0.05$) and 20µM ($p<0.05$). Amplitude of ReBl-PAT-hiPSC-CMs was significantly reduced at 15µM ($p<0.05$) and 20µM ($p<0.05$). Amplitude of CP1-hiPSC-CMs was significantly increased at 15µM ($p<0.05$). TOT of ReBl-PAT-hiPSC-CMs was significantly increased at 10µM ($p<0.05$), 15µM ($p<0.05$) and 20µM ($p<0.05$). TOT of CP1-WT-hiPSC-CMs was significantly increased at 10µM ($p<0.05$) and 20µM ($p<0.05$) but not 15µM ($p=0.53$). Stars denote significance in the change between basal and treated levels within the same hiPSC-CM line.

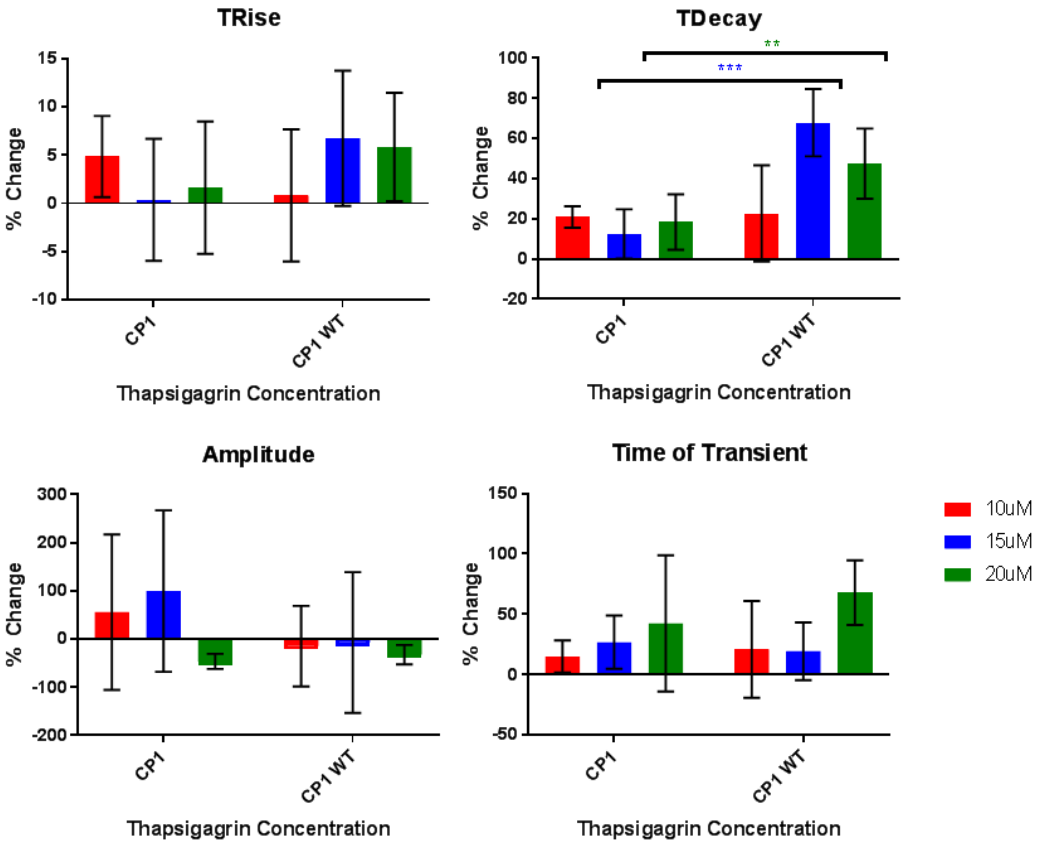


Figure 5-19 - % change in calcium handling parameters across hiPSC-CM panel in response to different doses of thapsigargin

hiPSC-CMs were seeded into Matrigel coated 96-well plates at a density of $5x10^4$ per well to create a confluent monolayer. All hiPSC-CMs in this study were between d30-35 post differentiation. hiPSC-CMs were stained with intracellular calcium label FURA2-AM and transients were recorded on the CellOPTIQ platform. Statistical analysis was carried out to assess if there were any significant differences in the magnitude of response of TRise, TDecay, amplitude or TOT between CP1 and CP1-WT after exposure to thapsigargin. A significantly different magnitude of response was observed in TDecay between CP1 and CP1-WT when exposed to 15uM (12.53±12.56% vs 67.87±16.75%, $p<0.05$, n=5, unpaired t-test) and 20uM (18.4±13.85% vs 47.5±17.49%, $p<0.05$, n=6, unpaired t-test) of thapsigargin. No significant differences were observed in the magnitude of response in relation to TRise, amplitude or TOT. Comparisons within these graphs relate to differences in % change between each cell line when exposed to same concentration of drug.

5.2.10 Assessment of NCX blockade in healthy-hiPSC-CMs and CPVT-hiPSC-CMs

One of the key processes during EC coupling is the removal of calcium ions from the cytosol of the cardiac myocyte after contraction (Roux-Buisson et al, 2012). This is achieved primarily through two mechanisms: the NCX which accounts for around 30% of Ca^{2+} removal and SERCA, which accounts for 70% of Ca^{2+} removal (Bassani et al, 1994; Shigekawa and Iwamoto, 2001). In CPVT there is excessive leakage from the SR which results in Ca^{2+} accumulation in the cytosol (Roux-Buisson et al, 2012). Therefore blocking the NCX pump may have a differential effect in CPVT-hiPSC-CMs when compared to healthy controls.

To investigate this hiPSC-CMs were seeded into a 96-well plate at a density of $5x10^4$ per well. These hiPSC-CMs were stained with the intracellular labelling dye Fura2-AM and basal recordings were taken using the CellOPTIQ system. ORM-10103 (ORM) was added at 10µM, 15µM and 20µM and incubated on the cells for 30 minutes. After this incubation a second recording was taken. To assess changes one-way ANOVA with Dunnett's multiple comparisons test was used to compare treated hiPSC-CMs to basal hiPSC-CMs within the same cell line, n=6 (Figure 5.20).

In ReBl-PAT-hiPSC-CMs TRise was significantly decreased at 15µM and 20µM. TDecay significantly decreased at 15µM and 20µM. Amplitude also significantly decreased at 15µM and 20µM. TOT significantly decreased at 20µM. In CP1-hiPSC-CMs TRise was significantly decreased at 10µM, 15µM and 20µM. However in CP1-WT-hiPSC-CMs, TOT was significantly increased at 10µM.

Having established the response of the hiPSC-CMs panel to the NCX block, the follow up question was to assess whether the magnitude of response was different between CP1-hiPSC-CMs and CP1-WT-hiPSC-CMs (Figure 5.21). To assess if a significantly different effect was observed unpaired t tests were undertaken. In all cases n=6 There was difference which was found to be significant in the magnitude of response between CP1-hiPSC-CMs and CP1-WT-hiPSC-CMs with regard to TRise when exposed to 15uM of ORM10103. The TOT of CP1-WT was found to exhibit a significantly different magnitude of response when exposed to 10uM and 15uM of ORM10103.

Table 5-7 - Effect of ORM on calcium handling mechanics

	Condition	Trise (ms)	SD	% Change	Tdecay (ms)	SD	% Change	Amplitude (au)	SD	% Change	TOT (ms)	SD	% Change
R-PAT	Basal	327.88	15.73		349.63	53.79		0.22	0.10		1076.03	127.49	
	10uM	316.10	21.04	-3.59	322.95	77.35	-7.63	0.17	0.11	-21.79	1015.17	153.89	29.42
	15uM	294.78	24.46	-10.09	215.04	36.56	-38.49	0.08	0.05	-63.56	793.38	57.78	-26.27
	20uM	303.32	18.77	-7.49	194.45	32.67	-44.38	0.04	0.03	-83.18	777.62	46.50	-27.73
CP1	Basal	367.75	18.98		455.98	69.01		0.47	0.18		1392.57	233.01	
	10uM	336.28	31.93	-8.56	386.67	80.10	-15.20	0.47	0.15	-0.74	1189.73	179.43	-14.57
	15uM	341.98	18.53	-7.01	419.72	90.86	-7.95	0.44	0.20	-6.12	1233.43	256.55	-11.43
	20uM	331.12	6.68	-9.96	376.42	47.93	-17.45	0.52	0.15	10.36	1148.08	95.56	-17.56
CP1 WT	Basal	338.18	9.75		501.41	101.60		0.11	0.06		1630.73	235.88	
	10uM	332.15	12.77	-1.78	529.17	171.73	5.54	0.07	0.04	-41.70	2173.83	733.65	33.30
	15uM	346.25	24.77	2.39	523.07	80.25	4.32	0.06	0.04	-45.12	1632.43	253.22	0.10
	20uM	320.20	25.59	-5.32	455.18	69.69	-9.22	0.06	0.03	-47.43	1725.20	352.41	5.79

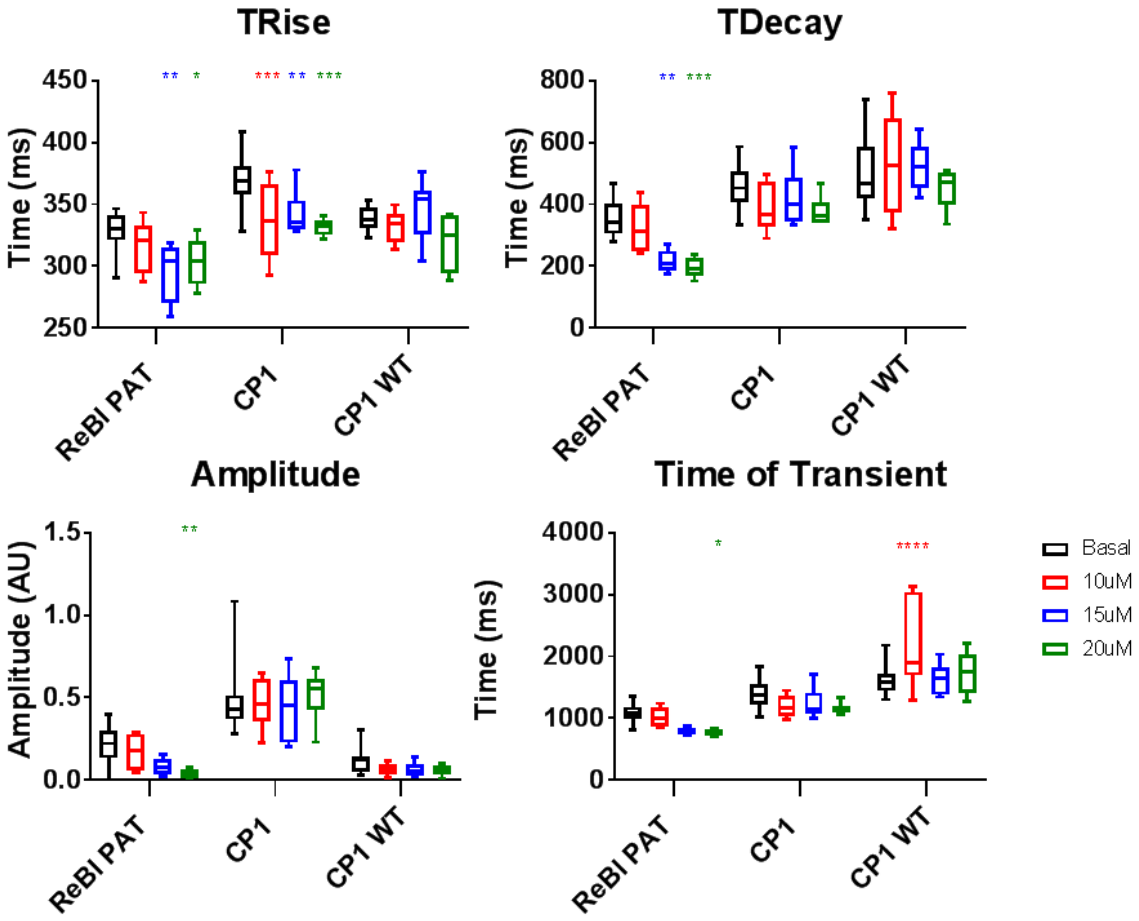


Figure 5-20 - Assessment of hiPSC-CM calcium handling response to NCX blocker ORM10103

hiPSC-CMs were seeded into Matrigel coated 96-well plates at a density of $5x10^4$ per well to create a confluent monolayer. All hiPSC-CMs in this study were between d30-35 post differentiation. hiPSC-CMs were stained with intracellular calcium label FURA2-AM and transients were recorded on the CellOPTIQ platform. Statistical analysis was carried out on each parameter (TRise, TDecay, amplitude and TOT) for each hiPSC-CM line across all concentrations tested to assess if drug exposure resulted in any significant changes. To assess changes one-way ANOVA with Dunnett's multiple comparisons test was used to compare treated hiPSC-CMs to basal hiPSC-CMs within the same cell line, n=6. TRise of ReBl-PAT-hiPSC-CMs was significantly decreased at 15µM ($p<0.05$) and 20µM ($p<0.05$). TRise of CP1-hiPSC-CMs was significantly decreased at 10µM ($p<0.05$), 15µM ($p<0.05$) and 20µM ($p<0.05$). TDecay of ReBl-PAT-hiPSC-CMs was significantly decreased at 15µM ($p<0.05$) and 20µM ($p<0.05$). Amplitude of ReBl-PAT-hiPSC-CMs was significantly decreased at 15µM ($p<0.05$) and 20µM ($p<0.05$). TOT of ReBl-PAT-hiPSC-CMs was significantly decreased at 20µM ($p<0.05$). TOT of CP1-WT-hiPSC-CMs was significantly increased at 10µM ($p<0.05$). Stars denote significance in the change between basal and treated levels within the same hiPSC-CM line.

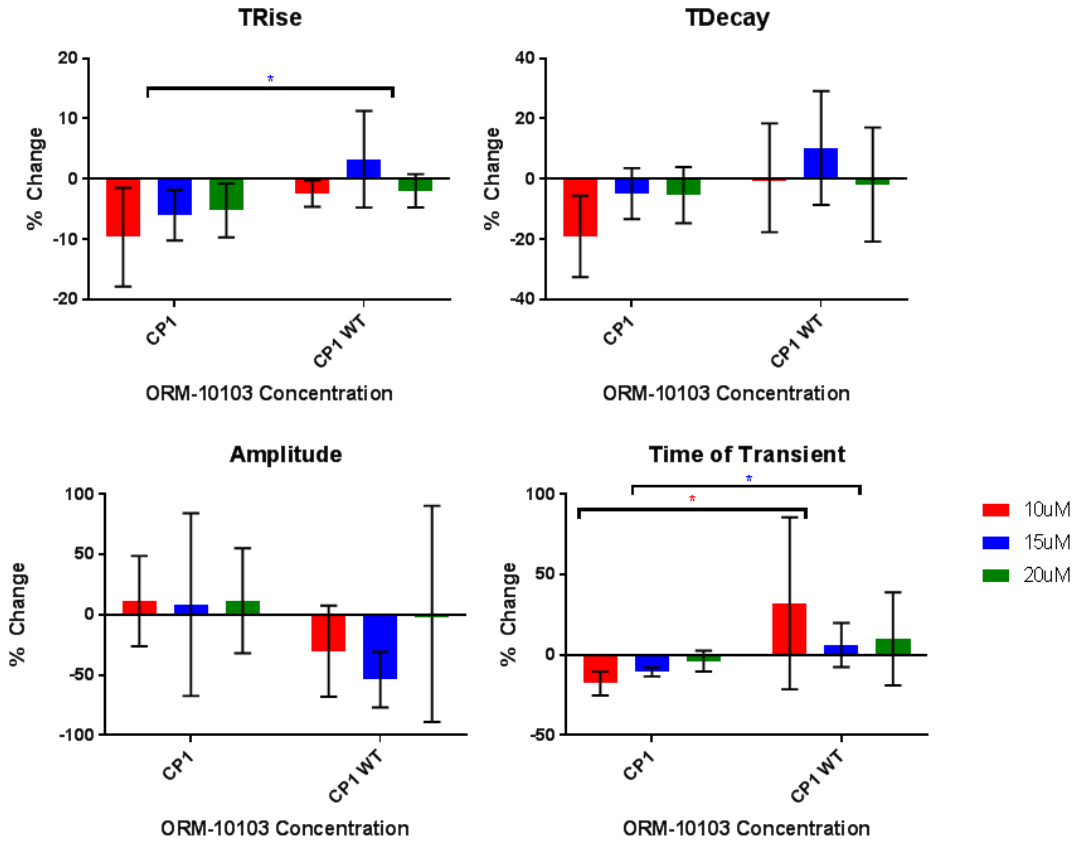


Figure 5-21 - change in calcium handling parameters across hiPSC-CM panel in response to different doses of ORM10103

hiPSC-CMs were seeded into Matrigel coated 96-well plates at a density of $5x10^4$ per well to create a confluent monolayer. All hiPSC-CMs in this study were between d30-35 post differentiation. hiPSC-CMs were stained with intracellular calcium label FURA2-AM and transients were recorded on the CellOPTIQ platform. Statistical analysis was carried out to assess if there were any significant differences in the magnitude of response of TRise, TDecay, amplitude or TOT between CP1 and CP1-WT after exposure to ORM10103. There was found to be a significant difference in the magnitude of response between CP1-hiPSC-CMs and CP1-WT-hiPSC-CMs with regard to TRise when exposed to 15uM of ORM10103 (-6±8.16% vs 3.29±8%, $p<0.05$, n=6, unpaired t-test). The TOT of CP1-WT was found to be exhibit a significantly different magnitude of response when exposed to 10uM (-17.7±7.42% vs 32.22±53.52%, $p<0.05$, n=6, unpaired t-test) and 15uM of ORM10103 (-10.47±2.79% vs 6.31±13.69%, $p<0.05$, n=6, unpaired t-test).

5.2.11 Assessment of IP3R blockade in healthy-hiPSC-CMs and CPVT-hiPSC-CMs

The role of IP3 in the cardiac myocytes handling of calcium remains controversial. It has been postulated that this secondary messenger is more functional in the fetal heart and its role is taken over by RYR in the adult heart (Rosemblit et al, 1999). Given that hiPSC-CMs are more likely to display a fetal like phenotype rather than an adult one it was prudent to assess the response of the calcium transit to IP3R blockade using 5μM xestospognin C, a known blocker of these receptors (Oka et al, 2002).

To investigate this hiPSC-CMs were seeded into a 96-well plate at a density of $5x10^4$ per well. These hiPSC-CMs were then stained with the intracellular labelling dye Fura2-AM and basal recordings taken using the CellOPTIQ system. xestospongin C was added at increasing concentrations and incubated on the cells for 30 minutes. After this incubation a second recording was taken. To assess changes one-way ANOVA with Dunnett's multiple comparisons test was used to compare treated hiPSC-CMs to basal hiPSC-CMs within the same cell line, n=6 (Figure 5.22).

Across all three cell lines no significant changes were observed in TRise, TDecay, amplitude or TOT when exposed to 5μM of xestospongin C.

Having established the response our hiPSC-CMs panel to IP3R block, the next question was then to assess whether the magnitude of response was different between CP1-hiPSC-CMs and CP1-WT-hiPSC-CMs (Figure 5.23). To assess if a significantly different effect was observed unpaired t tests were undertaken. In all cases n=6.

In all parameters tested, TRise, TDecay, amplitude and TOT, no significant differences were observed after treatment with 5μM of xestospongin C between CP1-hiPSC-CMs and CP1-WT-hiPSC-CMs.

Table 5-8 - Effect of xestospongin c on calcium handling mechanics

R-PAT	Condition	Trise (ms)	SD	% Change	Tdecay (ms)	SD	% Change	Amplitude (au)	SD	% Change	TOT (ms)	SD	% Change
	Basal	345.82	9.69		520.47	120.01		0.24	0.10		1482.80	281.86	
	5uM	340.62	5.99	-1.50	567.10	119.66	8.96	0.27	0.13	11.75	1581.60	270.81	8.17
CP1	Basal	375.37	7.92		501.75	51.21		0.30	0.11		1603.97	311.62	
	5uM	370.82	4.69	-1.21	544.77	74.33	8.57	0.26	0.10	-12.60	1864.90	257.04	16.27
CP1 WT	Basal	331.85	15.40		436.95	67.28		0.14	0.06		1486.87	176.32	
	5uM	330.55	9.99	-0.39	439.22	66.47	0.52	0.15	0.07	7.62	1417.02	225.05	-4.70

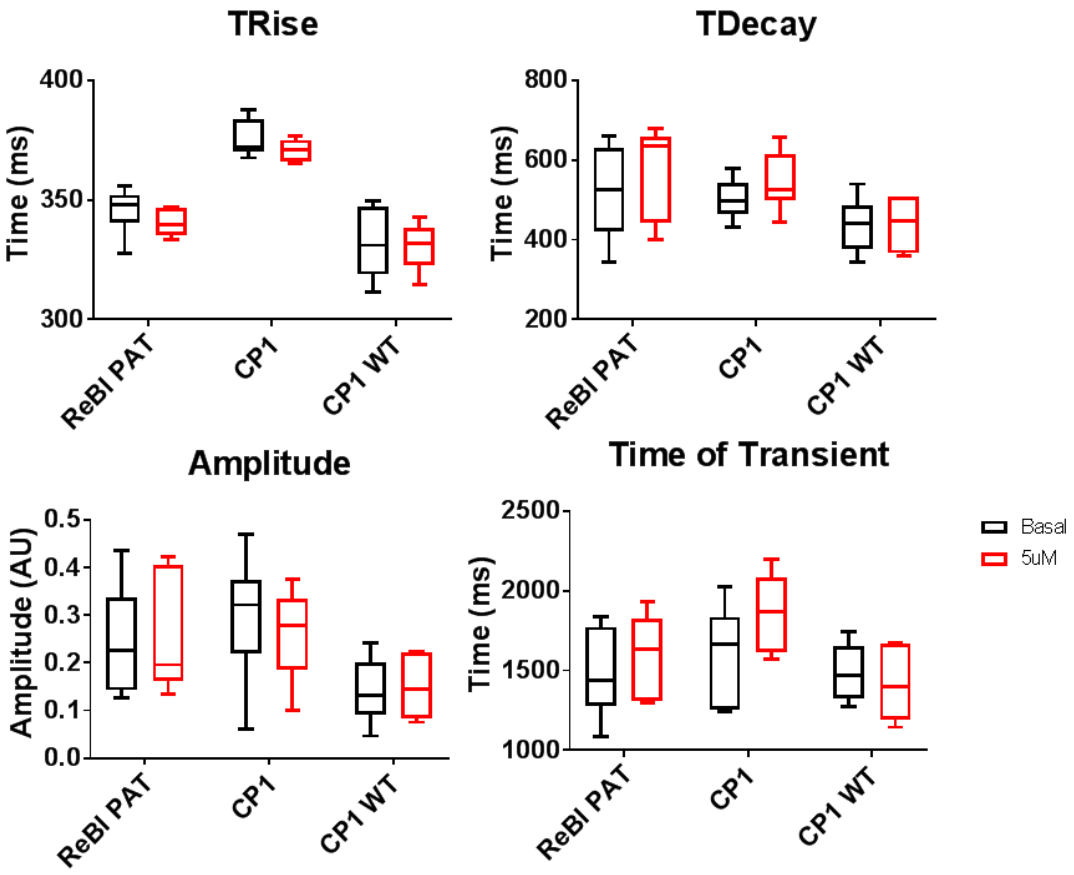


Figure 5-22 - Assessment of hiPSC-CM calcium handling response to IP3R blocker xestospongin C

hiPSC-CMs were seeded into Matrigel coated 96-well plates at a density of $5x10^4$ per well to create a confluent monolayer. All hiPSC-CMs in this study were between d30-35 post differentiation. hiPSC-CMs were stained with intracellular calcium label FURA2-AM and transients were recorded on the CellOPTIQ platform. Statistical analysis was carried out on each parameter (TRise, TDecay, amplitude and TOT) for each hiPSC-CM line across all concentrations tested to assess if drug exposure resulted in any significant changes. In this thesis no parameters were significantly altered in any of the hiPSC-CM lines tested when exposed to xestospongin C.

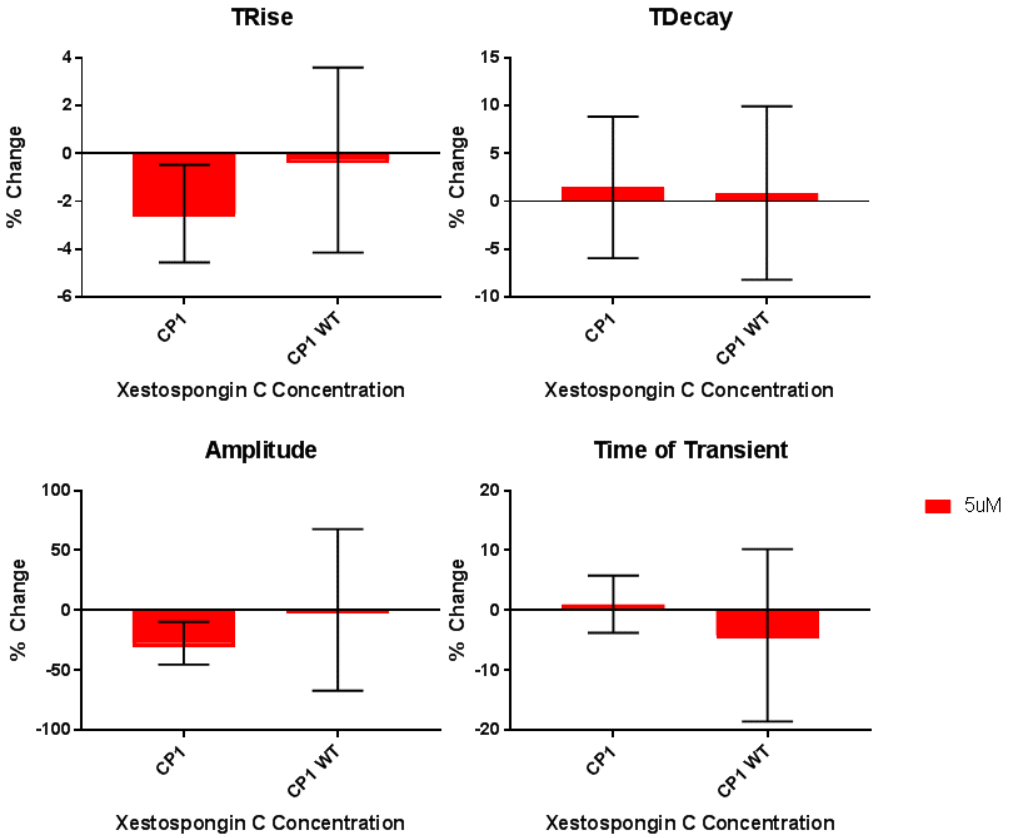


Figure 5-23 - % change in calcium handling parameters across hiPSC-CM panel in response to 5µM xestospongin C

hiPSC-CMs were seeded into Matrigel coated 96-well plates at a density of $5x10^4$ per well to create a confluent monolayer. All hiPSC-CMs in this study were between d30-35 post differentiation. hiPSC-CMs were stained with intracellular calcium label FURA2-AM and transients were recorded on the CellOPTIQ platform. Statistical analysis was carried out to assess if there were any significant differences in the magnitude of response of TRise, TDecay, amplitude or TOT between CP1 and CP1-WT after exposure to xestospongin C. There were no significant differences observed in the magnitude of response in regards to TRise, TDecay, amplitude or TOT after exposure to xestospongin C.

5.3 Discussion

Attempting to edit CP1-hiPSC using the oligonucleotide method was unsuccessful in this thesis as a result of inactive Cas9 protein from a commercial supplier. However reports in the literature have confirmed that the oligonucleotide method is able to successfully edit hiPSCs genome (Bialk et al, 2015). In future gene editing experiments it may be prudent to optimise a new protocol purchasing Cas9 protein from a more reliable supplier given the simplicity and non-integrative nature of this method. In this thesis a plasmid based method was successfully utilised to correct the T>C at base pair 6737 in exon 44 of the *RYR2* gene using a modified PiggyBac transposon system within the targeting construct in order to insert two arms of homology with the corrected sequence within them. This was then excised leaving no footprint as has previously been performed to correct the β-thalasssemia mutation in hiPSCs (Xie et al, 2014). Although the plasmid based strategy requires more time and passages than the oligonucleotide based method it could be argued it is a more robust system. This is due to the two selection steps which are not present in the oligonucleotide method. Although the oligonucleotide method requires no integration it also represents a greater chance of screening multiple negative colonies. One note to make regarding screening when using the oligonucleotide method is the importance of adding a unique restriction site. In this thesis a unique restriction site was removed, however any incomplete cutting would therefore have generated a false positive in the diagnostic digest. This should be avoided and restriction sites added instead, to give a clearer indication of success as cutting should only occur when successful targeting has occurred.

Basal characteristics of calcium handling showed that CP1-hiPSC-CMs displayed significantly shorter TRise times compared to ReBl-PAT-hiPSC-CMs and a significantly shorter TOT. This is not necessarily what was expected given that dysfunction of the *RYR2* is suggested to lead to calcium leak, however CPVT does not result in a phenotype at basal levels. Indeed recent reports suggest that length of the calcium transient is not different between healthy-hiPSC-CMs and CPVT-hiPSC-CMs (Sasaki et al, 2016). The reason for this unexpected result may lie in the cells immaturity, with underdeveloped structural properties and gene expression more typical of fetal than adult cardiomyocytes these hiPSC-CMs may behave atypically. However given that Sasaki also used hiPSC-CMs a more likely explanation would be that genetic variability between the lines is the cause of this difference (Sinnecker et al, 2014), this underlines the need for isogenic controls when analysing calcium handling properties of cells as highlighted previously (Bellin et al, 2013).

When CP1-hiPSC-CMs were compared to CP1-WT-hiPSC-CMs they displayed longer TRise, larger amplitude and shorter TOT. These changes were unexpected as CPVT does not exhibit a phenotype at basal levels (MacLennan and Zvaritch, 2011; Kim et al, 2014). CPVT-hiPSC-CMs at basal have previously been shown to exhibit aberrant events such as double peaks (Penttinen et al, 2015). In this study none were observed. A logical follow on experiment from this would be to assess the response of CP1 and CP1-WT to adrenergic stimulation, potentially by isoprenaline exposure. Time pressure in this thesis meant this was not possible. However increased basal amplitude in CP1-hiPSC-CMs over CP1-WT-hiPSC-CMs may indicate Ca^{2+} leak from the SR, potentially a manifestation of the CPVT phenotype. Although this would not be expected at basal levels it is important to note that the immature phenotype of hiPSC-CMs may result in different calcium handling properties from native adult cardiomyocytes.

The two healthy lines, CP1-WT-hiPSC-CMs and ReBl-PAT-hiPSC-CMs were assessed to determine if genetic correction returned CP1-WT-hiPSC-CMs back to a "normal" phenotype. It was observed that these hiPSC-CMs displayed significant differences in TRise, TDecay, amplitude and TOT. Given the differences observed between ReBl-PAT-hiPSC-CMs and CP1-WT-hiPSC-CMs it is likely the case that genetic variability underlies these differences (Sinnecker et al, 2014). This further underlines the importance of generating isogenic controls for disease modelling studies in relation to calcium handling. Given the unexpected results observed in these experiments repeating them across a larger panel of hiPSC lines would elucidate this further to increase the understanding of baseline calcium handling properties which often go underreported. The TRise times in this thesis of between 335.4 – 365.8ms are longer than some TRise reports in the literature of between 200-300ms (Shinnawi et al, 2015). Furthermore the TDecay times observed in this thesis at baseline levels are between 458.3-502.2ms in comparison to published TDecay times in the region of 600-800ms (Shinnawi et al, 2015). The variation between this thesis and the values reported in Shinnawi's publication may be a number of factors such as method of reprogramming or method of differentiation (Liang and Zhang, 2013) underlining a need to standardise such phenotyping assays across the field.

Table 5-9 - Overall effect of the drug on cell lines

		Nifedipine effect	Ryanodine effect	Thapsigargin effect	ORM effect	Xestospongin C effect
R-PAT	TRise	<	-	<	<	-
	TDecay	-	>	>	<	-
	Amplitude	-	-	<	<	-
	TOT	-	>	>	-	-
CP1	TRise	<	-	-	<	-
	TDecay	-	-	-	-	-
	Amplitude	-	-	-	-	-
	TOT	-	-	>	-	-
CP1-WT	TRise	<	<	-	-	-
	TDecay	-	>	>	-	-
	Amplitude	-	-	-	-	-
	TOT	-	-	>	-	-

5-24 - > indicates increase, < indicates decrease while - indicates no change

Ca^{2+} entry via LTCC is vital for the initiation of calcium transients. In the hiPSC-CM panel tested in this thesis all hiPSC-CMs stopped beating upon addition of 1000nM of nifedipine, this is consistent with reports in the literature (Itzhaki et al, 2011). Exposure to nifedipine was found to decrease the TRise time across all cells lines, this is potentially as a result of less LTCC being able to transport Ca^{2+} into the cell and thus hiPSC-CMs reach the peak of their transient sooner as they will potentially rely more heavily on Ca^{2+} from SR stores. However once the hiPSC-CM has depolarised the reuptake and extrusion machinery are unaffected and therefore operates to its standard timeframe. Intracellular Ca^{2+} may not be affected by this as previous reports have shown the SR to be a functional store of Ca^{2+} in hiPSC-CMs (Itzhaki et al, 2011). Exposure to nifedipine was not observed to cause any response in TDecay, amplitude or TOT in ReBl-

PAT-hiPSC-CMs or CP1-hiPSC-CMs until the amelioration of the transients at 1000nM. There was significant reductions in TDecay, amplitude and TOT observed in CP1-WT at 100nM although these statistics will be influenced by the 83% of wells which stopped exhibiting calcium transients at this concentration. Reports in the literature have shown nifedipine is able to reduce the TOT in hiPSC-CMs (Klimas et al, 2016). In addition to that previous reports have shown that nifedipine results in significant decreases in calcium transient amplitude (Itzhaki et al, 2011; Dempsey et al, 2016). Given the variability between the results in this thesis and the published literature it would be prudent to replicate the experiments within this thesis across a greater panel of hiPSC-CMs. However what should be pointed out is the scarcity of reports in the literature with regards to the calcium handling machinery within hiPSC-CMs and more specifically CPVT-hiPSC-CMs.

Significant differences were observed in the magnitude of response to nifedipine between CP1-hiPSC-CMs and CP1-WT-hiPSC-CMs. CP1-WT-hiPSC-CMs were found to decrease their TRise time to a greater level than CP1-hiPSC-CMs. In addition to this TDecay was decreased to a significantly greater level and as well as amplitude and TOT at 100nM of nifedipine. Although this could be a consequence of the CRISPR/Cas9 editing process described in this chapter it is important to remember that all but 1 well of the 100nM CP1-WT-hiPSC-CMs stopped beating which is likely skewing the data. This experiment should be replicated to assess whether CP1-WT-hiPSC-CMs are more sensitive to LTCC blockade than CP1-hiPSC-CMs. Theoretically this may indicate that in a CP1-hiPSC-CM with leaky RYR2 intracellular Ca^{2+} is able to compensate for the loss of Ca^{2+} through the LTCC. Having corrected the mutation this may not be the case in CP1-WT-hiPSC-CMs. To assess this more Ca^{2+} imaging experiments may be performed in addition to possible recombination studies of single receptors of both CP1 and CP1-WT RYR2.

Exposure to ryanodine resulted in a significant drop in TRise for CP1-WT, not seen in CP1. This could indicate a more prominent role for RYR in calcium release in CP1-WT. Previous reports in the literature have shown that upstroke velocity was decreased in RYR-/- in mouse ES cells indicating that without RYR2 TRise may decrease (Fu et al, 2005). TDecay of ReBl-PAT and CP1-WT was increased but no changes were seen in CP1. This may indicate a higher degree of functionality in the CP1-WT-hiPSC-CMs which is not reflected in the CP1-hiPSC-CMs. Amplitude decreased in response to ryanodine exposure but not to a statistically significant level. Reports in the literature have shown amplitude to decrease in response to 10µM ryanodine by between 5-29% in control-CMs and 23-52% in CPVT-CMs (Lee et al, 2011; Novak et al, 2015). This was dose responsive as increased doses reduced the amplitude (Itzhaki et al,

2011). The reason this was not observed in this thesis may potentially indicate that Ca^{2+} is being released through a secondary mechanism or cycled through the LTCC and NCX. In this respect the extracellular Ca^{2+} of the medium is important, in the experiments performed in this thesis extracellular calcium concentration was 1.8mM. Future experiments may wish to optimise this further and perhaps assess the relative changes in calcium transients in response to variations in extracellular Ca^{2+} content. The TOT of ReBl-PAT was increased, this was not seen in CP1 or CP1-WT. It is not clear whether blockade of the RYR would lead to increased TOT as less Ca^{2+} extruded from the SR would require less reuptake by SERCA and extrusion by NCX. A drawback of these experiments is the poorly understood cycling of calcium in these hiPSC-CMs as a result of the absence of t-tubules and therefore couplons which are vital in efficient propagation of EC coupling (Franzini-Armstrong et al, 1999; Brette et al, 2002). In this thesis caffeine was not administered in order to assess the relative levels of Ca^{2+} stored in the SR. The reason for this was due to the need to "puff" caffeine on the cell not being possible due to technical constraints of the CellOPTIQ system. However, it would be prudent in future to test the response of hiPSC-CMs to caffeine puff to assess the volume of Ca^{2+} stored in the SR as this has been achieved before (Itzhaki et al, 2011).

The variation in magnitude of response which was observed between CP1-hiPSC-CMs and CP1-WT-hiPSC-CMs with regard to TRise and TDecay at 10µM and 15µM of ryanodine indicates a differential level of functionality of the ryanodine receptor between the two hiPSC-CM lines. This may indicate that the CRISPR/Cas9 genome editing has successfully changed and potentially corrected the diseased phenotype. However to prove this will require a number of further experiments. To further assess the differential phenotype between these two hiPSC-CMs it would be prudent to assess response to β-adrenergic stimulation with isoprenaline as this has been shown to elucidate a phenotype in patient cells (MacLennan and Zvaritch, 2011; Kim et al, 2014). The second experiment would be to assess the Ca^{2+} spark frequency after incubation with µM concentrations of ryanodine as this should block the receptor, any efflux from the SR at this time may indicate calcium leak. Thirdly, it would be interesting to clone the individual receptors for single receptor analysis to assess their gating properties.

Treatment with thapsigargin to block SERCA resulted in a decrease in TRise in ReBl-PAT but not CP1 or CP1-WT. This could be considered an unexpected consequence as SERCA is predominantly involved in reuptake after the transient has peaked therefore no effect on TRise was expected. However as the hiPSC-CMs were incubated for 30 minutes this may be

an adaptive mechanism to the loss of functionality of SERCA. TDecay increased in ReBl-PAT and CP1-WT but not CP1. Blockade of SERCA should result in either defective reuptake of calcium back into the SR or the overcompensation of NCX to extrude more calcium than usual for the cell. Interestingly in this thesis the two healthy lines responded appropriately whereas CP1-hiPSC-CMs did not exhibit an effect in the TDecay time in response to SERCA blockade. Amplitude decreased in ReBl-PAT-hiPSC-CMs at 15µM and 20µM as well as in CP1-hiPSC-CMs at 15µM. However no decrease was observed in CP1-WT-hiPSC-CMs. Reports in the literature have previously suggested that 20µM of thapsigargin would lead to total amelioration of calcium transients (Itzhaki et al, 2011). Given the important role in reuptake it is possible that the hiPSC-CMs in this thesis are simply cycling Ca^{2+} through the LTCC and NCX, therefore bypassing the SR mediated Ca^{2+} stores, this is closely linked to the level of extracellular Ca^{2+} content in culture medium. In order to test this it would be interesting to block SERCA in addition to the blockade of NCX and LTTC, both separately and all three at once. This experiment would further elucidate the role each is playing in hiPSC-CM calcium cycling. TOT increased in ReBl-PAT and CP1-WT also in CP1 but only at 20µM. The increase in TOT may be an expected occurrence in response to SERCA blockade as the inability of the hiPSC-CM to extrude calcium could lead to an elongation of the transients. Although the contribution of NCX to calcium relaxation has been shown to upregulate in response to inadequate SR Ca^{2+} uptake (Piacentino et al, 2003) a potentially rate limiting step is energy availability as the NCX is driven by ATP hydrolysis (Periasamy and Kalyanasundaram, 2007).

Exposure to 15µM and 20µM of thapsigargin causes a significantly greater increase in TDecay time in CP1-WT-hiPSC-CMs than in CP1-hiPSC-CMs. This is further indication that the CRISPR/Cas9 gene editing has resulted in a change in function within calcium handling of these hiPSC-CMs, this is particularly interesting in the case of SERCA as its role is related to SR reuptake. A leaking RYR2 channel would indicate dysfunctional handling of Ca^{2+} within the SR, given the differential magnitude of response between these two lines it would be interesting to investigate this further by repeating this experiment with higher concentrations of thapsigargin to assess if CP1-hiPSC-CMs have a blunted response to SERCA blockade in comparison to CP1-WT-hiPSC-CMs.

ORM-10103 was used to block the NCX within the hiPSC-CM panel in this thesis. TRise decreased for ReBl-PAT-hiPSC-CMs and CP1-hiPSC-CMs but not CP1-WT-hiPSC-CMs. It is difficult to interpret these data as there remains a lack of research into the role of NCX in calcium influx (Kane et al, 2015). However as amplitude is decreased in ReBl-PAT-hiPSC-CMs,

this may suggest that the NCX is involved in Ca^{2+} influx early in the cardiac calcium transient. The NCX was blocked using ORM which demonstrated that TDecay decreased for ReBl-PAT-hiPSC-CMs and CP1-WT-hiPSC-CMs but not CP1-hiPSC-CMs. To test the relative role of each of these calcium extrusion mechanisms it may be interesting to assess the effect of their blockade in cells which are younger and older than those used in this study. In addition to this gene expression assays would be a good complement to such a study.

There was not much of a differential response to the effect of NCX blockade between CP1-hiPSC-CMs and CP1-WT-hiPSC-CMs. Interestingly this reflects the trend observed throughout these experiments which showed larger differential effects between mechanisms directly related to the SR, where CPVT dysfunction exists, as opposed to those indirectly involved such as LTCC, IP3 and NCX. TOT of the CP1-WT-hiPSC-CMs were found to be significantly different from CP1-hiPSC-CMs response at 10µM and 15µM but given that this effect was not maintained at 20µM a replication of this experiment may be required to fully elucidate whether this is a true result.

Administration of xestospongin C did not result in any changes to any of the hiPSC-CMs in any of the parameters tested. Previous research has indicated that blockade of IP3R has resulted in a decrease in amplitude depending on drug of up to 100% suggesting IP3 mediated calcium release is necessary for hiPSC-CMs (Itzhaki et al, 2011). Why this was not the case in this thesis may be down to a number of factors. In Itzhaki's research IP3 was not blocked with xestospongin C it was instead blocked with 2-Aminoethoxydiphenyl borate (2-APB) and the phosopholipase C inhibitor U73122. The second reason why this drug may have had no effect could be that IP3 is not responsible for any aspect of calcium handling in the hiPSC-CMs assessed in this thesis. Finally only 1 concentration of the drug was able to be tested in this thesis due to scarcity of the drug, it would be prudent in the future to repeat these experiments with a wider selection of concentrations. In addition to this alternative drugs should also be tested as there remains some dubiety about the efficacy of xestospongin C in blocking IP3R (Oka et al, 2002; Saleem et al, 2014). Potential alternatives are Aminoethoxydiphenyl borate (2-APB) and the phosopholipase C inhibitor U73122 (Itzhaki et al, 2011).

Overall in this chapter the gene editing of the CP1 hiPSC line was successfully performed using a plasmid based system. Although this is more intrusive than the simpler oligonucleotide system it is more robust as a result of its selection process. The CP1-WT-hiPSC line exhibits a clean homozygous WT G nucleotide at position 2246 in the *RYR2* gene. Furthermore

recombination sites at the left and right arms of homology show clean recombination with no indels or frameshift mutations. Furthermore there was clean recombination at the TTAA site. With respect to the analysis of the hiPSC-CMs calcium handling machinery this chapter reports interesting but preliminary data. The hiPSC-CMs in this thesis responded appropriately to the known LTCC blocker nifedipine, providing confidence in the assay and the hiPSC-CMs. However blockade with ryanodine did not result in the decreased amplitude shown in other reports in the literature. In addition to this the overall variable response in much of this calcium transient analysis raises many questions. The next step in this analysis should be to plot each individual data point to assess whether there is a clustering of hiPSC-CMs within certain parameters while others would be considered "outliers" potentially identifying sub-populations within the larger population. Such analysis would be vital in investigating whether the behaviour with respect to calcium handling properties of hiPSC-CMs is widely variable or if a more representative mean population is present alongside outlying hiPSC-CMs. Should this prove to be the case it may be beneficial in future to assess hiPSC-CMs within a tighter window to ensure the hiPSC-CMs analysed are more representative of the mean population and to avoid outliers skewing data.

6 General Discussion

The emergence of hiPSC technology has provided the research community with a powerful tool to study disease progression in a way which would not be feasible *in vivo* using human models. Sudden cardiac death (SCD) is a major global healthcare challenge as it accounts for nearly 20% of the deaths in industrialised countries with up to 50% of these patients having no previous heart disease diagnosis (Wellens et al, 2014). Furthermore it is estimated that up to 10% of SCD cases have an underlying genetic cause (Napolitano et al, 2012). There remains an inadequacy in risk stratification strategies, treatment options and methods of diagnosis for these conditions (Rajamohan et al, 2013; Wellens et al, 2014).

hiPSC have become a valuable source of *in vitro* cardiomyocytes with higher efficiencies and marked improvements in yields demonstrated in recent years (Burridge et al, 2011; Burridge et al, 2014). These *de novo* hiPSC-CMs have been demonstrated as a novel source for *in vitro* drug screening and toxicity assays which may complement animal models and heterologous overexpression systems to assess of drug efficacy and safety (Ebert et al, 2012; Liang et al, 2013; Rajamohan et al, 2013).

6.1 Generating Disease Models

6.1.1 Non-integrative reprogramming technology

Initial methods to generate hiPSCs using non-integrative methods were beset by laborious techniques such as mRNA delivery (Warren et al, 2010) or by very low reprogramming efficiencies such as in the initial reports of episomal plasmids (Yu et al, 2009). However among these newer methods Sendai virus stands out as one of the most attractive owing to its ease of use, only requiring one transduction, and it's relatively high reprogramming efficiency of around 0.04-0.31% in feeder free conditions (MacArthur et al, 2012; Yamasaki et al, 2016). Sendai virus was the most efficient reprogramming method tested in this thesis displaying an efficiency of 0.51%.

This thesis is the first to report the successful derivation of hiPSC lines using the GET peptide delivery system. This system has previously been used to deliver a variety of biologically active cargo (Dixon et al, 2016). The benefit of such a system is the simplicity of its use, requiring only one transfection, and the ability to generate the peptide at low cost, potentially indicating an improvement over SeV.

It is now a decade since the seminal reports of hiPSC generation from Yamanka and Thomson's labs and the growth of the field in that time has meant that it can now realistically be said that hiPSC generation is a technique which can be employed in any lab around the world. This is due to the commercial non-integrating reprogramming kits widely available such as CytoTune2.0 and Epi5 kits (Thermo Fisher) and the ReproRNA kit (STEMCELL Technologies).

6.2 Using hiPSC-CMs to model cardiac channelopathies

6.2.1 LQTS2

In this thesis an elongation of the APD was observed between LQT2-hiSPC-CMs and healthy-hiPSC-CMs when using voltage sensitive dyes. This confirms what has been shown in the literature previously by single cell analysis, using patch clamp electrophysiology, and cluster analysis with MEA based systyems (Matsa et al, 2011; Itzhaki et al, 2011; Kuusela et al, 2016). In this thesis the LQTS2-hiPSC-CMs were not subjected to adrenergic stimulation, although this has induced EADs in some models in the past. The variable results displayed across reported LQTS2-hiPSC disease models with regards to the generation of EADs in response to adrenergic stimulation can be explained by a number of factors. The first is different hiPSC and hiPSC-CM generation techniques. A second explanation may be the method of phenotyping as analysis of hiPSC-CMs at a single cell level for patch clamp electrophysiology elicits a differential response to the same hiPSC-CMs analysed as clusters on MEA system (Matsa et al, 2011). Furthermore it is possible that the reason for variable results between LQT2-hiPSC-CM disease models is underpinned by the inherent genetic variability which exists between different cell lines, especially in disorders such as LQTS which is known to exhibit variable penetrance even within multiple members of the same family who share the same mutation (Giudicessi et al, 2013: van Meer et al, 2016). Overall this underlines the need for greater standardisation across the field regarding culture methods, hiPSC-CM generation, phenotyping assays and the parameters to measure. Projects such as the CiPA consortium will be vital in establishing a new paradigm. The aim of CiPA is to facilitate a new method of analysis to ascertain compounds which are arrhythmogenic which is not solely focussed on hERG block but more holistically around the ion channels of the heart. CiPA seeks to use mechanistically based *in vitro* assays alongside *in silico* reconstructions of cellular cardiac electrophysiological activity to elucidate toxic compounds in the pre-clinical trial stage before confirming these findings using hPSC-CMs.

6.3 Therapeutic options for LQTS2

6.3.1 β-blockers

Nadolol and propranolol are the most effective β-blockers available to treat LQTS2 patients (Chockalingham et al, 2012; Abu-Zeitone et al, 2014). It is therefore a cause of concern that nadolol, the most commonly used LQTS2 β-blocker, has recently been discontinued in the UK for commercial reasons (Ackerman et al, 2017). This development underlines a need for improved pharmacological treatment options to prevent clinicians undertaking more aggressive treatment options such as ICD implantation. Propranolol was tested on LQTS2-hiPSC-CMs in this thesis and shown to result in no significant changes to APD50, APD90 or the triangularisation time indicating its role in LQTS2 is to prevent increased heart rate not modulation of the cardiac action potential. By preventing an increase in heart rate under adrenergic stimulation β-blockers do not address the underlying issue within the patient, a prolonged period of cardiac repolarisation. It is for this reason that this thesis investigated a number of ion channel modulators to assess if the underlying cardiac repolarisation could be improved.

6.3.2 I_{katp} agonists

The main manifestation of the LQTS2 phenotype is a limited amount of K^+ efflux during cardiac repolarisation through the hERG channel as I_{kr} current. Attempts to mediate this process by increasing K^+ efflux via alternative channels are an attractive treatment option.

6.3.2.1 Nicorandil

In this thesis nicorandil was demonstrated to reduce APD50 by 20%, APD90 by 18% and triangularisation by 14%, these data indicate a similar reduction to that observed in previous reports (Matsa et al, 2011). The potential of nicorandil to increase K^+ efflux and potentially treat LQTS has been reported on previously, prior to the advent of hiPSC technology animal models indicated that activation of the I_{katp} current could improve repolarisation (Shimizu and Antzelevtich, 2000; Chinushi et al, 2002). Published LQTS2-hiPSC disease models have reported nicorandil to be effective in reducing the APD of LQTS2-hiPSC-CM disease model by shortening the APD and abolishing the observed EADs in response to adrenergic stimulation (Matsa et al, 2011; Liang et al, 2013). In this thesis nicorandil was used as a reference compound to validate the LQT2-hiPSC-CM disease model by showing that APD could be decreased using this drug using the system tested in this thesis, confirming previous reports.

6.3.2.2 Minoxidil

In this thesis minoxidil was shown to result in a reduction of 19% in APD50, 18% in APD90 and 16% in triangularsation time. Traditionally minoxidil has been used as a vasodilator which can cause tachycardia and thus this effect must be mitigated in patients, an important consideration in LQTS2 patients. One of its more unfortunate side effects is hypertrichosis which is ultimately why it is commonly used in hair growth products (Sica, 2004). Indeed it has been reported that treatment of dermal papilla cells derived from hiPSCs with minoxidil increased expression of dermal papilla markers (Veraitch et al, 2017). Furthermore, minoxidil has been proposed as a treatment for impotence due to its vasodilation potential (Cavillini, 1991). Overall the effect of minoxidil on LQTS2 and repolarisation warrants further investigation as it is a drug which is commonly available on the market in the UK and any beneficial effects for LQTS patients would markedly improve patient outlook and quality of life.

Reports in the literature have identified other I_{katp} openers which were not tested in this thesis but exhibit the ability to improve repolarisation. The I_{katp} agonist pinacidil has been shown to reduce APD in LQTS-hiPSC-CMs as well as abolishing EADs and other arrhythmic events (Itzhaki et al, 2011). This further underlines the potential which I_{katp} agonists show in treating LQTS2, something which should be studied in greater depth.

6.3.3 I_{kr} agonists

The loss of functionality or expression of the hERG channel in the human heart leads to a decrease in I_{kr} current which is vital for repolarisation of the ventricles during the cardiac action potential. Increasing this current by activating the channels in the LQTS2 heart which are functional is an attractive treatment option.

6.3.3.1 NS1643

In this thesis NS1643 was demonstrated to result in a reduction in APD50 of 21%, in APD90 of 20% and in triangularisation time of 16%. NS1643 is an organic small molecule compound which was first discovered to interact with the hERG channel in heterologous overexpression models (Hansen et al, 2005; Cassis et al, 2006). NS1643 has been shown to reduce field potential duration, a surrogate for the QT interval, in LQTS1-hiPSC-CM models (Zhang et al, 2014). Further testing in LQTS1-hiPSC-CM disease models indicated that NS1643 was able to reduce the time for repolarisation but only at concentrations >100µM and its effects were far less potent than that of LUF7346 (Sala et al, 2016). NS1643 has also been tested in 3D

engineered heart tissue (EHT) format, providing a decrease in the time for the relaxation of the EHT, this is in direct contrast to the known I_{kr} blocker E4031 which increased this relaxation time (Mannhardt et al, 2016).

6.3.3.2 Ginsenoside RG3 (RG3)

Exposure of LQTS2-hiPSC-CMs to RG3 was demonstrated in this thesis to result in a reduction of ADP50 by 9%, APD90 by 8% and triangularisation time by 7%. RG3 is derived from the medicinal plant *Panax ginseng* and has been reported to have an anti-proliferative and anti-migratory effect in both colon and prostate cancers (Kim et al, 2004; Junmin et al, 2015). In addition to the potential benefits the compound may bring in cancer treatment it has also been demonstrated that it exhibits an anti-apoptotic and anti-inflammatory effect in thus improving cardiac function in rat models which have been subjected to myocardial infarction (Zhang et al, 2016). Further investigation of the pharmacological properties of RG3 reported that the drug was also able to activate the *KCNE1* subunit which co-assembles with *KCNQ1*, increasing activation of the I_{ks} channel and thus increasing K^+ efflux through mediation of the I_{ks} current (Choi et al, 2010; Choi et al, 2014).

Further research will be required on the use of I_{kr} agonists to treat LQTS2 and the use of LQTS2-hiPSC-CM models will allow further investigation of the pathogenesis of the disease. As the hERG channel is dysfunctional in LQTS2 it remains to be seen if activation of the functional channels which are present will enable greater and more efficient repolarisation *in vivo* or if a more prudent strategy will be the activation of alternative channels for K^+ efflux.

6.3.4 PPARδ agonists

The activation the I_{kr} current through hERG channels represents an attractive potential avenue for treatment for LQTS as described in Section 6.3.3.

6.3.4.1 Telmisartan

In this thesis telmisartan was demonstrated to result in a reduction of APD50 by 15%, APD90 by 14% and the triangularisation time by 12%. Telmisartan is thought to be an effective anti-fibrotic and has been suggested as a potential treatment option for hypertensive patients (Mikami et al, 2014). The drug has also been proposed as a potential treatment for type 2 diabetes although this effect is thought to be mediated through its ability to activate the PPARγ receptor (Miura et al, 2005). More recently there has been interest in using telmisartan as cancer drug due to its apoptotic effect on cancer cells across a number of types of cancer (Wu et al, 2016; Kozako et al, 2016). Large scale clinical trials in humans indicate that the drug

can play a role in reducing blood pressure (ONTARGET investigators, 2008) and a generic form of telmisartan was approved for use by the FDA in 2014.

6.3.4.2 GW0742

In this thesis exposure of LQTS2-hiPSC-CMs to GW0742 was demonstrated to result ina reduction of APD50 by 15%, APD90 by 14% and the triangularisation time by 12%.Studies in murine models have demonstrated that GW0742 may play a role in preventing lung inflammation (Galuppo et al, 2010). Furthermore experiments in rats demonstrated a potential cardioprotective effect against ischemic injury when GW0742 was administered (Yue et al, 2008). However in spite of these findings there has been no reported experiments on the use of GW0742 in modulating the APD in humanised models.

Despite the abundance of PPARδ receptors present in the heart (Yue et al, 2008) there remains a relative lack of information relating to the effect PPARδ agonists, or indeed antagonists, play in cardiac electrophysiology. This thesis reports that both PPARδ agonists tested on an LQTS2-hiPSC-CM disease model exhibit significant effects in reducing APD. In addition to this the triangularisation time, a measurement of repolarisation, was significantly enhanced in response to both drugs. This effect was found to be more potent when using GW0742 in comparison to telmisartan. Nevertheless both of these drugs require further investigation to examine in greater depth their potential as LQTS2 therapeutic compounds.

6.3.5 I_{ks} agonists

6.3.5.1 ML277

ML277 was tested in this thesis and shown to result in a reduction of APD50 by 42%, APD90 by 46% and the triangularisaton time by 58%. A compound library screen identified the compound ML227 as a potent activator of *KCNQ1* (Mattmann et al, 2012). ML277 has been trialled in a number of LQTS-hiPSC-CM disease models with results indicating that it is able to reduce APD by up to 11% when tested at concentrations of between 1µM and 2µM (Kuusela et al, 2016). In a LQTS1-hiPSC-CM disease model, treatment with ML277 was found to enhance activation of the I_{ks} current in addition to reducing the APD in both LQTS1-hiPSC-CMs and healthy-hiPSC-CMs (Ma et al, 2015). The ability of I_{ks} to potentially augment K^+ efflux in LQTS2 patients exhibiting a decreased I_{kr} current is an attractive prospect to treat LQTS2.

It is worth noting that in the case of I_{ks} current there remains dubiety as to whether this current is expressed in hPSC-CMs. Reports in the literature have shown that I_{ks} block resulted in no effect on hiPSC-CMs (Qu and Vargas, 2015). However another report has indicated that

exposure to ML277 restored I_{ks} function in a LQTS1-hiPSC model (Ma et al, 2015). Interestingly it has been reported that hiPSCs derived from cardiac-stromal progenitor cells exhibited an I_{ks} current when hiPSCs derived from a skin biopsy from the same patient did not, potentially indicating that hiPSC-CM phenotype may be linked to the original starting cell population that was reprogrammed (Altomare et al, 2016). In order to elucidate this further a greater panel of hPSC-CMs should be evaluated for the presence of I_{ks} current, this is something being carried out presently by our lab. What must also be noted is that ML277 is not necessarily only having an effect on the I_{ks} current, given that no response was evident until concentrations of >300nM were used in this thesis it would be prudent to assess whether the drug is able to bind to other receptors.

6.4 Modelling CPVT

Calcium handling is a highly spatial and temporal process which relies on the efficient movement of calcium into the cell, via the LTCC, to activate the RYR2 on the membrane of SR and induce calcium induce calcium release and contraction of the cardiac myocyte. Calcium is then taken back into the SR by SERCA or extruded from the cell by the NCX. Changes in the morphology and structure of cardiomyocytes have been shown to result in changes in the way in which the cardiomyocyte handles calcium (Louch et al, 2015).

Modelling of CPVT is made more complex by the suggestion that the disease primarily manifests itself in the His-purkinje system (Cerrone et al. 2007). Given that current cardiac differentiation protocols are as yet unable generate specific subtypes it may not be possible to accurately model CPVT *in vitro* at this time. Although attempts to use subtype specific promoters to drive fluorescent proteins have recently be used to enable more rapid identification of subtypes within cultures for specific analysis of the effects on those subtypes (Chen et al, 2017). However, it has been suggested that hiPSC-CMs exhibit a degree of plasticity meaning that the action potential characteristics of hiPSC-CMs, commonly used to define subtype, vary based on call seeding density (Du et al, 2015). In this thesis hiPSC-CMs were consistently seeded at the same density for all assays to limit the variability in this respect.

This thesis demonstrated that the hiPSC-CMs responded appropriately to nifedipine exposure by stopping calcium transients at concentrations of around 1µM which has previously been shown in the literature (Itzhaki et al, 2011). Reports regarding the nature of calcium handling mechanics in hPSC-CMs are scarce. Given the knowledge that hPSC-CMs have markedly

different structure from mature adult cardiomyocytes it is intuitive that their mechanism for cycling calcium may be different due to the temporal and spatial nature of calcium cycling. This thesis sought to gain a greater understanding of the way in which calcium is being cycled in hiPSC-CMs. The experiments within this thesis sought to block different aspects of the calcium handling machinery in order to assess the relative importance it played. However for many of the results observed the variation within the dataset appears to obscure the importance each component plays. This fits with the wider literature which cites a high degree of variation in calcium data (George and Edwards, 2017). To this end it is vital that this variation is reduced to improve the power of the findings in such experiments. This could be achieved by improvement of the maturation of the hiPSC-CMs, however differences in cell size would likely still play a role in variation of calcium mechanics. It is also possible that within populations there are typical and atypical results, it would be intersting if atypical or outlying samples could be excluded on the basis of basal characteristics allowing researchers to focus on the hiPSC-CMs which behave more typically. However this would require further investigation as no evidence has been published which shows typical hiPSC-CM calcium handling behaviour, the field must move towards more reporting of variance in calcium handling data to allow a greater understanding of how hPSC-CMs handle calcium and how this differs from native adult cardiomyoctytes.The logical next step from the work contained within this thesis would be to assess whether “sub populations” or a “mean population” exist within the dataset to gain a greater appreciation of the variance of the data within this thesis.

6.5 The current outlook for disease modelling using hiPSC-CMs

6.5.1 Utility of hPSC-CMs as disease models

As described in Section 1.5, hPSC-CMs are able to faithfully recapitulate many of the ion channels, accessory subunits and regulatory proteins which are present *in vivo*. When compared to the use of immortalised cell lines, such as HEK or CHO, overexpressing a single ion channel, this humanised model of cardiac function is able to greatly enhance the understanding of drug interaction at the ion channel level. Such limitations of single ion channel studies highlight the need for improved humanised models for drug screening. Indeed in this thesis two PPARδ agonists were tested and displayed efficacy in improving repolarisation of the LQTS2-hiPSC-CM disease model. Such compounds would be unable to exert an effect on heterologous overexpression models as the PPARδ agonists operate by

signalling through multiple factors which are present in hPSC-CMs but not in HEKs or CHOs overexpressing hERG (Lee and Kim, 2015).

Furthermore, *in vitro* hPSC-CMs have been extensively shown to faithfully recapitulate *in vivo* pharmacological response of over 60 compounds to date with a wide range of drugs with varied targets (Rajamohan et al, 2013). For example hPSC-CMs have both increased and decreased their beat rate in response to β1-adrenoceptor agonists and antagonists (Norström et al, 2006). Furthermore agonists of the β2-adrenoceptor such as isoprenaline can also increase beat rate (Matsa et al, 2011), something which was also observed in this thesis. Moreover they display the functionality of a multitude of K^+ channels such as I_{kr}, which can be blocked resulting in a prolonged APD, (Matsa et al, 2011) and I_{katp} openers which can shorten the APD by increasing K^+ efflux during phase 3 of the cardiac AP (Matsa et al, 2011). Both of these effects were observed in this thesis using the LQTS2-hiPSC-CM model. The ability of these hiPSC-CMs to faithfully recapitulate clinical observations has been demonstrated by reports of increased cardiac repolarisation in hiPSC-CMs in response to known APD elongating drugs – cisapride, erythromycin, sotalol, quinidine and E4031 (Kuusela et al, 2016).

Changes in cell behaviour mean variability is increased if a small and defined time window with regards to age of hPSC-CMs for assays is not adopted (Dolnikov et al, 2005). In this thesis all hiPSC-CMs were assessed between day 30 -35 post-differentiation. Cryopreservation of hiPSC-CMs would enable standardisation of CM ages when used in assays however this leads to increases in beat rate when compared to fresh hiPSC-CMs (Kim et al, 2011). Furthermore cryopreservation and thaw of hiPSC-CMs has been shown to result in variable viability after thaw and this loss of hiPSC-CMs must be factored in when choosing this strategy. Changes in the phenotype of hiPSC-CMs before and after cryopreservation were not tested in this thesis, however the evidence in the literature suggest that cross comparison of fresh and thawed hiPSC-CMs may introduce an additional layer of variability which should be avoided.

A further drawback is the use of a healthy control hiPSC line from a different patient with a separate genetic background, as a result of the millions of other polymorphisms within the genome which can account for phenotypic variability even within multiple healthy patients (Shen et al, 2013). This issue can be overcome by the generation of an isogenic control using genome engineering techniques (Bellin et al, 2013). Despite these limitations, hiPSC-CMs remain a valuable disease model which can complement the findings of *in vitro* overexpression models and *in vivo* animal models. The key caveat to any *in vitro* hiPSC-CM disease model is

the need to validate the system as was performed in this thesis using multiple hiPSC-CM lines and reference compounds.

Taken together these findings illustrate that key ionic channels within the heart which regulate voltage and calcium events in hPSC-CMs are present and functional. It has been established in multiple reports that I_{kr}, the current affected by LQTS2, is a major repolarising current in hPSC-CMs demonstrating the suitability of hPSC-CM models to investigate I_{kr} dysfunction. However to model a disease such as CPVT it is imperative that the RYR2 is expressed and functional, this has been shown to be the case indicating that hPSC-CMs are able to display functional characteristics of the channel. However, what remains under addressed is the role different aspect of the calcium handling play within hPSC-CMs and how their structural immaturity influences this due to the highly spatial and temporal nature of calcium cycling.

6.5.2 Limitations of hPSC-CM

6.5.2.1 The immature phenotype of hPSC-CMs

Although *in vitro* modelling provides resources which were not available before hPSC technology there remain some limitations to its use regarding the maturity both functionally and structurally for the hiPSC-CMs, this was described in Section 1.5. Inducing maturation in vitro

In vitro maturation of hPSC-CMs is perhaps the most pressing issue facing the cardiac disease modelling field at the present time. Given the limitations of hPSC-CMs outlined above there remains room for improvement in order for hPSC-CMs to reach their full potential as tools to model disease, assess drug toxicity/efficacy and be used for stem cell transplantations. Interestingly it has been shown that transplantation of immature hPSC-CMs into the working myocardium of a model species results in an increase in structural and functional maturation (Kadota et al, 2017). Attempts to modulate maturation of hPSC-CMs *in vitro* are discussed below.

6.5.2.2 *In vitro* maturation

The simplicity and ease of use regarding medium additives in facilitating hPSC-CM maturation make them an attractive proposition for the field in general. It has been shown that Triiodothyronine (T3) results in functional maturation of hPSC-CMs with improvements in twitch force, calcium transient upstroke and downstroke as well as enhanced oxygen consumption rates (Yang et al, 2014). However it appears that medium additives alone will be insufficient to induce hPSC-CM maturation and as such other factors which can be modulated

are also being investigated (Denning et al, 2016). Altering substrate stiffness and chemistry also hold promise in improving maturation, maintaining rat cardiomyocytes on a substrate with an elastic modulus of ~10kPa, the native rat hearts elastic modulus, was found to result in a greater alignment of the hPSC-CMs sarcomeres as well as functional maturation of calcium transients and SERCA expression (Jacot et al, 2008). Large scale screens for optimal hPSC-CM substrates have previously reported that chemically-defined methacrylate co-polymers (isobornyl and tert-butylamino-ethyl) resulted in hPSC-CMs with 6 fold quicker upstroke velocities and significantly increased sarcomeric length when compared to gelatin control plates (Patel et al, 2015).

In addition to altering the substrate aiding alignment to rod shaped cells thorugh cell patterning is thought of as a potentially beneficial avenue as the shape of the cardiomyocyte is vital in driving sarcomeric alignment (Bray et al, 2008). Stimulation of the hPSC-CM, electrically or mechanically, has been hypothesised as a potential route to ensure synchronous contractions (Yang et al, 2014). As native cardiomyocytes undergo mechanical stimulation *in vivo* it has been suggested that mimicry of such an event may lead to maturation of hPSC-CMs. It has been reported that seeding hESC-CMs onto a gelatin 3D scaffold which is then subjected to stretch has resulted in functional maturation of the hPSC-CMs tested in that study (Mihic et al, 2014). The use of 3D cultures is considered a viable methodology which may enable *in vitro* maturation of the cardiomyocytes. One report using 3D engineered structures used cardiomyocytes to form what they termed engineered heart tissue (EHT) which were developed by mixing dissociated hPSC-CMs with fibrin and collagen into rectangle moulds which sit between two silicon posts (Hansen et al, 2010; Schaff et al, 2011). The use of these EHTs has been shown to improve sarcomeric alignment and improve cellular organisation in both hPSC-CMs and using neonatal rat heart cells (Hansen et al, 2010; Schaff et al, 2011).

6.6 Study limitations and future work

6.6.1 Use of only 1 hiPSC line per condition

In this thesis the LQTS2 *in vitro* drug assay has indicated that a number of the drugs tested may exhibit beneficial effects for LQTS2 patients. However one limitation of this work is that the drug assay was only carried out on ReBl-hiPSC-CMs. Given the genetic variability observed across different hiPSCs and indeed the variability which can be introduced as a result of reprogramming and differentiation method it would be wise to investigate these results further (Burridge et al, 2012; Liang and Zhang, 2013). To do this a larger panel of both healthy

and LQTS2 hiPSC lines should be differentiated to cardiomyocytes and assessed using the assay template from this thesis. This will achieve two aims – the first is to further confirm that these drugs are able to increase K^+ efflux during phase 2 and 3 of the cardiac action potential and therefore improve repolarisation time, a key aspect in treating LQTS2. The second outcome this will achieve will be to gain an understanding of whether treatment with these drugs in the healthy hiPSC-CM may induce excessive APD shortening. Together these two outcomes will help build a broader picture about whether these drugs should be considered candidates for use in LQTS2 patients.

6.6.2 Use of cell permeable fluorescent dyes

In this thesis the two major phenotyping experiments were carried out using fluorescent dyes – FluoVolt for voltage and Fura2-AM for calcium. Although cellular phenotyping using dye based systems are well established an alternative to these are the use of genetically encoded indicators. This enables long term imaging without loss of signal or cytotoxicity. Genetically encoded indicators have been reported for both calcium and voltage (Zhao et al, 2011; Broussard et al, 2014). Such systems can also be ratiometric in order to account for movement of the hiPSC-CM, in this thesis Fura2-AM was used to image calcium which is ratiometric. However the FluoVolt dye used to image voltage is not. Despite the potential benefits of using genetically encoded indicators one of the major drawbacks of such systems is the time they take to generate in addition to variable expression levels in such a transgenic system (Rose et al, 2014).

6.6.3 Lack of other cell types in phenotyping assays

In this thesis cells were analysed as part of a monolayer culture rather than as single cells as is typically the case for patch clamp electrophysiology. This was decided as it could be argued that single cells will behave differently than cells acting within a monolayer, which is more commonly the case *in vivo*, research has shown that hiPSC-CMs behave differently between single cells and clusters (Matsa et al, 2011). However it can also be argued that cardiomyocytes do not act alone *in vivo* as there is substantial contribution from other cell types such as cardiac fibroblasts, endothelial cells and vascular smooth muscle cells (Souders et al, 2009). Therefore it may be the case that in order to fully recapitulate the *in vivo* phenotype other cell types must be included as part of disease models.

Initial investigations in this area have been favourable with reports demonstrating that cardiac tissue structure could be improved in EHTs by the introduction of tubular channels to the EHT which were populated by endothelial cells to mimic *in vivo* vasculature (Vollert et al, 2014). In addition to this the co-culture of endothelial cells and engineered myocardium has been shown to improve the function of this myocardium by a mechanism speculated to be biomimicry of vascular network's *in vivo* properties for functional cell assembly therefore resulting in greater orientation of the cardiomyocytes (Chiu et al, 2012). Co-culture of cardiomyocytes with cardiac fibroblasts has been shown to result in increased expression of Cx-43 as well as integrin-β1, this is potentially achieved via the growth factors and extra cellular matrix which are secreted by the cardiac fibroblasts *in vivo* (Ieda et al, 2013; Saini et al, 2015). However despite these indications of improved cardiomyocyte phenotype when co-culturing with other cells found in the *in vivo* cardiac system there remain limited methods which are able to separate these cells *in vitro* robustly aside from promoter driven antibiotic resistance which requires the generation of a transgenic hiPSC line. As a result of this, there remains a challenge when analysing fluorescent based dyes on monolayers of hiPSC-CMs when other cell types are present (Lee et al, 2012; Herron, 2016).

6.6.4 Lack of patch clamp investigation

Although the use of monolayers and fluorescent dyes was able to greatly improve throughput in this thesis it is unable to determine the effect drugs have on specific ion channels. It would be prudent in future to investigate the drugs tested in this thesis with patch clamp electrophysiology to gain a greater understanding of how drugs affect specific current densities (Obergrussberger et al, 2016). In this respect the monolayer based assays using fluorescent dyes are able to screen many compounds in a higher throughput fashion than manual or automated patch clamp electrophysiology. However these techniques are required downstream to gain a greater mechanistic understanding of the effect the compound has specifically on each ion channel.

6.6.5 Variability of calcium handling data

The inherent variability of calcium handling parameters has been established in the literature (George and Edwards, 2017). In this thesis the CPVT-hiPSC disease model was used in a calcium handling assay to ascertain whether there existed any differences between the CPVT-hiPSC-CMs and their CRISPR/Cas9 genetically corrected CPVT-WT-hiPSC-CM isogenic pair. Although some interesting data was gathered, there remains a great degree of variability within the

findings, in this case a new analytical framework may be required to further investigate calcium handling properties. Such a framework has been proposed, by assessing factors such as synchronization, amplitude, length, and variability of oscillation (SALVO) a team in Cardiff have reported a single index of *in vitro* cytotoxicity that was able to correctly stratify the effect of astemizole, thioridazine, cisapride, flecainide, valdecoxib, sotalol, and nadolol using Ca^{2+} signalling in hPSC-CMs (Lewis et al, 2015). It would be interesting to use such a system to analyse the data set reported in this thesis.

6.7 Final remarks

The rate of advancement of disease modelling using hiPSC has been rapid, only a decade ago were hiPSCs first generated by Shinya Yamanaka and already they have been trialled in humans for a patient suffering macular degeneration. The high rate of drug attrition which currently besets the pharmaceutical industry could be radically altered by an improvement of pre-clinical screening procedures. hiPSCs have the potential to be that radical change. This thesis has demonstrated that hiPSC generation and their subsequent differentiation to cardiomyocytes can result in high quality hiPSC lines, as assessed by pluripotency and tri-lineage differentiation potential, and hiPSC-CMs which can be produced in large quantities at high differentiation efficiencies. Automation of this system is possible, and has been trialled in our lab, and promises to greatly enhance the output of hiPSC-CMs as and when required. Furthermore this thesis established a drug screening assay using LQTS2-hiPSC-CMs which yielded a number of promising compounds with respect to improving the repolarisation time of hiPSC-CMs and these will require further investigation. With respect to CPVT, it appears clear that the structural immaturity of hiPSC-CMs will hold back progress in modelling this disease due to the spatial and temporal nature of calcium cycling. In this respect the maturation of hiPSC-CMs will be the next major breakthrough in the field of cardiac disease modelling.

7 Bibliography

AASEN, T., RAYA, A., BARRERO, M. J., GARRETA, E., CONSIGLIO, A., GONZALEZ, F., VASSENA, R., BILIĆ, J., PEKARIK, V., TISCORNIA, G., EDEL, M., BOUÉ, S. & IZPISÚA BELMONTE, J. C. 2008. Efficient and rapid generation of induced pluripotent stem cells from human keratinocytes. *Nat Biotechnol,* 26**,** 1276-84.

ABE, K., NIWA, H., IWASE, K., TAKIGUCHI, M., MORI, M., ABÉ, S. I. & YAMAMURA, K. I. 1996. Endoderm-specific gene expression in embryonic stem cells differentiated to embryoid bodies. *Exp Cell Res,* 229**,** 27-34.

ABOUT, I., BOTTERO, M. J., DE DENATO, P., CAMPS, J., FRANQUIN, J. C. & MITSIADIS, T. A. 2000. Human dentin production in vitro. *Exp Cell Res,* 258**,** 33-41.

ABU-ZEITONE, A., PETERSON, D. R., POLONSKY, B., MCNITT, S. & MOSS, A. J. 2014. Efficacy of different beta-blockers in the treatment of long QT syndrome. *J Am Coll Cardiol,* 64**,** 1352-8.

ACKERMAN, M. J. 2004. Cardiac channelopathies: it's in the genes. *Nat Med,* 10**,** 463-4.

ADEWUMI, O., AFLATOONIAN, B., AHRLUND-RICHTER, L., AMIT, M., ANDREWS, P. W., BEIGHTON, G., BELLO, P. A., BENVENISTY, N., BERRY, L. S., BEVAN, S., BLUM, B., BROOKING, J., CHEN, K. G., CHOO, A. B., CHURCHILL, G. A., CORBEL, M., DAMJANOV, I., DRAPER, J. S., DVORAK, P., EMANUELSSON, K., FLECK, R. A., FORD, A., GERTOW, K., GERTSENSTEIN, M., GOKHALE, P. J., HAMILTON, R. S., HAMPL, A., HEALY, L. E., HOVATTA, O., HYLLNER, J., IMREH, M. P., ITSKOVITZ-ELDOR, J., JACKSON, J., JOHNSON, J. L., JONES, M., KEE, K., KING, B. L., KNOWLES, B. B., LAKO, M., LEBRIN, F., MALLON, B. S., MANNING, D., MAYSHAR, Y., MCKAY, R. D., MICHALSKA, A. E., MIKKOLA, M., MILEIKOVSKY, M., MINGER, S. L., MOORE, H. D., MUMMERY, C. L., NAGY, A., NAKATSUJI, N., O'BRIEN, C. M., OH, S. K., OLSSON, C., OTONKOSKI, T., PARK, K. Y., PASSIER, R., PATEL, H., PATEL, M., PEDERSEN, R., PERA, M. F., PIEKARCZYK, M. S., PERA, R. A., REUBINOFF, B. E., ROBINS, A. J., ROSSANT, J., RUGG-GUNN, P., SCHULZ, T. C., SEMB, H., SHERRER, E. S., SIEMEN, H., STACEY, G. N., STOJKOVIC, M., SUEMORI, H., SZATKIEWICZ, J., TURETSKY, T., TUURI, T., VAN DEN BRINK, S., VINTERSTEN, K., VUORISTO, S., WARD, D., WEAVER, T. A., YOUNG, L. A., ZHANG, W. & INITIATIVE, I. S. C. 2007. Characterization of human embryonic stem cell lines by the International Stem Cell Initiative. *Nat Biotechnol,* 25**,** 803-16.

AFZAL, M. Z., GARTZ, M., KLYACHKO, E. A., KHAN, S. S., SHAH, S. J., GUPTA, S., SHAPIRO, A. D., VAUGHAN, D. E. & STRANDE, J. L. 2016. Generation of human iPSCs from urine derived cells of a patient with a novel homozygous PAI-1 mutation. *Stem Cell Res,* 17**,** 657-660.

AKHRAS, F. & RICKARDS, A. F. 1981. The relationship between QT interval and heart rate during physiological exercise and pacing. *Jpn Heart J,* 22**,** 345-51.

ALTOMARE, C., PIANEZZI, E., CERVIO, E., BOLIS, S., BIEMMI, V., BENZONI, P., CAMICI, G. G., MOCCETTI, T., BARILE, L. & VASSALLI, G. 2016. Human-induced pluripotent stem cell-derived cardiomyocytes from cardiac progenitor cells: effects of selective ion channel blockade. *Europace,* 18**,** iv67-iv76.

AMBROSI, A., CATTOGLIO, C. & DI SERIO, C. 2008. Retroviral integration process in the human genome: is it really non-random? A new statistical approach. *PLoS Comput Biol,* 4**,** e1000144.

ANDERLINI, P. 2009. Effects and safety of granulocyte colony-stimulating factor in healthy volunteers. *Curr Opin Hematol,* 16**,** 35-40.

ANTZELEVITCH, C. & BURASHNIKOV, A. 2011. Overview of Basic Mechanisms of

Cardiac Arrhythmia. *Cardiac electrophysiology clinics,* 3**,** 23-45.
ANTZELEVITCH, C. & OLIVA, A. 2006. Amplification of spatial dispersion of repolarization underlies sudden cardiac death associated with catecholaminergic polymorphic VT, long QT, short QT and Brugada syndromes. *J Intern Med,* 259**,** 48-58.
ANTZELEVITCH, C. & SICOURI, S. 2012. Mechanisms Underlying Arrhythmogenesis in Long QT Syndrome. *Cardiac Electrophysiology Clinics,* 4**,** 17-27.
ANTZELEVITCH, C., SICOURI, S., LITOVSKY, S. H., LUKAS, A., KRISHNAN, S. C., DI DIEGO, J. M., GINTANT, G. A. & LIU, D. W. 1991. Heterogeneity within the ventricular wall. Electrophysiology and pharmacology of epicardial, endocardial, and M cells. *Circ Res,* 69**,** 1427-49.
AOI, T., YAE, K., NAKAGAWA, M., ICHISAKA, T., OKITA, K., TAKAHASHI, K., CHIBA, T. & YAMANAKA, S. 2008. Generation of pluripotent stem cells from adult mouse liver and stomach cells. *Science,* 321**,** 699-702.
ARÉCHIGA-FIGUEROA, I. A., RODRÍGUEZ-MARTÍNEZ, M. & SÁNCHEZ-CHAPULA, J. A. 2011. Voltage-dependent potassium currents in feline sino-atrial node myocytes. *Pflugers Arch,* 462**,** 385-96.
ASAKURA, K., HAYASHI, S., OJIMA, A., TANIGUCHI, T., MIYAMOTO, N., NAKAMORI, C., NAGASAWA, C., KITAMURA, T., OSADA, T., HONDA, Y., KASAI, C., ANDO, H., KANDA, Y., SEKINO, Y. & SAWADA, K. 2015. Improvement of acquisition and analysis methods in multi-electrode array experiments with iPS cell-derived cardiomyocytes. *J Pharmacol Toxicol Methods,* 75**,** 17-26.
BADYAL, D. K. & DESAI, C. 2014. Animal use in pharmacology education and research: the changing scenario. *Indian J Pharmacol,* 46**,** 257-65.
BAN, H., NISHISHITA, N., FUSAKI, N., TABATA, T., SAEKI, K., SHIKAMURA, M., TAKADA, N., INOUE, M., HASEGAWA, M., KAWAMATA, S. & NISHIKAWA, S. 2011a. Efficient generation of transgene-free human induced pluripotent stem cells (iPSCs) by temperature-sensitive Sendai virus vectors. *Proc Natl Acad Sci U S A,* 108**,** 14234-9.
BANASIK, M. B. & MCCRAY, P. B. 2010. Integrase-defective lentiviral vectors: progress and applications. *Gene Ther,* 17**,** 150-7.
BARRANGOU, R., FREMAUX, C., DEVEAU, H., RICHARDS, M., BOYAVAL, P., MOINEAU, S., ROMERO, D. A. & HORVATH, P. 2007. CRISPR provides acquired resistance against viruses in prokaryotes. *Science,* 315**,** 1709-12.
BARUSCOTTI, M. & ROBINSON, R. B. 2007. Electrophysiology and pacemaker function of the developing sinoatrial node. *Am J Physiol Heart Circ Physiol,* 293**,** H2613-23.
BASSANI, J. W., BASSANI, R. A. & BERS, D. M. 1994. Relaxation in rabbit and rat cardiac cells: species-dependent differences in cellular mechanisms. *J Physiol,* 476**,** 279-93.
BASTIAENEN, R. & BEHR, E. R. 2011a. Sudden death and ion channel disease: pathophysiology and implications for management. *Heart,* 97**,** 1365-72.
BAZETT, H. C. 1997. AN ANALYSIS OF THE TIME-RELATIONS OF ELECTROCARDIOGRAMS. *Annals of Noninvasive Electrocardiology,* 2**,** 177-194.
BECK, C., CAYEUX, S., LUPTON, S. D., DÖRKEN, B. & BLANKENSTEIN, T. 1995. The thymidine kinase/ganciclovir-mediated "suicide" effect is variable in different tumor cells. *Hum Gene Ther,* 6**,** 1525-30.
BEDUT, S., SEMINATORE-NOLE, C., LAMAMY, V., CAIGNARD, S., BOUTIN, J. A., NOSJEAN, O., STEPHAN, J. P. & COGE, F. 2016. High-throughput drug profiling with voltage- and calcium-sensitive fluorescent probes in human iPSC-

derived cardiomyocytes. *Am J Physiol Heart Circ Physiol,* 311**,** H44-53.
BEERS, J., LINASK, K. L., CHEN, J. A., SINISCALCHI, L. I., LIN, Y., ZHENG, W., RAO, M. & CHEN, G. 2015. A cost-effective and efficient reprogramming platform for large-scale production of integration-free human induced pluripotent stem cells in chemically defined culture. *Sci Rep,* 5**,** 11319.
BENSON, D. W., WANG, D. W., DYMENT, M., KNILANS, T. K., FISH, F. A., STRIEPER, M. J., RHODES, T. H. & GEORGE, A. L. 2003a. Congenital sick sinus syndrome caused by recessive mutations in the cardiac sodium channel gene (SCN5A). *J Clin Invest,* 112**,** 1019-28.
BEROUKHIM, R., MERMEL, C. H., PORTER, D., WEI, G., RAYCHAUDHURI, S., DONOVAN, J., BARRETINA, J., BOEHM, J. S., DOBSON, J., URASHIMA, M., MC HENRY, K. T., PINCHBACK, R. M., LIGON, A. H., CHO, Y. J., HAERY, L., GREULICH, H., REICH, M., WINCKLER, W., LAWRENCE, M. S., WEIR, B. A., TANAKA, K. E., CHIANG, D. Y., BASS, A. J., LOO, A., HOFFMAN, C., PRENSNER, J., LIEFELD, T., GAO, Q., YECIES, D., SIGNORETTI, S., MAHER, E., KAYE, F. J., SASAKI, H., TEPPER, J. E., FLETCHER, J. A., TABERNERO, J., BASELGA, J., TSAO, M. S., DEMICHELIS, F., RUBIN, M. A., JANNE, P. A., DALY, M. J., NUCERA, C., LEVINE, R. L., EBERT, B. L., GABRIEL, S., RUSTGI, A. K., ANTONESCU, C. R., LADANYI, M., LETAI, A., GARRAWAY, L. A., LODA, M., BEER, D. G., TRUE, L. D., OKAMOTO, A., POMEROY, S. L., SINGER, S., GOLUB, T. R., LANDER, E. S., GETZ, G., SELLERS, W. R. & MEYERSON, M. 2010. The landscape of somatic copy-number alteration across human cancers. *Nature,* 463**,** 899-905.
BERS, D. M. 2002. Cardiac excitation-contraction coupling. *Nature,* 415**,** 198-205.
BHATT, N., GHOSH, R., ROY, S., GAO, Y., ARMANIOS, M., CHENG, L. & FRANCO, S. 2016. Integration-free erythroblast-derived human induced pluripotent stem cells (iPSCs) from an individual with Ataxia-Telangiectasia (A-T). *Stem Cell Res,* 17**,** 205-207.
BIALK, P., RIVERA-TORRES, N., STROUSE, B. & KMIEC, E. B. 2015a. Regulation of Gene Editing Activity Directed by Single-Stranded Oligonucleotides and CRISPR/Cas9 Systems. *PLoS One,* 10**,** e0129308.
BIERMANN, J., WU, K., ODENING, K. E., ASBACH, S., KOREN, G., PENG, X., ZEHENDER, M., BODE, C. & BRUNNER, M. 2011. Nicorandil normalizes prolonged repolarisation in the first transgenic rabbit model with Long-QT syndrome 1 both in vitro and in vivo. *Eur J Pharmacol,* 650**,** 309-16.
BIRKET, MATTHEW J., CASINI, S., KOSMIDIS, G., ELLIOTT, DAVID A., GERENCSER, AKOS A., BAARTSCHEER, A., SCHUMACHER, C., MASTROBERARDINO, PIER G., ELEFANTY, ANDREW G., STANLEY, ED G. & MUMMERY, CHRISTINE L. 2013. PGC-1α and Reactive Oxygen Species Regulate Human Embryonic Stem Cell-Derived Cardiomyocyte Function. *Stem Cell Reports,* 1**,** 560-574.
BLAYNEY, L. M. & LAI, F. A. 2009. Ryanodine receptor-mediated arrhythmias and sudden cardiac death. *Pharmacol Ther,* 123**,** 151-77.
BLELLOCH, R., VENERE, M., YEN, J. & RAMALHO-SANTOS, M. 2007a. Generation of induced pluripotent stem cells in the absence of drug selection. *Cell Stem Cell,* 1**,** 245-7.
BOCH, J. 2011. TALEs of genome targeting. *Nat Biotechnol,* 29**,** 135-6.
BOCH, J. & BONAS, U. 2010. Xanthomonas AvrBs3 family-type III effectors: discovery and function. *Annu Rev Phytopathol,* 48**,** 419-36.
BOCH, J., SCHOLZE, H., SCHORNACK, S., LANDGRAF, A., HAHN, S., KAY, S., LAHAYE, T., NICKSTADT, A. & BONAS, U. 2009. Breaking the code of DNA binding specificity of TAL-type III effectors. *Science,* 326**,** 1509-12.
BOHNEN, M. S., PENG, G., ROBEY, S. H., TERRENOIRE, C., IYER, V., SAMPSON, K. J. &

KASS, R. S. 2017. Molecular Pathophysiology of Congenital Long QT Syndrome. *Physiol Rev,* 97**,** 89-134.
BOS, J. M., BOS, K. M., JOHNSON, J. N., MOIR, C. & ACKERMAN, M. J. 2013a. Left cardiac sympathetic denervation in long QT syndrome: analysis of therapeutic nonresponders. *Circ Arrhythm Electrophysiol,* 6**,** 705-11.
BRAMBRINK, T., FOREMAN, R., WELSTEAD, G. G., LENGNER, C. J., WERNIG, M., SUH, H. & JAENISCH, R. 2008. Sequential expression of pluripotency markers during direct reprogramming of mouse somatic cells. *Cell Stem Cell,* 2**,** 151-9.
BRAY, M. A., SHEEHY, S. P. & PARKER, K. K. 2008. Sarcomere alignment is regulated by myocyte shape. *Cell Motil Cytoskeleton,* 65**,** 641-51.
BRETTE, F., KOMUKAI, K. & ORCHARD, C. H. 2002. Validation of formamide as a detubulation agent in isolated rat cardiac cells. *Am J Physiol Heart Circ Physiol,* 283**,** H1720-8.
BRIDGE, J. H., SMOLLEY, J. R. & SPITZER, K. W. 1990a. The relationship between charge movements associated with ICa and INa-Ca in cardiac myocytes. *Science,* 248**,** 376-8.
BRIGGS, R. & KING, T. J. 1952. Transplantation of Living Nuclei From Blastula Cells into Enucleated Frogs' Eggs. *Proc Natl Acad Sci U S A,* 38**,** 455-63.
BRILLANTES, A. B., ONDRIAS, K., SCOTT, A., KOBRINSKY, E., ONDRIASOVÁ, E., MOSCHELLA, M. C., JAYARAMAN, T., LANDERS, M., EHRLICH, B. E. & MARKS, A. R. 1994. Stabilization of calcium release channel (ryanodine receptor) function by FK506-binding protein. *Cell,* 77**,** 513-23.
BRITO-MARTINS, M., HARDING, S. E. & ALI, N. N. 2008. beta(1)- and beta(2)-adrenoceptor responses in cardiomyocytes derived from human embryonic stem cells: comparison with failing and non-failing adult human heart. *Br J Pharmacol,* 153**,** 751-9.
BROUSSARD, G. J., LIANG, R. & TIAN, L. 2014. Monitoring activity in neural circuits with genetically encoded indicators. *Front Mol Neurosci,* 7**,** 97.
BRUNELLI, L., CIESLIK, K. A., ALCORN, J. L., VATTA, M. & BALDINI, A. 2007. Peroxisome proliferator-activated receptor-delta upregulates 14-3-3 epsilon in human endothelial cells via CCAAT/enhancer binding protein-beta. *Circ Res,* 100**,** e59-71.
BUCK, E., ZIMANYI, I., ABRAMSON, J. J. & PESSAH, I. N. 1992. Ryanodine stabilizes multiple conformational states of the skeletal muscle calcium release channel. *J Biol Chem,* 267**,** 23560-7.
BURRIDGE, P. W., ANDERSON, D., PRIDDLE, H., BARBADILLO MUÑOZ, M. D., CHAMBERLAIN, S., ALLEGRUCCI, C., YOUNG, L. E. & DENNING, C. 2007. Improved human embryonic stem cell embryoid body homogeneity and cardiomyocyte differentiation from a novel V-96 plate aggregation system highlights interline variability. *Stem Cells,* 25**,** 929-38.
BURRIDGE, P. W., HOLMSTRÖM, A. & WU, J. C. 2015. Chemically Defined Culture and Cardiomyocyte Differentiation of Human Pluripotent Stem Cells. *Curr Protoc Hum Genet,* 87**,** 21.3.1-15.
BURRIDGE, P. W., KELLER, G., GOLD, J. D. & WU, J. C. 2012. Production of de novo cardiomyocytes: human pluripotent stem cell differentiation and direct reprogramming. *Cell Stem Cell,* 10**,** 16-28.
BURRIDGE, P. W., MATSA, E., SHUKLA, P., LIN, Z. C., CHURKO, J. M., EBERT, A. D., LAN, F., DIECKE, S., HUBER, B., MORDWINKIN, N. M., PLEWS, J. R., ABILEZ, O. J., CUI, B., GOLD, J. D. & WU, J. C. 2014. Chemically defined generation of human cardiomyocytes. *Nat Methods,* 11**,** 855-60.
BURRIDGE, P. W., THOMPSON, S., MILLROD, M. A., WEINBERG, S., YUAN, X., PETERS,

A., MAHAIRAKI, V., KOLIATSOS, V. E., TUNG, L. & ZAMBIDIS, E. T. 2011a. A universal system for highly efficient cardiac differentiation of human induced pluripotent stem cells that eliminates interline variability. *PLoS One,* 6**,** e18293.

BYRNE, S. M., MALI, P. & CHURCH, G. M. 2014. Genome editing in human stem cells. *Methods Enzymol,* 546**,** 119-38.

CAMPUZANO, O., BELTRAN-ALVAREZ, P., IGLESIAS, A., SCORNIK, F., PEREZ, G. & BRUGADA, R. 2010a. Genetics and cardiac channelopathies. *Genet Med,* 12**,** 260-267.

CARDANO, M., MARSONER, F., MARCATILI, M., KARNAVAS, T., ZASSO, J., LANTERNA, L. A. & CONTI, L. 2016. Establishment of induced pluripotent stem cell (iPSC) line from 55-year old male patient with hemorrhagic Moyamoya disease. *Stem Cell Res,* 17**,** 623-626.

CARROLL, D. 2011. Genome Engineering With Zinc-Finger Nucleases. *Genetics,* 188**,** 773-782.

CASIS, O., OLESEN, S.-P. & SANGUINETTI, M. C. 2006a. Mechanism of Action of a Novel Human ether-a-go-go-Related Gene Channel Activator. *Molecular Pharmacology,* 69**,** 658.

CATTOGLIO, C., FACCHINI, G., SARTORI, D., ANTONELLI, A., MICCIO, A., CASSANI, B., SCHMIDT, M., VON KALLE, C., HOWE, S., THRASHER, A. J., AIUTI, A., FERRARI, G., RECCHIA, A. & MAVILIO, F. 2007. Hot spots of retroviral integration in human CD34+ hematopoietic cells. *Blood,* 110**,** 1770-8.

CERRONE, M., NOUJAIM, S. F., TOLKACHEVA, E. G., TALKACHOU, A., O'CONNELL, R., BERENFELD, O., ANUMONWO, J., PANDIT, S. V., VIKSTROM, K., NAPOLITANO, C., PRIORI, S. G. & JALIFE, J. 2007. Arrhythmogenic mechanisms in a mouse model of catecholaminergic polymorphic ventricular tachycardia. *Circ Res,* 101**,** 1039-48.

CHAMBERS, I., COLBY, D., ROBERTSON, M., NICHOLS, J., LEE, S., TWEEDIE, S. & SMITH, A. 2003. Functional expression cloning of Nanog, a pluripotency sustaining factor in embryonic stem cells. *Cell,* 113**,** 643-55.

CHAN, K. K., ZHANG, J., CHIA, N. Y., CHAN, Y. S., SIM, H. S., TAN, K. S., OH, S. K., NG, H. H. & CHOO, A. B. 2009. KLF4 and PBX1 directly regulate NANOG expression in human embryonic stem cells. *Stem Cells,* 27**,** 2114-25.

CHANDLER, N. J., GREENER, I. D., TELLEZ, J. O., INADA, S., MUSA, H., MOLENAAR, P., DIFRANCESCO, D., BARUSCOTTI, M., LONGHI, R., ANDERSON, R. H., BILLETER, R., SHARMA, V., SIGG, D. C., BOYETT, M. R. & DOBRZYNSKI, H. 2009. Molecular Architecture of the Human Sinus Node. *Circulation,* 119**,** 1562.

CHEN, A. T. & ZOU, S. 2016. Evaluation of drug-mediated arrhythmic changes in spontaneous beating cardiomyocytes by AFM. *Analyst,* 141**,** 6303-6313.

CHEN, L. Y., BALLEW, J. D., HERRON, K. J., RODEHEFFER, R. J. & OLSON, T. M. 2007. A common polymorphism in SCN5A is associated with lone atrial fibrillation. *Clin Pharmacol Ther,* 81**,** 35-41.

CHEN, V. C., YE, J., SHUKLA, P., HUA, G., CHEN, D., LIN, Z., LIU, J. C., CHAI, J., GOLD, J., WU, J., HSU, D. & COUTURE, L. A. 2015. Development of a scalable suspension culture for cardiac differentiation from human pluripotent stem cells. *Stem Cell Res,* 15**,** 365-75.

CHEN, Y. T. & BRADLEY, A. 2000. A new positive/negative selectable marker, puDeltatk, for use in embryonic stem cells. *Genesis,* 28**,** 31-5.

CHEN, Z., XIAN, W., BELLIN, M., DORN, T., TIAN, Q., GOEDEL, A., DREIZEHNTER, L., SCHNEIDER, C. M., WARD-VAN OOSTWAARD, D., NG, J. K., HINKEL, R., PANE, L. S., MUMMERY, C. L., LIPP, P., MORETTI, A., LAUGWITZ, K. L. & SINNECKER,

D. 2017. Subtype-specific promoter-driven action potential imaging for precise disease modelling and drug testing in hiPSC-derived cardiomyocytes. *Eur Heart J,* 38**,** 292-301.

CHENG, H., LEDERER, W. J. & CANNELL, M. B. 1993. Calcium sparks: elementary events underlying excitation-contraction coupling in heart muscle. *Science,* 262**,** 740.

CHINUSHI, M., KASAI, H., TAGAWA, M., WASHIZUKA, T., HOSAKA, Y., CHINUSHI, Y. & AIZAWA, Y. 2002. Triggers of ventricular tachyarrhythmias and therapeutic effects of nicorandil in canine models of LQT2 and LQT3 syndromes. *J Am Coll Cardiol,* 40**,** 555-62.

CHIU, L. L., MONTGOMERY, M., LIANG, Y., LIU, H. & RADISIC, M. 2012. Perfusable branching microvessel bed for vascularization of engineered tissues. *Proc Natl Acad Sci U S A,* 109**,** E3414-23.

CHO, Y. 2016. Management of Patients with Long QT Syndrome. *Korean Circ J,* 46**,** 747-752.

CHOI, S. H., LEE, B. H., KIM, H. J., JUNG, S. W., KIM, H. S., SHIN, H. C., LEE, J. H., KIM, H. C., RHIM, H., HWANG, S. H., HA, T. S., CHO, H. & NAH, S. Y. 2014. Ginseng gintonin activates the human cardiac delayed rectifier K+ channel: involvement of Ca2+/calmodulin binding sites. *Mol Cells,* 37**,** 656-63.

CHOI, S. H., SHIN, T. J., HWANG, S. H., LEE, B. H., KANG, J., KIM, H. J., JO, S. H., CHOE, H. & NAH, S. Y. 2011a. Ginsenoside Rg(3) decelerates hERG K(+) channel deactivation through Ser631 residue interaction. *Eur J Pharmacol,* 663**,** 59-67.

CHOI, S. H., SHIN, T. J., LEE, B. H., CHU, D. H., CHOE, H., PYO, M. K., HWANG, S. H., KIM, B. R., LEE, S. M., LEE, J. H., KIM, D. H., KIM, H. C., RHIM, H. W. & NAH, S. Y. 2010a. Ginsenoside Rg3 activates human KCNQ1 K+ channel currents through interacting with the K318 and V319 residues: a role of KCNE1 subunit. *Eur J Pharmacol,* 637**,** 138-47.

CHRIST, T., HORVATH, A. & ESCHENHAGEN, T. 2015a. LQT1-phenotypes in hiPSC: Are we measuring the right thing? *Proc Natl Acad Sci U S A,* 112**,** E1968.

CHUNG, H. C., LIN, R. C., LOGAN, G. J., ALEXANDER, I. E., SACHDEV, P. S. & SIDHU, K. S. 2012. Human induced pluripotent stem cells derived under feeder-free conditions display unique cell cycle and DNA replication gene profiles. *Stem Cells Dev,* 21**,** 206-16.

CONG, L., RAN, F. A., COX, D., LIN, S., BARRETTO, R., HABIB, N., HSU, P. D., WU, X., JIANG, W., MARRAFFINI, L. A. & ZHANG, F. 2013. Multiplex Genome Engineering Using CRISPR/Cas Systems. *Science (New York, N.Y.),* 339**,** 819-823.

COSTELLO, I., PIMEISL, I. M., DRÄGER, S., BIKOFF, E. K., ROBERTSON, E. J. & ARNOLD, S. J. 2011. The T-box transcription factor Eomesodermin acts upstream of Mesp1 to specify cardiac mesoderm during mouse gastrulation. *Nat Cell Biol,* 13**,** 1084-91.

COWAN, C. A., ATIENZA, J., MELTON, D. A. & EGGAN, K. 2005. Nuclear reprogramming of somatic cells after fusion with human embryonic stem cells. *Science,* 309**,** 1369-73.

CRANEFIELD, P. F. 1977. Action potentials, afterpotentials, and arrhythmias. *Circ Res,* 41**,** 415-23.

CROTTI, L., CELANO, G., DAGRADI, F. & SCHWARTZ, P. J. 2008. Congenital long QT syndrome. *Orphanet J Rare Dis,* 3**,** 18.

CSEPE, T. A., KALYANASUNDARAM, A., HANSEN, B. J., ZHAO, J. & FEDOROV, V. V. 2015. Fibrosis: a structural modulator of sinoatrial node physiology and

dysfunction. *Frontiers in Physiology,* 6**,** 37.
CURRIE, S., LOUGHREY, C. M., CRAIG, M. A. & SMITH, G. L. 2004. Calcium/calmodulin-dependent protein kinase IIdelta associates with the ryanodine receptor complex and regulates channel function in rabbit heart. *Biochem J,* 377**,** 357-66.
DAMBROT, C., BRAAM, S. R., TERTOOLEN, L. G., BIRKET, M., ATSMA, D. E. & MUMMERY, C. L. 2014a. Serum supplemented culture medium masks hypertrophic phenotypes in human pluripotent stem cell derived cardiomyocytes. *J Cell Mol Med,* 18**,** 1509-18.
DAMIANO, R. J., ASANO, T., SMITH, P. K. & COX, J. L. 1990. Effect of the right ventricular isolation procedure on ventricular vulnerability to fibrillation. *J Am Coll Cardiol,* 15**,** 730-6.
DAUSSE, E., BERTHET, M., DENJOY, I., ANDRÉ-FOUET, X., CRUAUD, C., BENNACEUR, M., FAURÉ, S., COUMEL, P., SCHWARTZ, K. & GUICHENEY, P. 1996. A mutation in HERG associated with notched T waves in long QT syndrome. *J Mol Cell Cardiol,* 28**,** 1609-15.
DAVID, R., JARSCH, V. B., SCHWARZ, F., NATHAN, P., GEGG, M., LICKERT, H. & FRANZ, W.-M. 2011. Induction of MesP1 by Brachyury(T) generates the common multipotent cardiovascular stem cell. *Cardiovascular Research,* 92**,** 115-122.
DAVIS, R. P., CASINI, S., VAN DEN BERG, C. W., HOEKSTRA, M., REMME, C. A., DAMBROT, C., SALVATORI, D., OOSTWAARD, D. W., WILDE, A. A., BEZZINA, C. R., VERKERK, A. O., FREUND, C. & MUMMERY, C. L. 2012. Cardiomyocytes derived from pluripotent stem cells recapitulate electrophysiological characteristics of an overlap syndrome of cardiac sodium channel disease. *Circulation,* 125**,** 3079-91.
DE LA CRUZ, M., SANCHEZ GOMEZ, C. & CAYRE, R. 1991. The developmental components of the ventricles: their significance in congenital cardiac malformations. Cardiology Young.
DEMPSEY, G. T., CHAUDHARY, K. W., ATWATER, N., NGUYEN, C., BROWN, B. S., MCNEISH, J. D., COHEN, A. E. & KRALJ, J. M. 2016. Cardiotoxicity screening with simultaneous optogenetic pacing, voltage imaging and calcium imaging. *J Pharmacol Toxicol Methods,* 81**,** 240-50.
DENNING, C., BORGDORFF, V., CRUTCHLEY, J., FIRTH, K. S., GEORGE, V., KALRA, S., KONDRASHOV, A., HOANG, M. D., MOSQUEIRA, D., PATEL, A., PRODANOV, L., RAJAMOHAN, D., SKARNES, W. C., SMITH, J. G. & YOUNG, L. E. 2016. Cardiomyocytes from human pluripotent stem cells: From laboratory curiosity to industrial biomedical platform. *Biochim Biophys Acta,* 1863**,** 1728-48.
DEVALLA, H. D., GÉLINAS, R., ABURAWI, E. H., BEQQALI, A., GOYETTE, P., FREUND, C., CHAIX, M. A., TADROS, R., JIANG, H., LE BÉCHEC, A., MONSHOUWER-KLOOTS, J. J., ZWETSLOOT, T., KOSMIDIS, G., LATOUR, F., ALIKASHANI, A., HOEKSTRA, M., SCHLAEPFER, J., MUMMERY, C. L., STEVENSON, B., KUTALIK, Z., DE VRIES, A. A., RIVARD, L., WILDE, A. A., TALAJIC, M., VERKERK, A. O., AL-GAZALI, L., RIOUX, J. D., BHUIYAN, Z. A. & PASSIER, R. 2016. TECRL, a new life-threatening inherited arrhythmia gene associated with overlapping clinical features of both LQTS and CPVT. *EMBO Mol Med,* 8**,** 1390-1408.
DHAR, D. & HSI-EN HO, J. 2009. Stem cell research policies around the world. *Yale J Biol Med,* 82**,** 113-5.
DHEIN, S. 1998. Gap junction channels in the cardiovascular system: pharmacological and physiological modulation. *Trends Pharmacol Sci,* 19**,** 229-41.
DI DIEGO, J. M., DOSS, M. X., GOODROW, R., WU, Y., CORDEIRO, J. M., TREAT, J. &

ANTZELEVITCH, C. Role of I_{Kr} In Maintaining Resting Membrane Potential in Human iPS-Cardiomyocytes. *Heart Rhythm,* 8**,** 1822-1823.

DICK, E., KALRA, S., ANDERSON, D., GEORGE, V., RITSON, M., LAVAL, S., BARRESI, R., AARTSMA-RUS, A., LOCHMULLER, H. & DENNING, C. 2013. Exon skipping and gene transfer restore dystrophin expression in hiPSC-cardiomyocytes harbouring DMD mutations. *Stem Cells Dev*.

DICK, E., MATSA, E., YOUNG, L. E., DARLING, D. & DENNING, C. 2011b. Faster generation of hiPSCs by coupling high-titer lentivirus and column-based positive selection. *Nat Protoc,* 6**,** 701-14.

DINESS, T. G., YEH, Y. H., QI, X. Y., CHARTIER, D., TSUJI, Y., HANSEN, R. S., OLESEN, S. P., GRUNNET, M. & NATTEL, S. 2008. Antiarrhythmic properties of a rapid delayed-rectifier current activator in rabbit models of acquired long QT syndrome. *Cardiovasc Res,* 79**,** 61-9.

DOLNIKOV, K., SHILKRUT, M., ZEEVI-LEVIN, N., DANON, A., GERECHT-NIR, S., ITSKOVITZ-ELDOR, J. & BINAH, O. 2005. Functional properties of human embryonic stem cell-derived cardiomyocytes. *Ann N Y Acad Sci,* 1047**,** 66-75.

DOSS, M. X., DI DIEGO, J. M., GOODROW, R. J., WU, Y., CORDEIRO, J. M., NESTERENKO, V. V., BARAJAS-MARTÍNEZ, H., HU, D., URRUTIA, J., DESAI, M., TREAT, J. A., SACHINIDIS, A. & ANTZELEVITCH, C. 2012. Maximum Diastolic Potential of Human Induced Pluripotent Stem Cell-Derived Cardiomyocytes Depends Critically on IKr. *PLOS ONE,* 7**,** e40288.

DOUDNA, J. A. & CHARPENTIER, E. 2014. Genome editing. The new frontier of genome engineering with CRISPR-Cas9. *Science,* 346**,** 1258096.

DOYLE, D. A., MORAIS CABRAL, J., PFUETZNER, R. A., KUO, A., GULBIS, J. M., COHEN, S. L., CHAIT, B. T. & MACKINNON, R. 1998. The structure of the potassium channel: molecular basis of K+ conduction and selectivity. *Science,* 280**,** 69-77.

DRÁBEROVÁ, E., DEL VALLE, L., GORDON, J., MARKOVÁ, V., SMEJKALOVÁ, B., BERTRAND, L., DE CHADARÉVIAN, J. P., AGAMANOLIS, D. P., LEGIDO, A., KHALILI, K., DRÁBER, P. & KATSETOS, C. D. 2008. Class III beta-tubulin is constitutively coexpressed with glial fibrillary acidic protein and nestin in midgestational human fetal astrocytes: implications for phenotypic identity. *J Neuropathol Exp Neurol,* 67**,** 341-54.

DU, DAVID T., HELLEN, N., KANE, C. & TERRACCIANO, CESARE M. 2015. Action Potential Morphology of Human Induced Pluripotent Stem Cell-Derived Cardiomyocytes Does Not Predict Cardiac Chamber Specificity and Is Dependent on Cell Density. *Biophysical Journal,* 108**,** 1-4.

DU, G. G., GUO, X., KHANNA, V. K. & MACLENNAN, D. H. 2001. Functional characterization of mutants in the predicted pore region of the rabbit cardiac muscle Ca(2+) release channel (ryanodine receptor isoform 2). *J Biol Chem,* 276**,** 31760-71.

DUPRE, A., VIEAU, S. & IAIZZO, P. A. 2009. Basic ECG Theory, 12-Lead Recordings and Their Interpretation. *In:* IAIZZO, P. A. (ed.) *Handbook of Cardiac Anatomy, Physiology, and Devices.* Totowa, NJ: Humana Press.

DURDAGI, S., GUO, J., LEES-MILLER, J. P., NOSKOV, S. Y. & DUFF, H. J. 2012. Structure-guided topographic mapping and mutagenesis to elucidate binding sites for the human ether-a-go-go-related gene 1 potassium channel (KCNH2) activator NS1643. *J Pharmacol Exp Ther,* 342**,** 441-52.

DZHURA, I., WU, Y., COLBRAN, R. J., BALSER, J. R. & ANDERSON, M. E. 2000. Calmodulin kinase determines calcium-dependent facilitation of L-type calcium channels. *Nat Cell Biol,* 2**,** 173-7.

EDEN, M., MEDER, B., VÖLKERS, M., POOMVANICHA, M., DOMES, K., BRANCHEREAU, M., MARCK, P., WILL, R., BERNT, A., RANGREZ, A., BUSCH, M., HRABĚ DE ANGELIS, M., HEYMES, C., ROTTBAUER, W., MOST, P., HOFMANN, F., FREY, N. & CONSORTIUM, G. M. C. 2016. Myoscape controls cardiac calcium cycling and contractility via regulation of L-type calcium channel surface expression. *Nat Commun,* 7**,** 11317.

EDER, A., VOLLERT, I., HANSEN, A. & ESCHENHAGEN, T. 2016. Human engineered heart tissue as a model system for drug testing. *Advanced Drug Delivery Reviews,* 96**,** 214-224.

EGAN, K. R., RALPHE, J. C., WEINHAUS, L. & MAGINOT, K. R. 2013. Just Sinus Bradycardia or Something More Serious? *Case Reports in Pediatrics,* 2013**,** 5.

EGASHIRA, T., YUASA, S., SUZUKI, T., AIZAWA, Y., YAMAKAWA, H., MATSUHASHI, T., OHNO, Y., TOHYAMA, S., OKATA, S., SEKI, T., KURODA, Y., YAE, K., HASHIMOTO, H., TANAKA, T., HATTORI, F., SATO, T., MIYOSHI, S., TAKATSUKI, S., MURATA, M., KUROKAWA, J., FURUKAWA, T., MAKITA, N., AIBA, T., SHIMIZU, W., HORIE, M., KAMIYA, K., KODAMA, I., OGAWA, S. & FUKUDA, K. 2012a. Disease characterization using LQTS-specific induced pluripotent stem cells. *Cardiovasc Res,* 95**,** 419-29.

EGUSA, H., OKITA, K., KAYASHIMA, H., YU, G., FUKUYASU, S., SAEKI, M., MATSUMOTO, T., YAMANAKA, S. & YATANI, H. 2010. Gingival fibroblasts as a promising source of induced pluripotent stem cells. *PLoS One,* 5**,** e12743.

EL CHEMALY, A., MAGAUD, C., PATRI, S., JAYLE, C., GUINAMARD, R. & BOIS, P. 2007. The heart rate-lowering agent ivabradine inhibits the pacemaker current I(f) in human atrial myocytes. *J Cardiovasc Electrophysiol,* 18**,** 1190-6.

EMINLI, S., FOUDI, A., STADTFELD, M., MAHERALI, N., AHFELDT, T., MOSTOSLAVSKY, G., HOCK, H. & HOCHEDLINGER, K. 2009. Differentiation stage determines potential of hematopoietic cells for reprogramming into induced pluripotent stem cells. *Nat Genet,* 41**,** 968-76.

EVANS, M. J. & KAUFMAN, M. H. 1981a. Establishment in culture of pluripotential cells from mouse embryos. *Nature,* 292**,** 154-6.

EVANS, R. M., BARISH, G. D. & WANG, Y. X. 2004. PPARs and the complex journey to obesity. *Nat Med,* 10**,** 355-61.

FAGGIONI, M., KRYSHTAL, D. O. & KNOLLMANN, B. C. 2012. Calsequestrin mutations and catecholaminergic polymorphic ventricular tachycardia. *Pediatr Cardiol,* 33**,** 959-67.

FARRE, C. & FERTIG, N. 2012. HTS techniques for patch clamp-based ion channel screening - advances and economy. *Expert Opin Drug Discov,* 7**,** 515-24.

FATIMA, A., XU, G., SHAO, K., PAPADOPOULOS, S., LEHMANN, M., ARNÁIZ-COT, J. J., ROSA, A. O., NGUEMO, F., MATZKIES, M., DITTMANN, S., STONE, S. L., LINKE, M., ZECHNER, U., BEYER, V., HENNIES, H. C., ROSENKRANZ, S., KLAUKE, B., PARWANI, A. S., HAVERKAMP, W., PFITZER, G., FARR, M., CLEEMANN, L., MORAD, M., MILTING, H., HESCHELER, J. & SARIC, T. 2011. In vitro modeling of ryanodine receptor 2 dysfunction using human induced pluripotent stem cells. *Cell Physiol Biochem,* 28**,** 579-92.

FENG, X., LUO, Z., MA, L., MA, S., YANG, D., ZHAO, Z., YAN, Z., HE, H., CAO, T., LIU, D. & ZHU, Z. 2011a. Angiotensin II receptor blocker telmisartan enhances running endurance of skeletal muscle through activation of the PPAR-δ/AMPK pathway. *J Cell Mol Med,* 15**,** 1572-81.

FINK, M., NOBLE, P. J. & NOBLE, D. 2011. Ca(2+)-induced delayed afterdepolarizations are triggered by dyadic subspace Ca(2+) affirming that increasing SERCA reduces aftercontractions. *American Journal of Physiology -*

Heart and Circulatory Physiology, 301**,** H921-H935.
FISCHER, T. H., HERTING, J., TIRILOMIS, T., RENNER, A., NEEF, S., TOISCHER, K., ELLENBERGER, D., FÖRSTER, A., SCHMITTO, J. D., GUMMERT, J., SCHÖNDUBE, F. A., HASENFUSS, G., MAIER, L. S. & SOSSALLA, S. 2013. Ca2+/calmodulin-dependent protein kinase II and protein kinase A differentially regulate sarcoplasmic reticulum Ca2+ leak in human cardiac pathology. *Circulation,* 128**,** 970-81.
FONOUDI, H., ANSARI, H., ABBASALIZADEH, S., LARIJANI, M. R., KIANI, S., HASHEMIZADEH, S., ZARCHI, A. S., BOSMAN, A., BLUE, G. M., PAHLAVAN, S., PERRY, M., ORR, Y., MAYORCHAK, Y., VANDENBERG, J., TALKHABI, M., WINLAW, D. S., HARVEY, R. P., AGHDAMI, N. & BAHARVAND, H. 2015. A Universal and Robust Integrated Platform for the Scalable Production of Human Cardiomyocytes From Pluripotent Stem Cells. *Stem Cells Transl Med,* 4**,** 1482-94.
FRANK, K. F., BÖLCK, B., ERDMANN, E. & SCHWINGER, R. H. 2003. Sarcoplasmic reticulum Ca2+-ATPase modulates cardiac contraction and relaxation. *Cardiovasc Res,* 57**,** 20-7.
FRANZINI-ARMSTRONG, C., PROTASI, F. & RAMESH, V. 1999. Shape, size, and distribution of Ca(2+) release units and couplons in skeletal and cardiac muscles. *Biophysical Journal,* 77**,** 1528-1539.
FROM, A. M., MALESZEWSKI, J. J. & RIHAL, C. S. 2011. Current status of endomyocardial biopsy. *Mayo Clin Proc,* 86**,** 1095-102.
FUSAKI, N., BAN, H., NISHIYAMA, A., SAEKI, K. & HASEGAWA, M. 2009a. Efficient induction of transgene-free human pluripotent stem cells using a vector based on Sendai virus, an RNA virus that does not integrate into the host genome. *Proc Jpn Acad Ser B Phys Biol Sci,* 85**,** 348-62.
FÖLDES, G., MIOULANE, M., WRIGHT, J. S., LIU, A. Q., NOVAK, P., MERKELY, B., GORELIK, J., SCHNEIDER, M. D., ALI, N. N. & HARDING, S. E. 2011. Modulation of human embryonic stem cell-derived cardiomyocyte growth: a testbed for studying human cardiac hypertrophy? *J Mol Cell Cardiol,* 50**,** 367-76.
GABURJAKOVA, M., BAL, N. C., GABURJAKOVA, J. & PERIASAMY, M. 2013. Functional interaction between calsequestrin and ryanodine receptor in the heart. *Cell Mol Life Sci,* 70**,** 2935-45.
GALAT, V., GALAT, Y., PEREPITCHKA, M., JENNINGS, L. J., IANNACCONE, P. M. & HENDRIX, M. J. 2016. Transgene Reactivation in Induced Pluripotent Stem Cell Derivatives and Reversion to Pluripotency of Induced Pluripotent Stem Cell-Derived Mesenchymal Stem Cells. *Stem Cells Dev,* 25**,** 1060-72.
GALETTA, F., FRANZONI, F., FALLAHI, P., TOCCHINI, L., GRACI, F., CARPI, A., ANTONELLI, A. & SANTORO, G. 2010. Effect of telmisartan on QT interval variability and autonomic control in hypertensive patients with left ventricular hypertrophy. *Biomed Pharmacother,* 64**,** 516-20.
GALUPPO, M., DI PAOLA, R., MAZZON, E., ESPOSITO, E., PATERNITI, I., KAPOOR, A., THIEMERMANN, C. & CUZZOCREA, S. 2010a. GW0742, a high affinity PPAR-β/δ agonist reduces lung inflammation induced by bleomycin instillation in mice. *Int J Immunopathol Pharmacol,* 23**,** 1033-46.
GALVAN, D. L., NAKAZAWA, Y., KAJA, A., KETTLUN, C., COOPER, L. J., ROONEY, C. M. & WILSON, M. H. 2009. Genome-wide mapping of PiggyBac transposon integrations in primary human T cells. *J Immunother,* 32**,** 837-44.
GAMBIT, M. O. T. S. 2001. New approaches to antiarrhythmic therapy, Part I: emerging therapeutic applications of the cell biology of cardiac arrhythmias. *Circulation,* 104**,** 2865-73.

GARCIA, C. M., KWON, G. P. & BEEBE, D. C. 2006. alpha-Smooth muscle actin is constitutively expressed in the lens epithelial cells of several species. *Exp Eye Res,* 83**,** 999-1001.

GARNEAU, J. E., DUPUIS, M., VILLION, M., ROMERO, D. A., BARRANGOU, R., BOYAVAL, P., FREMAUX, C., HORVATH, P., MAGADÁN, A. H. & MOINEAU, S. 2010. The CRISPR/Cas bacterial immune system cleaves bacteriophage and plasmid DNA. *Nature,* 468**,** 67-71.

GEORGE, C. H. & EDWARDS, D. H. 2017. Decoding Ca2+ Signals as a Non-electrophysiological Method for Assessing Drug Toxicity in Stem Cell-Derived Cardiomyocytes. *In:* CLEMENTS, M. & ROQUEMORE, L. (eds.) *Stem Cell-Derived Models in Toxicology.* New York, NY: Springer New York.

GETI, I., ORMISTON, M. L., ROUHANI, F., TOSHNER, M., MOVASSAGH, M., NICHOLS, J., MANSFIELD, W., SOUTHWOOD, M., BRADLEY, A., RANA, A. A., VALLIER, L. & MORRELL, N. W. 2012. A practical and efficient cellular substrate for the generation of induced pluripotent stem cells from adults: blood-derived endothelial progenitor cells. *Stem Cells Transl Med,* 1**,** 855-65.

GHERGHICEANU, M., BARAD, L., NOVAK, A., REITER, I., ITSKOVITZ-ELDOR, J., BINAH, O. & POPESCU, L. M. 2011a. Cardiomyocytes derived from human embryonic and induced pluripotent stem cells: comparative ultrastructure. *J Cell Mol Med,* 15**,** 2539-51.

GINTANT, G. A. 1996. Two components of delayed rectifier current in canine atrium and ventricle. Does IKs play a role in the reverse rate dependence of class III agents? *Circ Res,* 78**,** 26-37.

GORZA, L., SCHIAFFINO, S. & VOLPE, P. 1993. Inositol 1,4,5-trisphosphate receptor in heart: evidence for its concentration in Purkinje myocytes of the conduction system. *The Journal of Cell Biology,* 121**,** 345.

GRAU, J., BOCH, J. & POSCH, S. 2013. TALENoffer: genome-wide TALEN off-target prediction. *Bioinformatics,* 29**,** 2931-2.

GREAVES, P., WILLIAMS, A. & EVE, M. 2004. First dose of potential new medicines to humans: how animals help. *Nat Rev Drug Discov,* 3**,** 226-236.

GRIMM, F. A., IWATA, Y., SIRENKO, O., BITTNER, M. & RUSYN, I. 2015. High-Content Assay Multiplexing for Toxicity Screening in Induced Pluripotent Stem Cell-Derived Cardiomyocytes and Hepatocytes. *Assay Drug Dev Technol,* 13**,** 529-46.

GROS, D., THÉVENIAU-RUISSY, M., BERNARD, M., CALMELS, T., KOBER, F., SÖHL, G., WILLECKE, K., NARGEOT, J., JONGSMA, H. J. & MANGONI, M. E. 2010. Connexin 30 is expressed in the mouse sino-atrial node and modulates heart rate. *Cardiovasc Res,* 85**,** 45-55.

GUNDRY, M. C., BRUNETTI, L., LIN, A., MAYLE, A. E., KITANO, A., WAGNER, D., HSU, J. I., HOEGENAUER, K. A., ROONEY, C. M., GOODELL, M. A. & NAKADA, D. 2016. Highly Efficient Genome Editing of Murine and Human Hematopoietic Progenitor Cells by CRISPR/Cas9. *Cell Rep,* 17**,** 1453-1461.

GUO, L., ABRAMS, R. M. C., BABIARZ, J. E., COHEN, J. D., KAMEOKA, S., SANDERS, M. J., CHIAO, E. & KOLAJA, K. L. 2011a. Estimating the Risk of Drug-Induced Proarrhythmia Using Human Induced Pluripotent Stem Cell–Derived Cardiomyocytes. *Toxicological Sciences,* 123**,** 281-289.

GUO, L., QIAN, J. Y., ABRAMS, R., TANG, H. M., WEISER, T., SANDERS, M. J. & KOLAJA, K. L. 2011b. The electrophysiological effects of cardiac glycosides in human iPSC-derived cardiomyocytes and in guinea pig isolated hearts. *Cell Physiol Biochem,* 27**,** 453-62.

GURDON, J. B. 1962. The Developmental Capacity of Nuclei taken from Intestinal

Epithelium Cells of Feeding Tadpoles. *Journal of Embryology and Experimental Morphology,* 10**,** 622-640.

HACEIN-BEY-ABINA, S., GARRIGUE, A., WANG, G. P., SOULIER, J., LIM, A., MORILLON, E., CLAPPIER, E., CACCAVELLI, L., DELABESSE, E., BELDJORD, K., ASNAFI, V., MACINTYRE, E., DAL CORTIVO, L., RADFORD, I., BROUSSE, N., SIGAUX, F., MOSHOUS, D., HAUER, J., BORKHARDT, A., BELOHRADSKY, B. H., WINTERGERST, U., VELEZ, M. C., LEIVA, L., SORENSEN, R., WULFFRAAT, N., BLANCHE, S., BUSHMAN, F. D., FISCHER, A. & CAVAZZANA-CALVO, M. 2008. Insertional oncogenesis in 4 patients after retrovirus-mediated gene therapy of SCID-X1. *J Clin Invest,* 118**,** 3132-42.

HAFT, D. H., SELENGUT, J., MONGODIN, E. F. & NELSON, K. E. 2005. A guild of 45 CRISPR-associated (Cas) protein families and multiple CRISPR/Cas subtypes exist in prokaryotic genomes. *PLoS Comput Biol,* 1**,** e60.

HAKAMATA, Y., NAKAI, J., TAKESHIMA, H. & IMOTO, K. 1992. Primary structure and distribution of a novel ryanodine receptor/calcium release channel from rabbit brain. *FEBS Lett,* 312**,** 229-35.

HAMLIN, R. L. & ALTSCHULD, R. A. 2011. Extrapolation From Mouse to Man. *Circulation: Cardiovascular Imaging,* 4**,** 2.

HANNA, J., SAHA, K., PANDO, B., VAN ZON, J., LENGNER, C. J., CREYGHTON, M. P., VAN OUDENAARDEN, A. & JAENISCH, R. 2009. Direct cell reprogramming is a stochastic process amenable to acceleration. *Nature,* 462**,** 595-601.

HANSEN, A., EDER, A., BÖNSTRUP, M., FLATO, M., MEWE, M., SCHAAF, S., AKSEHIRLIOGLU, B., SCHWOERER, A. P., SCHWÖRER, A., UEBELER, J. & ESCHENHAGEN, T. 2010. Development of a drug screening platform based on engineered heart tissue. *Circ Res,* 107**,** 35-44.

HANSEN, R. S., DINESS, T. G., CHRIST, T., DEMNITZ, J., RAVENS, U., OLESEN, S.-P. & GRUNNET, M. 2005a. Activation of Human ether-a-go-go-Related Gene Potassium Channels by the Diphenylurea 1,3-Bis-(2-hydroxy-5-trifluoromethyl-phenyl)-urea (NS1643). *Molecular Pharmacology,* 69**,** 266.

HARAGUCHI, Y., OHTSUKI, A., OKA, T. & SHIMIZU, T. 2015. Electrophysiological analysis of mammalian cells expressing hERG using automated 384-well-patch-clamp. *BMC Pharmacol Toxicol,* 16**,** 39.

HARDY, K., HANDYSIDE, A. H. & WINSTON, R. M. 1989. The human blastocyst: cell number, death and allocation during late preimplantation development in vitro. *Development,* 107**,** 597-604.

HARVEY, R. P. 2002. Patterning the vertebrate heart. *Nat Rev Genet,* 3**,** 544-556.

HAYASHI, S., HORIE, M. & OKADA, Y. 1993. Ionic mechanism of minoxidil sulfate-induced shortening of action potential durations in guinea pig ventricular myocytes. *J Pharmacol Exp Ther,* 265**,** 1527-33.

HAZELTINE, L. B., SIMMONS, C. S., SALICK, M. R., LIAN, X., BADUR, M. G., HAN, W., DELGADO, S. M., WAKATSUKI, T., CRONE, W. C., PRUITT, B. L. & PALECEK, S. P. 2012. Effects of substrate mechanics on contractility of cardiomyocytes generated from human pluripotent stem cells. *Int J Cell Biol,* 2012**,** 508294.

HE, H., YANG, D., MA, L., LUO, Z., MA, S., FENG, X., CAO, T., YAN, Z., LIU, D., TEPEL, M. & ZHU, Z. 2010. Telmisartan Prevents Weight Gain and Obesity Through Activation of Peroxisome Proliferator-Activated Receptor-δ–Dependent Pathways. *Hypertension,* 55**,** 869.

HE, J.-Q., MA, Y., LEE, Y., THOMSON, J. A. & KAMP, T. J. 2003a. Human Embryonic Stem Cells Develop Into Multiple Types of Cardiac Myocytes: Action Potential Characterization. *Circulation Research,* 93**,** 32-39.

HEALY, L. J., JIANG, Y. & HSU, E. W. 2011. Quantitative comparison of myocardial fiber structure between mice, rabbit, and sheep using diffusion tensor cardiovascular magnetic resonance. *J Cardiovasc Magn Reson,* 13**,** 74.

HEIDBÜCHEL, H., CORRADO, D., BIFFI, A., HOFFMANN, E., PANHUYZEN-GOEDKOOP, N., HOOGSTEEN, J., DELISE, P., HOFF, P. I., PELLICCIA, A. & REHABILITATION, S. G. O. S. C. O. T. E. A. F. C. P. A. 2006. Recommendations for participation in leisure-time physical activity and competitive sports of patients with arrhythmias and potentially arrhythmogenic conditions. Part II: ventricular arrhythmias, channelopathies and implantable defibrillators. *Eur J Cardiovasc Prev Rehabil,* 13**,** 676-86.

HEMATTI, P., HONG, B. K., FERGUSON, C., ADLER, R., HANAWA, H., SELLERS, S., HOLT, I. E., ECKFELDT, C. E., SHARMA, Y., SCHMIDT, M., VON KALLE, C., PERSONS, D. A., BILLINGS, E. M., VERFAILLIE, C. M., NIENHUIS, A. W., WOLFSBERG, T. G., DUNBAR, C. E. & CALMELS, B. 2004. Distinct genomic integration of MLV and SIV vectors in primate hematopoietic stem and progenitor cells. *PLoS Biol,* 2**,** e423.

HENDEL, A., BAK, R. O., CLARK, J. T., KENNEDY, A. B., RYAN, D. E., ROY, S., STEINFELD, I., LUNSTAD, B. D., KAISER, R. J., WILKENS, A. B., BACCHETTA, R., TSALENKO, A., DELLINGER, D., BRUHN, L. & PORTEUS, M. H. 2015. Chemically modified guide RNAs enhance CRISPR-Cas genome editing in human primary cells. *Nat Biotechnol,* 33**,** 985-9.

HERRON, T. J. 2016. Calcium and voltage mapping in hiPSC-CM monolayers. *Cell Calcium,* 59**,** 84-90.

HOCHEDLINGER, K. & PLATH, K. 2009. Epigenetic reprogramming and induced pluripotency. *Development (Cambridge, England),* 136**,** 509-523.

HOCKEMEYER, D., SOLDNER, F., COOK, E. G., GAO, Q., MITALIPOVA, M. & JAENISCH, R. 2008. A drug-inducible system for direct reprogramming of human somatic cells to pluripotency. *Cell Stem Cell,* 3**,** 346-53.

HOF, T., SIMARD, C., ROUET, R., SALLÉ, L. & GUINAMARD, R. 2013. Implication of the TRPM4 nonselective cation channel in mammalian sinus rhythm. *Heart Rhythm,* 10**,** 1683-9.

HOLLINGSHEAD, H. E., KILLINS, R. L., BORLAND, M. G., GIRROIR, E. E., BILLIN, A. N., WILLSON, T. M., SHARMA, A. K., AMIN, S., GONZALEZ, F. J. & PETERS, J. M. 2007. Peroxisome proliferator-activated receptor-β/δ (PPARβ/δ) ligands do not potentiate growth of human cancer cell lines. *Carcinogenesis,* 28**,** 2641-2649.

HONG, H., TAKAHASHI, K., ICHISAKA, T., AOI, T., KANAGAWA, O., NAKAGAWA, M., OKITA, K. & YAMANAKA, S. 2009. Suppression of induced pluripotent stem cell generation by the p53–p21 pathway. *Nature,* 460**,** 1132-1135.

HORTIGON-VINAGRE, M. P., ZAMORA, V., BURTON, F. L., GREEN, J., GINTANT, G. A. & SMITH, G. L. 2016. The Use of Ratiometric Fluorescence Measurements of the Voltage Sensitive Dye Di-4-ANEPPS to Examine Action Potential Characteristics and Drug Effects on Human Induced Pluripotent Stem Cell-Derived Cardiomyocytes. *Toxicol Sci,* 154**,** 320-331.

HOWE, S. J., MANSOUR, M. R., SCHWARZWAELDER, K., BARTHOLOMAE, C., HUBANK, M., KEMPSKI, H., BRUGMAN, M. H., PIKE-OVERZET, K., CHATTERS, S. J., DE RIDDER, D., GILMOUR, K. C., ADAMS, S., THORNHILL, S. I., PARSLEY, K. L., STAAL, F. J., GALE, R. E., LINCH, D. C., BAYFORD, J., BROWN, L., QUAYE, M., KINNON, C., ANCLIFF, P., WEBB, D. K., SCHMIDT, M., VON KALLE, C., GASPAR, H. B. & THRASHER, A. J. 2008. Insertional mutagenesis combined with acquired somatic mutations causes leukemogenesis following gene therapy

of SCID-X1 patients. *J Clin Invest,* 118**,** 3143-50.
HSU, P. D., LANDER, E. S. & ZHANG, F. 2014. Development and applications of CRISPR-Cas9 for genome engineering. *Cell,* 157**,** 1262-78.
HUANGFU, D., OSAFUNE, K., MAEHR, R., GUO, W., EIJKELENBOOM, A., CHEN, S., MUHLESTEIN, W. & MELTON, D. A. 2008. Induction of pluripotent stem cells from primary human fibroblasts with only Oct4 and Sox2. *Nat Biotechnol,* 26**,** 1269-75.
HWANG, H. S., KRYSHTAL, D. O., FEASTER, T. K., SÁNCHEZ-FREIRE, V., ZHANG, J., KAMP, T. J., HONG, C. C., WU, J. C. & KNOLLMANN, B. C. 2015a. Comparable calcium handling of human iPSC-derived cardiomyocytes generated by multiple
IEDA, M. 2013. Heart Development and Regeneration via Cellular Interactionand Reprogramming. *The Keio Journal of Medicine,* 62**,** 99-106.
IKEDA, Y., HOSHIJIMA, M. & CHIEN, K. R. 2008. Toward biologically targeted therapy of calcium cycling defects in heart failure. *Physiology (Bethesda),* 23**,** 6-16.
INGBER, D. E. 2006. Mechanical control of tissue morphogenesis during embryological development. *Int J Dev Biol,* 50**,** 255-66.
INVESTIGATORS, O. 2008. Telmisartan, Ramipril, or Both in Patients at High Risk for Vascular Events. *New England Journal of Medicine,* 358**,** 1547-1559.
ISHINO, Y., SHINAGAWA, H., MAKINO, K., AMEMURA, M. & NAKATA, A. 1987. Nucleotide sequence of the iap gene, responsible for alkaline phosphatase isozyme conversion in Escherichia coli, and identification of the gene product. *J Bacteriol,* 169**,** 5429-33.
ITO, H. & ONO, K. 1995. A rapidly activating delayed rectifier K+ channel in rabbit sinoatrial node cells. *Am J Physiol,* 269**,** H443-52.
ITZHAKI, I., MAIZELS, L., HUBER, I., GEPSTEIN, A., ARBEL, G., CASPI, O., MILLER, L., BELHASSEN, B., NOF, E., GLIKSON, M. & GEPSTEIN, L. 2012a. Modeling of catecholaminergic polymorphic ventricular tachycardia with patient-specific human-induced pluripotent stem cells. *J Am Coll Cardiol,* 60**,** 990-1000.
ITZHAKI, I., MAIZELS, L., HUBER, I., ZWI-DANTSIS, L., CASPI, O., WINTERSTERN, A., FELDMAN, O., GEPSTEIN, A., ARBEL, G., HAMMERMAN, H., BOULOS, M. & GEPSTEIN, L. 2011a. Modelling the long QT syndrome with induced pluripotent stem cells. *Nature,* 471**,** 225-9.
JACOT, J. G., MCCULLOCH, A. D. & OMENS, J. H. 2008. Substrate stiffness affects the functional maturation of neonatal rat ventricular myocytes. *Biophys J,* 95**,** 3479-87.
JANSE, M. J. & WIT, A. L. 1989. Electrophysiological mechanisms of ventricular arrhythmias resulting from myocardial ischemia and infarction. *Physiological Reviews,* 69**,** 1049.
JANSEN, R., EMBDEN, J. D., GAASTRA, W. & SCHOULS, L. M. 2002. Identification of genes that are associated with DNA repeats in prokaryotes. *Mol Microbiol,* 43**,** 1565-75.
JASINSKIENE, N., COATES, C. J., ASHIKYAN, A. & JAMES, A. A. 2003. High efficiency, site-specific excision of a marker gene by the phage P1 cre–loxP system in the yellow fever mosquito, Aedes aegypti. *Nucleic Acids Research,* 31**,** e147-e147.
JERVELL, A. & LANGE-NIELSEN, F. 1957. Congenital deaf-mutism, functional heart disease with prolongation of the Q-T interval, and sudden death. *American Heart Journal,* 54**,** 59-68.
JI, J., TONG, X., HUANG, X., ZHANG, J., QIN, H. & HU, Q. 2016. Patient-Derived Human Induced Pluripotent Stem Cells From Gingival Fibroblasts Composited With

Defined Nanohydroxyapatite/Chitosan/Gelatin Porous Scaffolds as Potential Bone Graft Substitutes. *Stem Cells Transl Med,* 5**,** 95-105.

JIANG, D., XIAO, B., YANG, D., WANG, R., CHOI, P., ZHANG, L., CHENG, H. & CHEN, S. R. 2004. RyR2 mutations linked to ventricular tachycardia and sudden death reduce the threshold for store-overload-induced Ca2+ release (SOICR). *Proc Natl Acad Sci U S A,* 101**,** 13062-7.

JIN, L., HAN, Z., PLATISA, J., WOOLTORTON, J. R. A., COHEN, L. B. & PIERIBONE, V. A. 2012. Single action potentials and subthreshold electrical events imaged in neurons with a novel fluorescent protein voltage probe. *Neuron,* 75**,** 779-785.

JONES, E. M., ROTI ROTI, E. C., WANG, J., DELFOSSE, S. A. & ROBERTSON, G. A. 2004. Cardiac IKr channels minimally comprise hERG 1a and 1b subunits. *J Biol Chem,* 279**,** 44690-4.

JOST, N., ACSAI, K., HORVÁTH, B., BÁNYÁSZ, T., BACZKÓ, I., BITAY, M., BOGÁTS, G. & NÁNÁSI, P. P. 2009. Contribution of I Kr and I K1 to ventricular repolarization in canine and human myocytes: is there any influence of action potential duration? *Basic Res Cardiol,* 104**,** 33-41.

JOST, N., NAGY, N., CORICI, C., KOHAJDA, Z., HORVÁTH, A., ACSAI, K., BILICZKI, P., LEVIJOKI, J., POLLESELLO, P., KOSKELAINEN, T., OTSOMAA, L., TÓTH, A., PAPP, J. G., VARRÓ, A. & VIRÁG, L. 2013. ORM-10103, a novel specific inhibitor of the Na+/Ca2+ exchanger, decreases early and delayed afterdepolarizations in the canine heart. *Br J Pharmacol,* 170**,** 768-78.

JOST, N., VIRÁG, L., BITAY, M., TAKÁCS, J., LENGYEL, C., BILICZKI, P., NAGY, Z., BOGÁTS, G., LATHROP, D. A., PAPP, J. G. & VARRÓ, A. 2005. Restricting excessive cardiac action potential and QT prolongation: a vital role for IKs in human ventricular muscle. *Circulation,* 112**,** 1392-9.

JUNG, C. B., MORETTI, A., MEDEROS Y SCHNITZLER, M., IOP, L., STORCH, U., BELLIN, M., DORN, T., RUPPENTHAL, S., PFEIFFER, S., GOEDEL, A., DIRSCHINGER, R. J., SEYFARTH, M., LAM, J. T., SINNECKER, D., GUDERMANN, T., LIPP, P. & LAUGWITZ, K. L. 2012. Dantrolene rescues arrhythmogenic RYR2 defect in a patient-specific stem cell model of catecholaminergic polymorphic ventricular tachycardia. *EMBO Mol Med,* 4**,** 180-91.

JUNMIN, S., HONGXIANG, L., ZHEN, L., CHAO, Y. & CHAOJIE, W. 2015. Ginsenoside Rg3 inhibits colon cancer cell migration by suppressing nuclear factor kappa B activity. *J Tradit Chin Med,* 35**,** 440-4.

KADOTA, S., PABON, L., REINECKE, H. & MURRY, C. E. 2017. In Vivo Maturation of Human Induced Pluripotent Stem Cell-Derived Cardiomyocytes in Neonatal and Adult Rat Hearts. *Stem Cell Reports,* 8**,** 278-289.

KAESTNER, L., SCHOLZ, A., TIAN, Q., RUPPENTHAL, S., TABELLION, W., WIESEN, K., KATUS, H. A., MÜLLER, O. J., KOTLIKOFF, M. I. & LIPP, P. 2014a. Genetically encoded Ca2+ indicators in cardiac myocytes. *Circ Res,* 114**,** 1623-39.

KAESTNER, L., TIAN, Q., KAISER, E., XIAN, W., MÜLLER, A., OBERHOFER, M., RUPPENTHAL, S., SINNECKER, D., TSUTSUI, H., MIYAWAKI, A., MORETTI, A. & LIPP, P. 2015. Genetically Encoded Voltage Indicators in Circulation Research. *Int J Mol Sci,* 16**,** 21626-42.

KAFTAN, E., MARKS, A. R. & EHRLICH, B. E. 1996. Effects of rapamycin on ryanodine receptor/Ca(2+)-release channels from cardiac muscle. *Circ Res,* 78**,** 990-7.

KAGAN, A., MELMAN, Y. F., KRUMERMAN, A. & MCDONALD, T. V. 2002. 14-3-3 amplifies and prolongs adrenergic stimulation of HERG K+ channel activity. *EMBO J,* 21**,** 1889-98.

KAJI, K., NORRBY, K., PACA, A., MILEIKOVSKY, M., MOHSENI, P. & WOLTJEN, K. 2009.

Virus-free induction of pluripotency and subsequent excision of reprogramming factors. *Nature,* 458**,** 771-5.
KAMAKURA, T., MAKIYAMA, T., SASAKI, K., YOSHIDA, Y., WURIYANGHAI, Y., CHEN, J., HATTORI, T., OHNO, S., KITA, T., HORIE, M., YAMANAKA, S. & KIMURA, T. 2013. Ultrastructural maturation of human-induced pluripotent stem cell-derived cardiomyocytes in a long-term culture. *Circ J,* 77**,** 1307-14.
KANE, C., COUCH, L. & TERRACCIANO, C. M. N. 2015. Excitation–contraction coupling of human induced pluripotent stem cell-derived cardiomyocytes. *Frontiers in Cell and Developmental Biology,* 3**,** 59.
KANG, X., YU, Q., HUANG, Y., SONG, B., CHEN, Y., GAO, X., HE, W., SUN, X. & FAN, Y. 2015a. Effects of Integrating and Non-Integrating Reprogramming Methods on Copy Number Variation and Genomic Stability of Human Induced Pluripotent Stem Cells. *PLoS One,* 10**,** e0131128.
KATTMAN, S. J., WITTY, A. D., GAGLIARDI, M., DUBOIS, N. C., NIAPOUR, M., HOTTA, A., ELLIS, J. & KELLER, G. 2011a. Stage-specific optimization of activin/nodal and BMP signaling promotes cardiac differentiation of mouse and human pluripotent stem cell lines. *Cell Stem Cell,* 8**,** 228-40.
KEHAT, I., KENYAGIN-KARSENTI, D., SNIR, M., SEGEV, H., AMIT, M., GEPSTEIN, A., LIVNE, E., BINAH, O., ITSKOVITZ-ELDOR, J. & GEPSTEIN, L. 2001. Human embryonic stem cells can differentiate into myocytes with structural and functional properties of cardiomyocytes. *J Clin Invest,* 108**,** 407-14.
KEHLER, J., TOLKUNOVA, E., KOSCHORZ, B., PESCE, M., GENTILE, L., BOIANI, M., LOMELÍ, H., NAGY, A., MCLAUGHLIN, K. J., SCHÖLER, H. R. & TOMILIN, A. 2004. Oct4 is required for primordial germ cell survival. *EMBO Rep,* 5**,** 1078-83.
KELLY, R. G., BUCKINGHAM, M. E. & MOORMAN, A. F. 2014. Heart fields and cardiac morphogenesis. *Cold Spring Harb Perspect Med,* 4.
KENTISH, J. C., BARSOTTI, R. J., LEA, T. J., MULLIGAN, I. P., PATEL, J. R. & FERENCZI, M. A. 1990. Calcium release from cardiac sarcoplasmic reticulum induced by photorelease of calcium or Ins(1,4,5)P3. *American Journal of Physiology - Heart and Circulatory Physiology,* 258**,** H610.
KHAN, J. M., LYON, A. R. & HARDING, S. E. 2013. The case for induced pluripotent stem cell-derived cardiomyocytes in pharmacological screening. *Br J Pharmacol,* 169**,** 304-17.
KIM, C., WONG, J., WEN, J., WANG, S., WANG, C., SPIERING, S., KAN, N. G., FORCALES, S., PURI, P. L., LEONE, T. C., MARINE, J. E., CALKINS, H., KELLY, D. P., JUDGE, D. P. & CHEN, H. S. 2013. Studying arrhythmogenic right ventricular dysplasia with patient-specific iPSCs. *Nature,* 494**,** 105-10.
KIM, D., KIM, C. H., MOON, J. I., CHUNG, Y. G., CHANG, M. Y., HAN, B. S., KO, S., YANG, E., CHA, K. Y., LANZA, R. & KIM, K. S. 2009. Generation of human induced pluripotent stem cells by direct delivery of reprogramming proteins. *Cell Stem Cell,* 4**,** 472-6.
KIM, H. S., LEE, E. H., KO, S. R., CHOI, K. J., PARK, J. H. & IM, D. S. 2004. Effects of ginsenosides Rg3 and Rh2 on the proliferation of prostate cancer cells. *Arch Pharm Res,* 27**,** 429-35.
KIM, N. D., KANG, S. Y., PARK, J. H. & SCHINI-KERTH, V. B. 1999. Ginsenoside Rg3 mediates endothelium-dependent relaxation in response to ginsenosides in rat aorta: role of K+ channels. *Eur J Pharmacol,* 367**,** 41-9.
KIM, Y. Y., KU, S. Y., LIU, H. C., CHO, H. J., OH, S. K., MOON, S. Y. & CHOI, Y. M. 2011. Cryopreservation of human embryonic stem cells derived-cardiomyocytes induced by BMP2 in serum-free condition. *Reprod Sci,* 18**,** 252-60.

KITAJIMA, S., TAKAGI, A., INOUE, T. & SAGA, Y. 2000. MesP1 and MesP2 are essential for the development of cardiac mesoderm. *Development,* 127**,** 3215-26.
KLIMAS, A., AMBROSI, C. M., YU, J., WILLIAMS, J. C., BIEN, H. & ENTCHEVA, E. 2016. OptoDyCE as an automated system for high-throughput all-optical dynamic cardiac electrophysiology. *Nat Commun,* 7**,** 11542.
KLÉBER, A. G. & RUDY, Y. 2004. Basic mechanisms of cardiac impulse propagation and associated arrhythmias. *Physiol Rev,* 84**,** 431-88.
KOLA, I. & LANDIS, J. 2004. Can the pharmaceutical industry reduce attrition rates? *Nat Rev Drug Discov,* 3**,** 711-5.
KOZAKO, T., SOEDA, S., YOSHIMITSU, M., ARIMA, N., KUROKI, A., HIRATA, S., TANAKA, H., IMAKYURE, O., TONE, N., HONDA, S. I. & SOEDA, S. 2016. Angiotensin II type 1 receptor blocker telmisartan induces apoptosis and autophagy in adult T-cell leukemia cells. *FEBS Open Bio,* 6**,** 442-460.
KRAMER, J., OBEJERO-PAZ, C. A., MYATT, G., KURYSHEV, Y. A., BRUENING-WRIGHT, A., VERDUCCI, J. S. & BROWN, A. M. 2013. MICE models: superior to the HERG model in predicting Torsade de Pointes. *Sci Rep,* 3**,** 2100.
KRANIAS, E. G. & HAJJAR, R. J. 2012. Modulation of cardiac contractility by the phospholamban/SERCA2a regulatome. *Circ Res,* 110**,** 1646-60.
KUMAR, S., CURRAN, J. E., GLAHN, D. C. & BLANGERO, J. 2016. Utility of Lymphoblastoid Cell Lines for Induced Pluripotent Stem Cell Generation. *Stem Cells International,* 2016**,** 2349261.
KUUSELA, J., KUJALA, V. J., KIVIAHO, A., OJALA, M., SWAN, H., KONTULA, K. & AALTO-SETÄLÄ, K. 2016. Effects of cardioactive drugs on human induced pluripotent stem cell derived long QT syndrome cardiomyocytes. *Springerplus,* 5**,** 234.
KWON, C., QIAN, L., CHENG, P., NIGAM, V., ARNOLD, J. & SRIVASTAVA, D. 2009. A regulatory pathway involving Notch1/beta-catenin/Isl1 determines cardiac progenitor cell fate. *Nat Cell Biol,* 11**,** 951-7.
LAHAT, H., PRAS, E., OLENDER, T., AVIDAN, N., BEN-ASHER, E., MAN, O., LEVY-NISSENBAUM, E., KHOURY, A., LORBER, A., GOLDMAN, B., LANCET, D. & ELDAR, M. 2001. A Missense Mutation in a Highly Conserved Region of CASQ2 Is Associated with Autosomal Recessive Catecholamine-Induced Polymorphic Ventricular Tachycardia in Bedouin Families from Israel. *The American Journal of Human Genetics,* 69**,** 1378-1384.
LAHTI, A. L., KUJALA, V. J., CHAPMAN, H., KOIVISTO, A. P., PEKKANEN-MATTILA, M., KERKELÄ, E., HYTTINEN, J., KONTULA, K., SWAN, H., CONKLIN, B. R., YAMANAKA, S., SILVENNOINEN, O. & AALTO-SETÄLÄ, K. 2012. Model for long QT syndrome type 2 using human iPS cells demonstrates arrhythmogenic characteristics in cell culture. *Dis Model Mech,* 5**,** 220-30.
LANNER, J. T., GEORGIOU, D. K., JOSHI, A. D. & HAMILTON, S. L. 2010. Ryanodine receptors: structure, expression, molecular details, and function in calcium release. *Cold Spring Harb Perspect Biol,* 2**,** a003996.
LAVER, D. R. 2007. Ca2+ stores regulate ryanodine receptor Ca2+ release channels via luminal and cytosolic Ca2+ sites. *Clin Exp Pharmacol Physiol,* 34**,** 889-96.
LEDFORD, H. 2011. Translational research: 4 ways to fix the clinical trial. *Nature,* 477**,** 526-8.
LEE, P., KLOS, M., BOLLENSDORFF, C., HOU, L., EWART, P., KAMP, T. J., ZHANG, J., BIZY, A., GUERRERO-SERNA, G., KOHL, P., JALIFE, J. & HERRON, T. J. 2012a. Simultaneous Voltage and Calcium Mapping of Genetically Purified Human iPS Cell-Derived Cardiac Myocyte Monolayers. *Circulation research,* 110**,** 1556-1563.
LEE, W. S. & KIM, J. 2015a. Peroxisome Proliferator-Activated Receptors and the

Heart: Lessons from the Past and Future Directions. *PPAR Res,* 2015**,** 271983.
LEE, Y. K., NG, K. M., LAI, W. H., CHAN, Y. C., LAU, Y. M., LIAN, Q., TSE, H. F. & SIU, C. W. 2011a. Calcium homeostasis in human induced pluripotent stem cell-derived cardiomyocytes. *Stem Cell Rev,* 7**,** 976-86.
LEENHARDT, A., LUCET, V., DENJOY, I., GRAU, F., NGOC, D. D. & COUMEL, P. 1995. Catecholaminergic Polymorphic Ventricular Tachycardia in Children: A 7-Year Follow-up of 21 Patients. *Circulation,* 91**,** 1512-1519.
LELOVAS, P. P., KOSTOMITSOPOULOS, N. G. & XANTHOS, T. T. 2014. A comparative anatomic and physiologic overview of the porcine heart. *J Am Assoc Lab Anim Sci,* 53**,** 432-8.
LEWIS, K. J., SILVESTER, N. C., BARBERINI-JAMMAERS, S., MASON, S. A., MARSH, S. A., LIPKA, M. & GEORGE, C. H. 2014. A New System for Profiling Drug-Induced Calcium Signal Perturbation in Human Embryonic Stem Cell–Derived Cardiomyocytes. *Journal of Biomolecular Screening,* 20**,** 330-340.
LEYTON-MANGE, J. S., MILLS, R. W., MACRI, V. S., JANG, M. Y., BUTTE, F. N., ELLINOR, P. T. & MILAN, D. J. 2014. Rapid cellular phenotyping of human pluripotent stem cell-derived cardiomyocytes using a genetically encoded fluorescent voltage sensor. *Stem Cell Reports,* 2**,** 163-70.
LI, C., HU, D., SHANG, L., MA, S., LIU, W., LI, Y., MA, Z., TANG, C., MEI, Y. & WANG, L. 2005. Surgical left cardiac sympathetic denervation for long QT syndrome: effects on QT interval and heart rate. *Heart Vessels,* 20**,** 137-41.
LI, H. O., ZHU, Y. F., ASAKAWA, M., KUMA, H., HIRATA, T., UEDA, Y., LEE, Y. S., FUKUMURA, M., IIDA, A., KATO, A., NAGAI, Y. & HASEGAWA, M. 2000. A cytoplasmic RNA vector derived from nontransmissible Sendai virus with efficient gene transfer and expression. *J Virol,* 74**,** 6564-9.
LI, L., LUO, Z., YU, H., FENG, X., WANG, P., CHEN, J., PU, Y., ZHAO, Y., HE, H., ZHONG, J., LIU, D. & ZHU, Z. 2013. Telmisartan Improves Insulin Resistance of Skeletal Muscle Through Peroxisome Proliferator–Activated Receptor-δ Activation. *Diabetes,* 62**,** 762-774.
LI, M. & BELMONTE, J. C. 2017. Ground rules of the pluripotency gene regulatory network. *Nat Rev Genet*.
LIAN, X., HSIAO, C., WILSON, G., ZHU, K., HAZELTINE, L. B., AZARIN, S. M., RAVAL, K. K., ZHANG, J., KAMP, T. J. & PALECEK, S. P. 2012. Robust cardiomyocyte differentiation from human pluripotent stem cells via temporal modulation of canonical Wnt signaling. *Proc Natl Acad Sci U S A,* 109**,** E1848-57.
LIANG, G. & ZHANG, Y. 2013. Genetic and epigenetic variations in iPSCs: potential causes and implications for application. *Cell Stem Cell,* 13**,** 149-59.
LIANG, P., LAN, F., LEE, A. S., GONG, T., SANCHEZ-FREIRE, V., WANG, Y., DIECKE, S., SALLAM, K., KNOWLES, J. W., WANG, P. J., NGUYEN, P. K., BERS, D. M., ROBBINS, R. C. & WU, J. C. 2013a. Drug screening using a library of human induced pluripotent stem cell-derived cardiomyocytes reveals disease-specific patterns of cardiotoxicity. *Circulation,* 127**,** 1677-91.
LIAO, J., LI, H., ZENG, W., SAUER, D. B., BELMARES, R. & JIANG, Y. 2012. Structural insight into the ion-exchange mechanism of the sodium/calcium exchanger. *Science,* 335**,** 686-90.
LIEU, D. K., LIU, J., SIU, C.-W., MCNERNEY, G. P., TSE, H.-F., ABU-KHALIL, A., HUSER, T. & LI, R. A. 2009. Absence of Transverse Tubules Contributes to Non-Uniform Ca(2+) Wavefronts in Mouse and Human Embryonic Stem Cell–Derived Cardiomyocytes. *Stem Cells and Development,* 18**,** 1493-1500.
LINDSAY, A. R., TINKER, A. & WILLIAMS, A. J. 1994. How does ryanodine modify ion handling in the sheep cardiac sarcoplasmic reticulum Ca(2+)-release

channel? *J Gen Physiol,* 104**,** 425-47.
LIPSKAIA, L., CHEMALY, E. R., HADRI, L., LOMPRE, A.-M. & HAJJAR, R. J. 2010. Sarcoplasmic reticulum Ca(2+) ATPase as a therapeutic target for heart failure. *Expert opinion on biological therapy,* 10**,** 29-41.
LITWIN, S. E., LI, J. & BRIDGE, J. H. 1998. Na-Ca exchange and the trigger for sarcoplasmic reticulum Ca release: studies in adult rabbit ventricular myocytes. *Biophysical Journal,* 75**,** 359-371.
LIU, C. Y., LEE, C. F., HONG, C. H. & WEI, Y. H. 2004. Mitochondrial DNA mutation and depletion increase the susceptibility of human cells to apoptosis. *Ann N Y Acad Sci,* 1011**,** 133-45.
LIU, D.-W. & ANTZELEVITCH, C. 1995. Characteristics of the Delayed Rectifier Current (I_{Kr} and I_{Ks}) in Canine Ventricular Epicardial, Midmyocardial, and Endocardial Myocytes. *Circulation Research,* 76**,** 351.
LIU, G. H., SUZUKI, K., QU, J., SANCHO-MARTINEZ, I., YI, F., LI, M., KUMAR, S., NIVET, E., KIM, J., SOLIGALLA, R. D., DUBOVA, I., GOEBL, A., PLONGTHONGKUM, N., FUNG, H. L., ZHANG, K., LORING, J. F., LAURENT, L. C. & IZPISUA BELMONTE, J. C. 2011. Targeted gene correction of laminopathy-associated LMNA mutations in patient-specific iPSCs. *Cell Stem Cell,* 8**,** 688-94.
LIU, H., YE, Z., KIM, Y., SHARKIS, S. & JANG, Y. Y. 2010. Generation of endoderm-derived human induced pluripotent stem cells from primary hepatocytes. *Hepatology,* 51**,** 1810-9.
LIU, J., LAKSMAN, Z. & BACKX, P. H. 2016. The electrophysiological development of cardiomyocytes. *Advanced Drug Delivery Reviews,* 96**,** 253-273.
LOH, Y. H., AGARWAL, S., PARK, I. H., URBACH, A., HUO, H., HEFFNER, G. C., KIM, K., MILLER, J. D., NG, K. & DALEY, G. Q. 2009. Generation of induced pluripotent stem cells from human blood. *Blood,* 113**,** 5476-9.
LONG, Y. & LI, Z. 2012. *Drug Screening and Drug Safety Evaluation by Patch Clamp Technique*, InTech.
LOPASCHUK, G. D. & JASWAL, J. S. 2010. Energy metabolic phenotype of the cardiomyocyte during development, differentiation, and postnatal maturation. *J Cardiovasc Pharmacol,* 56**,** 130-40.
LOU, Q., JANARDHAN, A. & EFIMOV, I. R. 2012. Remodeling of Calcium Handling in Human Heart Failure. *Advances in experimental medicine and biology,* 740**,** 1145-1174.
LOUCH, W. E., KOIVUMÄKI, J. T. & TAVI, P. 2015. Calcium signalling in developing cardiomyocytes: implications for model systems and disease. *J Physiol,* 593**,** 1047-63.
LUNDY, S. D., ZHU, W. Z., REGNIER, M. & LAFLAMME, M. A. 2013. Structural and functional maturation of cardiomyocytes derived from human pluripotent stem cells. *Stem Cells Dev,* 22**,** 1991-2002.
LUQUET, S., GAUDEL, C., HOLST, D., LOPEZ-SORIANO, J., JEHL-PIETRI, C., FREDENRICH, A. & GRIMALDI, P. A. 2005. Roles of PPAR delta in lipid absorption and metabolism: a new target for the treatment of type 2 diabetes. *Biochim Biophys Acta,* 1740**,** 313-7.
LÓPEZ-SÁNCHEZ, C. & GARCÍA-MARTÍNEZ, V. 2011. Molecular determinants of cardiac specification. *Cardiovasc Res,* 91**,** 185-95.
MA, D., WEI, H., LU, J., HUANG, D., LIU, Z., LOH, L. J., ISLAM, O., LIEW, R., SHIM, W. & COOK, S. A. 2015. Characterization of a novel KCNQ1 mutation for type 1 long QT syndrome and assessment of the therapeutic potential of a novel IKs activator using patient-specific induced pluripotent stem cell-derived

cardiomyocytes. *Stem Cell Res Ther,* 6**,** 39.
MA, J., GUO, L., FIENE, S. J., ANSON, B. D., THOMSON, J. A., KAMP, T. J., KOLAJA, K. L., SWANSON, B. J. & JANUARY, C. T. 2011a. High purity human-induced pluripotent stem cell-derived cardiomyocytes: electrophysiological properties of action potentials and ionic currents. *Am J Physiol Heart Circ Physiol,* 301**,** H2006-17.
MACARTHUR, C. C., FONTES, A., RAVINDER, N., KUNINGER, D., KAUR, J., BAILEY, M., TALIANA, A., VEMURI, M. C. & LIEU, P. T. 2012. Generation of human-induced pluripotent stem cells by a nonintegrating RNA Sendai virus vector in feeder-free or xeno-free conditions. *Stem Cells Int,* 2012**,** 564612.
MACLENNAN, D. H. & ZVARITCH, E. 2011. Mechanistic models for muscle diseases and disorders originating in the sarcoplasmic reticulum. *Biochim Biophys Acta,* 1813**,** 948-64.
MAEKAWA, M., YAMAGUCHI, K., NAKAMURA, T., SHIBUKAWA, R., KODANAKA, I., ICHISAKA, T., KAWAMURA, Y., MOCHIZUKI, H., GOSHIMA, N. & YAMANAKA, S. 2011. Direct reprogramming of somatic cells is promoted by maternal transcription factor Glis1. *Nature,* 474**,** 225-229.
MAKAROVA, K. S., HAFT, D. H., BARRANGOU, R., BROUNS, S. J., CHARPENTIER, E., HORVATH, P., MOINEAU, S., MOJICA, F. J., WOLF, Y. I., YAKUNIN, A. F., VAN DER OOST, J. & KOONIN, E. V. 2011. Evolution and classification of the CRISPR-Cas systems. *Nat Rev Microbiol,* 9**,** 467-77.
MALI, P., ESVELT, K. M. & CHURCH, G. M. 2013. Cas9 as a versatile tool for engineering biology. *Nat Meth,* 10**,** 957-963.
MALTSEV, V. A., VINOGRADOVA, T. M., BOGDANOV, K. Y., LAKATTA, E. G. & STERN, M. D. 2004. Diastolic calcium release controls the beating rate of rabbit sinoatrial node cells: numerical modeling of the coupling process. *Biophys J,* 86**,** 2596-605.
MANDEL, Y., WEISSMAN, A., SCHICK, R., BARAD, L., NOVAK, A., MEIRY, G., GOLDBERG, S., LORBER, A., ROSEN, M. R., ITSKOVITZ-ELDOR, J. & BINAH, O. 2012. Human Embryonic and Induced Pluripotent Stem Cell–Derived Cardiomyocytes Exhibit Beat Rate Variability and Power-Law Behavior. *Circulation,* 125**,** 883-893.
MANNHARDT, I., BRECKWOLDT, K., LETUFFE-BRENIÈRE, D., SCHAAF, S., SCHULZ, H., NEUBER, C., BENZIN, A., WERNER, T., EDER, A., SCHULZE, T., KLAMPE, B., CHRIST, T., HIRT, M. N., HUEBNER, N., MORETTI, A., ESCHENHAGEN, T. & HANSEN, A. 2016a. Human Engineered Heart Tissue: Analysis of Contractile Force. *Stem Cell Reports,* 7**,** 29-42.
MANOACH, M. 1984. Factors influencing maintenance and spontaneous termination of ventricular fibrillation. *Int J Cardiol,* 5**,** 398-402.
MANZO, A., OOTAKI, Y., OOTAKI, C., KAMOHARA, K. & FUKAMACHI, K. 2009. Comparative study of heart rate variability between healthy human subjects and healthy dogs, rabbits and calves. *Lab Anim,* 43**,** 41-5.
MARBAN, E. 2002. Cardiac channelopathies. *Nature,* 415**,** 213-218.
MARCATILI, M., MARSONER, F., D'AGOSTINO, A., KARNAVAS, T., BOTTAI, D., SCARONE, S. & CONTI, L. 2016. Establishment of an induced pluripotent stem cell (iPSC) line from a patient with Clozapine-responder Schizophrenia. *Stem Cell Res,* 17**,** 630-633.
MARK, M. D. & HERLITZE, S. 2000. G-protein mediated gating of inward-rectifier K+ channels. *European Journal of Biochemistry,* 267**,** 5830-5836.
MARKS, A. R. 2000. Cardiac intracellular calcium release channels: role in heart failure. *Circ Res,* 87**,** 8-11.

MARTHERUS, R. S., VANHERLE, S. J., TIMMER, E. D., ZEIJLEMAKER, V. A., BROERS, J. L., SMEETS, H. J., GERAEDTS, J. P. & AYOUBI, T. A. 2010. Electrical signals affect the cardiomyocyte transcriptome independently of contraction. *Physiol Genomics,* 42A**,** 283-9.

MARTINSEN, B. J. & LOHR, J. L. Cardiac Development. *In:* IAIZZO, P. A. (ed.) *Handbook of Cardiac anatomy, Physiology and Devices.* Totowa, NJ: Humana Press Inc.

MARX, S. O., ONDRIAS, K. & MARKS, A. R. 1998. Coupled gating between individual skeletal muscle Ca2+ release channels (ryanodine receptors). *Science,* 281**,** 818-21.

MARX, S. O., REIKEN, S., HISAMATSU, Y., JAYARAMAN, T., BURKHOFF, D., ROSEMBLIT, N. & MARKS, A. R. 2000. PKA Phosphorylation Dissociates FKBP12.6 from the Calcium Release Channel (Ryanodine Receptor): Defective Regulation in Failing Hearts. *Cell,* 101**,** 365-376.

MATHUR, A., LOSKILL, P., SHAO, K., HUEBSCH, N., HONG, S., MARCUS, S. G., MARKS, N., MANDEGAR, M., CONKLIN, B. R., LEE, L. P. & HEALY, K. E. 2015. Human iPSC-based cardiac microphysiological system for drug screening applications. *Sci Rep,* 5**,** 8883.

MATSA, E., RAJAMOHAN, D., DICK, E., YOUNG, L., MELLOR, I., STANIFORTH, A. & DENNING, C. 2011a. Drug evaluation in cardiomyocytes derived from human induced pluripotent stem cells carrying a long QT syndrome type 2 mutation. *Eur Heart J,* 32**,** 952-62.

MATSUURA, K., MASUDA, S. & SHIMIZU, T. 2014. Cell sheet-based cardiac tissue engineering. *Anat Rec (Hoboken),* 297**,** 65-72.

MATSUURA, K., WADA, M., SHIMIZU, T., HARAGUCHI, Y., SATO, F., SUGIYAMA, K., KONISHI, K., SHIBA, Y., ICHIKAWA, H., TACHIBANA, A., IKEDA, U., YAMATO, M., HAGIWARA, N. & OKANO, T. 2012. Creation of human cardiac cell sheets using pluripotent stem cells. *Biochem Biophys Res Commun,* 425**,** 321-7.

MATTMANN, M. E., YU, H., LIN, Z., XU, K., HUANG, X., LONG, S., WU, M., MCMANUS, O. B., ENGERS, D. W., LE, U. M., LI, M., LINDSLEY, C. W. & HOPKINS, C. R. 2012. Identification of (R)-N-(4-(4-methoxyphenyl)thiazol-2-yl)-1-tosylpiperidine-2-carboxamide, ML277, as a novel, potent and selective K(v)7.1 (KCNQ1) potassium channel activator. *Bioorganic & medicinal chemistry letters,* 22**,** 5936-5941.

MEDEIROS-DOMINGO, A., ITURRALDE-TORRES, P. & ACKERMAN, M. J. 2007a. [Clinical and genetic characteristics of long QT syndrome]. *Rev Esp Cardiol,* 60**,** 739-52.

MENG, J., SHI, C., LI, L., DU, Y. & XU, Y. 2013. Compound ICA-105574 prevents arrhythmias induced by cardiac delayed repolarization. *Eur J Pharmacol,* 718**,** 87-97.

MENG, X., NEISES, A., SU, R. J., PAYNE, K. J., RITTER, L., GRIDLEY, D. S., WANG, J., SHENG, M., LAU, K. H., BAYLINK, D. J. & ZHANG, X. B. 2012. Efficient reprogramming of human cord blood CD34+ cells into induced pluripotent stem cells with OCT4 and SOX2 alone. *Mol Ther,* 20**,** 408-16.

MEYER, T., BOVEN, K. H., GÜNTHER, E. & FEJTL, M. 2004a. Micro-electrode arrays in cardiac safety pharmacology: a novel tool to study QT interval prolongation. *Drug Saf,* 27**,** 763-72.

MIHIC, A., LI, J., MIYAGI, Y., GAGLIARDI, M., LI, S. H., ZU, J., WEISEL, R. D., KELLER, G. & LI, R. K. 2014. The effect of cyclic stretch on maturation and 3D tissue formation of human embryonic stem cell-derived cardiomyocytes. *Biomaterials,* 35**,** 2798-808.

MIKAMI, D., KIMURA, H., KAMIYAMA, K., TORII, K., KASUNO, K., TAKAHASHI, N.,

YOSHIDA, H. & IWANO, M. 2014a. Telmisartan activates endogenous peroxisome proliferator-activated receptor-δ and may have anti-fibrotic effects in human mesangial cells. *Hypertens Res,* 37**,** 422-31.
MINAMI, I., YAMADA, K., OTSUJI, T. G., YAMAMOTO, T., SHEN, Y., OTSUKA, S., KADOTA, S., MORONE, N., BARVE, M., ASAI, Y., TENKOVA-HEUSER, T., HEUSER, J. E., UESUGI, M., AIBA, K. & NAKATSUJI, N. 2012. A small molecule that promotes cardiac differentiation of human pluripotent stem cells under defined, cytokine- and xeno-free conditions. *Cell Rep,* 2**,** 1448-60.
MITSUI, K., TOKUZAWA, Y., ITOH, H., SEGAWA, K., MURAKAMI, M., TAKAHASHI, K., MARUYAMA, M., MAEDA, M. & YAMANAKA, S. 2003. The homeoprotein Nanog is required for maintenance of pluripotency in mouse epiblast and ES cells. *Cell,* 113**,** 631-42.
MIZUGUCHI, H., XU, Z., ISHII-WATABE, A., UCHIDA, E. & HAYAKAWA, T. 2000. IRES-dependent second gene expression is significantly lower than cap-dependent first gene expression in a bicistronic vector. *Mol Ther,* 1**,** 376-82.
MONFREDI, O., DOBRZYNSKI, H., MONDAL, T., BOYETT, M. R. & MORRIS, G. M. 2010a. The Anatomy and Physiology of the Sinoatrial Node—A Contemporary Review. *Pacing and Clinical Electrophysiology,* 33**,** 1392-1406.
MOORMAN, A., WEBB, S., BROWN, N. A., LAMERS, W. & ANDERSON, R. H. 2003. Development of the heart: (1) formation of the cardiac chambers and arterial trunks. *Heart,* 89**,** 806-14.
MORETTI, A., BELLIN, M., WELLING, A., JUNG, C. B., LAM, J. T., BOTT-FLÜGEL, L., DORN, T., GOEDEL, A., HÖHNKE, C., HOFMANN, F., SEYFARTH, M., SINNECKER, D., SCHÖMIG, A. & LAUGWITZ, K. L. 2010a. Patient-specific induced pluripotent stem-cell models for long-QT syndrome. *N Engl J Med,* 363**,** 1397-409.
MOSCHELLA, M. C. & MARKS, A. R. 1993. Inositol 1,4,5-trisphosphate receptor expression in cardiac myocytes. *The Journal of Cell Biology,* 120**,** 1137.
MOSCOU, M. J. & BOGDANOVE, A. J. 2009. A simple cipher governs DNA recognition by TAL effectors. *Science,* 326**,** 1501.
MOSS, A. J., ZAREBA, W., KAUFMAN, E. S., GARTMAN, E., PETERSON, D. R., BENHORIN, J., TOWBIN, J. A., KEATING, M. T., PRIORI, S. G., SCHWARTZ, P. J., VINCENT, G. M., ROBINSON, J. L., ANDREWS, M. L., FENG, C., HALL, W. J., MEDINA, A., ZHANG, L. & WANG, Z. 2002. Increased risk of arrhythmic events in long-QT syndrome with mutations in the pore region of the human ether-a-go-go-related gene potassium channel. *Circulation,* 105**,** 794-9.
MUMMERY, C., WARD, D., VAN DEN BRINK, C. E., BIRD, S. D., DOEVENDANS, P. A., OPTHOF, T., BRUTEL DE LA RIVIERE, A., TERTOOLEN, L., VAN DER HEYDEN, M. & PERA, M. 2002. Cardiomyocyte differentiation of mouse and human embryonic stem cells. *J Anat,* 200**,** 233-42.
MUMMERY, C., WARD-VAN OOSTWAARD, D., DOEVENDANS, P., SPIJKER, R., VAN DEN BRINK, S., HASSINK, R., VAN DER HEYDEN, M., OPTHOF, T., PERA, M., DE LA RIVIERE, A. B., PASSIER, R. & TERTOOLEN, L. 2003. Differentiation of human embryonic stem cells to cardiomyocytes: role of coculture with visceral endoderm-like cells. *Circulation,* 107**,** 2733-40.
MUMMERY, C. L., ZHANG, J., NG, E. S., ELLIOTT, D. A., ELEFANTY, A. G. & KAMP, T. J. 2012. Differentiation of human embryonic stem cells and induced pluripotent stem cells to cardiomyocytes: a methods overview. *Circ Res,* 111**,** 344-58.
MURAMATSU, H., ZOU, A. R., BERKOWITZ, G. A. & NATHAN, R. D. 1996. Characterization of a TTX-sensitive Na+ current in pacemaker cells isolated

from rabbit sinoatrial node. *Am J Physiol,* 270**,** H2108-19.
NAKAGAWA, M., KOYANAGI, M., TANABE, K., TAKAHASHI, K., ICHISAKA, T., AOI, T., OKITA, K., MOCHIDUKI, Y., TAKIZAWA, N. & YAMANAKA, S. 2008. Generation of induced pluripotent stem cells without Myc from mouse and human fibroblasts. *Nat Biotechnol,* 26**,** 101-6.
NAKAGAWA, M., TAKIZAWA, N., NARITA, M., ICHISAKA, T. & YAMANAKA, S. 2010a. Promotion of direct reprogramming by transformation-deficient Myc. *Proc Natl Acad Sci U S A,* 107**,** 14152-7.
NAKAI, J., IMAGAWA, T., HAKAMAT, Y., SHIGEKAWA, M., TAKESHIMA, H. & NUMA, S. 1990. Primary structure and functional expression from cDNA of the cardiac ryanodine receptor/calcium release channel. *FEBS Lett,* 271**,** 169-77.
NAPOLITANO, C., BLOISE, R., MONTEFORTE, N. & PRIORI, S. G. 2012. Sudden cardiac death and genetic ion channelopathies: long QT, Brugada, short QT, catecholaminergic polymorphic ventricular tachycardia, and idiopathic ventricular fibrillation. *Circulation,* 125**,** 2027-34.
NAPOLITANO , C., PRIORI, S. & BLOISE, R. 2004. Catecholaminergic Polymorphic Ventricular Tachycardia.
NAPOLITANO, C., PRIORI, S. G., SCHWARTZ, P. J., BLOISE, R., RONCHETTI, E., NASTOLI, J., BOTTELLI, G., CERRONE, M. & LEONARDI, S. 2005. Genetic testing in the long QT syndrome: development and validation of an efficient approach to genotyping in clinical practice. *JAMA,* 294**,** 2975-80.
NARSINH, K. H., JIA, F., ROBBINS, R. C., KAY, M. A., LONGAKER, M. T. & WU, J. C. 2011. Generation of Adult Human Induced Pluripotent Stem Cells Using Non-Viral Minicircle DNA Vectors. *Nature protocols,* 6**,** 78-88.
NAVARRETE, E. G., LIANG, P., LAN, F., SANCHEZ-FREIRE, V., SIMMONS, C., GONG, T., SHARMA, A., BURRIDGE, P. W., PATLOLLA, B., LEE, A. S., WU, H., BEYGUI, R. E., WU, S. M., ROBBINS, R. C., BERS, D. M. & WU, J. C. 2013. Screening Drug-Induced Arrhythmia Using Human Induced Pluripotent Stem Cell–Derived Cardiomyocytes and Low-Impedance Microelectrode Arrays. *Circulation,* 128**,** S3.
NERBONNE, J. M. 2004. Studying cardiac arrhythmias in the mouse--a reasonable model for probing mechanisms? *Trends Cardiovasc Med,* 14**,** 83-93.
NG, E. S., DAVIS, R. P., AZZOLA, L., STANLEY, E. G. & ELEFANTY, A. G. 2005a. Forced aggregation of defined numbers of human embryonic stem cells into embryoid bodies fosters robust, reproducible hematopoietic differentiation. *Blood,* 106**,** 1601-3.
NICHOLS, J., ZEVNIK, B., ANASTASSIADIS, K., NIWA, H., KLEWE-NEBENIUS, D., CHAMBERS, I., SCHÖLER, H. & SMITH, A. 1998. Formation of pluripotent stem cells in the mammalian embryo depends on the POU transcription factor Oct4. *Cell,* 95**,** 379-91.
NISHIMASU, H., RAN, F. A., HSU, P. D., KONERMANN, S., SHEHATA, S. I., DOHMAE, N., ISHITANI, R., ZHANG, F. & NUREKI, O. 2014. Crystal structure of Cas9 in complex with guide RNA and target DNA. *Cell,* 156**,** 935-49.
NORSTRÖM, A., AKESSON, K., HARDARSON, T., HAMBERGER, L., BJÖRQUIST, P. & SARTIPY, P. 2006. Molecular and pharmacological properties of human embryonic stem cell-derived cardiomyocytes. *Exp Biol Med (Maywood),* 231**,** 1753-62.
NOVAK, A., BARAD, L., LORBER, A., GHERGHICEANU, M., REITER, I., EISEN, B., ELDOR, L., ITSKOVITZ-ELDOR, J., ELDAR, M., ARAD, M. & BINAH, O. 2015. Functional abnormalities in iPSC-derived cardiomyocytes generated from CPVT1 and CPVT2 patients carrying ryanodine or calsequestrin mutations. *Journal of*

Cellular and Molecular Medicine, 19**,** 2006-2018.
NUNES, S. S., MIKLAS, J. W., LIU, J., ASCHAR-SOBBI, R., XIAO, Y., ZHANG, B., JIANG, J., MASSE, S., GAGLIARDI, M., HSIEH, A., THAVANDIRAN, N., LAFLAMME, M. A., NANTHAKUMAR, K., GROSS, G. J., BACKX, P. H., KELLER, G. & RADISIC, M. 2013. Biowire: a platform for maturation of human pluripotent stem cell-derived cardiomyocytes. *Nat Meth,* 10**,** 781-787.
NYEGAARD, M., OVERGAARD, MICHAEL T., SØNDERGAARD, MADS T., VRANAS, M., BEHR, ELIJAH R., HILDEBRANDT, LASSE L., LUND, J., HEDLEY, PAULA L., CAMM, A. J., WETTRELL, G., FOSDAL, I., CHRISTIANSEN, M. & BØRGLUM, ANDERS D. 2012. Mutations in Calmodulin Cause Ventricular Tachycardia and Sudden Cardiac Death. *The American Journal of Human Genetics,* 91**,** 703-712.
NÄBAUER, M., BEUCKELMANN, D. J., UBERFUHR, P. & STEINBECK, G. 1996a. Regional differences in current density and rate-dependent properties of the transient outward current in subepicardial and subendocardial myocytes of human left ventricle. *Circulation,* 93**,** 168-77.
OBERGRUSSBERGER, A., HAARMANN, C., STÖLZLE-FEIX, S., BECKER, N., OHTSUKI, A., BRÜGGEMANN, A., GEORGE, M. & FERTIG, N. 2017. Automated Patch Clamp Recordings of Human Stem Cell-Derived Cardiomyocytes. *In:* CLEMENTS, M. & ROQUEMORE, L. (eds.) *Stem Cell-Derived Models in Toxicology.* New York, NY: Springer New York.
OKA, T., SATO, K., HORI, M., OZAKI, H. & KARAKI, H. 2002a. Xestospongin C, a novel blocker of IP3 receptor, attenuates the increase in cytosolic calcium level and degranulation that is induced by antigen in RBL-2H3 mast cells. *Br J Pharmacol,* 135**,** 1959-66.
OKITA, K., ICHISAKA, T. & YAMANAKA, S. 2007. Generation of germline-competent induced pluripotent stem cells. *Nature,* 448**,** 313-7.
ONO, K., SHIBATA, S. & IIJIMA, T. 2000. Properties of the delayed rectifier potassium current in porcine sino-atrial node cells. *J Physiol,* 524 Pt 1**,** 51-62.
ONO, M., HAMADA, Y., HORIUCHI, Y., MATSUO-TAKASAKI, M., IMOTO, Y., SATOMI, K., ARINAMI, T., HASEGAWA, M., FUJIOKA, T., NAKAMURA, Y. & NOGUCHI, E. 2012a. Generation of induced pluripotent stem cells from human nasal epithelial cells using a Sendai virus vector. *PLoS One,* 7**,** e42855.
ONO, M., HAMADA, Y., HORIUCHI, Y., MATSUO-TAKASAKI, M., IMOTO, Y., SATOMI, K., ARINAMI, T., HASEGAWA, M., FUJIOKA, T., NAKAMURA, Y. & NOGUCHI, E. 2012b. Generation of induced pluripotent stem cells from human nasal epithelial cells using a Sendai virus vector. *PLoS One,* 7**,** e42855.
OTTOLIA, M., TORRES, N., BRIDGE, J. H., PHILIPSON, K. D. & GOLDHABER, J. I. 2013. Na/Ca exchange and contraction of the heart. *J Mol Cell Cardiol,* 61**,** 28-33.
PAPADIMITRIOU, D., XANTHOS, T., DONTAS, I., LELOVAS, P. & PERREA, D. 2008. The use of mice and rats as animal models for cardiopulmonary resuscitation research. *Lab Anim,* 42**,** 265-76.
PARK, F. 2007. Lentiviral vectors: are they the future of animal transgenesis? *Physiol Genomics,* 31**,** 159-73.
PARK, I. H., ARORA, N., HUO, H., MAHERALI, N., AHFELDT, T., SHIMAMURA, A., LENSCH, M. W., COWAN, C., HOCHEDLINGER, K. & DALEY, G. Q. 2008a. Disease-specific induced pluripotent stem cells. *Cell,* 134**,** 877-86.
PARK, I. H., LEROU, P. H., ZHAO, R., HUO, H. & DALEY, G. Q. 2008b. Generation of human-induced pluripotent stem cells. *Nat Protoc,* 3**,** 1180-6.
PAUKLIN, S. & VALLIER, L. 2013. The cell-cycle state of stem cells determines cell fate propensity. *Cell,* 155**,** 135-47.

PENTTINEN, K., SWAN, H., VANNINEN, S., PAAVOLA, J., LAHTINEN, A. M., KONTULA, K. & AALTO-SETÄLÄ, K. 2015. Antiarrhythmic Effects of Dantrolene in Patients with Catecholaminergic Polymorphic Ventricular Tachycardia and Replication of the Responses Using iPSC Models. *PLoS One,* 10**,** e0125366.

PERIASAMY, M. & KALYANASUNDARAM, A. 2007. SERCA pump isoforms: their role in calcium transport and disease. *Muscle Nerve,* 35**,** 430-42.

PETERS, N. S., SEVERS, N. J., ROTHERY, S. M., LINCOLN, C., YACOUB, M. H. & GREEN, C. R. 1994. Spatiotemporal relation between gap junctions and fascia adherens junctions during postnatal development of human ventricular myocardium. *Circulation,* 90**,** 713.

PIACENTINO, V., WEBER, C. R., CHEN, X., WEISSER-THOMAS, J., MARGULIES, K. B., BERS, D. M. & HOUSER, S. R. 2003. Cellular basis of abnormal calcium transients of failing human ventricular myocytes. *Circ Res,* 92**,** 651-8.

PIPER, D. R., SANGUINETTI, M. C. & TRISTANI-FIROUZI, M. 2005. Voltage sensor movement in the hERG K+ channel. *Novartis Found Symp,* 266**,** 46-52; discussion 52-6, 95-9.

POINDEXTER, B. J., SMITH, J. R., BUJA, L. M. & BICK, R. J. 2001. Calcium signaling mechanisms in dedifferentiated cardiac myocytes: comparison with neonatal andadult cardiomyocytes. *Cell Calcium,* 30**,** 373-382.

POSTMA, A. V., DENJOY, I., KAMBLOCK, J., ALDERS, M., LUPOGLAZOFF, J. M., VAKSMANN, G., DUBOSQ-BIDOT, L., SEBILLON, P., MANNENS, M. M., GUICHENEY, P. & WILDE, A. A. 2005. Catecholaminergic polymorphic ventricular tachycardia: RYR2 mutations, bradycardia, and follow up of the patients. *J Med Genet,* 42**,** 863-70.

PRADHAPAN, P., KUUSELA, J., VIIK, J., AALTO-SETÄLÄ, K. & HYTTINEN, J. 2013. Cardiomyocyte MEA Data Analysis (CardioMDA) – A Novel Field Potential Data Analysis Software for Pluripotent Stem Cell Derived Cardiomyocytes. *PLOS ONE,* 8**,** e73637.

PREININGER, M. K., JHA, R., MAXWELL, J. T., WU, Q., SINGH, M., WANG, B., DALAL, A., MCEACHIN, Z. T., ROSSOLL, W., HALES, C. M., FISCHBACH, P. S., WAGNER, M. B. & XU, C. 2016a. A human pluripotent stem cell model of catecholaminergic polymorphic ventricular tachycardia recapitulates patient-specific drug responses. *Dis Model Mech,* 9**,** 927-39.

PREININGER, M. K., JHA, R., MAXWELL, J. T., WU, Q., SINGH, M., WANG, B., DALAL, A., MCEACHIN, Z. T., ROSSOLL, W., HALES, C. M., FISCHBACH, P. S., WAGNER, M. B. & XU, C. 2016b. A human pluripotent stem cell model of catecholaminergic polymorphic ventricular tachycardia recapitulates patient-specific drug responses. *Dis Model Mech,* 9**,** 927-39.

PRIORI, S. G. & CHEN, S. R. 2011. Inherited dysfunction of sarcoplasmic reticulum Ca2+ handling and arrhythmogenesis. *Circ Res,* 108**,** 871-83.

PRIORI, S. G. & CORR, P. B. 1990. The Importance of α-Adrenergic Stimulation of Cardiac Tissue and its Contribution to Arrhythmogenesis During Ischemia. *Journal of Cardiovascular Electrophysiology,* 1**,** 529-542.

PRIORI, S. G., NAPOLITANO, C., SCHWARTZ, P. J., GRILLO, M., BLOISE, R., RONCHETTI, E., MONCALVO, C., TULIPANI, C., VEIA, A., BOTTELLI, G. & NASTOLI, J. 2004b. Association of long QT syndrome loci and cardiac events among patients treated with beta-blockers. *JAMA,* 292**,** 1341-4.

PRIORI, S. G., NAPOLITANO, C., TISO, N., MEMMI, M., VIGNATI, G., BLOISE, R., SORRENTINO, V. & DANIELI, G. A. 2001a. Mutations in the Cardiac Ryanodine Receptor Gene (hRyR2) Underlie Catecholaminergic Polymorphic Ventricular Tachycardia. *Circulation,* 103**,** 196-200.

PRIORI, S. G., SCHWARTZ, P. J., NAPOLITANO, C., BLOISE, R., RONCHETTI, E., GRILLO, M., VICENTINI, A., SPAZZOLINI, C., NASTOLI, J., BOTTELLI, G., FOLLI, R. & CAPPELLETTI, D. 2003. Risk Stratification in the Long-QT Syndrome. *New England Journal of Medicine,* 348**,** 1866-1874.

QU, X., LIU, T., SONG, K., LI, X. & GE, D. 2012. Induced pluripotent stem cells generated from human adipose-derived stem cells using a non-viral polycistronic plasmid in feeder-free conditions. *PLoS One,* 7**,** e48161.

QU, Y. & VARGAS, H. M. 2015. Proarrhythmia Risk Assessment in Human Induced Pluripotent Stem Cell-Derived Cardiomyocytes Using the Maestro MEA Platform. *Toxicol Sci,* 147**,** 286-95.

RAHMOUNE, H., THOMPSON, P. W., WARD, J. M., SMITH, C. D., HONG, G. & BROWN, J. 2005a. Glucose transporters in human renal proximal tubular cells isolated from the urine of patients with non-insulin-dependent diabetes. *Diabetes,* 54**,** 3427-34.

RAJAMOHAN, D., KALRA, S., DUC HOANG, M., GEORGE, V., STANIFORTH, A., RUSSELL, H., YANG, X. & DENNING, C. 2016. Automated Electrophysiological and Pharmacological Evaluation of Human Pluripotent Stem Cell-Derived Cardiomyocytes. *Stem Cells Dev,* 25**,** 439-52.

RAJAMOHAN, D., MATSA, E., KALRA, S., CRUTCHLEY, J., PATEL, A., GEORGE, V. & DENNING, C. 2013a. Current status of drug screening and disease modelling in human pluripotent stem cells. *Bioessays,* 35**,** 281-98.

RAMACHANDRAN, R., FAUSETT, B. V. & GOLDMAN, D. 2010. Ascl1a regulates Müller glia dedifferentiation and retinal regeneration through a Lin-28-dependent, let-7 microRNA signalling pathway. *Nat Cell Biol,* 12**,** 1101-7.

RAMIREZ, R. J., SAH, R., LIU, J., ROSE, R. A. & BACKX, P. H. 2011. Intracellular [Na+] modulates synergy between Na+/Ca2+ exchanger and L-type Ca2+ current in cardiac excitation–contraction coupling during action potentials. *Basic Research in Cardiology,* 106**,** 967-977.

RAN, F. A., HSU, P. D., LIN, C. Y., GOOTENBERG, J. S., KONERMANN, S., TREVINO, A. E., SCOTT, D. A., INOUE, A., MATOBA, S., ZHANG, Y. & ZHANG, F. 2013a. Double nicking by RNA-guided CRISPR Cas9 for enhanced genome editing specificity. *Cell,* 154**,** 1380-9.

RAO, C., PRODROMAKIS, T., KOLKER, L., CHAUDHRY, U. A., TRANTIDOU, T., SRIDHAR, A., WEEKES, C., CAMELLITI, P., HARDING, S. E., DARZI, A., YACOUB, M. H., ATHANASIOU, T. & TERRACCIANO, C. M. 2013a. The effect of microgrooved culture substrates on calcium cycling of cardiac myocytes derived from human induced pluripotent stem cells. *Biomaterials,* 34**,** 2399-411.

RAO, M. S. & MALIK, N. 2012. Assessing iPSC reprogramming methods for their suitability in translational medicine. *J Cell Biochem,* 113**,** 3061-8.

RATH, D., AMLINGER, L., RATH, A. & LUNDGREN, M. 2015. The CRISPR-Cas immune system: biology, mechanisms and applications. *Biochimie,* 117**,** 119-28.

RECCHIA, A., BONINI, C., MAGNANI, Z., URBINATI, F., SARTORI, D., MURARO, S., TAGLIAFICO, E., BONDANZA, A., STANGHELLINI, M. T., BERNARDI, M., PESCAROLLO, A., CICERI, F., BORDIGNON, C. & MAVILIO, F. 2006. Retroviral vector integration deregulates gene expression but has no consequence on the biology and function of transplanted T cells. *Proc Natl Acad Sci U S A,* 103**,** 1457-62.

REN, Y., LEE, M. Y., SCHLIFFKE, S., PAAVOLA, J., AMOS, P. J., GE, X., YE, M., ZHU, S., SENYEI, G., LUM, L., EHRLICH, B. E. & QYANG, Y. 2011. Small molecule Wnt inhibitors enhance the efficiency of BMP-4-directed cardiac differentiation of human pluripotent stem cells. *J Mol Cell Cardiol,* 51**,** 280-7.

RIVOLTA, M. W., BEVAN, G. H., GUREV, V., RICE, J. J., LOPES, C. M. & COUDERC, J. P. T-wave morphology depends on transmural heterogeneity in a high-resolution human left-ventricular wedge model. 2015 Computing in Cardiology Conference (CinC), 6-9 Sept. 2015 2015. 433-436.

RODEN, D. M., BALSER, J. R., GEORGE, A. L. & ANDERSON, M. E. 2002. Cardiac ion channels. *Annu Rev Physiol,* 64**,** 431-75.

ROMANO, C., GEMME, G. & PONGIGLIONE, R. 1963. [RARE CARDIAC ARRYTHMIAS OF THE PEDIATRIC AGE. II. SYNCOPAL ATTACKS DUE TO PAROXYSMAL VENTRICULAR FIBRILLATION. (PRESENTATION OF 1ST CASE IN ITALIAN PEDIATRIC LITERATURE)]. *Clin Pediatr (Bologna),* 45**,** 656-83.

ROSE, T., GOLTSTEIN, P. M., PORTUGUES, R. & GRIESBECK, O. 2014. Putting a finishing touch on GECIs. *Frontiers in Molecular Neuroscience,* 7**,** 88.

ROSEMBLIT, N., MOSCHELLA, M. C., ONDRIAŠOVÁ, E., GUTSTEIN, D. E., ONDRIAŠ, K. & MARKS, A. R. 1999. Intracellular calcium release channel expression during embryogenesis. *Dev Biol,* 206**,** 163-77.

ROUX-BUISSON, N., CACHEUX, M., FOUREST-LIEUVIN, A., FAUCONNIER, J., BROCARD, J., DENJOY, I., DURAND, P., GUICHENEY, P., KYNDT, F., LEENHARDT, A., LE MAREC, H., LUCET, V., MABO, P., PROBST, V., MONNIER, N., RAY, P. F., SANTONI, E., TRÉMEAUX, P., LACAMPAGNE, A., FAURÉ, J., LUNARDI, J. & MARTY, I. 2012. Absence of triadin, a protein of the calcium release complex, is responsible for cardiac arrhythmia with sudden death in human. *Hum Mol Genet,* 21**,** 2759-67.

ROWLAND, B. D., BERNARDS, R. & PEEPER, D. S. 2005a. The KLF4 tumour suppressor is a transcriptional repressor of p53 that acts as a context-dependent oncogene. *Nat Cell Biol,* 7**,** 1074-82.

SAAD, M., MAHMOUD, A., ELGENDY, I. Y. & RICHARD CONTI, C. 2016. Ranolazine in Cardiac Arrhythmia. *Clin Cardiol,* 39**,** 170-8.

SAFFITZ, J. E., KANTER, H. L., GREEN, K. G., TOLLEY, T. K. & BEYER, E. C. 1994. Tissue-specific determinants of anisotropic conduction velocity in canine atrial and ventricular myocardium. *Circ Res,* 74**,** 1065-70.

SAIMI, Y. & KUNG, C. 2002. Calmodulin as an ion channel subunit. *Annu Rev Physiol,* 64**,** 289-311.

SAINI, H., NAVAEI, A., VAN PUTTEN, A. & NIKKHAH, M. 2015. 3D cardiac microtissues encapsulated with the co-culture of cardiomyocytes and cardiac fibroblasts. *Adv Healthc Mater,* 4**,** 1961-71.

SAITO, H., IWABUCHI, K., FUSAKI, N. & ITO, F. 2016. Generation of Induced Pluripotent Stem Cells from Human Melanoma Tumor-infiltrating Lymphocytes. *J Vis Exp*.

SAITO, H., KATO, A., MATSUMOTO, K. & OKAYAMA, Y. 2006. Culture of human mast cells from peripheral blood progenitors. *Nat Protoc,* 1**,** 2178-83.

SALA, L., YU, Z., WARD-VAN OOSTWAARD, D., VAN VELDHOVEN, J. P. D., MORETTI, A., LAUGWITZ, K. L., MUMMERY, C. L., IJZERMAN, A. P. & BELLIN, M. 2016. A new hERG allosteric modulator rescues genetic and drug-induced long-QT syndrome phenotypes in cardiomyocytes from isogenic pairs of patient induced pluripotent stem cells. *EMBO Molecular Medicine*.

SALAMA, G. & LONDON, B. 2007. Mouse models of long QT syndrome. *The Journal of Physiology,* 578**,** 43-53.

SALEEM, H., TOVEY, S. C., MOLINSKI, T. F. & TAYLOR, C. W. 2014. Interactions of antagonists with subtypes of inositol 1,4,5-trisphosphate (IP3) receptor. *British Journal of Pharmacology,* 171**,** 3298-3312.

SANGUINETTI, M. C., JIANG, C., CURRAN, M. E. & KEATING, M. T. 1995. A mechanistic

link between an inherited and an acquired cardiac arrhythmia: HERG encodes the IKr potassium channel. *Cell,* 81**,** 299-307.

SARTIANI, L., BETTIOL, E., STILLITANO, F., MUGELLI, A., CERBAI, E. & JACONI, M. E. 2007. Developmental changes in cardiomyocytes differentiated from human embryonic stem cells: a molecular and electrophysiological approach. *Stem Cells,* 25**,** 1136-44.

SASAKI, K., MAKIYAMA, T., YOSHIDA, Y., WURIYANGHAI, Y., KAMAKURA, T., NISHIUCHI, S., HAYANO, M., HARITA, T., YAMAMOTO, Y., KOHJITANI, H., HIROSE, S., CHEN, J., KAWAMURA, M., OHNO, S., ITOH, H., TAKEUCHI, A., MATSUOKA, S., MIURA, M., SUMITOMO, N., HORIE, M., YAMANAKA, S. & KIMURA, T. 2016a. Patient-Specific Human Induced Pluripotent Stem Cell Model Assessed with Electrical Pacing Validates S107 as a Potential Therapeutic Agent for Catecholaminergic Polymorphic Ventricular Tachycardia. *PLoS One,* 11**,** e0164795.

SATIN, J., ITZHAKI, I., RAPOPORT, S., SCHRODER, E. A., IZU, L., ARBEL, G., BEYAR, R., BALKE, C. W., SCHILLER, J. & GEPSTEIN, L. 2008. Calcium handling in human embryonic stem cell-derived cardiomyocytes. *Stem Cells,* 26**,** 1961-72.

SAUCERMAN, J. J. & BERS, D. M. 2008. Calmodulin mediates differential sensitivity of CaMKII and calcineurin to local Ca2+ in cardiac myocytes. *Biophys J,* 95**,** 4597-612.

SCHAPER, J., MEISER, E. & STÄMMLER, G. 1985. Ultrastructural morphometric analysis of myocardium from dogs, rats, hamsters, mice, and from human hearts. *Circ Res,* 56**,** 377-91.

SCHIMPF, R., VELTMANN, C., WOLPERT, C. & BORGGREFE, M. 2009. Channelopathies: Brugada syndrome, long QT syndrome, short QT syndrome, and CPVT. *Herz,* 34**,** 281-8.

SCHLAEGER, T. M., DAHERON, L., BRICKLER, T. R., ENTWISLE, S., CHAN, K., CIANCI, A., DEVINE, A., ETTENGER, A., FITZGERALD, K., GODFREY, M., GUPTA, D., MCPHERSON, J., MALWADKAR, P., GUPTA, M., BELL, B., DOI, A., JUNG, N., LI, X., LYNES, M. S., BROOKES, E., CHERRY, A. B., DEMIRBAS, D., TSANKOV, A. M., ZON, L. I., RUBIN, L. L., FEINBERG, A. P., MEISSNER, A., COWAN, C. A. & DALEY, G. Q. 2015. A comparison of non-integrating reprogramming methods. *Nat Biotechnol,* 33**,** 58-63.

SCHNEIDER, H., STEINMETZ, M., KRAUSE, U., KRIEBEL, T., RUSCHEWSKI, W. & PAUL, T. 2013a. Left cardiac sympathetic denervation for the management of life-threatening ventricular tachyarrhythmias in young patients with catecholaminergic polymorphic ventricular tachycardia and long QT syndrome. *Clinical Research in Cardiology,* 102**,** 33-42.

SCHRAM, G., POURRIER, M., MELNYK, P. & NATTEL, S. 2002a. Differential distribution of cardiac ion channel expression as a basis for regional specialization in electrical function. *Circ Res,* 90**,** 939-50.

SCHWARTZ, P. 1984. *Sympathetic imbalance and cardiac arrhythmias. In: RandallWC, editor. Nervous control of cardiovascular function*.

SCHWARTZ, P. J., CROTTI, L. & INSOLIA, R. 2012a. Long-QT syndrome: from genetics to management. *Circ Arrhythm Electrophysiol,* 5**,** 868-77.

SCHWARTZ, P. J., PRIORI, S. G., CERRONE, M., SPAZZOLINI, C., ODERO, A., NAPOLITANO, C., BLOISE, R., DE FERRARI, G. M., KLERSY, C., MOSS, A. J., ZAREBA, W., ROBINSON, J. L., HALL, W. J., BRINK, P. A., TOIVONEN, L., EPSTEIN, A. E., LI, C. & HU, D. 2004a. Left cardiac sympathetic denervation in the management of high-risk patients affected by the long-QT syndrome.

Circulation, 109**,** 1826-33.
SCHWARTZ, P. J., PRIORI, S. G., SPAZZOLINI, C., MOSS, A. J., VINCENT, G. M., NAPOLITANO, C., DENJOY, I., GUICHENEY, P., BREITHARDT, G., KEATING, M. T., TOWBIN, J. A., BEGGS, A. H., BRINK, P., WILDE, A. A., TOIVONEN, L., ZAREBA, W., ROBINSON, J. L., TIMOTHY, K. W., CORFIELD, V., WATTANASIRICHAIGOON, D., CORBETT, C., HAVERKAMP, W., SCHULZE-BAHR, E., LEHMANN, M. H., SCHWARTZ, K., COUMEL, P. & BLOISE, R. 2001a. Genotype-phenotype correlation in the long-QT syndrome: gene-specific triggers for life-threatening arrhythmias. *Circulation,* 103**,** 89-95.
SCHWARTZ, P. J., VANOLI, E., CROTTI, L., SPAZZOLINI, C., FERRANDI, C., GOOSEN, A., HEDLEY, P., HERADIEN, M., BACCHINI, S., TURCO, A., LA ROVERE, M. T., BARTOLI, A., GEORGE, A. L. & BRINK, P. A. 2008a. Neural control of heart rate is an arrhythmia risk modifier in long QT syndrome. *J Am Coll Cardiol,* 51**,** 920-9.
SCHÖLER, H. R., RUPPERT, S., SUZUKI, N., CHOWDHURY, K. & GRUSS, P. 1990. New type of POU domain in germ line-specific protein Oct-4. *Nature,* 344**,** 435-9.
SCOOTE, M. & WILLIAMS, A. J. 2002. The cardiac ryanodine receptor (calcium release channel)Emerging role in heart failure and arrhythmia pathogenesis. *Cardiovascular Research,* 56**,** 359-372.
SEGEV, H., KENYAGIN-KARSENTI, D., FISHMAN, B., GERECHT-NIR, S., ZISKIND, A., AMIT, M., COLEMAN, R. & ITSKOVITZ-ELDOR, J. 2005. Molecular analysis of cardiomyocytes derived from human embryonic stem cells. *Dev Growth Differ,* 47**,** 295-306.
SEIBLER, P., GRAZIOTTO, J., JEONG, H., SIMUNOVIC, F., KLEIN, C. & KRAINC, D. 2011. Mitochondrial Parkin recruitment is impaired in neurons derived from mutant PINK1 induced pluripotent stem cells. *J Neurosci,* 31**,** 5970-6.
SHABANI, P., GHAZIZADEH, Z., PAHLAVAN, S., HASHEMIZADEH, S., BAHARVAND, H., AGHDAMI, N. & DOOSTI, M. 2015. Exogenous treatment with eicosapentaenoic acid supports maturation of cardiomyocytes derived from embryonic stem cells. *Biochem Biophys Res Commun,* 461**,** 281-6.
SHAFA, M., KRAWETZ, R., ZHANG, Y., RATTNER, J. B., GODOLLEI, A., DUFF, H. J. & RANCOURT, D. E. 2011. Impact of stirred suspension bioreactor culture on the differentiation of murine embryonic stem cells into cardiomyocytes. *BMC Cell Biol,* 12**,** 53.
SHALEM, O., SANJANA, N. E., HARTENIAN, E., SHI, X., SCOTT, D. A., MIKKELSEN, T. S., HECKL, D., EBERT, B. L., ROOT, D. E., DOENCH, J. G. & ZHANG, F. 2014. Genome-scale CRISPR-Cas9 knockout screening in human cells. *Science,* 343**,** 84-7.
SHAO, L. & WU, W. S. 2010. Gene-delivery systems for iPS cell generation. *Expert Opin Biol Ther,* 10**,** 231-42.
SHEN, H., LI, J., ZHANG, J., XU, C., JIANG, Y., WU, Z., ZHAO, F., LIAO, L., CHEN, J., LIN, Y., TIAN, Q., PAPASIAN, C. J. & DENG, H. W. 2013. Comprehensive characterization of human genome variation by high coverage whole-genome sequencing of forty four Caucasians. *PLoS One,* 8**,** e59494.
SHI, G. & JIN, Y. 2010. Role of Oct4 in maintaining and regaining stem cell pluripotency. *Stem Cell Res Ther,* 1**,** 39.
SHI, W., WYMORE, R. S., WANG, H. S., PAN, Z., COHEN, I. S., MCKINNON, D. & DIXON, J. E. 1997. Identification of two nervous system-specific members of the erg potassium channel gene family. *J Neurosci,* 17**,** 9423-32.
SHIBA, Y., HAUCH, K. D. & LAFLAMME, M. A. 2009. Cardiac applications for human pluripotent stem cells. *Curr Pharm Des,* 15**,** 2791-806.

SHIGEKAWA, M. & IWAMOTO, T. 2001. Cardiac Na⁺-Ca²⁺ Exchange. *Circulation Research,* 88**,** 864.

SHIH, H. T. 1994a. Anatomy of the action potential in the heart. *Texas Heart Institute Journal,* 21**,** 30-41.

SHIMIZU, W. & ANTZELEVITCH, C. 2000. Effects of a K(+) channel opener to reduce transmural dispersion of repolarization and prevent torsade de pointes in LQT1, LQT2, and LQT3 models of the long-QT syndrome. *Circulation,* 102**,** 706-12.

SHINNAWI, R., HUBER, I., MAIZELS, L., SHAHEEN, N., GEPSTEIN, A., ARBEL, G., TIJSEN, A. J. & GEPSTEIN, L. 2015a. Monitoring Human-Induced Pluripotent Stem Cell-Derived Cardiomyocytes with Genetically Encoded Calcium and Voltage Fluorescent Reporters. *Stem Cell Reports,* 5**,** 582-96.

SICA, D. A. 2004. Minoxidil: An Underused Vasodilator for Resistant or Severe Hypertension. *The Journal of Clinical Hypertension,* 6**,** 283-287.

SINNECKER, D., LAUGWITZ, K. L. & MORETTI, A. 2014. Induced pluripotent stem cell-derived cardiomyocytes for drug development and toxicity testing. *Pharmacol Ther,* 143**,** 246-52.

SITSAPESAN, R. & WILLIAMS, A. J. 1994. Regulation of the gating of the sheep cardiac sarcoplasmic reticulum Ca(2+)-release channel by luminal Ca2+. *J Membr Biol,* 137**,** 215-26.

SMITH, J. L., ANDERSON, C. L., BURGESS, D. E., ELAYI, C. S., JANUARY, C. T. & DELISLE, B. P. 2016. Molecular pathogenesis of long QT syndrome type 2. *J Arrhythm,* 32**,** 373-380.

SOCHACKI, J., DEVALLE, S., REIS, M., MATTOS, P. & REHEN, S. 2016. Generation of urine iPS cell lines from patients with Attention Deficit Hyperactivity Disorder (ADHD) using a non-integrative method. *Stem Cell Res,* 17**,** 102-106.

SOMIA, N. & VERMA, I. M. 2000. Gene therapy: trials and tribulations. *Nat Rev Genet,* 1**,** 91-9.

SOMMER, C. A., SOMMER, A. G., LONGMIRE, T. A., CHRISTODOULOU, C., THOMAS, D. D., GOSTISSA, M., ALT, F. W., MURPHY, G. J., KOTTON, D. N. & MOSTOSLAVSKY, G. 2010. Excision of reprogramming transgenes improves the differentiation potential of iPS cells generated with a single excisable vector. *Stem Cells,* 28**,** 64-74.

SOMMER, C. A., STADTFELD, M., MURPHY, G. J., HOCHEDLINGER, K., KOTTON, D. N. & MOSTOSLAVSKY, G. 2009. Induced pluripotent stem cell generation using a single lentiviral stem cell cassette. *Stem Cells,* 27**,** 543-9.

SORRENTINO, V. & VOLPE, P. 1993. Ryanodine receptors: how many, where and why? *Trends Pharmacol Sci,* 14**,** 98-103.

SOUDERS, C. A., BOWERS, S. L. K. & BAUDINO, T. A. 2009. Cardiac Fibroblast. *Circulation Research,* 105**,** 1164.

SPECTOR, P. 2013. Principles of cardiac electric propagation and their implications for re-entrant arrhythmias. *Circ Arrhythm Electrophysiol,* 6**,** 655-61.

STADTFELD, M., MAHERALI, N., BREAULT, D. T. & HOCHEDLINGER, K. 2008. Defining molecular cornerstones during fibroblast to iPS cell reprogramming in mouse. *Cell Stem Cell,* 2**,** 230-40.

STILLITANO, F., LONARDO, G., ZICHA, S., VARRO, A., CERBAI, E., MUGELLI, A. & NATTEL, S. 2008. Molecular basis of funny current (If) in normal and failing human heart. *J Mol Cell Cardiol,* 45**,** 289-99.

SUMI, T., TSUNEYOSHI, N., NAKATSUJI, N. & SUEMORI, H. 2007. Apoptosis and differentiation of human embryonic stem cells induced by sustained activation of c-Myc. *Oncogene,* 26**,** 5564-76.

SUN, N., YAZAWA, M., LIU, J., HAN, L., SANCHEZ-FREIRE, V., ABILEZ, O. J., NAVARRETE, E. G., HU, S., WANG, L., LEE, A., PAVLOVIC, A., LIN, S., CHEN, R., HAJJAR, R. J., SNYDER, M. P., DOLMETSCH, R. E., BUTTE, M. J., ASHLEY, E. A., LONGAKER, M. T., ROBBINS, R. C. & WU, J. C. 2012a. Patient-specific induced pluripotent stem cells as a model for familial dilated cardiomyopathy. *Sci Transl Med,* 4**,** 130ra47.

SUN, X., MEYERS, E. N., LEWANDOSKI, M. & MARTIN, G. R. 1999. Targeted disruption of Fgf8 causes failure of cell migration in the gastrulating mouse embryo. *Genes Dev,* 13**,** 1834-46.

SWAN, H., PIIPPO, K., VIITASALO, M., HEIKKILÄ, P., PAAVONEN, T., KAINULAINEN, K., KERE, J., KETO, P., KONTULA, K. & TOIVONEN, L. 1999. Arrhythmic disorder mapped to chromosome 1q42–q43 causes malignant polymorphic ventricular tachycardia in structurally normal hearts. *Journal of the American College of Cardiology,* 34**,** 2035-2042.

SWARTS, D. C., MOSTERD, C., VAN PASSEL, M. W. & BROUNS, S. J. 2012. CRISPR interference directs strand specific spacer acquisition. *PLoS One,* 7**,** e35888.

SYNNERGREN, J., AMÉEN, C., JANSSON, A. & SARTIPY, P. 2012. Global transcriptional profiling reveals similarities and differences between human stem cell-derived cardiomyocyte clusters and heart tissue. *Physiol Genomics,* 44**,** 245-58.

TAKAHASHI, K., TANABE, K., OHNUKI, M., NARITA, M., ICHISAKA, T., TOMODA, K. & YAMANAKA, S. 2007. Induction of pluripotent stem cells from adult human fibroblasts by defined factors. *Cell,* 131**,** 861-72.

TAKAHASHI, K. & YAMANAKA, S. 2006a. Induction of pluripotent stem cells from mouse embryonic and adult fibroblast cultures by defined factors. *Cell,* 126**,** 663-76.

TAKEDA, A., IGARASHI, H., KAWADA, M., TSUKAMOTO, T., YAMAMOTO, H., INOUE, M., IIDA, A., SHU, T., HASEGAWA, M. & MATANO, T. 2008. Evaluation of the immunogenicity of replication-competent V-knocked-out and replication-defective F-deleted Sendai virus vector-based vaccines in macaques. *Vaccine,* 26**,** 6839-43.

TAKESHIMA, H., NISHIMURA, S., MATSUMOTO, T., ISHIDA, H., KANGAWA, K., MINAMINO, N., MATSUO, H., UEDA, M., HANAOKA, M. & HIROSE, T. 1989. Primary structure and expression from complementary DNA of skeletal muscle ryanodine receptor. *Nature,* 339**,** 439-45.

TAN, H. K., TOH, C. X., MA, D., YANG, B., LIU, T. M., LU, J., WONG, C. W., TAN, T. K., LI, H., SYN, C., TAN, E. L., LIM, B., LIM, Y. P., COOK, S. A. & LOH, Y. H. 2014. Human finger-prick induced pluripotent stem cells facilitate the development of stem cell banking. *Stem Cells Transl Med,* 3**,** 586-98.

TERENTYEV, D., VIATCHENKO-KARPINSKI, S., GYÖRKE, I., VOLPE, P., WILLIAMS, S. C. & GYÖRKE, S. 2003. Calsequestrin determines the functional size and stability of cardiac intracellular calcium stores: Mechanism for hereditary arrhythmia. *Proc Natl Acad Sci U S A,* 100**,** 11759-64.

TISO, N., STEPHAN, D. A., NAVA, A., BAGATTIN, A., DEVANEY, J. M., STANCHI, F., LARDERET, G., BRAHMBHATT, B., BROWN, K., BAUCE, B., MURIAGO, M., BASSO, C., THIENE, G., DANIELI, G. A. & RAMPAZZO, A. 2001. Identification of mutations in the cardiac ryanodine receptor gene in families affected with arrhythmogenic right ventricular cardiomyopathy type 2 (ARVD2). *Human Molecular Genetics,* 10**,** 189-194.

TORRENTE, A. G., MESIRCA, P., NECO, P., RIZZETTO, R., DUBEL, S., BARRERE, C., SINEGGER-BRAUNS, M., STRIESSNIG, J., RICHARD, S., NARGEOT, J., GOMEZ,

A. M. & MANGONI, M. E. 2016. L-type Cav1.3 channels regulate ryanodine receptor-dependent Ca2+ release during sino-atrial node pacemaker activity. *Cardiovascular Research,* 109**,** 451-461.

TRIPATHY, A. & MEISSNER, G. 1996. Sarcoplasmic reticulum lumenal Ca2+ has access to cytosolic activation and inactivation sites of skeletal muscle Ca2+ release channel. *Biophys J,* 70**,** 2600-15.

TRUDEAU, M. C., WARMKE, J. W., GANETZKY, B. & ROBERTSON, G. A. 1995. HERG, a human inward rectifier in the voltage-gated potassium channel family. *Science,* 269**,** 92-5.

TSENG, G. N. 2001. I(Kr): the hERG channel. *J Mol Cell Cardiol,* 33**,** 835-49.

TULLOCH, N. L., MUSKHELI, V., RAZUMOVA, M. V., KORTE, F. S., REGNIER, M., HAUCH, K. D., PABON, L., REINECKE, H. & MURRY, C. E. 2011. Growth of engineered human myocardium with mechanical loading and vascular coculture. *Circ Res,* 109**,** 47-59.

URNOV, F. D., REBAR, E. J., HOLMES, M. C., ZHANG, H. S. & GREGORY, P. D. 2010. Genome editing with engineered zinc finger nucleases. *Nat Rev Genet,* 11**,** 636-46.

VAN DER WERF, C., KANNANKERIL, P. J., SACHER, F., KRAHN, A. D., VISKIN, S., LEENHARDT, A., SHIMIZU, W., SUMITOMO, N., FISH, F. A., BHUIYAN, Z. A., WILLEMS, A. R., VAN DER VEEN, M. J., WATANABE, H., LABORDERIE, J., HAÏSSAGUERRE, M., KNOLLMANN, B. C. & WILDE, A. A. 2011. Flecainide therapy reduces exercise-induced ventricular arrhythmias in patients with catecholaminergic polymorphic ventricular tachycardia. *J Am Coll Cardiol,* 57**,** 2244-54.

VAN HOORN, F., CAMPIAN, M. E., SPIJKERBOER, A., BLOM, M. T., PLANKEN, R. N., VAN ROSSUM, A. C., DE BAKKER, J. M., WILDE, A. A., GROENINK, M. & TAN, H. L. 2012. SCN5A mutations in Brugada syndrome are associated with increased cardiac dimensions and reduced contractility. *PLoS One,* 7**,** e42037.

VAN MEER, B. J., TERTOOLEN, L. G. & MUMMERY, C. L. 2016. Concise Review: Measuring Physiological Responses of Human Pluripotent Stem Cell Derived Cardiomyocytes to Drugs and Disease. *Stem Cells,* 34**,** 2008-15.

VAROTHAI, S. & BERGFELD, W. F. 2014. Androgenetic alopecia: an evidence-based treatment update. *Am J Clin Dermatol,* 15**,** 217-30.

VERAITCH, O., MABUCHI, Y., MATSUZAKI, Y., SASAKI, T., OKUNO, H., TSUKASHIMA, A., AMAGAI, M., OKANO, H. & OHYAMA, M. 2017. Induction of hair follicle dermal papilla cell properties in human induced pluripotent stem cell-derived multipotent LNGFR(+)THY-1(+) mesenchymal cells. *Sci Rep,* 7**,** 42777.

VERHEIJCK, E. E., VAN GINNEKEN, A. C., BOURIER, J. & BOUMAN, L. N. 1995. Effects of delayed rectifier current blockade by E-4031 on impulse generation in single sinoatrial nodal myocytes of the rabbit. *Circ Res,* 76**,** 607-15.

VERHEIJCK, E. E., VAN KEMPEN, M. J., VEERESCHILD, M., LURVINK, J., JONGSMA, H. J. & BOUMAN, L. N. 2001. Electrophysiological features of the mouse sinoatrial node in relation to connexin distribution. *Cardiovasc Res,* 52**,** 40-50.

VERKERK, A. O., WILDERS, R., VAN BORREN, M. M., PETERS, R. J., BROEKHUIS, E., LAM, K., CORONEL, R., DE BAKKER, J. M. & TAN, H. L. 2007. Pacemaker current (I(f)) in the human sinoatrial node. *Eur Heart J,* 28**,** 2472-8.

VILLA-DIAZ, L. G., ROSS, A. M., LAHANN, J. & KREBSBACH, P. H. 2013. Concise review: The evolution of human pluripotent stem cell culture: from feeder cells to synthetic coatings. *Stem Cells,* 31**,** 1-7.

VOGT, E. J., MEGLICKI, M., HARTUNG, K. I., BORSUK, E. & BEHR, R. 2012. Importance of the pluripotency factor LIN28 in the mammalian nucleolus during early

embryonic development. *Development,* 139**,** 4514-23.
VOLDERS, P. G., STENGL, M., VAN OPSTAL, J. M., GERLACH, U., SPÄTJENS, R. L., BEEKMAN, J. D., SIPIDO, K. R. & VOS, M. A. 2003. Probing the contribution of IKs to canine ventricular repolarization: key role for beta-adrenergic receptor stimulation. *Circulation,* 107**,** 2753-60.
VOLLERT, I., SEIFFERT, M., BACHMAIR, J., SANDER, M., EDER, A., CONRADI, L., VOGELSANG, A., SCHULZE, T., UEBELER, J., HOLNTHONER, W., REDL, H., REICHENSPURNER, H., HANSEN, A. & ESCHENHAGEN, T. 2014. In vitro perfusion of engineered heart tissue through endothelialized channels. *Tissue Eng Part A,* 20**,** 854-63.
WADA, N., WANG, B., LIN, N. H., LASLETT, A. L., GRONTHOS, S. & BARTOLD, P. M. 2011. Induced pluripotent stem cell lines derived from human gingival fibroblasts and periodontal ligament fibroblasts. *J Periodontal Res,* 46**,** 438-47.
WADDINGTON, C. H. 1957. The Strategy of the Genes. London: George Allen and Unwin.
WAINGER, B. J., DEGENNARO, M., SANTORO, B., SIEGELBAUM, S. A. & TIBBS, G. R. 2001. Molecular mechanism of cAMP modulation of HCN pacemaker channels. *Nature,* 411**,** 805-810.
WAKAYAMA, T., PERRY, A. C., ZUCCOTTI, M., JOHNSON, K. R. & YANAGIMACHI, R. 1998. Full-term development of mice from enucleated oocytes injected with cumulus cell nuclei. *Nature,* 394**,** 369-74.
WANG, H., HAO, J. & HONG, C. C. 2011. Cardiac Induction of Embryonic Stem Cells by a Small Molecule Inhibitor of Wnt/β-catenin signaling. *ACS chemical biology,* 6**,** 192-197.
WANG, T., WEI, J. J., SABATINI, D. M. & LANDER, E. S. 2014. Genetic screens in human cells using the CRISPR-Cas9 system. *Science,* 343**,** 80-4.
WANG, W., LIN, C., LU, D., NING, Z., COX, T., MELVIN, D., WANG, X., BRADLEY, A. & LIU, P. 2008. Chromosomal transposition of PiggyBac in mouse embryonic stem cells. *Proc Natl Acad Sci U S A,* 105**,** 9290-5.
WANG, Y., HU, Z., SUN, B., XU, J., JIANG, J. & LUO, M. 2015. Ginsenoside Rg3 attenuates myocardial ischemia/reperfusion injury via Akt/endothelial nitric oxide synthase signaling and the B-cell lymphoma/B-cell lymphoma-associated X protein pathway. *Mol Med Rep,* 11**,** 4518-24.
WANG, Z., FERMINI, B. & NATTEL, S. 1993. Delayed rectifier outward current and repolarization in human atrial myocytes. *Circ Res,* 73**,** 276-85.
WARD, O. C. 1964. A NEW FAMILIAL CARDIAC SYNDROME IN CHILDREN. *J Ir Med Assoc,* 54**,** 103-6.
WARMKE, J. W. & GANETZKY, B. 1994. A family of potassium channel genes related to eag in Drosophila and mammals. *Proc Natl Acad Sci U S A,* 91**,** 3438-42.
WATANABE, H., CHOPRA, N., LAVER, D., HWANG, H. S., DAVIES, S. S., ROACH, D. E., DUFF, H. J., RODEN, D. M., WILDE, A. A. & KNOLLMANN, B. C. 2009. Flecainide prevents catecholaminergic polymorphic ventricular tachycardia in mice and humans. *Nat Med,* 15**,** 380-3.
WATANABE, M., ROLLINS, M. A., POLO-PARADA, L., MA, P., GU, S. & JENKINS, W. M. 2016. Probing the Electrophysiology of the Developing Heart. *Journal of Cardiovascular Development and Disease,* 3.
WEHRENS, X. H., KIRCHHOFF, S. & DOEVENDANS, P. A. 2000. Mouse electrocardiography: an interval of thirty years. *Cardiovasc Res,* 45**,** 231-7.
WEHRENS, X. H., LEHNART, S. E., REIKEN, S. R. & MARKS, A. R. 2004. Ca2+/calmodulin-dependent protein kinase II phosphorylation regulates the

cardiac ryanodine receptor. *Circ Res,* 94**,** e61-70.
WEISS, J. N., GARFINKEL, A., KARAGUEUZIAN, H. S., CHEN, P. S. & QU, Z. 2010. Early afterdepolarizations and cardiac arrhythmias. *Heart Rhythm,* 7**,** 1891-9.
WELLENS, H. J., SCHWARTZ, P. J., LINDEMANS, F. W., BUXTON, A. E., GOLDBERGER, J. J., HOHNLOSER, S. H., HUIKURI, H. V., KÄÄB, S., LA ROVERE, M. T., MALIK, M., MYERBURG, R. J., SIMOONS, M. L., SWEDBERG, K., TIJSSEN, J., VOORS, A. A. & WILDE, A. A. 2014. Risk stratification for sudden cardiac death: current status and challenges for the future. *Eur Heart J,* 35**,** 1642-51.
WETTWER, E., AMOS, G. J., POSIVAL, H. & RAVENS, U. 1994. Transient outward current in human ventricular myocytes of subepicardial and subendocardial origin. *Circ Res,* 75**,** 473-82.
WIEDENHEFT, B., STERNBERG, S. H. & DOUDNA, J. A. 2012. RNA-guided genetic silencing systems in bacteria and archaea. *Nature,* 482**,** 331-338.
WIESE, C., GRIESKAMP, T., AIRIK, R., MOMMERSTEEG, M. T., GARDIWAL, A., DE GIER-DE VRIES, C., SCHUSTER-GOSSLER, K., MOORMAN, A. F., KISPERT, A. & CHRISTOFFELS, V. M. 2009. Formation of the sinus node head and differentiation of sinus node myocardium are independently regulated by Tbx18 and Tbx3. *Circ Res,* 104**,** 388-97.
WILLIAMS, A. J., WEST, D. J. & SITSAPESAN, R. 2001. Light at the end of the Ca(2+)-release channel tunnel: structures and mechanisms involved in ion translocation in ryanodine receptor channels. *Q Rev Biophys,* 34**,** 61-104.
WOBUS, A. M. & LÖSER, P. 2011. Present state and future perspectives of using pluripotent stem cells in toxicology research. *Arch Toxicol,* 85**,** 79-117.
WU, C. & DUNBAR, C. E. 2011. Stem cell gene therapy: the risks of insertional mutagenesis and approaches to minimize genotoxicity. *Frontiers of medicine,* 5**,** 356-371.
WU, T. T., NIU, H. S., CHEN, L. J., CHENG, J. T. & TONG, Y. C. 2016. Increase of human prostate cancer cell (DU145) apoptosis by telmisartan through PPAR-delta pathway. *Eur J Pharmacol,* 775**,** 35-42.
XIE, F., YE, L., CHANG, J. C., BEYER, A. I., WANG, J., MUENCH, M. O. & KAN, Y. W. 2014a. Seamless gene correction of β-thalassemia mutations in patient-specific iPSCs using CRISPR/Cas9 and piggyBac. *Genome Res,* 24**,** 1526-33.
XU, C., POLICE, S., HASSANIPOUR, M., LI, Y., CHEN, Y., PRIEST, C., O'SULLIVAN, C., LAFLAMME, M. A., ZHU, W. Z., VAN BIBER, B., HEGEROVA, L., YANG, J., DELAVAN-BOORSMA, K., DAVIES, A., LEBKOWSKI, J. & GOLD, J. D. 2011a. Efficient generation and cryopreservation of cardiomyocytes derived from human embryonic stem cells. *Regen Med,* 6**,** 53-66.
YAGI, T., ITO, D., OKADA, Y., AKAMATSU, W., NIHEI, Y., YOSHIZAKI, T., YAMANAKA, S., OKANO, H. & SUZUKI, N. 2011. Modeling familial Alzheimer's disease with induced pluripotent stem cells. *Hum Mol Genet,* 20**,** 4530-9.
YAMAKAGE, M. & NAMIKI, A. 2002. Calcium channels — basic aspects of their structure, function and gene encoding; anesthetic action on the channels — a review. *Canadian Journal of Anesthesia,* 49**,** 151-164.
YAMASAKI, S., HAMADA, A., AKAGI, E., NAKATAO, H., OHTAKA, M., NISHIMURA, K., NAKANISHI, M., TORATANI, S. & OKAMOTO, T. 2016. Generation of cleidocranial dysplasia-specific human induced pluripotent stem cells in completely serum-, feeder-, and integration-free culture. *In Vitro Cell Dev Biol Anim,* 52**,** 252-64.
YAN, X., QIN, H., QU, C., TUAN, R. S., SHI, S. & HUANG, G. T. 2010a. iPS cells reprogrammed from human mesenchymal-like stem/progenitor cells of dental tissue origin. *Stem Cells Dev,* 19**,** 469-80.

YANG, X., PABON, L. & MURRY, C. E. 2014a. Engineering adolescence: maturation of human pluripotent stem cell-derived cardiomyocytes. *Circ Res,* 114**,** 511-23.
YANG, X., RODRIGUEZ, M., PABON, L., FISCHER, K. A., REINECKE, H., REGNIER, M., SNIADECKI, N. J., RUOHOLA-BAKER, H. & MURRY, C. E. 2014b. Tri-iodo-l-thyronine promotes the maturation of human cardiomyocytes-derived from induced pluripotent stem cells. *J Mol Cell Cardiol,* 72**,** 296-304.
YAZAWA, M., HSUEH, B., JIA, X., PASCA, A. M., BERNSTEIN, J. A., HALLMAYER, J. & DOLMETSCH, R. E.
YE, Z., ZHAN, H., MALI, P., DOWEY, S., WILLIAMS, D. M., JANG, Y. Y., DANG, C. V., SPIVAK, J. L., MOLITERNO, A. R. & CHENG, L. 2009. Human-induced pluripotent stem cells from blood cells of healthy donors and patients with acquired blood disorders. *Blood,* 114**,** 5473-80.
YOKOO, N., BABA, S., KAICHI, S., NIWA, A., MIMA, T., DOI, H., YAMANAKA, S., NAKAHATA, T. & HEIKE, T. 2009. The effects of cardioactive drugs on cardiomyocytes derived from human induced pluripotent stem cells. *Biochem Biophys Res Commun,* 387**,** 482-8.
YONEMITSU, Y., KITSON, C., FERRARI, S., FARLEY, R., GRIESENBACH, U., JUDD, D., STEEL, R., SCHEID, P., ZHU, J., JEFFERY, P. K., KATO, A., HASAN, M. K., NAGAI, Y., MASAKI, I., FUKUMURA, M., HASEGAWA, M., GEDDES, D. M. & ALTON, E. W. 2000. Efficient gene transfer to airway epithelium using recombinant Sendai virus. *Nat Biotechnol,* 18**,** 970-3.
YU, J., CHAU, K. F., VODYANIK, M. A., JIANG, J. & JIANG, Y. 2011. Efficient feeder-free episomal reprogramming with small molecules. *PLoS One,* 6**,** e17557.
YU, J. & THOMSON, J. A. 2008. Pluripotent stem cell lines. *Genes Dev,* 22**,** 1987-97.
YU, J., VODYANIK, M. A., SMUGA-OTTO, K., ANTOSIEWICZ-BOURGET, J., FRANE, J. L., TIAN, S., NIE, J., JONSDOTTIR, G. A., RUOTTI, V., STEWART, R., SLUKVIN, I. I. & THOMSON, J. A. 2007. Induced pluripotent stem cell lines derived from human somatic cells. *Science,* 318**,** 1917-20.
YUE, T. L., NERURKAR, S. S., BAO, W., JUCKER, B. M., SAROV-BLAT, L., STEPLEWSKI, K., OHLSTEIN, E. H. & WILLETTE, R. N. 2008. In vivo activation of peroxisome proliferator-activated receptor-delta protects the heart from ischemia/reperfusion injury in Zucker fatty rats. *J Pharmacol Exp Ther,* 325**,** 466-74.
ZAREBA, W., MOSS, A. J., DAUBERT, J. P., HALL, W. J., ROBINSON, J. L. & ANDREWS, M. 2003a. Implantable cardioverter defibrillator in high-risk long QT syndrome patients. *J Cardiovasc Electrophysiol,* 14**,** 337-41.
ZHANG, H., ZOU, B., YU, H., MORETTI, A., WANG, X., YAN, W., BABCOCK, J. J., BELLIN, M., MCMANUS, O. B., TOMASELLI, G., NAN, F., LAUGWITZ, K. L. & LI, M. 2012a. Modulation of hERG potassium channel gating normalizes action potential duration prolonged by dysfunctional KCNQ1 potassium channel. *Proc Natl Acad Sci U S A,* 109**,** 11866-71.
ZHANG, J., KLOS, M., WILSON, G. F., HERMAN, A. M., LIAN, X., RAVAL, K. K., BARRON, M. R., HOU, L., SOERENS, A. G., YU, J., PALECEK, S. P., LYONS, G. E., THOMSON, J. A., HERRON, T. J., JALIFE, J. & KAMP, T. J. 2012b. Extracellular matrix promotes highly efficient cardiac differentiation of human pluripotent stem cells: the matrix sandwich method. *Circ Res,* 111**,** 1125-36.
ZHANG, J., RATANASIRINTRAWOOT, S., CHANDRASEKARAN, S., WU, Z., FICARRO, S. B., YU, C., ROSS, C. A., CACCHIARELLI, D., XIA, Q., SELIGSON, M., SHINODA, G., XIE, W., CAHAN, P., WANG, L., NG, S. C., TINTARA, S., TRAPNELL, C., ONDER, T., LOH, Y. H., MIKKELSEN, T., SLIZ, P., TEITELL, M. A., ASARA, J. M., MARTO, J. A., LI, H., COLLINS, J. J. & DALEY, G. Q. 2016a. LIN28 Regulates Stem Cell

Metabolism and Conversion to Primed Pluripotency. *Cell Stem Cell,* 19**,** 66-80.

ZHANG, J., WILSON, G. F., SOERENS, A. G., KOONCE, C. H., YU, J., PALECEK, S. P., THOMSON, J. A. & KAMP, T. J. 2009. Functional cardiomyocytes derived from human induced pluripotent stem cells. *Circ Res,* 104**,** e30-41.

ZHANG, L., TIMOTHY, K. W., VINCENT, G. M., LEHMANN, M. H., FOX, J., GIULI, L. C., SHEN, J., SPLAWSKI, I., PRIORI, S. G., COMPTON, S. J., YANOWITZ, F., BENHORIN, J., MOSS, A. J., SCHWARTZ, P. J., ROBINSON, J. L., WANG, Q., ZAREBA, W., KEATING, M. T., TOWBIN, J. A., NAPOLITANO, C. & MEDINA, A. 2000. Spectrum of ST-T-wave patterns and repolarization parameters in congenital long-QT syndrome: ECG findings identify genotypes. *Circulation,* 102**,** 2849-55.

ZHANG, L. P., JIANG, Y. C., YU, X. F., XU, H. L., LI, M., ZHAO, X. Z. & SUI, D. Y. 2016b. Ginsenoside Rg3 Improves Cardiac Function after Myocardial Ischemia/Reperfusion via Attenuating Apoptosis and Inflammation. *Evid Based Complement Alternat Med,* 2016**,** 6967853.

ZHANG, M., D'ANIELLO, C., VERKERK, A. O., WROBEL, E., FRANK, S., WARD-VAN OOSTWAARD, D., PICCINI, I., FREUND, C., RAO, J., SEEBOHM, G., ATSMA, D. E., SCHULZE-BAHR, E., MUMMERY, C. L., GREBER, B. & BELLIN, M. 2014a. Recessive cardiac phenotypes in induced pluripotent stem cell models of Jervell and Lange-Nielsen syndrome: disease mechanisms and pharmacological rescue. *Proc Natl Acad Sci U S A,* 111**,** E5383-92.

ZHANG, S. & CUI, W. 2014. Sox2, a key factor in the regulation of pluripotency and neural differentiation. *World J Stem Cells,* 6**,** 305-11.

ZHANG WY, DE ALMEIDA PE & JC., W. 2012. Teratoma formation: A tool for monitoring pluripotency in stem cell research. Cambridge (MA): Harvard Stem Cell Institute.

ZHANG, Y., MCNEILL, E., TIAN, H., SOKER, S., ANDERSSON, K. E., YOO, J. J. & ATALA, A. 2008. Urine derived cells are a potential source for urological tissue reconstruction. *J Urol,* 180**,** 2226-33.

ZHAO, Y., ARAKI, S., WU, J., TERAMOTO, T., CHANG, Y.-F., NAKANO, M., ABDELFATTAH, A. S., FUJIWARA, M., ISHIHARA, T., NAGAI, T. & CAMPBELL, R. E. 2011. An Expanded Palette of Genetically Encoded Ca(2+) Indicators. *Science (New York, N.Y.),* 333**,** 1888-1891.

ZHAO, Y., YIN, X., QIN, H., ZHU, F., LIU, H., YANG, W., ZHANG, Q., XIANG, C., HOU, P., SONG, Z., LIU, Y., YONG, J., ZHANG, P., CAI, J., LIU, M., LI, H., LI, Y., QU, X., CUI, K., ZHANG, W., XIANG, T., WU, Y., LIU, C., YU, C., YUAN, K., LOU, J., DING, M. & DENG, H. 2008b. Two supporting factors greatly improve the efficiency of human iPSC generation. *Cell Stem Cell,* 3**,** 475-9.

ZHOU, H., WU, S., JOO, J. Y., ZHU, S., HAN, D. W., LIN, T., TRAUGER, S., BIEN, G., YAO, S., ZHU, Y., SIUZDAK, G., SCHÖLER, H. R., DUAN, L. & DING, S. 2009. Generation of induced pluripotent stem cells using recombinant proteins. *Cell Stem Cell,* 4**,** 381-4.

ZHOU, T., BENDA, C., DUZINGER, S., HUANG, Y., LI, X., LI, Y., GUO, X., CAO, G., CHEN, S., HAO, L., CHAN, Y. C., NG, K. M., HO, J. C., WIESER, M., WU, J., REDL, H., TSE, H. F., GRILLARI, J., GRILLARI-VOGLAUER, R., PEI, D. & ESTEBAN, M. A. 2011. Generation of induced pluripotent stem cells from urine. *J Am Soc Nephrol,* 22**,** 1221-8.

ZHU, R., BLAZESKI, A., POON, E., COSTA, K. D., TUNG, L. & BOHELER, K. R. 2014. Physical developmental cues for the maturation of human pluripotent stem cell-derived cardiomyocytes. *Stem Cell Res Ther,* 5**,** 117.

ZIMA, A. V., BOVO, E., MAZUREK, S. R., ROCHIRA, J. A., LI, W. & TERENTYEV, D. 2014. Ca handling during excitation–contraction coupling in heart failure. *Pflügers Archiv - European Journal of Physiology,* 466**,** 1129-1137.

ZIPES, D. P., CAMM, A. J., BORGGREFE, M., BUXTON, A. E., CHAITMAN, B., FROMER, M., GREGORATOS, G., KLEIN, G., MOSS, A. J., MYERBURG, R. J., PRIORI, S. G., QUINONES, M. A., RODEN, D. M., SILKA, M. J. & TRACY, C. 2006. ACC/AHA/ESC 2006 guidelines for management of patients with ventricular arrhythmias and the prevention of sudden cardiac death—executive summaryA report of the American College of Cardiology/American Heart Association Task Force and the European Society of Cardiology Committee for Practice Guidelines (Writing Committee to Develop Guidelines for Management of Patients with Ventricular Arrhythmias and the Prevention of Sudden Cardiac Death) Developed in collaboration with the European Heart Rhythm Association and the Heart Rhythm Society. *European Heart Journal,* 27**,** 2099-2140.

ZYGMUNT, A. C., EDDLESTONE, G. T., THOMAS, G. P., NESTERENKO, V. V. & ANTZELEVITCH, C. 2001. Larger late sodium conductance in M cells contributes to electrical heterogeneity in canine ventricle. *Am J Physiol Heart Circ Physiol,* 281**,** H689-97.